

***In Vitro* and *In Vivo* Characterization and  
Evaluation of Some Naturally Occurring  
Small Molecules Based Nanoformulation  
for Diabetes Management**

**Thesis submitted by**

**SK MOSIUR RAHAMAN**

**Doctor of Philosophy (Pharmacy)**

**Department of Pharmaceutical Technology  
Faculty of Engineering & Technology  
Jadavpur University  
Kolkata-700032, WB, India**

**2024**



**JADAVPUR UNIVERSITY KOLKATA**

**700032**

**WEST BENGAL, INDIA**

**INDEX NO: 287/19/Ph.**

**1. Title of the thesis:**

*In Vitro* and *In Vivo* Characterization and Evaluation of Some Naturally Occurring Small Molecules Based Nanoformulation for Diabetes Management

**2. Name, Designation & Institution of the supervisor:**

**Dr. Ranu Biswas**

Assistant Professor  
Department of Pharmaceutical Technology  
Jadavpur University,  
188, Raja S C Mullick Road, Kolkata 700032  
West Bengal, India.

**3. List of Publications:**

**A. Related to the thesis works (2)**

- i. Rahaman SM**, Chandra A. Biswas, R. RP-HPLC method development and validation for simultaneous estimation of curcumin and resveratrol in nano-micelle: dual drug dual form simultaneous estimation. *Int J App Pharm.* 2024;16(3):109–118. <https://doi.org/10.22159/ijap.2024v16i3.50276>
- ii. Rahaman SM**, Dutta G, Biswas R, Sugumaran A, Salem MM, Gamal M, Abdelrahman M, Salem-Bekhit MM. Succinyl curcumin conjugated chitosan polymer-prodrug nanomicelles: A potential treatment for Type-II diabetes in diabetic Balb/C mice. *Acta Chim Slov.* 2024;71:401–415. DOI: 10.17344/acsi.2024.8658

**4. List of patents: Nil**

**5. List of presentations in national/international seminar/conferences: (2)**

- i. **Rahaman SM**, Bhutia GT, Bera T, “Type-II anti-diabetic potential of chitosan di-curcumin conjugated nanomicelles” oral presentation dated 29-30th July 2022 at National Seminar on “Recent Advances in Drug Discovery and Developments” organized by Calcutta Institute of Pharmaceutical Technology & AHS, Uluberia, WB, India.
- ii. **Rahaman SM**, Bhutia GT, Bera T, “Type-II anti-diabetic potential of solid dispersion of curcumin & resveratrol containing D- $\alpha$ -tocopheryl polyethylene glycol succinate and mannitol formulation”. Oral presented in the National Conference entitled “Drug Repositioning: A Novel Approach to Drug Discovery”. R B Science. Bhopal, Madhya Pradesh, India held on September 18, 2022.

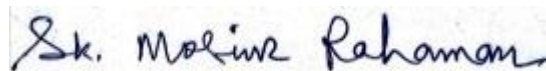


## “Statement of Originality”

I **Sk Mosiur Rahaman** research scholar of Department of Pharmaceutical Technology, Jadavpur University, Kolkata, India registered on **24/06/2019** do here by declare that this thesis entitled “***In Vitro* and *In Vivo* Characterization and Evaluation of Some Naturally Occurring Small Molecules Based Nanoformulation for Diabetes Management**” contains literature survey and original research work done by the undersigned candidate as part of Doctoral studies.

All information in this thesis have been obtained and presented in accordance with existing academic rules and ethical conduct. I declare that, as required by these rules and conduct. The cited and referred materials and results are not original to this work.

I also declare that I have checked this thesis as per the “Policy on Anti Plagiarism, Jadavpur University, 2019”, and the level of similarity as checked by iThenticate software is 7 %



**Signature of Candidate:**

**Date: 21/06/2024**



**Certified by Supervisor(s):**

**(Signature with date, seal)**

**Dr. Ranu Biswas**  
Assistant Professor  
Dept. of Pharmaceutical Technology  
Jadavpur University  
Kolkata-700032, W.B. India



## CERTIFICATE FROM THE SUPERVISORS

This is to certify that the thesis entitled “*In Vitro* and *In Vivo* Characterization and Evaluation of Some Naturally Occurring Small Molecules Based Nanoformulation for Diabetes Management” submitted by Mr. **Sk Mosiur Rahaman** who got his name registered on 24<sup>th</sup> June, 2019 for the award of Ph. D. (Pharmacy) degree of Jadavpur University is absolutely based upon his own work under the supervision of **Dr. Ranu Biswas**, Assistant Professor and that neither his thesis nor any part of the thesis has been submitted for any degree/diploma or any other academic award anywhere before.

A handwritten signature in blue ink, appearing to read 'Ranu Biswas', with a date '21/6/24' written below it. The signature is written over a dotted line.

**Signature of Supervisor**

**(Dr. Ranu Biswas)**

Assistant Professor

Department of Pharmaceutical Technology

Jadavpur University

Kolkata 700032

West Bengal, India.



## **Acknowledgements**

*It has been a great experience to work for my PhD thesis which has provided me with wonderful period of time to learn from great teachers and friends and colleagues. I am pleased to be at this stage of my PhD program where I recall several personalities without whose kind support, patience and encouragement my thesis would have been just a dream.*

*I take this opportunity to express my sincere thanks and deepest sense of gratitude to my guide/supervisor **Dr. Ranu Biswas**, Assistant Professor, Department of Pharmaceutical Technology, Jadavpur University, Kolkata-700032, for his valuable guidance, suggestions, constant encouragement and untiring help, without which my thesis would never have been completed.*

*It is great feelings to express my cordial gratitude and thanks to **Prof (Dr.) Amalesh Samanta**, HOD, Department of Pharmaceutical Technology, Jadavpur University, Kolkata-700032. Without his encouragement and guidance, I would not be able to attain this stage of my career now. His kind patience, constructive guidance and criticism have improved the quality of work as well as expression to a significant extent.*

*I am grateful to all **the faculties of Department of Pharmaceutical Technology**, Jadavpur University, Kolkata, India, for their cordial and expert helms. I must be thankful to the authorities of Jadavpur University for providing necessary supports throughout the possession of my Ph. D. research. It has been an outstanding opportunity to work in Jadavpur University with the exceptional amenities being offered to me.*

*I would like to extend my deepest gratitude to **Dr. Abimanyu Sugumaran**, former professor Department of Pharmaceutics, SRM College of Pharmacy, SRM Institute of Science and Technology, Kattankulathur 603203, Tamilnadu, India, and his scholar **Mr. Gouranga Dutta** for kindly helping a great deal. The Chemical and morphological study of nanomicelles as well as ideas obtained from his laboratory were absolutely essential to carry out these studies.*

*I am also grateful to **Dr. Sanmoy Karmakar**, Ex. Head of the Department, **Dr. Biswajit Mukherjee**, Ex Head of the Department, **Dr. Kunal Roy**, Ex Head of the Department, **Dr. Pallab Kanti Haldar**, Dept. Pharmaceutical Technology, Jadavpur University for rendering me valuable helps and necessary laboratory facilities to carry out this thesis work.*

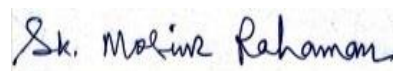
*This is as well to express very sincere thanks to **the Vice-Chancellor, the Registrar, the Controller of Examination**, Jadavpur University and **the Dean, FET**, Jadavpur University for giving me the opportunity to do my work at this University.*

*I am thankful to my senior colleagues **Dr. Suman Das** and **Dr. Asit De** for their support during the tenure of my research. I extend my heart full thanks to **Mr. Gyamcho Tshering Bhutia** for his cooperation and immense help I received from him during my work.*

*Last but not the least; I would like to thank my family: my wife (**Mrs. Salima Khatun**), My son (**Shaikh Abeed Rahaman**) and my daughter (**Shaikh Maheera**) for supporting me and kind co-operation throughout my research work and writing this thesis.*

Date: 21/06/2024

Place: Kolkata

A handwritten signature in blue ink that reads "Sk. Mosiur Rahaman". The signature is written in a cursive style with a clear, legible font.

**Sk Mosiur Rahaman**



***Dedicated to my  
beloved  
Parents***





## Index

<b>Chapter</b>	<b>Content</b>	<b>Page. No</b>
<b>Chapter 1</b>	<b>Introduction</b>	<b>1-38</b>
1.1	Diabetes mellitus	2
1.2	Classification of Diabetes Mellitus	5
1.3	Curcumin	14
1.4	Resveratrol	21
1.5	Nanomicelles	27
1.6	Aim and Objectives	37
<b>Chapter 2</b>	<b>Review of Literature</b>	<b>39-56</b>
2.1	Awareness of Diabetes Mellitus	40
2.2	Assessment of Diabetes	40
2.3	Diabetes Management	42
2.4	The Effects of Curcumin in Diabetes Mellitus	43
2.5	Potential of Resveratrol	48
2.6	Effects of resveratrol on glucose control and insulin sensitivity	52
2.7	Nanomedicine for the treatment of diabetes-associated diseases	53
2.8	Nanomicelles	55
<b>Chapter 3</b>	<b>Synthesis of chitosan-curcumin conjugates</b>	<b>57-70</b>
3.1	Synthesis of Succinyl-Curcumin conjugates	58
3.2	Synthesis of chitosan succinyl curcumin conjugated prodrug	58
3.3	Structural identification of chitosan succinyl-curcumin conjugated prodrug	59
3.3.1	UV–Vis and fluorescence spectroscopy	59
3.3.2	FT-IR Spectroscopy	60
3.3.3	<sup>1</sup> H-NMR Spectroscopy	60
3.4	Results and discussions	60
3.5	Conclusions	70
<b>Chapter 4</b>	<b>Preparation and Characterization of Curcumin nanomicelles</b>	<b>71-86</b>
4.1	Introduction	72

4.2	Preparation of conjugated and free curcumin containing nanomicelle (CDSCM-CCMN)	72
4.3	Determination of Drug loading and entrapment efficacy	74
4.4	CCMN release study from CDSCM-CCMN	74
4.5	Stability of CDSCM-CCMN containing CCMN in physiological conditions	75
4.6	Determination of Critical micelle concentration of CDSCM-CCMN	75
4.7	Blood compatibility	76
4.8	Characterizations of CDSCM-CCMN	76
4.8.1	Measurement of zeta potential and hydrodynamic particle size of CDSCM-CCMN	76
4.8.2	Differential Scanning Calorimetry	77
4.8.3	Sample preparation for X-ray diffraction	77
4.8.4	Sample preparation for SEM, TEM and AFM	77
4.9	Results and discussions	78
4.10	Conclusions	86
<b>Chapter 5</b>	<b>Preparation and characterization of curcumin-resveratrol nanomicelles</b>	<b>87-100</b>
5.1	Introduction	88
5.2	Preparation of conjugated curcumin and free resveratrol containing nanomicelle (CDSCM-RSV)	88
5.3	Determination of Critical micelle concentration of CDSCM-RSV	90
5.4	Blood compatibility	90
5.5	Characterizations of CDSCM-RSV	91
5.5.1	Measurement of zeta potential and hydrodynamic particle size of CDSCM-CCMN	91
5.5.2	Differential Scanning Calorimetry	91
5.5.3	X-Ray diffraction	91
5.5.4	Sample preparation for SEM, TEM and AFM	92
5.6	Results and Discussions	92
5.7	Conclusions	99
<b>Chapter 6</b>	<b>HPLC method development for estimation of curcumin and resveratrol</b>	<b>101-118</b>

6.1	Introduction	102
6.2	Materials and methods	102
6.2.1	Chemicals and reagents	102
6.2.2	Instrumentation and chromatographic conditions	102
6.2.3	Preparation of calibration standards and sample solution	103
6.2.4	Method validation	104
6.2.5	In-vitro release study of CCMN and RSV from nanomicelle	106
6.2.6	Stability of CDSCM-RSV containing CCMN and RSV in physiological pH	106
6.3	Data analysis	106
6.4	Results and discussions	106
6.5	Conclusions	118
<b>Chapter 7</b>	<b><i>In-vivo</i> study of CDSCM-CCMN and CDSCM-RSV as antidiabetic nanoformulation</b>	<b>119-138</b>
7.1	Introduction	119
7.2	Experimental animals	119
7.3	Experiment design for <i>In-vivo</i> study	122
7.3.1	Induction of Type-II diabetes mellitus	123
7.3.2	Sampling of blood to estimate FBG level	123
7.3.3	Measurement of body weight	123
7.3.4	Analysis of biochemical parameters level	123
7.3.5	Carbohydrate metabolizing enzymes estimation	124
7.4	Histopathology of pancreas	124
7.5	Statistical analysis	124
7.6	Results and discussions	124
7.7	Conclusions	137
<b>Chapter 8</b>	<b>Summary and Conclusions</b>	<b>139-148</b>
	<b>References</b>	<b>149-168</b>

## List of Figures

<b>Figure No</b>	<b>Title</b>	<b>Page No</b>
<b>1.1</b>	Proinsulin, Insulin and Insulin binding	3
<b>1.2</b>	Number of people with diabetes worldwide and per IDF	4
<b>1.3</b>	Chemical structures of keto and enol form of curcumin and its source	14
<b>1.4</b>	Resveratrol and its isomers. (A) trans-3,5,4'-trihydroxystilbene, and (B) cis-3,5,4'-trihydroxystilbene.	21
<b>1.5</b>	Plant source of resveratrol	24
<b>1.6</b>	Overall research lay-out	38
<b>2.1</b>	Pathophysiology of diabetes mellitus.	44
<b>2.2</b>	Effects of curcumin	44
<b>2.3</b>	Mechanism of improving insulin resistance by RSV	50
<b>2.4</b>	Mechanism of enhancement of glucose uptake by RSV	52
<b>3.1</b>	Synthesis of Curcumin monosuccinate	58
<b>3.2</b>	Synthesis of chitosan succinyl curcumin	59
<b>3.3</b>	(a) UV–Vis and (b) fluorescence spectroscopy of CCMN and CHT-di(SUC-CCMN)	60
<b>3.4</b>	FT-IR Spectra of Curcumin, Curcumin-monosuccinate, Chitosan, and CHT di(SUC-CCMN)	62
<b>3.5</b>	<sup>1</sup> H-NMR of Curcumin	64
<b>3.6</b>	<sup>1</sup> H-NMR of Succinyl-Curcumin	65
<b>3.7</b>	<sup>1</sup> H-NMR of Chitosan	66
<b>3.8</b>	<sup>1</sup> H-NMR of Chitosan di-succinyl curcumin	67
<b>3.9</b>	<sup>1</sup> H NMR spectra of Curcumin, Curcumin-monosuccinate, Chitosan, and CHT-di(SUC-CCMN).	68
<b>4.1</b>	Schematic presentation of CDSCM-CCMN formation	73
<b>4.2</b>	Calibration curve of CCMN	78
<b>4.3</b>	CCMN release nature from CDSCM-CCMN	79
<b>4.4</b>	Stability of CDSCM-CCMN containing CCMN	79
<b>4.5</b>	Determination of Critical Micelle Concentration of CDSCM-CCMN	80
<b>4.6</b>	Hemolysis of CDSCM-CCMN	80
<b>4.7</b>	Zeta Potential of CDSCM-CCMN	81
<b>4.8</b>	Hydrodynamic particle size of CDSCM-CCMN	81
<b>4.9</b>	DSC thermogram of CDSCM-CCMN (NP), Physical mixture and CCMN	82
<b>4.10</b>	XRD of CDSCM-CCMN (NP), Physical mixture and CCMN	83

<b>4.11</b>	FE-SEM of CDSCM-CCMN	84
<b>4.12</b>	TEM of CDSCM-CCMN	84
<b>4.13</b>	2d AFM of CDSCM-CCMN	85
<b>4.14</b>	3d AFM of CDSCM-CCMN	85
<b>5.1</b>	Schematic presentation of CDSCM-RSV formation	89
<b>5.2</b>	Determination of Critical Micelle Concentration of CDSCM-RSV	93
<b>5.3</b>	Hemolysis of CDSCM-RSV	93
<b>5.4</b>	Zeta Potential of CDSCM-RSV	94
<b>5.5</b>	Hydrodynamic particle size of CDSCM-RSV	95
<b>5.6</b>	DSC thermogram of CDSCM-RSV (NP), Physical mixture, CCMN, and RSV	96
<b>5.7</b>	XRD of CDSCM-RSV (NP), Physical mixture, CCMN and RSV	97
<b>5.8</b>	FE-SEM of CDSCM-CCMN	97
<b>5.9</b>	TEM of CDSCM-RSV	98
<b>5.10</b>	2d AFM of CDSCM-RSV	99
<b>5.11</b>	3d AFM of CDSCM-RSV	99
<b>6.1</b>	Superimposition UV spectrum of CCMN and RSV	107
<b>6.2</b>	RP-HPLC chromatogram of resveratrol and curcumin standard	108
<b>6.3</b>	RP-HPLC chromatogram of resveratrol standard (tR-8.15 min)	108
<b>6.4</b>	RP-HPLC chromatogram of Curcumin standard (tR-11.41 min)	108
<b>6.5</b>	Calibration curve of CCMN	110
<b>6.6</b>	Calibration curve of RSV	110
<b>6.7</b>	A blank sample RP-HPLC chromatogram	114
<b>6.8</b>	RP-HPLC chromatogram of CCMN and RSV treated with 2N HCl	115
<b>6.9</b>	Nano-micelle sample RP-HPLC chromatogram	115
<b>6.10</b>	Cumulative percent release pattern of CCMN and RSV in pH 5.0 and pH 7.4	116
<b>6.11</b>	Stability study of CDSCM-RSV containing CCMN at pH 7.4	117
<b>6.12</b>	Stability study of CDSCM-RSV containing RSV at pH 7.4	118
<b>7.1</b>	Experimental protocol	121
<b>7.2</b>	Schematic testing protocol	121
<b>7.3</b>	Fasting blood glucose level assessment	126
<b>7.4</b>	Fasting blood glucose level after 21 days	127
<b>7.5</b>	Body weight variation	128
<b>7.6</b>	Comparison of liver weight after 21 days	128
<b>7.7</b>	Glycated hemoglobin (HbA1c) after 21 days of treatment	130
<b>7.8</b>	Level of (a) Serum creatinine, (b) Serum uric acid, (c) Serum cholesterol, (d) Serum triglycerides	131
<b>7.9</b>	Level of (a) SGPT, (b) SGOT, (c) HDL cholesterol, (d) LDL cholesterol, (e) ALP	132

<b>7.10</b>	Level of (a) Hexokinase, (b) G6PD, (c) HDL cholesterol, (d) LDH, (e) Inter group comparison of HbA1c, Serum creatinine, Serum uric acid, hexokinase	134
<b>7.11</b>	Inter group comparison of Serum cholesterol, Serum triglycerides, SGOT, HDL cholesterol, LDL cholesterol, ALP, G6PD and HDL	135
<b>7.12</b>	Histopathology of pancreas of (A) Normal Gr-I: NDc, (B) STZ Gr-II: Dc, (C) Free drug Gr-III: Dc-F-CCMN, (D) Nanoparticle Gr-IV:Dc-M-CCMN, (E) Nanoparticle Gr-V:Dc-M-RSV and (F) Standard drug Gr-VI: Dc-SD animals	136

## List of Tables

<b>Table No</b>	<b>Title</b>	<b>Page No</b>
<b>1.1</b>	Comparison between type I and type II diabetes mellitus	7
<b>1.2</b>	Classification of hypoglycemic drugs and their example	12
<b>1.3</b>	Treatment of Diabetes mellitus	13
<b>1.4</b>	Physicochemical properties of curcumin	16
<b>1.5</b>	Physicochemical properties of resveratrol	21
<b>1.6</b>	Resveratrol Content in Different Sources	24
<b>3.1</b>	FT-IR spectrum Analysis	63
<b>6.1</b>	System suitability of the developed method	109
<b>6.2</b>	Validation parameters for curcumin and resveratrol	110
<b>6.3</b>	Summary of intra-day and inter-day precision and accuracy of the method	111
<b>6.4</b>	Intra-day analysis results of CCMN and RSV	111
<b>6.5</b>	Inter-day analysis results of CCMN and RSV	112
<b>6.6</b>	Summary of robustness of method	113
<b>6.7</b>	Cumulative percent release results of CCMN and RSV in pH 5.0 and pH 7.4	116
<b>7.1</b>	Group division of animals for treatment	122
<b>7.2</b>	Fasting blood glucose level (mg/dL) at the treatment	126
<b>7.3</b>	Body weight and liver weight assessment	127
<b>7.4</b>	Study of biochemical parameters after 21 days	129

## List of Abbreviations

Abbreviated Form	Full Form
%	Percentage
°C	Degree Celsius
2d	Two dimension
3d	Three dimension
ACP	Acid phosphatase
ACN	Acetonitrile
AFM	Atomic force microscopy
ALP	Alkaline phosphatase
AMPK	AMP-activated kinase
ANOVA	Analysis of Variance
AUC	Area Under the Curve
BMI	Body mass index
BUN	Blood Urea Nitrogen
CCMN	Curcumin
CDSCM	Chitosan -di(succinyl curcumin) micelles
CDSCM-CCMN	Curcumin nanomicelle
CDSCM-CCMN	Resveratrol nanomicelle
CHT	Chitosan
CHT-di(SUC-CCMN)	Chitosan di-succinyl curcumin
CMC	Critical micelle concentration
CRP	C-Reactive Protein
DCC	N, N'-Dicyclohexylcarbodiimide
DKA	Diabetic ketoacidosis
DL	Drug Loading
DLE	Drug Loading Efficacy
DLS	Dynamic Light Scattering
DM	Diabetes Mellitus
DMAP	4-dimethylaminopyridine

DMSO	Dimethyl Sulfoxide
DPP-4i	Dipeptidyl peptidase 4 inhibitor
DPX	Dibutylphthalate Polystyrene Xylene
DSC	Differential Scanning Calorimeter
FBG	Fasting blood glucose
FESEM	Field Emission Scanning Electron Microscope
FTIR	Fourier Transform Infrared Spectroscopy
G6PD	Glucose-6-phosphate dehydrogenase
GLP-1 RA	Glucagon-like peptide 1 receptor agonist
gm	Gram
GRAS	Generally regarded as safe
GSH	Glutathione
h / hr	Hour
HbA1C	Glycated hemoglobin
HbA1c	Glycated Hemoglobin/Hemoglobin A1c
HDL	High Density Lipoprotein
HFD	High fat diet
HIP	Hyperglycemia in pregnancy
HK	Hexokinase
HNF	Hepatocyte nuclear factor
HOMA-IR	Homeostasis model assessment of insulin resistance
HOMA-IR	Homeostasis Model Assessment of Insulin Resistance
HOMA- $\beta$	Homeostasis model assessment-beta
Hp	Hemolysis percentage
HPLC	High Pressure/Performance Liquid Chromatography
i.e.	That is
ICAM-1	Intracellular Adhesion molecule 1
ICH	International Conference on Harmonization
IDDM	Insulin-dependent diabetes mellitus
IDF	International Diabetes Forum
IFG	Impair fasting glucose
IGT	Impair glucose tolerance
IL-1	Interlucin-1
IL-1 $\beta$	Interleukin-1beta



IL-6	interleukin-6
IPF	Insulin promoter factor
kg	Kilogram
LADA	Latent autoimmune diabetes in adults
LDH	Lactate Dehydrogenase
LDL	Low Density Lipoprotein
$\lambda_{\text{max}}$	Wavelength maxima
LOD	Limit of Detection
LOQ	Limit of Quantification
m.p.	Melting point
MCR	Metabolic Clearance Rate
MDA	Malondialdehyde
mg	Milli grams
ml	Milliliter
mM	Millimolar
MODY	Maturity onset diabetes
mV	Milli Volt
MW	Molecular weight
N	Normality
NeuroD1/BETA2	Neurogenic differentiation 1/beta cell E-box trans-activator 2
NIDDM	Noninsulin-dependent diabetes mellitus
NIH	National Institute of Health
nm	Nanometers
NMR	Nuclear Magnetic Resonance
NO <sub>2</sub>	Nitrogen dioxide radicals
NP	Nanoparticles
OGTT	Oral glucose tolerance test
PBS	Phosphate Buffer Solution
PDA	Photo Diode Array
PDK4	Pyruvate dehydrogenase kinase 4
pH	Logarithmic and inversely indicates the concentration of hydrogen ions in the solution
PPAR	Peroxisome proliferator-activated receptor

PPAR $\gamma$	Peroxisomal-proliferator-activated-reactive-gamma
ppm	Parts per million
R <sup>2</sup>	The proportion of the variance for a dependent variable
RBC	Red blood Cell
ROS	Reactive oxygen species
RP-HPLC	Reverse Phase High Pressure/Performance Liquid Chromatography
rpm	Revolutions Per Minute
RSD	Relative standard deviation
RSV	Resveratrol
SAR	Superoxide anion radical
SD	Standard Deviation
SEM	Scanning electron microscope
SGL T2i	Sodium and glucose transporter 2 inhibitor
SGOT	Serum Glutamic Oxaloacetic Transaminase
SGPT	Serum Glutamic Pyruvic Transaminase
SOD	Superoxide dismutase
STZ	Streptozotocine
SUC-CMN	Curcumin-monosuccinate
T1DM	Type I Diabetes Mellitus
T2DM	Type II Diabetes Mellitus
TEM	Transmission electron microscopes
TGF- $\beta$ 1	Transforming growth factor beta 1
TNF-A	Tumor necrosis factor-A
TNF-B	Tumor necrosis factor-A
TNF- $\alpha$	Tumor necrosis factor-alpha
TZD	Thiazolidinedione
UV	Ultra Violet
VCAM-1	Vascular cell adhesion protein 1
w/w	Weight/weight
XRD	X-Ray diffraction
$\mu$ l	Microliter

# Chapter 1

## Introduction

- 1.1 Diabetes mellitus
- 1.2 Classification of Diabetes Mellitus
- 1.3 Curcumin
- 1.4 Resveratrol
- 1.5 Nanomicelles
- 1.6 Aim and Objectives

## 1.1 DIABETES MELLITUS

The pancreas is one of the most important endocrine glands that regulate our blood glucose levels. Insulin is produced by the "Islets of Langerhans," which are made up of  $\alpha$ ,  $\beta$ , and  $\delta$  cells. A cascade of cleavage enzymes results in the production of insulin from its precursor, proinsulin (**Figure 1.1**). Insulin, sometimes referred to as the "anti-diabetic hormone," regulates how carbs are metabolized and indirectly affects how proteins and fats are metabolized. A crisis in the metabolism of carbohydrates brought on by insufficient insulin synthesis or an inability to carry out its functions resulted in Diabetes Mellitus (DM) [1, 2]. Diabetes Mellitus was formerly called as "madhumeha and Honey Urine," and several plants were used to treat it. It was originally used in modern medicine by Celsius and Aretaeus in 1921 A.D. Mellitus means honey, and diabetes denotes polyuria. A widespread disorder of the metabolism of carbohydrates, diabetes mellitus is primarily caused by insulin and is characterized by hyperglycemia, frequent urination, abnormalities of the eyesight, hepatomegaly, xanthelasma, and mucosal candidiasis in addition to other symptoms.

Approximately half a billion people worldwide currently suffer from diabetes, a major health issue with startlingly high rates. The International Diabetes Forum (IDF) Diabetes Atlas is a reliable source of information on diabetes prevalence, associated mortality, and health care costs connected with diabetes at the national, regional, and worldwide levels. Every two years, the subject matter experts from each of the seven IDF Regions comprise the IDF Diabetes Atlas Committee, which looks into the data sources and methods utilized to produce the estimates and projections in the Atlas. **Figure 1.2;** shows the composition of this committee. Based on information from the most current IDF 9th edition, diabetes mellitus is one of the worldwide health issues of the twenty-first century that is growing at the fastest pace. Globally, 463 million people are predicted to have diabetes in 2019, and by 2030, that number is projected to increase to 578 million, and by 2045, to 700 million. Two thirds of diabetics live in metropolitan areas, and three out of every four are of working age. 2019 will see an estimated four million people between the ages of 20 and 79 die from diabetes mellitus. An increasing number of children and teens (those under 19) receive a diabetes diagnosis each year. In 2019, the number of children and teenagers with type 1 diabetes mellitus (T1DM) exceeded one million. There are significant regional variations in the incidence of diabetes in this age group, with an estimated 136 million persons over 65 having the disease.

Furthermore, the IDF Diabetes Atlas edition shows that hyperglycemia in pregnancy (HIP) affects around one in six pregnancies. Another worrying statistic is the startlingly high prevalence of diabetes going undiagnosed (mainly type 2 diabetes), which is already above 50%. This highlights the pressing need to identify those with diabetes who are still undiagnosed and to start treating all diabetics as soon as feasible with adequate and prompt care. The chapter on diabetic complications includes explanations of co-morbidities and complications associated to diabetes, and it is based on current research.

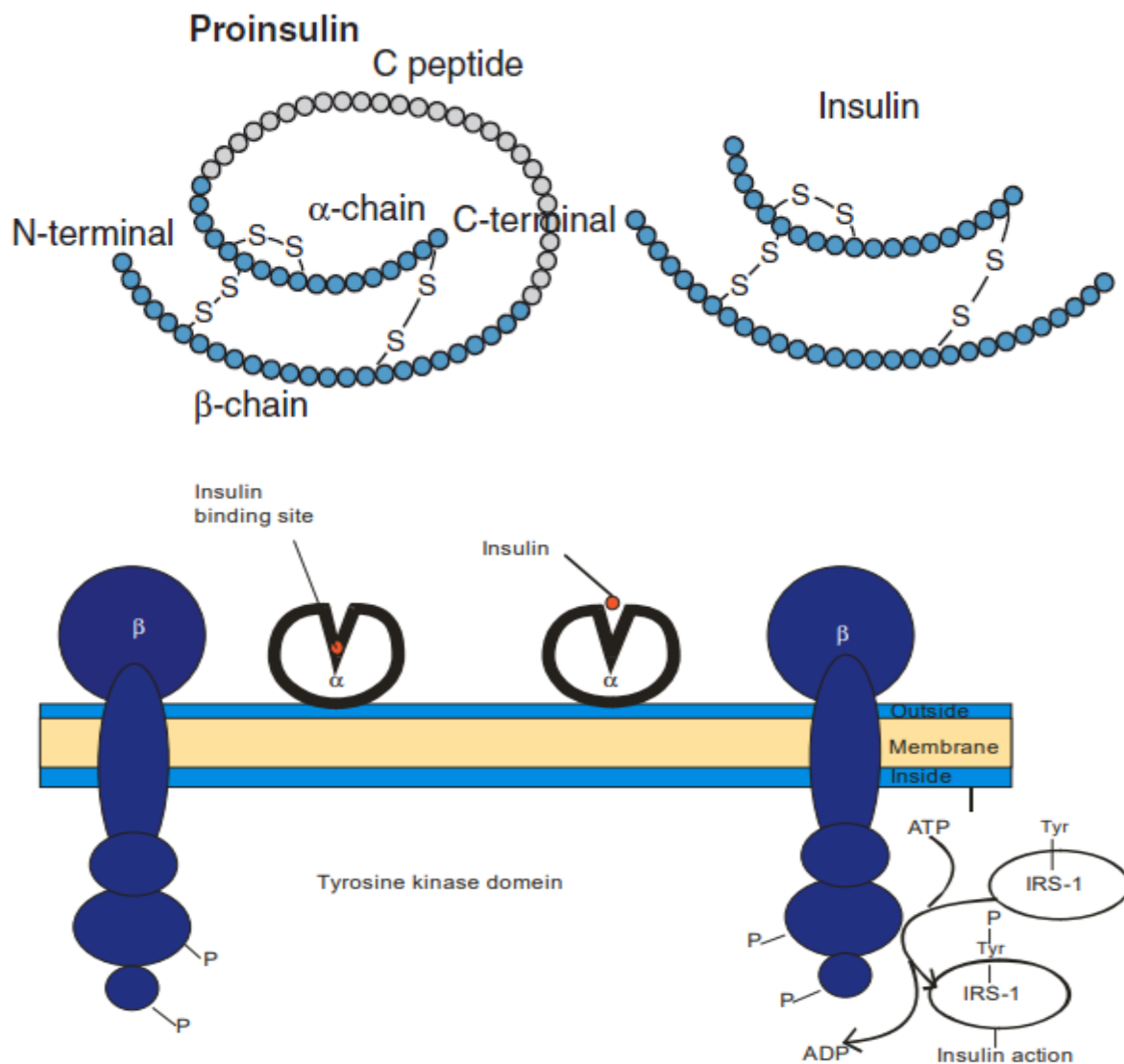


**Fig. 1.1:** Proinsulin, Insulin and Insulin binding

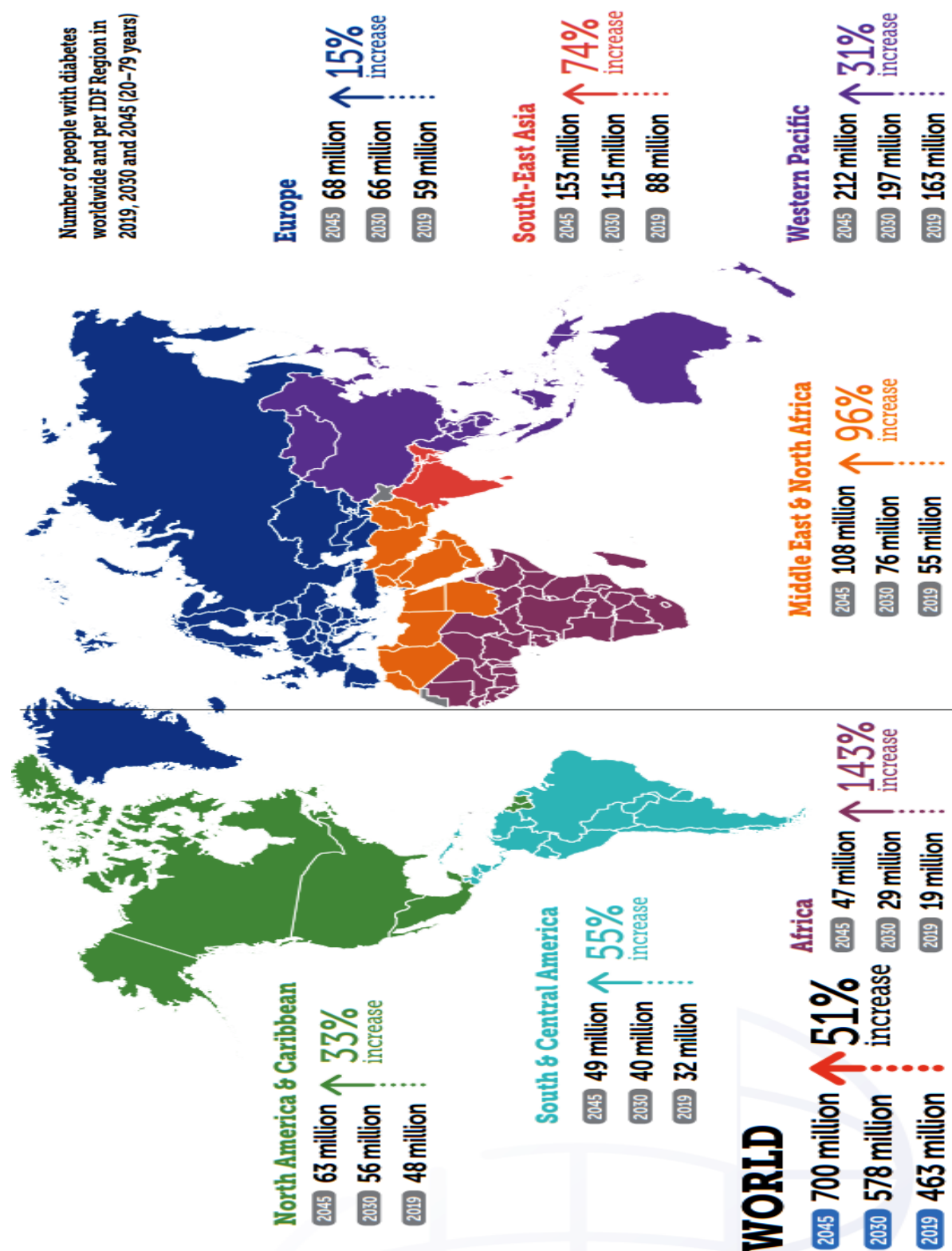


Fig. 1.2: Number of people with diabetes worldwide and per IDF

## 1.2 Classification of Diabetes Mellitus

Since ancient times, a distinct kind of diabetes has been recognized, but it was not properly classified. All types of diabetes mellitus have its unique signs; symptoms and etiology. The causes of different diabetes mellitus are also different. Initially it was observed as primary and secondary diabetes. The etiological outcomes of primary and secondary diabetes consider as not related to other disease and related to damage or disease of pancreas cause by other disease or factors respectively. Type-I Diabetes Mellitus (T1DM), also known as insulin-dependent diabetes mellitus (IDDM), and Type-II Diabetes Mellitus (T2DM), also known as noninsulin-dependent diabetes mellitus (NIDDM), are the two main classes of diabetes mellitus that have recently been separated.

### **Type I Diabetes Mellitus**

The pancreas which situated in the upper abdomen of human body is the vital organ that control blood glucose level. Insufficient insulin production led to development of T1DM. There are numerous reasons for insufficient insulin production; the main ones are damage, degeneration, or destruction of the  $\beta$ -cells found in the pancreatic islets of Langerhans. Viral infection, congenital disorders, and autoimmune diseases are the precursors to this condition, where antibodies develop against the  $\beta$ -cells' progression. Compared to Type II diabetes, the progression of Type I diabetes is more rapid. Although acidosis or ketosis may be linked to T1DM, obesity is not a component in the condition. Insulin-dependent diabetic mellitus, or T1DM, can strike anyone at any age, although it is more common in those who are 40 years of age or younger. Juvenile diabetes is another name for this form of diabetes mellitus that can develop in children if it does. Numerous other variations of type 1 diabetes mellitus occur, such as maturity-onset diabetes in young people (MODY) and latent autoimmune diabetes in adults (LADA). In case of LADA there have slow progression and slow onset in compare to IDDM and it occur after 35 years of age.

Sometime it is difficult to differentiate between type II diabetes mellitus and LADA. In case of LADA it take more time in compare to IDDM to diminish (or stop) the secretion of insulin. In case of MODY it happens in young individual of less than 25 years age group of people. It is a congenital disease where insulin secretion diminishes in a certain level that led to development of such kind of disease. On the basis of congenital defect in different gene, MODY can be

categories into MODY-1 (defect in HNF-4 $\alpha$  producing gene), MODY-2 (defect in Glucokinase producing gene), MODY-3 (defect in HNF-1 $\alpha$  producing gene), MODY-4 (defect in IPF1 producing gene), MODY-5 (defect in HNF-1 $\beta$  producing gene) and MODY-6 (defect in NeuroD1/BETA2 producing gene) [3]

### **Type II Diabetes Mellitus**

According to a WHO report, 90% of cases of diabetes worldwide are Type II diabetes mellitus, also known as non-insulin-dependent diabetic diabetes (NIDDM). Individuals with a variety of etiological conditions eventually become insulin resistant, which triggers the onset of type 2 diabetes. The pancreatic  $\beta$ -cells in the islets of Langerhans are capable of producing enough insulin in type 2 diabetes (T2DM); however, the unfavorable heterogeneous etiological conditions cumulatively inhibit the islets of Langerhans from secreting insulin and also hinder the released insulin from binding to the desired cell receptor.

The inability to bind insulin with its desire receptor of cell that leads to prevention of entry of glucose into cell, but the digestive system gradually increases the extent of glucose in systemic circulation and it is not being utilized by the cell as result glucose level increase many fold in systemic circulation. Sometimes in T2DM the minor defect in insulin gene that produces defective insulin which has less capacity in transport of glucose into cell. Except above reason there are many factors which leads to develop T2DM are life style associated with less exercise, bad eating habit which leads to obesity and stressful life. In most of the T2DM obesity is common but ketoacidosis may not be common.

Pre-Diabetes, also known as borderline diabetes or sub-clinical diabetes is a type of Type II diabetes mellitus in which the patient exhibits elevated glucose levels but does not exhibit the true etiology of the disease. This condition has been observed to develop frequently between non-diabetic and diabetic etiological conditions. This patient has an increased likelihood of getting type 2 diabetes.

Another form of T2DM is **Gestational diabetes**. It occurs in pregnant mother who doesn't have diabetes before pregnancy and it is happen due to change of different hormonal level and or change of life style but after delivery of child the symptoms disappear. In this case the chance of recurrence diabetes mellitus for this woman is higher.

### **Risk factors of T II DM**

---



- Diabetes in the family (parent or sibling with type 2 diabetes, for example)
- Being obese (BMI  $\geq 25$  kg/m<sup>2</sup>)
- Regularly not exercising
- Racial or ethnic background (such as Asian American, African American, Latino, or Pacific Islander)
- Previously recognized impaired glucose tolerance (IGT) or impaired fasting glucose (IFG)
- GDM history or baby delivery of more than 4 kg (9 lb)
- Hypertension ( $>140/90$  mmHg in blood pressure)
- A triglyceride level  $>250$  mg/dL (2.82 mmol/L) and/or an HDL cholesterol level  $<35$  mg/dL (0.90 mmol/L)
- Candhosis nigricans, also known as polycystic ovarian syndrome
- Past vascular illness history

**Table 1.1: Type I and type II diabetes mellitus comparison**

Key features	T1DM	T2DM
Prime cause	Insufficient insulin production	Prevention of insulin-receptor interaction, Retard secretion of insulin from Islets of Langerhans
Congenital cause	Yes	May or may not be
Deficiency of insulin	Yes	Partial right
Family history of diabetes	Uncommon	Common
Autommune destruction of $\beta$ -cells	Yes	No
Autoantibodies	Positive in 80–90%	Negative
Insulin resistance	No	Yes
Except pancreas other endocrine disorders	No	Yes
Occurrence in age group	Usually $\leq 40$ years of age	Usually $\geq 40$ years of age
Treatment by insulin	Always	In preliminary stage not require but may require in later stage

Key features	T1DM	T2DM
Can be control by oral hypoglycemic agents	No	Yes
Appearing of symptoms	Rapidly	Slowly
Effect on body weight	Usually lesser than standard body weight	Usually higher than standard body weight (Obese)
Stress-induced obesity	No	Yes
Keto-acidosis	Yes	May or may not be
Ketonuria	Yes	No
Rapid death in non-insulin treatment	Yes	No

### Secondary Diabetes Mellitus

Except T1DM and T2DM there is another form of diabetes mellitus which is very rare about 2% diabetes patient shows such type of diabetes mellitus known as secondary diabetes mellitus. This rare diabetes may or may not be permanent have different cause which lead to development of this type of diabetes like:-

1. “Pancreas malfunctioning” may happen in different disease condition of pancreas like chronic pancreatitis, hemochromatosis or emochromatosis (due to high iron intake by body leads to organ damage), fibrocalculous pancreatopathy, cystic fibrosis, neoplasia and carboxyl ester lipase gene mutation.
2. “Different diseases condition” those are develop by different endocrine gland dysfunction like Cushing’s syndrome, gigantism, glucagonoma, acromegaly, pheochromocytoma, hyperthyroidism, somatostatinoma and aldosteronoma. In above disease condition, continues over secretion of  $\beta$ -cells causes’ degradation and burning of  $\beta$ -cells that lead to permanent damage of  $\beta$ -cells which lead to development of permanent DM.
3. Liver disorder like fatty liver and Hepatitis-C
4. Celiac disease (autoimmune disease)
5. Surgical removal of pancreas

6. Drug related like excessive intake of diuretics (thiazides diuretics), beta blockers (antihypertensive),  $\beta$ -adrenergic agonists, oral contraceptive, steroids (glucocorticoids), chemotherapeutic drugs, thyroid hormone, protease inhibitors, and other drugs like phenytoin, clozapine, diazoxide, pentamidine,  $\alpha$ -interferon, Vacor.
7. Infections—Cytomegalovirus, congenital rubella, coxsackie
8. Over consumption of alcohol and opium
9. Diabetes caused by the immune system, such as "stiff-person" syndrome and anti-insulin receptor antibodies

### **Signs and Symptoms of Diabetes Mellitus**

**A. Hyperglycemia:** It is defined as the increase of fasting and random blood glucose level or plasma glucose level to a certain extent that exceed the normal standard limit.

As per WHO when random blood glucose level in a patient more than 11.1 mmol/L or 200mg/dL and fasting blood glucose (FBG) more than 7.0 mmol/L or 126mg/dL and 2 hours after carbohydrate intake the blood glucose level more than 11.1 mmol/L or 200mg/dL are consider as diabetic patient.

### **Symptoms of hyperglycemia**

- i. Glucosuria- glucose eliminated through urine
- ii. Thirst, polydipsia
- iii. Dry mouth
- iv. Polyuria
- v. Polyphagia
- vi. Nausea
- vii. Nocturia
- viii. Headache
- ix. Blurring of vision
- x. Exhaustion, weariness, sluggishness
- xi. Weight change (weight loss)
- xii. Balanitis (genital candidiasis), pruritus vulvae
- xiii. Hyperphagia, or an infatuation with sweets
- xiv. A shift in mood, trouble focusing, and indifference

**B. Ketoacidosis**

Diabetic ketoacidosis (DKA) typically occurs in Type 1 Diabetes (T1DM), whereas hyperglycemic hyperosmolar state (HHS) typically occurs in Type 2 Diabetes (T2DM). DKA was also discovered in patients with Type II DM who were using oral hypoglycemic medications and in people without the immunologic characteristics of Type I DM. DKA characterized by increased level of blood glucose, ketone bodies, metabolic acids, and destabilized the normal level of blood glucose regulatory hormones like insulin (decrease), glucagon (increase), catecholamines (increase), cortisol (increase), and growth hormone (increase). DKA precipitate when diabetic patient get infected with contagious disease, traumatic injury, and insufficient and or discontinuation of insulin treatment.

**Symptoms of diabetic ketoacidosis**

- i. Polyuria: excessive production of pee and increased frequency of urination
- ii. Thirst→increase frequency of water intaking
- iii. Weight loss→ decreasing of standard weight
- iv. Blurred vision
- v. Leg cramps
- vi. Weakness, asthenia
- vii. Abdominal pain
- viii. Nausea, vomiting

**Signs of diabetic ketoacidosis**

- i. Dehydration
- ii. Postural Hypotension
- iii. Tachycardia
- iv. Kussmaul breathing
- v. Cold extremities
- vi. Hypothermia
- vii. Peripheral cyanosis
- viii. Air hunger
- ix. Smell of acetone
- x. Delirium, drowsiness, coma

**Complications of diabetes**

## 1. Neuropathic or microvascular

i. Cataract and Retinopathy: Reduced eyesight ii. Renal failure due to nephropathy iii. Peripheral neuropathy: Motor weakness, pain, and sensory loss IV. Foot disease: Ulceration, Arthropathy, Postural hypotension, Gastrointestinal issues, Autonomic neuropathy

## 2. Macrovascular

i. Myocardial ischaemia/infarction in the coronary circulation ii. Transient ischemic attack and stroke in the cerebral circulation iii. Claudication and ischemia in the peripheral circulation

**Diagnostic Tests for Diabetes Mellitus**

For the diagnosis of DM following tests are available:

1. Fasting blood glucose
2. Insulin assay
3. Glycated hemoglobin (HbA1C)
4. Fructosamine assay
5. Proinsulin assay
6. Postprandial blood glucose
7. Glycated albumin
8. Oral glucose tolerance test (OGTT)
9. C-Peptide assay

**Table 1.2: Classification of hypoglycemic drugs and their example**

<b>Insulin</b>	Rapid acting	Insulin Lispro, Insulin aspart, Insulin glulisine		
	Short acting	Regular Insulin (soluble form)		
	Intermediate acting	Insulin zinc suspension, Neutral protamine hagedorn		
	Long acting	Insulin glargin, Insulin detemir		
<b>Oral anti-diabetic Drugs</b>	Insulin secretion enhancement	K-ATPase Channel blocker	Sulfonylureas (SU)	Tolbutamide, Glibenclamide, Gliclazide, Glipizide, limepiride
			Meglitinide / Phenylalanine analogues	Repaglidine, Nateglinide
		Dipeptidyl peptidase-4 inhibitors (DPP-4i)	Sitagliptin, Saxagliptin, Vildagliptin, Alogliptin, Linagliptin	
	Prevention of insulin resistance	Biguanide	Metformin	
		Thiazolidinedione (TZD)	Pioglitazone, rosiglitazone	
	Miscellaneous Drugs	Alpha-Glucosidase inhibitors	Acarbose, Miglitol, Voglibose	
		Amylin analogue	Pramlintide	
		Dopamin D2 Receptor agonist	Bromocriptine	
		Sodium-glucose cotransport-2 inhibitor (SGL-2i)	Dapagliflozin	

**Table 1.3: Treatment of Diabetes mellitus**

<b>Therapy</b>	<b>Drugs</b>	<b>Efficacy</b>	<b>Hypoglycemic Shock</b>	<b>Weight</b>	<b>Side-effect</b>	<b>Cost</b>
Mono Drug Therapy	Metformin	High	Low risk	Not/loss	GI, Lactic acidosis	Low
Dual Drug Therapy	Metformin + Insulin	High	High risk	Gain	Hypoglycemia	Moderate
	Metformin + TZD	High	Low risk	Gain	Oedema, heart failure	low
	Metformin + SGL T2i	Moderate	Low risk	Loss	Genitourinary, dehydration	High
	Metformin + SU	High	Moderate risk	Gain	Hypoglycemia	low
	Metformin+ DPP-4i	Moderate	Low risk	Not Change	Less occurrences	High
	Metformin+ GLP-1 RA	High	Low risk	Loss	GI	High
Triple Drug Therapy	Metformin + Insulin+ TZD/DPP-4i/GLP-1-RA/SGL T2i	High	High risk	Loss	Hypoglycemia, Oedema, heart failure	High
	Metformin + TZD + SU/DPP-4i/SGL T2i/GPL-1-RA/Insulin	High	Moderate risk	Gain	Hypoglycemia, Oedema, heart failure	High
	Metformin + SGL T2i + SU/DPP-4i/SGL T2i/Insulin	High	Moderate risk	Loss	Hypoglycemia, Genitourinary, dehydration,	High
	Metformin + SU + TZD/DPP-4i/SGL T2i/GPL-1-RA/Insulin	High	High risk	Gain	Hypoglycemia, Oedema, heart failure	High
	Metformin+ DPP-4i+ SU/TZD/SGLT2i / Insulin	High	Moderate risk	Loss	Hypoglycemia, Genitourinary,	High
	Metformin+ PLP-1 RA + SU/TZD/Insulin	High	Moderate risk	Loss	Hypoglycemia, Oedema	High
Multidrug with Injectable Therapy	Metformin + Basal Insulin + Mealtime insulin/GLP-1-RA	High	High risk	Loss	Hypoglycemia, Genitourinary,	High

## 1.3 CURCUMIN

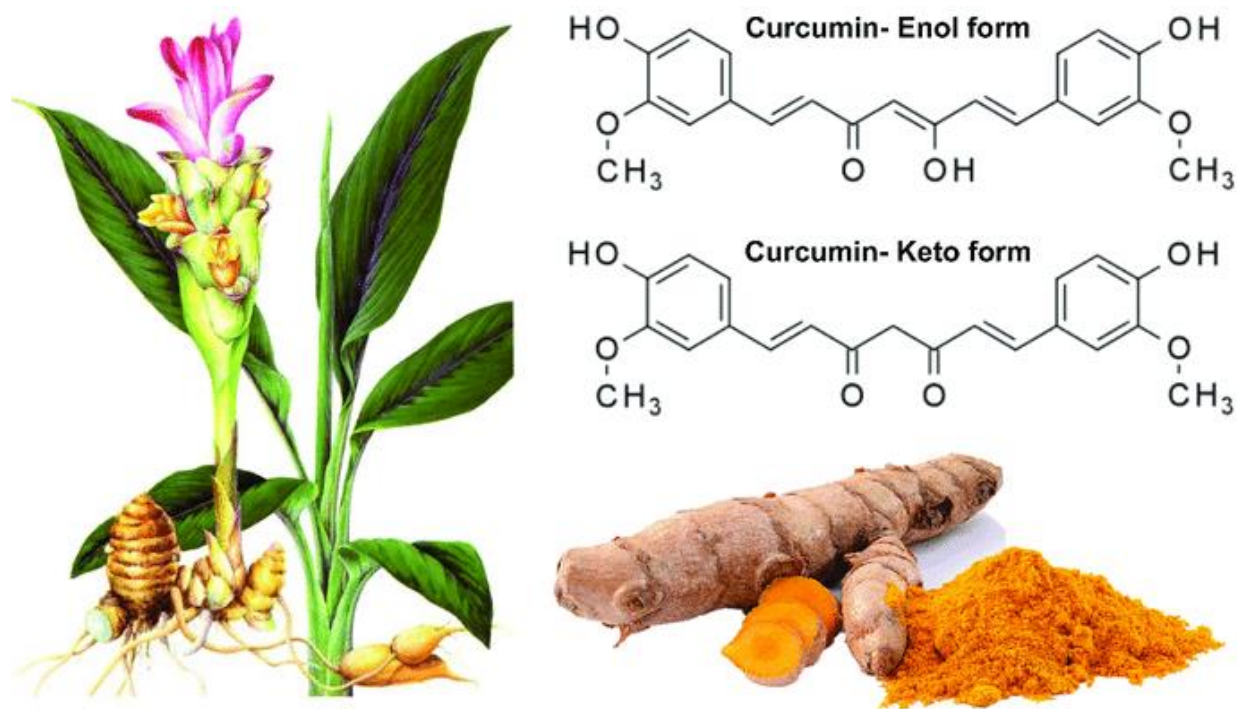


**Fig. 1.3:** Chemical structures of keto and enol form of curcumin and its source

### History

Turmeric contains more than 300 active ingredients, including phenolic and terpenoid compounds. One of these ingredients is curcumin (CCMN) which was first described about 200 years ago as a yellow coloring matter found in the rhizome of the turmeric plant, *Curcuma longa*. Vogel Jr. (1842) prepared a pure CCMN in 1842. Several chemists reported on its possible structure in the following decades. One of them reported on the chemical structure of the CCMN in the form of 1,6-heptadiene-3,5-dione-1,7-bis (4-hydroxy-3-methoxyphenyl)-(1E, 6E). Lamppe (1910) described the synthesis of this substance. In the following decades, several chemists reported on curcumin's chemical structure. One of them was Milobedzinski (1913). Srinivasan first used chromatography (1953).



One such material is CCMN, which was originally discovered to be the yellow coloring material from *Curcuma longa* rhizomes over 200 years ago. Turmeric has around 300 distinct components, including phenolics and terpenoids, in addition to CCMN, which is one of the most significant active ingredients. Vogel Jr. developed pure CCMN in 1842. Many scientists described the potential structure of CCMN in the decades that followed 1870. Milobedzka et al. (1910) identified structure of CCMN as diferuloylmethane. It was reported by Lampe and Milobedzka (1913) that CCMN was synthesized. However, the components of CCMN were separated and quantified using chromatography for the first time by Srinivasan (1953).

Since it has been utilized for over 6000 years, Jing Huang is also well-known for its active components and medicinal benefits. But a comprehensive investigation into their pharmacological effects was not carried out by scientists until the middle of the 20th century. Schraufstatter and Bernt (1949) found that CCMN exhibited a variety of antibacterial activities against *Salmonella*, *Streptococcus*, *Mucor*, *Mycobacterium*, and other microbes. Its lipid-lowering, anti-inflammatory, antioxidant, and antidiabetic properties were also discovered in the 1970s study. It was discovered to have anticancer properties in the 1980s. There have been numerous findings regarding the pharmacological and therapeutic effects of curcumin over the past thirty years.

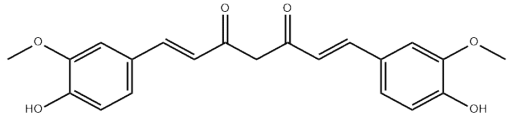
Over 35 clinical trials are currently underway, while over 65 clinical experiments involving humans have already been completed. Furthermore, research on CCMN compounds has gained popularity recently.

### **General information**

Phyto-constituents are generating a gigantic response in therapeutic applications because of less toxicity and very poor side effects concerning their synthetic embodiment. Curcumin, a polyphenolic phytochemical, obtained from plant like *Curcuma longa*, *Curcuma zedoaria*, *Curcuma xanthorrhiza*, *Curcuma caesia*, *Acorus calamus* and *Curcuma amada* (in rhizome) exhibits different kind of therapeutic activities and has evidence to be pharmacologically safe [4-5], it is also FDA's generally regarded as safe (GRAS) listed compound [6]. Beside CCMN (77%) there are two other CCMN derivative exist like demethoxycurcumin and bis-demethoxycurcumin. Though it has wide potential application and therapeutic activity, but its use being limited

primarily because of very less aqueous solubility, chemical instability, photo-sensitivity, first metabolism, insufficient tissue distribution and inadequate absorption, consummately leading to unsatisfied bioavailability [7-8].

**Table 1.4: Physicochemical properties of curcumin**

Chemical Name	Curcumin
Chemical Structure	
Molecular Formula	C <sub>21</sub> H <sub>20</sub> O <sub>6</sub>
Molecular Weight	368.383 Daltons
IUPAC Name	(1E,6E)-1,7-bis(4-hydroxy-3-methoxyphenyl) hepta-1,6-diene-3,5-dione
Synonyms	Halad, haldar, crucumin, kurkumin, Diferuloylmethane
Plant Source	<i>Curcuma longa</i> , <i>Curcuma zedoaria</i> , <i>Curcuma xanthorrhiza</i> , <i>Curcuma caesia</i> , <i>Acorus calamus</i>
Form	powder
Melting point	183 °C
Boiling point	418.73°C
Density	0.93
Refractive index	1.4155-1.4175
Color	Orange
Odor	Characteristics
Taste	Slight bitter
PH Range	7.8-9.2
pKa	8.09(at 25°C)
$\lambda_{\max}$	430nm
Solubility	Ethanol: 10 mg/mL. Also soluble in acetic acid, propylene glycol and alkali solution
Water Solubility	Slightly soluble
vapor density	13 (vs air)
Flash point	208.9±23.6°C

Storage temp.	2-8°C
Stability	Stable, photo-sensitive, heat sensitive, hygroscopic, destabilized when contacted with iron ion. Curcumin color turns from yellow to red at more than pH 8.
Major Application	In cosmetics formulations, skin diseases, wound healing, anti-inflammatory, skin-wrinkles remover, drug-eluting stents, obesity, treating alzheimer's disease, diabetes, antioxidant, cancer, leukemia, antimicrobial, antiviral, neurofibromas and in prostate cancer. [9-10]

### Reactivity Profile

CCMN reacts to light and pH fluctuations. It may also react with oxidizing substances.

### Biological Activity

It is having Antioxidant, Antitumour, Anti-inflammatory activity, Neuro- and Cardioprotective, Antimicrobial, and Anti-Diabetic properties. It can upregulate the expression of p53, Nrf2, EGFR, TNF- $\alpha$ , IL-1, IL-6, NF- $\kappa$  B and PPAR  $\gamma$ ; downregulate the expression of ROS Generating Enzymes (CYP, Lipoxygenase and iNOS).

### Biochemical Actions

CCMN, a phenolic molecule that occurs naturally, has strong anti-inflammatory, anti-oxidant, and anti-cancer properties. It has been mentioned as a potential chemical preservative in addition to being a chemical preservative. Curbol induces apoptosis in tumor cells. Protein C (Protein C-Esporbol) ester-inducible protein kinase activity is inhibited. Peripheral Blood Monocytes (PBCs) and Alveolar Macrophages (macrophages) are reported to produce inflammatory cytokines. Inhibits iNOS (Inducible Nitric Oxidase), Cyclooxygenase (COX) and Lipoxygenase (LOX). It readily passes through cell membranes and gathers in membrane structures such the nuclear envelope, endoplasmic reticulum, and plasma membrane.

### Mechanism of action

Turmeric's primary ingredient, curcuma longa, is thought to possess antioxidant and anti-inflammatory qualities. It specifically scavenges reactive oxygen species (ROS), such as hydroxyl radicals (H<sub>2</sub>O<sub>2</sub>), nitrogen dioxide radicals (NO<sub>2</sub>), and superoxide anion radicals

(SAR). It also has anti-inflammatory qualities by inhibiting the production of proinflammatory cytokines such as IL-1, TNF-A, and TNF-B and blocking the activation of certain transcription factors such as NF- $\kappa$ B and AP-1. Additionally, CCMN possesses anti-protective qualities. For instance, it inhibits the expression of UVB-induced matryluminesis-1/3 (MAPK-p38 / JNK pathway) and lowers the risk of skin cancer in SKH-1 hairless mice.

### **Pharmacology**

1. It has been demonstrated that CCMN is useful in the treatment of liver, lung, and other organ fibrosis. It has been demonstrated to inhibit the expression of extracellular matrices and lessen the release of inflammatory factors. Additionally, it has been demonstrated to prevent cells from growing by blocking transforming growth factors. It has also been demonstrated to activate caspase, which causes tumor cells to undergo apoptosis.
2. The anticancer activities of CCMN have received extensive research and attention globally, making them the best studied pharmacological effects of the herb. Additionally, it regulates cyclooxygenases, which are crucial to the cell cycle. Furthermore, CCMN has been demonstrated to trigger tumor cell death and prevent tumor cell migration by activating caspase.
3. CCMN effectively reduces inflammation in a variety of ways. Its mode of action might involve lowering the expression of leucotriene and prostaglandins, which would stop the release of several inflammatory agents. Similar to NSAIDs and glucocorticoids, CCMN has anti-inflammatory properties, but it is safer and has fewer adverse effects.
4. CCMN possesses potent antiviral and antibacterial properties. Curcumin has the ability to stop the growth and reproduction of parasites as well as bacteria, viruses, and fungi. According to scientific theories, curcumin may cause microbial cell membranes to rupture and genetic alterations in bacteria.
5. Curcumin's hypolipidemic action Many scientists believe CCMN could be developed into a medication to treat hypolipidemia. It has been demonstrated that CCMN lowers triglyceride, apolipoprotein A, and total blood cholesterol levels. In order to lower the amount of LDL in the body, it also speeds up the metabolism of low-density lipoproteins (LDL) and increases their excretion.

6. Purified CCMN was given orally to rats as a single dosage. In the gastrointestinal system, 60–65% of the curcumin was broken down. Within five days, 40% of the CCMN was eliminated by the stools. After three days, the plasma concentration reached its peak. CCMN underwent transformation during the liver-to-enlargement circulation phase.

### **Anti-diabetic effects of Curcumin**

One of the most popular natural products is curcumin, and it has a positive impact on glucose metabolism. *Curcuma longa* L., the main ingredient in this product, has been shown to have therapeutic potential for a range of diseases, including diabetes [11]. Previous research has suggested that CCMN may have biological properties that may be beneficial against a variety of pathological conditions [12]. CCMN has also been extensively studied for its ability to reduce glucose levels [11]. Two meta-analyses support curcumin's antidiabetic effects and provide evidence that the compound has only moderate side effects [13]. Some studies have identified a broad spectrum of molecular targets for curcumin, including numerous intracellular elements, routes, and key enzymes involved in glucose metabolism [14]. According to a few studies, curcumin lowers glucose concentrations by raising insulin levels, decreasing the activity of G6Pase (glucose 6-phosphatase), PEPCK (phosphoenol protein kinase), and activating AMP-activated protein kinase (AMP) [15].

Additionally, curcumin has demonstrated antioxidant and anti-inflammatory properties that appear to lower the following metabolic markers: Triglycerides, Total cholesterol, Uric acid, Total body fat, Inflammation (by decreasing the level of biomarkers TNF- $\alpha$ , IL6, ICAM-1, VCAM-1 and TGF- $\beta$ 1), apoptosis (by decreasing the level of biomarkers) and increase the Antioxidant biomarkers SOD and GSH [16]. Furthermore, curcumin has been demonstrated to have advantageous effects on the metabolism of glucose, resulting in a decrease in gluconeogenesis and an increase in glycolysis and glycogen synthesis [17]. However, more recent research has demonstrated that it has hypoglycemic impact through controlling the metabolism of incretins as well as the activity of several other metabolic enzymes, including glucose transporters, amylase, and  $\alpha$ -glucosidase. Additionally, it has been demonstrated to have anti-diabetic properties via controlling the synthesis of PPARG (peroxisomal proliferator-activated receptor-gamma).

Curcumin is a top contender for this objective because numerous studies have demonstrated its therapeutic effects in managing diabetes and its consequences by reducing insulin resistance, hyperglycemia, islet cell death, and necrosis [18]. Curcumin exerts its anti-diabetic action through a wide range of molecular targets, and has an enhanced safety profile [19]. Mechanism of action is highlighted in this review. For example, it has the capacity to inhibit enzymes such as alfa glucosidase (GLUT), alpha amylase (PDP-4), and diphosphonate phospholpyramid (DPP-4). Stimulate effects on insulin secretagogue (GLP-1) Some studies have shown that it can regulate GLUTs (glucose transporters) (GLUT2) Some reports have shown that it is possible to upregulated GLUT2 in response to glucosamine (GLUT1) It is also possible to inhibit GLUT1 in intestinal cells (GLUT4) GLUT4 upregulation in muscle cell can reduce glucose concentration. In addition, another important factor in curcumin's antidiabetic effects may be its anti-inflammatory and antioxidant properties. Additionally, some research has indicated that it possesses antioxidant and anti-inflammatory qualities. In conclusion, there is strong evidence supporting curcumin's potential as an antidiabetic in a number of diabetes pathogenesis-related domains. In addition to its well-known antioxidant and anti-inflammatory properties, this review has identified new mechanisms of action for curcumin antidiabetes therapy. However, some studies have shown contradictory results. Therefore, further research is needed to address these issues before clinical trials are conducted.

## 1.4 RESVERATROL

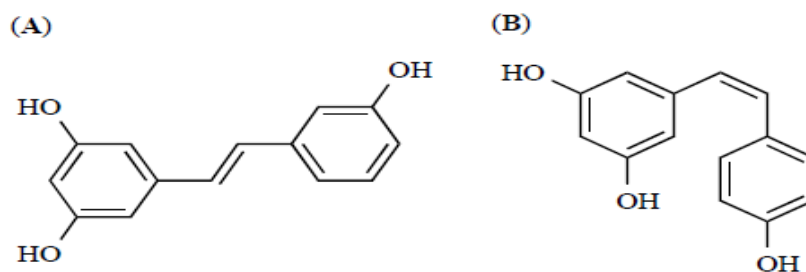


**Fig. 1.4:** Resveratrol and its isomers. (A) *trans*-3,5,4'-trihydroxystilbene, and (B) *cis*-3,5,4'-trihydroxystilbene.

### General information

Chemically known as 3,5,4'-trihydroxy-trans-stilbene, phytoalexin is a polyphenolic phytoconstituent resveratrol that has anticancer, anti-inflammatory, antioxidant, and type-2 anti-diabetic properties. It can be found in many different plant parts, including giant knotweed, giant grape skin, and in different berries. It prolongs the life of the SIRT1 gene and slows the progression of neurodegenerative disease [20]. Different publications are available which support its therapeutic potential against different ailments like Alzheimer disease, cancer, heart disease and diabetes [21, 22].

**Table 1.5: Physicochemical properties of resveratrol**

Chemical Name	Resveratrol
Chemical Structure	
Molecular Formula	C <sub>14</sub> H <sub>12</sub> O <sub>3</sub>
Molecular Weight	228.24 Daltons
IUPAC Name	5-[(E)-2-(4-hydroxyphenyl)ethenyl]benzene-1,3-diol
Synonyms	3,4',5- Trihydroxystilbene
Alternative Names	trans-resveratrol; 3,4',5-Trihydroxystilbene, 3,5,4'-Trihydroxystilbene; (E)-5-(p-Hydroxystyryl)resorcinol; (E)-5-(4-hydroxystyryl)benzene-1,3-diol
Plant Source	Grapes, rasoberries, blackberries, cranberries, blueberries,

	mulberries, peanut, coca
<b>Appearance</b>	off-white powder
<b>Melting point</b>	254 °C
<b>Boiling point</b>	449.1±14.0 °C
<b>Density</b>	1.359±0.06 g/cm <sup>3</sup>
<b>Refractive index</b>	1.762
<b>Color</b>	slight yellowish to off-white
<b>Odor</b>	characteristics
<b>PH Range</b>	6 to 9
<b>pKa</b>	9.22±0.10(Predicted)
<b>λ<sub>max</sub></b>	in water 304nm (trans-resveratrol) and 286nm (cis-resveratrol)
<b>solubility</b>	16 g/L in DMSO, 50 g/L in ethanol
<b>Water Solubility</b>	0.03 g/L in water
<b>Storage temp.</b>	Storage-20 °C
<b>Stability</b>	0.03 mg/mL in water, 16 g/L in DMSO, 50 g/L ethanol, to 374 mg/mL in polyethylene glycol 400 (PEG-400)
<b>Description</b>	Red grape, blueberry, and peanut skins are just a few examples of plant items that naturally contain resveratrol, a phenol and polyphenol. It is thought to provide several possible health advantages and is well-known for its antioxidant qualities. Reducing inflammation, preventing or treating specific cancers, enhancing heart health, and promoting brain health are a few possible advantages.
<b>Features And Benefits</b>	<ol style="list-style-type: none"> <li>1. Properties of antioxidants</li> <li>2. Reduction of inflammation</li> <li>3. UV defense</li> <li>4. Benefits against aging</li> <li>5. Brightening effects on the skin</li> <li>6. Promotes faster healing of wounds</li> <li>7. Promotes moisture and better skin texture</li> </ol>



## **History of Resveratrol**

An epidemiological study has proved the "French paradox," which is the phenomenon that red wine consumption is linked to a lower incidence of cardiovascular disease [23]. As a matter of fact, certain French communities seem to be less susceptible to heart disease even if they lead sedentary lifestyles and consume high-fat diets [23]. For example, compared to the rest of Europe, heart attack rates are almost 40% lower in France [24]. The discovery that moderate red wine drinking is good to health gave rise to the theory that phenolic chemicals may be the source of red wine's health benefits. Red wine's phenolic compounds, such as resveratrol, were thought to be responsible for these benefits [25]. The latest studies indicate that resveratrol is mostly responsible for the cardiovascular protection that wines and grapes offer [26].

Resveratrol gained notoriety for its part in the "French Paradox" around the beginning of the 1990s. At first, it was suggested that resveratrol, which is associated with red wine, could aid in the prevention of heart disease. Jang et al., 1997] demonstrated the compound's ability to inhibit the different phases of cancerogenesis. The phytochemical characteristics of resveratrol have piqued the interest of scientists in recent years, and research has demonstrated a broad spectrum of pharmacologic and biological actions at the cellular level. Antioxidant [28], anti-inflammatory [29], anticarcinogen [27, 30], cell cycle inhibitor [31], anti-aging [32], neuroprotective [33], and cardioprotective [34] are some of the classifications assigned to it. It has also been discovered to be particularly effective in treating diabetes and obesity more recently [35].

## **SOURCES OF RESVERATROL**

White hellebore is a plant in the genus *Veratrum*. It was from this plant that resveratrol was initially isolated in the 1940s. The dried root of Japanese knotweed, or *Ko-jockon* as it is called in Japan, was shown to contain resveratrol in 1963. Since ancient times, itadori tea—made from the Japanese knotweed plant—has been a staple of Japanese cuisine. Traditional Chinese and Japanese medicine has used it to treat a variety of conditions, including vasculature (inflammation of the blood vessels), dermatitis, fungus, athlete's foot, allergies, gonorrhea and heart disease. Since then, it has also been discovered in roughly 70 different kinds of fruits and plants. Red grapes, different berries, peanuts, groundnuts, pines, coconuts, and cocoa are a few plant species that contain resveratrol.

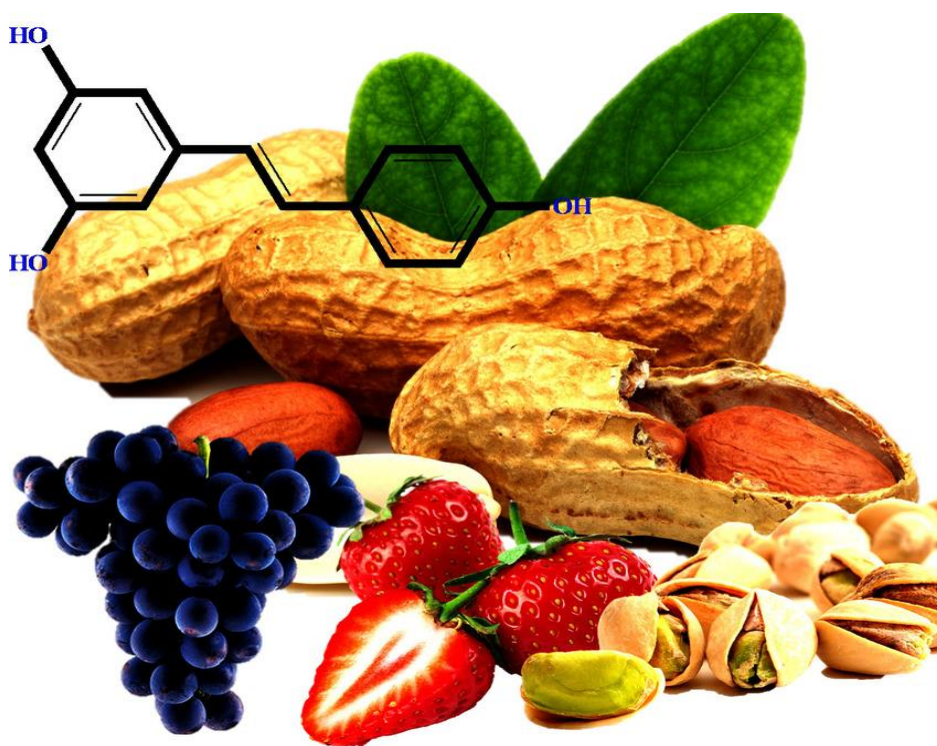


**Fig. 1.5:** Plant source of resveratrol

**Table 1.6: Resveratrol Content in Different Sources**

Sources	Serving	Total resveratrol/serving ( $\mu\text{g}$ )	Reference
Itadori roots	1 g	~2200	[36]
Itadori tea	200 ml	~2000	
Grapes	100 g	150-780	
Red wines	150 mL	80-2700	
Pistachio	28 g	2.5-47	
Raw peanuts	28 g	0.6-50	[36, 37]
Dark chocolate	15 g	3.8-6.5	[38, 39]
Raw peanuts	28 g	0.6-50	[36, 37, 39]
Grape juice	240 mL	0.12-0.26	

Cocoa powder	15 g	19-34	[39]
Milk chocolate	15 g	0.8-2.6	
Peanut butter	32 g	4.7-24	
Roasted peanuts	28 g	0.5-2.2	
Blueberry	100 g	86-170	[40]
Cranberry	100 g	~90	
Bilberry	100 g	~77	

Given that grapes are also used to make wine and other beverage. Since *Vitis varinifera* was originally discovered to have resveratrol in 1976, grapes have been known to contain it, and wine has been known to contain it since 1992. It is almost exclusively generated in the skin of grapes, especially when present in *Botrytis crucifera*, and is maximum in the skin right before the grapes ripen. Thus, the maximum quantity of resveratrol found in grape's skin (50–100 µg/gram) and its seeds (5–10%).

### Anticarcinogenic Activity

Resveratrol modulates a wide range of intracellular signals that play a role in multi-staged carcinogenesis and inflammation, as well as in cell cycle regulation and cell death [41]. Empirical data indicates a potential correlation between the anti-inflammatory and antioxidant properties. Although the exact mechanisms of action are unknown, they may involve the following: scavenging free radicals [42], inhibiting cell proliferation [44], suppressing COX (cyclo-oxygenase) activity [43], inducing apoptosis and inhibiting RNA-reductase [45], DNA (polymerases) [46], and PKA (protein kinase C) (Protein Kinase-C) [47]. The various cellular pathways that may contribute to the anti-tumour activity are discussed in the following sections.

### Antioxidant activity

Resveratrol's capacity to scavenge radicals such as hydroxyl and superoxide [48] and other harmful substances accounts for its preventive properties. Resveratrol shields DNA from reactive oxygen species damage and shields cell membranes from lipid oxidation [49]. The suppression of the protein Keap1, which encourages the dissociation of the dissociated Keap1, and the

activation of Nrf2, which is in charge of eliminating the reactive oxygen species, are the causes of the protective effects [50].

### **Anti-Inflammatory activity**

Inflammation mediators such as COX2, iNOS, IL-1, IL-8, and TNF- $\alpha$  play a role in cancer formation, particularly during the promotion and progression stages [49]. iNOS is an enzyme that aids prostaglandin synthesis, and IL-1, IL-8, and TNF- $\alpha$  are examples of these mediators.

Tumor growth is known to be aided by TGF- $\alpha$  and TGF- $\beta$ , while TGF- $\beta$  has been demonstrated to inhibit TGF- $\beta$  through blocking the Akt / CREB activation pathway, which is in charge of cell proliferation, differentiation, and adaptive responses. The synthesis of TNF- $\alpha$  and TNF- $\beta$  is inhibited by AP-1 [51] through the suppression of the expression of various pro-inflammatory signaling components, including NF- $\kappa$ B and AP-1. This decreases the amounts of intracellular  $Ca^{2+}$  and TNF- $\alpha$ .

### **Neuroprotective Effects**

Several neurological disorders, including Alzheimer, Parkinson and Huntington disease, have demonstrated neuroprotective effects [50], in addition to resveratrol's capacity to prevent cancer. Related to its neuroprotective properties are epilepsy and cerebral ischemia [52]. It seems that in Alzheimer's disease, as demonstrated by various cell lines, resveratrol reduces the levels of intracellular amyloid beta peptides and released amyloid beta peptides also. Actually, it encourages the intracellular proteasome to break down amyloid beta peptides rather than preventing its synthesis [53]. And resveratrol overexpresses the yeast sirtuin-coding SIR2 gene. Sirtuins, which are histone deacetylases that rely on NAD, have been shown to increase longevity and have been associated with certain age-related diseases [52]. The analogous human SIR2 gene is called SIR1. Since resveratrol shields AD neurons from oxidative stress (ROS), hydrogen cyanide ( $H_2O_2$ ), nitric oxides (NO), and A $\beta$  (A $\beta$ )-induced toxicity, SIRT1 expression by resveratrol may be essential for neuroprotective activity [52]. Furthermore, it has been demonstrated that in HD, SIRT1 (resveratrol induced SIRT1) in neurons protects neurons against polyQ toxicity [50] by inhibiting SIRT1. On the one hand, SIRT1 increases neuronal survival and decreases the apoptotic activity of Forkhead (Fox) transcription factors (FTEs). Conversely,

SIRT2 (NF- $\kappa$ B) protects AD neurons [52] from A $\beta$ -induced toxicity by suppressing cathepsin B and inhibiting iNOS (influxin), two toxic components of neurotoxicity.

### **Cardioprotective Activity**

Through a number of methods, resveratrol has been demonstrated to shield the cardiovascular system from atherosclerosis [54]. As an example, it has been proposed that it regulates erythrocyteinositol (NO) production, which could regulate the inflammatory response and shield against vascular injury [50]. Because resveratrol can prevent arachidonic acid from being used to synthesise eicosanoids, there is less platelet aggregation, which may help prevent atherosclerosis. Furthermore, resveratrol blocks TNF-Alpha from triggering coagulation factor expression, which in turn suppresses NF- $\kappa$ B-regulated iNOS expression in endothelial cells. Some studies have shown that resveratrol can protect the heart by increasing levels of the tumor suppressor P53.

### **Obesity and Diabetes Prevention**

It has been demonstrated to prevent and treat dyslipidemia, type 2 diabetes, and insulin resistance in addition to its anti-obesity and anti-diabetic qualities [55]. A high-calorie diet can activate SIRT1 (sIRT1) in one of the ways described above. It has also been demonstrated that phosphorylation contributes to some of the advantages of resveratrol. Because of this phosphorylation, AMPK is activated, which lessens the synthesis of fatty acids and aids in their oxidation. Furthermore, in diabetic rats, resveratrol reduces insulin sensitivity and promotes lipolysis [55]. Resveratrol has been shown to induce intracellular glucoside transport through a variety of methods. One example is the effect of resveratrol on glucose uptake by cells; it increases GLUT4 translocation to the plasma membrane. The liver glycogen store of diabetic rats is increased because it reduces glycogen phosphorylation and increases glycogen production [56].

## **1.5 NANOMICELLES**

Molecules with opposite water affinities make up micelles, also called amphiphilic colloids; their particle sizes range from 5 to 100 nm. Micelles, which are aggregates of amphiphilic molecules, occur at certain concentrations and temperatures.

Hydrophobic fragments are removed from aqueous environments and hydrogen bonds are formed in water, resulting in a reduction in the system's free energy. Micellas are used in drug carriers in many pharmaceutical industries. Micellae contain lipophilic molecules within their core. Polar molecules are bound to the micellar surface. Polymeric micelles. Polymer micelles provide better intestinal permeability. Polymeric micelles are a valuable target for tumor targeting due to their long circulating characteristics and significant tumour accumulation [58]. The polymeric micelles outperform the surfactant micelles in terms of stability, drug accumulation at target, dissociation rate, and CMC. The micelles' small size range is comparable to that of lipoprotein and virus molecules, which are crucial in deciding how their bodies are arranged when enhanced permeation retention (EPR) takes place [59]. Due to side effects, high medication toxicity makes appropriate treatment impossible.

For instance, adverse effects from cancer medications that affect both healthy and malignant tissues include nausea, hair loss, neuropathy, neutropenia, and renal failure [60]. Liposomal formulations for anti-cancer medications have already been licensed. Since this is the case, the drug-nanocarrier complex is highly selective, increasing delivery to injured tissue while decreasing delivery to unwanted locations [61]. For example, Doxil is a lipid-based version of the antiviral medication doxorubicin, used to treat multiple myeloma and Kaposi Sarcoma associated with AIDS [62]. This formulation has a lower cardiotoxicity profile and is more efficacious than the free-label medication doxorubicin [63]. Because of their tiny size, which allows them to get deep into tumor tissue, and their high drug loading capacity, nanomicellars are better suited for cancer therapy. Overcoming drug resistance is possible with nano-based pharmaceuticals due to the EPR effect, which raises local drug concentrations at the tumor site, making the drug more accessible and sensitive [64]. One component of nano-carrier drug delivery systems is regular micelles, which, when placed in a polar solvent, arrange themselves with a hydrophobic core and a hydrophilic exterior component.

Micellar encapsulation is used to improve the bioavailability of drugs and make them more soluble when taken orally [65]. In an un-ionized solvent, the hydrophobic parts of a reverse micelle are positioned on the exterior and the hydrophilic parts on the interior. Micelles are a great vehicle for the delivery and encapsulation of hydrophilic medicines and proteins, attemptpan blue [66], fluoresceins [67], and other solvents. When it comes to drug targeting,

micellar layers on solid supports, drug polymer linked micelles, synthesis of prodrugs, use of new polymers, and reverse micelle production are just a few of the benefits that micellars have over bigger systems [68]. Amphiphilic molecule aggregation provide several advantages, including enhanced solubility (compound that dissolves sparingly), stability, and simplicity in sterilizing. Within the micelles created by van der Waals pressures, lipophilic molecules form a hydrophobic nucleus [69]. A longer circulating time is achieved by the hydrophilic outer layer, which shields the construct from steric interference and keeps the RE from identifying and capturing the construct [70]. Through ligand conjugation, this aids in advancing the conjugation toward active targeting [71].

### **Preparation technique of nanomicelles**

A molecule that possesses both hydrophilic and hydrophobic components is called an amphiphilic molecule. These molecules self-assemble in the aqueous medium to create nanomicelles. The hydrophobic component of amphiphilic molecules forms the core of nanoparticles when they are dissolved in either a polar or hydrophilic solvent; the hydrophilic component, on the other hand, forms the exterior and orients towards the solvent. The hydrophilic, or polar, component can interact with an aqueous solvent, whereas the hydrophobic, or interior, component cannot. A normal micelle is the collection of these amphiphilic molecules arranged in this direction. Reverse micelles are amphiphilic molecules organized in the opposite orientation.

Amphiphilic nano-micellar polymers self-assemble form micelles that range in size from 20 to 200 nm. Amphiphilic polymers are designed to encapsulate and transport molecules that are poorly soluble in water by arranging hydrophobic cores with hydrophilic extrusions. A polymer's ability to self-assemble depends on how concentrated it is in the solution; in order for micelles to form, the concentration of critical micelles must be attained. In addition to their various benefits for drug delivery into the anterior segment, polymeric nano-micelles are also employed to carry medications, like rapamycin, into the posterior segment. Rapamycin is a light-sensitive, pH-sensitive, poorly soluble medication. In order to address the issue of rapamycin's low solubility, a non-invasive topical drug delivery method was created.



## **Features of nanomicelles**

### **Structural stability**

The thermodynamic and kinetic stability of nano-micelles is due to the binding of polymer chains inside the micelle's inner core. According to [72], the HLB of the co-polymer determines when a nano-micelle reaches thermodynamic stability, which occurs when the copolymer concentration surpasses its CMC. Since their CMC values are often lower than those of low-molecule-weight surfactants—between  $10^{-6}$  and  $10^{-7}$  M, nano-micelles are able to maintain their micelle-like structure even after being diluted several times. When circumstances for medication distribution are out of balance, kinetic stability becomes even more crucial. Additionally, when copolymer concentration drops below CMC, kinetic stability begins. When the concentration is below CMC, micelles breakdown much more slowly due to the high kinetic energy of their core structure. Their structural stability causes the gradual dissociation, which increases their bioavailability by retaining the drug content until it reaches the target site.

### **Its solubilize property of hydrophobic drug**

The most efficient drug carriers for solubilizing hydrophobic drugs are thought to be nano-micelles. One of the biggest obstacles to medication formulation is hydrophobia, which is the incapacity to produce a clear water solution with enough drug concentration to reach therapeutic levels. By trapping the medication inside a mixture of hydrophobic cores in the micellar and enclosing it in an outer shell composed of hydrophobic chains that stretch outward, nanocelles are able to solubile hydrophobic drugs, resulting in a clear water solution.

### **Physicochemical properties**

Block co-polymers are typically amphiphilic co-polymers. Diblock and triblock co-polymers are examples of block co-polymers. The majority of diblock co-polymers are of the A-B type, in which co-part A is hydrophilic and co-part B is hydrophobic. Triblock is a subset of both ABC and ABA. To create nano-micelle molecules, both the ABA and AB types are frequently employed [73]. These configurations improve loading efficiency and the drug's solubility. Hydrophobic interactions or electrostatic interactions resulting from macromolecules with opposite charges (polyion complex micelles, or PICs), which are also formed by metaligand



binding and hydrogen ion binding, stabilize the inner core of the hydrophobic block containing molecule [74]. Because of its contact with the cell, the hydrophilic molecule's outer shell is steric stable and important to the in-vivo environment [75]. Because of their structural makeup, micellas self-assemble in water, improve the medication's steric stability, and maintain their stability throughout the gastrointestinal tract.

### **pH sensitivity**

Drug release depends on intracellular signals, and these signals are mostly mediated by pH responsive mechanisms. The building blocks of drugs that are pH-sensitive are poly-bases or poly-acids and micelles [76]. Protonation can cause micelle instability. As a basic unit, amine is neutral at high pH and hydrophobic at low ones. The acidic core is carboxylic acid, which changes from an uncharged acidic base at low pH to a negatively charged acidic state at high pH. The pH has to be greater than the pKa value in order for a nanomicelle to develop. Controlled drug release, however, occurs when the pH drops below pKa because the polymers ionize and the micelle becomes unstable [77]. Drug absorption in the gut is facilitated by this pH gradient [78].

### **Mucoadhesive property**

Nanoparticles of oral medications often adhere to mucosa and pass through the mucosal barrier, resulting in low bioavailability. As the particles break down, the drugs adhere to the mucosa surface and are eventually removed by the mucus clearance process [79]. The mucosal retention property lengthens the time the medicine takes to release by delaying its transit through the gastrointestinal tract. High local drug concentrations are produced when mucoadhesive nanomicellar molecules fill and inflate the cervical mucosa, increasing the effective surface area [80]. Lastly, the medication concentration gradient linked to particle interaction with the mucosal surface is improved by bioadhesion [81]. For instance, positively charged polymicellae are hosted by the negatively charged intestinal mucosa, which is caused by the glycocalyx. Surface charges determine particle movement. Crater and Carrier demonstrated [82] that anionic particles disperse 20-30 times faster than cationic particles.

**Specific binding ability**

Because target ligand molecules are bound to the surface of micelles and the micelles are composed of stimuli-responsive amphiphilic copolymers, the elevated EPR effect makes targeted drug administration easier. To construct immunomicelles, monoclonal antibody molecules are attached to p-nitrophenyl carbonyl groups on the aqueous embedded ends of micelle corona. This process produces blocks with great binding selectivity and target ability [83].

**Classification of micelles****Regular micelles**

In an aqueous medium, regular micelles are amphiphilic copolymer structures that self-assemble. With an outer hydrophilic region and an interior hydrophobic zone, or the aqueous environment, they are fabricated in an aqueous solution.

**Reverse micelles**

Amphipathic co-polymers in a lipophilic medium form these self-assembling structures. They have an exterior hydrophobic zone and an interior lipophobic zone, and they are manufactured in an organic medium. Micelles of phosphazene in chloroform and PCL-P2VP in oleic acid are two examples.

**Single-molecule micelles**

A micelle can be formed by a single molecule of these polymers due to the abundance of hydrophilic and hydrophobic areas. Amphipathic molecules, such as Core PEG micelles, create these in a water-based media. Due to their one-of-a-kind molecular structures, they are resistant to extremes in dilution, temperature, pH, and ionic strength [84].

**Drug loading and release property of nanomicelle**

We will go over the three main approaches to loading drugs inside the core of micelle, in the sections that follow.

**Chemical conjugation**

One method involves using a pH-or enzyme-sensitive linker to chemically attach a medicine to the core. This generates a co-polymer block that, when cleaved, allows the medication to be

released into the cell in its active form. The conjugate then functions as a polymer prodrug by self-assembling into a core-shell structure. The stability and kind of the polymer-drug bond are solely dictated by the rate of drug release and the extent of drugs in the micelles. The stability of the drug conjugate linkage and the kind of polymer-drug linkage can be adjusted to control the pace of drug release and the efficacy of the prodrug. These micelles have acid-sensitive hydrazone linkers that doxorubicin is conjugated to hydrophobic segments. The study found that these micelles are stable at extracellular pH 7.4, but they degrade and release the free drug in endosomes and lysosomes at acidic pH 5.0 to 6.0. The complete elimination of solid tumors implanted in mice indicates that both modified conjugated doxorubicin concentration and block copolymer composition resulted in enhanced efficacy.

### **Captivity on a physical level**

For hydrophobic medicinal compounds in particular, micelle-forming polymer-drug conjugates are preferable than physical inclusion or solubilization into block copolymer micelles. Block copolymers developed for a particular class of medications are necessary since different biomolecules and medicinal substances do not contain the reactive functional groups necessary for chemical conjugation. But changing the shape of the core-forming section allows for the physical incorporation of many different medicines into the micelle core. In addition, by manipulating the molecular properties of a homologous copolymer series—including its molecular weight, content, and availability of the functional groups for active targeting—it is possible to maximize a medication's efficiency in a specific drug delivery scenario. While our team originally suggested the idea in the '80s under the moniker "micellar micro container," the term "micellar nanocontainer" has since become more popular. The solubilized medication was shown to improve neuroleptic action after encapsulating haloperidol in Pluronic block copolymer micelles and directing them towards the brain with the use of insulin or brain-specific antibodies.

### **Polyionic complexation**

Square copolymer micelles can be formed via electrostatic interactions between charged helpful operators and an ionic component of the copolymer that is oppositely charged. This method, which has been around for a while and was independently suggested in 1995 by Kabanov and Kataoka, uses square ionomer structures to combine various polynucleic acids to create non-viral

conveyance frameworks. Amount of medication that can be united inside micelles is determined by the production of stable square ionomer structures. This square ionomer micelle's sensitivity to salt and pH makes it a one-of-a-kind candidate for controlling the triggered arrival of the dynamic restorative substance. In addition, polyion exchange reactions—which are known to show that the helpful specialist and DNA are present in a functional structure inside cells—may be relevant to square ionomer structures. Numerous thorough investigations of square ionomer micelles as high-quality frameworks and drug delivery are available in the literature. In a similar vein, DNA constructs comprising cationic square copolymers have also had their physicochemical components evaluated recently.

### **Advantages of nanomicelles in drug delivery**

Due to their size and molecular composition, nanomicelle-based drug delivery technologies provide some benefits over traditional drug administration systems. Here are some of the benefits:

- A. Lipophilic drugs attach to the lipophilic cores of nanomicelles because they are amphiphilic molecules. This results in a transparent aqueous solution that greatly boosts the solubility of lipophilic drugs. [85]. In comparison, the ordinary Efavirenz (non-nanomicelle), which is poorly soluble in water, would have had a solubility of approximately 4 µg/ml. For example, the polymeric nanomicelle of the antiviral medicine Efavirenz has a solubility of 34 mg/ml. As a result, hydrophobic medications become more soluble when they are encapsulated in nanomicelles.
- B. Because of its active targeting capabilities, which maximize delivery and minimize side effects, nanomicelles are unique to specific targets. Specific targeting is achieved by conjugating them with target moieties. The interactions may involve specific surface receptors, transporter proteins, applied signal proteins, or phage fusion proteins [85]. Ahn et al. conjugated an antibody fragment with platinum-loaded nanomicelles to target pancreatic cancer on tumor xenografts [86].
- C. Because nanomicelles release medications in response to specific stimuli, such temperature or pH, they boost selectivity while reducing toxicity. The medicine is entrapped inside nanomicelles under normal physiological settings (pH 7.2); however,

under acidic conditions (produced by the acidic nature of tumor cells, lysosomes, and endosomes), the drug or therapeutic agent is released in the part of the body that is intended for it. This pH gradient functions as a trigger, causing the medication to release in the intended location [87]. For example, Bae et al. [88] produced pH-sensitive Polyethylene Glycol (PEG)-Poly Aspartate Hydrazone Adriamycin-loaded nanomicelles. Because of the acid-sensitive hydrazine linker, these nanomicelles leak at low pH levels.

- D. The fundamental components of nanomicelles are hydrophobic and biodegradable polymeric nanoparticles. When the drug accumulates at the desired site, these biodegradable nanoparticles act as its local depot. At the location of disease, such as solid tumors, this depot acts as a source of continuous administration of medicine or therapeutic agent encapsulated in a nanomicelle [89].
- E. Nanomicelles ( $>1\ \mu\text{m}$ ) are more suited for intravenous drug delivery due to their greater size. The body's tiniest capillary has a diameter of  $5.6\text{--}6\ \mu\text{m}$ . Nanomicelles ensure that medications are correctly transported into the bloodstream and prevent embolism since they are smaller than the body's smallest capillaries [89].

### **Nanomicelle drug delivery in several therapeutic treatments**

Targeted delivery of cancer medications has gained substantial interest thanks to the benefits that polymeric micelles that self-assemble from amphiphilic block copolymers offer over conventional nanocarriers in terms of both physical and biological properties. Their size ranges from 20 to 100 nm, and they have a hydrophobic core that helps poorly water-soluble medications be loaded effectively, and a hydrophilic shell that provides inherent sheath effect and colloidal stability [89, 90, 91]. These nanocarriers have the following effects: (i) they make anti-cancer drugs more soluble in water; (ii) they prolong the time that a drug is in circulation; (iii) they use the EPR effect to passively target tumor tissues; (iv) they increase bioavailability [93, 94]. The three mainstays of traditional cancer treatment are radiation therapy, chemotherapy, and surgical tumor excision. Because of their cytotoxicity and lack of specificity, chemotherapy medicines destroy both cancerous and healthy cells in an untargeted way. As a result, they have grave negative consequences. Because of their small molecular weight, polymeric micelles have shown to be an effective medication carrier that allows for non-selective biodistribution to both healthy and cancerous cells [95]. Due to their limited solubility in water, the majority of

anticancer medications have low bioavailability and absorption rates; hence, a drug delivery system that reaches the tumor is essential.

### **In eye treatment**

The application of nanomicellar formulation-based technology has significantly advanced the field of ocular medication delivery. This is because these formulations have many benefits, including compact size, easy preparation, high drug encapsulation capability, and lipophobic nanomicellar exterior part that generates hydrated solution. Micellar formulations also improve drug absorption in ocular tissues [96]. For the front area of the eye, for instance, dexamethasone-loaded nanomicelles were created using copolymers of PHEAC and PEGylated PHEAC [97]. Currently, scientists are figuring out how to create a medication to treat conditions affecting the back of the eye. The topical administration of hydrophobic medications seems to have a pharmaceutical carrier in this drug delivery technique.

When it comes to treating age-related eye diseases such as diabetic retinopathy, macular degeneration, diabetic macular oedema, and posterior uveitis, this method is both effective and highly complied with by patients [98].

### **In skin treatment**

For the same reason that it reacts strongly to hydrophobic and hydrophilic substances, the skin barrier prevents medications from entering the body easily. The utilization of nano-sized carriers is the most recent development in the field of drug administration through skin penetration [99].

Pharmaceutical compounds are encapsulated in nanocarriers to achieve functions including entering hair follicles and interacting with the lipids on the skin to assist delivery. Their large surface area to volume ratio allows them to strongly penetrate all channels, including the intracellular and intercellular pathways as well as the trans-appendage pathway of hair follicle shafts [100]. Some synthetic or semi-synthetic polymers, including chitosan, PLA, and PLGA, are safe and effective for topical medication delivery. There is reduced skin irritation from direct drug contact and controlled release with polymeric nano carriers, which are made possible by modifying the composition of the polymer [101].

## 1.6 Aim and Objectives

### Aim:

Diabetes is a chronic metabolic disorder that affects millions of people worldwide and takes a heavy toll on human life. Treatment of diabetes often possesses a problem in selection of the proper drug, its dose and unwanted side effect. Therefore, newer drugs with the least side effect but with highest efficacy are being continuously searched for. Diabetes mellitus is characterized by persistent hyperglycemia. High blood sugar can produce long term complication such as cardiovascular and renal disorder, retinopathy and poor blood flow.

Since ancient time compounds from various plants are in practice and some of which have been reported to possess pronounced antidiabetic properties. Curcumin and resveratrol are the most potent and frequently studied multifunctional polyphenolic compounds. However, because of their poor water solubility and bioavailability, a new water soluble antidiabetic derivative or nanoformulation need to be developed to increase the bioavailability.

So, the **aim of the study** is to develop a highly water soluble curcumin and resveratrol containing nanomicelle for the management of diabetes.

To fulfill our research goal the main **objectives** are as follows:

- Synthesis of chitosan-curcumin conjugated amphipathic prodrug for increasing the solubility of curcumin.
- Structural identification of amphipathic prodrug by FTIR, <sup>1</sup>H-NMR, UV-vis and Fluorescence spectroscopy, etc.
- Fabrication of nanomicelles from chitosan-curcumin conjugated prodrug to transport free form of curcumin and resveratrol with conjugated form of curcumin and simultaneously to increase therapeutic efficacy.
- Characterization of nanomicelles by TEM, SEM, AFM, XRD, Zeta Sizer etc.
- HPLC method development for the simultaneous estimation of conjugated curcumin and free form of resveratrol.
- *In vitro* evaluation of the formulated nanomicelles.
- *In vivo* evaluation of antidiabetic activity of the nanomicelles at pre-clinical stage.



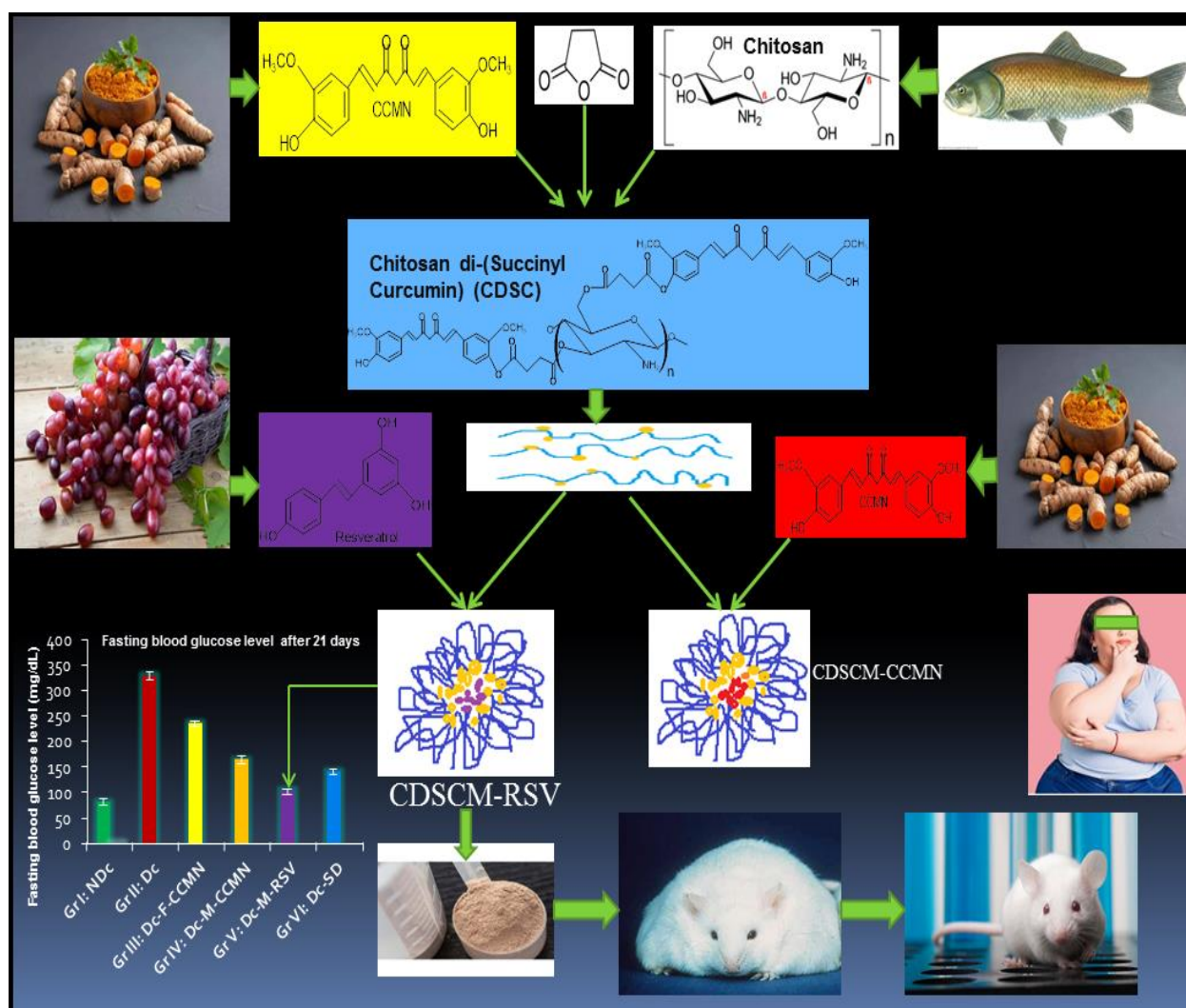


**Fig. 1.6:** Overall research lay-out



# Chapter 2

## Review of Literature

- 2.1 Awareness of Diabetes Mellitus
- 2.2 Assessment of Diabetes
- 2.3 Diabetes Management
- 2.4 The Effects of Curcumin in Diabetes Mellitus
- 2.5 Potential of Resveratrol
- 2.6 Effects of resveratrol on glucose control and insulin sensitivity
- 2.7 Nanomedicine for the treatment of diabetes-associated diseases
- 2.8 Nanomicelles

### **2.1. Awareness of Diabetes Mellitus**

In 2013, Maral F. Thabit investigated how well people with T2DM understood diabetes and its consequences [102]. This study aims to assess how well persons with T2DM understand their disease and its consequences. They concluded that the study's T2DM patients lacked sufficient understanding of a number of topics, including the genesis of the disease, appropriate measurements, complications, follow-up and management through dietary changes, medication therapy, and reliance on herbal remedies. James Jafali [103] studied diabetes mellitus in people with the disease in the Gambia in 2013. The paper presents a strong argument in favor of health promotion and instruction. Just 47% of the patients who were targeted and claimed to be aware of their condition understood what diabetic mellitus (DM) was. Similarly, 53% of research participants did not know the causes of diabetes mellitus (DM) and nearly 50% did not know how to prevent it. Of those with diabetes, 67% were aware that it can lead to blindness and 46% that it can slow the healing of wounds. Respondents' knowledge that diabetes can cause skin infection, heart failure, and stroke was very low. Half or more of the individuals had no idea how to avoid developing diabetes. The length of the illness, educational attainment, and a family member's awareness of diabetes were revealed to be important predictors in their study. They have concluded that the majority of patients who come to the Mayor's Office for People with Disabilities (MOPD) are not well-informed about the condition and its causes, problems, care, and prevention, among other relevant topics. Consequently, it is imperative that Gambian people become more aware of this deadly but concealed disease condition.

### **2.2. Assessment of diabetes**

Researchers Kanchana Dussa, Parimalakrishnan S., and Rakesh Sahay [104] examined 2015 diabetes awareness among patients with type 2 diabetes mellitus using a diabetes questionnaire. T2DMs had their diabetes knowledge tested using the Diabetes Knowledge Questionnaire (DKQ), and the researchers looked for a correlation between DKQ scores and HbA1c levels. The average age of the participants was 52–22 years old, and their ages varied from 36–75. In the study there were 78.38% female participants and 21.62% male; 59.45% illiterate; 75.67% only used oral hypoglycemic medications; 24.32% also used insulin; no one reported any of them to a diabetes educator; and 14.86% went to a dietician for advice. The DKQ score and the duration of

the illness were related, although the HbA1c levels were not. They have concluded that the diabetes patients who came to Osmania Hospital knew very little about the disease. Most people were either very poorly educated or had never attended school. Enhancing these people's knowledge of diabetes could aid in improving their glycaemic control. Including a clinical pharmacist and endocrinologist in the best diabetes management may assist achieve the objective of raising patient awareness of the condition when done over an extended period of time.

Anurekha Jain [105] studied diabetic mellitus (DM), commonly called high blood sugar, which is caused by a confluence of metabolic disorders, in 2015. Insufficient insulin production or cells that do not respond to insulin are the two main causes of diabetes. Characteristic symptoms of polyuria, polydipsia, and polyphagia are increased thirst, increased hunger, and increased urine caused by elevated blood sugar. Three main categories have been used to classify diabetes throughout history: The inability of the body to manufacture insulin, leading to the need for an insulin pump or injection, characterizes IDDM, also known as T1DM. The term "juvenile diabetes" can describe your condition. The inability of cells to fully or partially utilize insulin as intended is known as insulin resistance, and it is the root cause of type 2 diabetes (T2DM), sometimes called non-insulin-dependent diabetic mellitus (NIDDM). This variety was previously known as "adult-onset diabetes." Gestational diabetes, the third type of diabetes, occurs when pregnant women without a previous history of the disease have abnormally high blood glucose levels. It may occur before type 2 diabetes begins to manifest. Oral hypoglycemic medicines and insulin are the current pharmacological options for diabetes mellitus. One way these medications lower blood sugar levels is by improving glucose absorption and decreasing gluconeogenesis; another is by enhancing pancreatic insulin production.

However, the duration of these new drugs is insufficient to restore normal glucose homeostasis, and they have a long list of adverse effects, such as insulinoma, hepatotoxicity, hypoglycemia, kidney disease, GIT problems, and cardiac risk. Numerous herbal medicines have also demonstrated efficacy in the treatment of diabetes due to their medicinal components. Thus, the focus of this review will be on the physiological aspects of diabetes, its effects, goals for management, and the application of both synthetic and herbal diabetic cures.

### 2.3. Diabetes management

Thomas Haak [106] conducted study in 2013 to create and assess diabetic self-care strategies for glycaemic control. The predicted scale structure was confirmed by principal component analysis, which revealed a four-factor structure. As confirmed by confirmatory factor analysis, the four-component model was the most appropriate for the given data. The researchers came to the conclusion that the DSMQ is a reliable and practical tool for evaluating self-care practices related to glycemic control. The questionnaire should be beneficial for research on T1DM and T2DM patients in both clinical and scientific settings. As such, the DSMQ should prove valuable in future research as well as therapeutic situations.

Research on early disease management conducted in 2021 by Nicola Brew-Sam [107] recommends interdisciplinary care coordination encompassing the child, family, medical professionals, and other caregivers, such as teachers. Early diabetes diagnosis is frequently associated with psychological stress for the kid or teenager as well as the parents because of the demands of round-the-clock disease management. Adapting to intricate treatment plans and always fearing the repercussions of inadequate blood glucose regulation, particularly hypoglycemia, are two examples of this stress (**Figure 2.1 and 2.2**). Physiological changes associated with puberty, increasing independence from parents, the complexity of daily tasks, psychological demands, and peer pressure are some of the unique obstacles that adolescents with diabetes face when trying to manage their condition.

To attain ideal blood glucose management, adolescents with type 1 diabetes need to effectively handle three crucial components: insulin administration, glucose monitoring, and correlation between insulin administration, glucose monitoring. Adolescents with T1DM require expert supervision of three critical components—glucose monitoring, insulin delivery, and communication networks between the two (2)—to achieve optimal blood glucose control. Specific information is provided by glucose measurements in the blood or dermal interstitial fluid when administering exogenous insulin into subcutaneous tissues through insulin injection or pump. To prevent both immediate complications and more serious complications in the future, this type of treatment is essential. Glucose monitoring options include continuous glucose

---

monitoring (CGM) systems that provide real-time access to subcutaneous interstitial fluid glucose testing, flash glucose monitoring (FGM) systems that provide intermittent access, and self-management of blood glucose through finger stick blood collection.

#### **2.4. The Effects of Curcumin in Diabetes Mellitus**

Diabetes mellitus (DM), which could soon trigger global pandemic illnesses, was the subject of research by Patricia Cincotto dos Santos Bueno [108]. Lifelong medication therapy and behavioral changes are part of beneficiary management, which is incredibly difficult due to the intricacy of the disease. More and more studies are looking at the possibility that herbal supplements can help with diabetes mellitus, both in prevention and therapy. One of *Curcuma longa*'s bioactive compounds, CCMN, has a number of useful physiological and pharmacological effects, including reducing inflammation and cancer risk, protecting nerves, and preventing diabetes. Our goal is to study the impact of *Curcuma longa* (CCMN) on DM for each of these factors in great detail. After searching databases like PUBMED and EMBASE, sixteen papers were found that met the inclusion requirements. Thousands of people all around the globe are impacted by type 2 diabetes, which has a complex origin. Possible treatments include dietary changes, physical activity, and lifestyle adjustments, as well as long-term medication-assisted therapy. Naturally occurring CCMN offers a low-cost, safe alternative to the current treatment strategy for this ailment; however, its exact dosage is still unclear. CCMN also acts as an anti-inflammatory and anti-diabetic. We recommend larger, more trustworthy randomized controlled studies to determine CCMN's function in T2DM therapy.

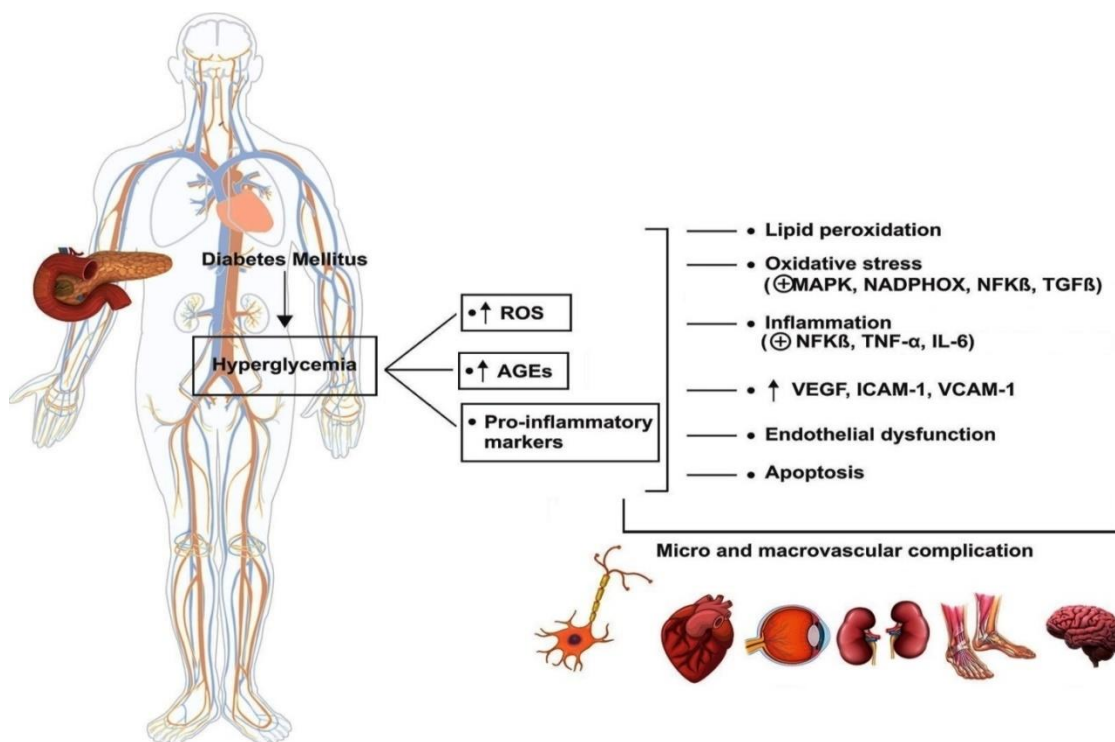


**Fig. 2.1:** Pathophysiology of diabetes mellitus.

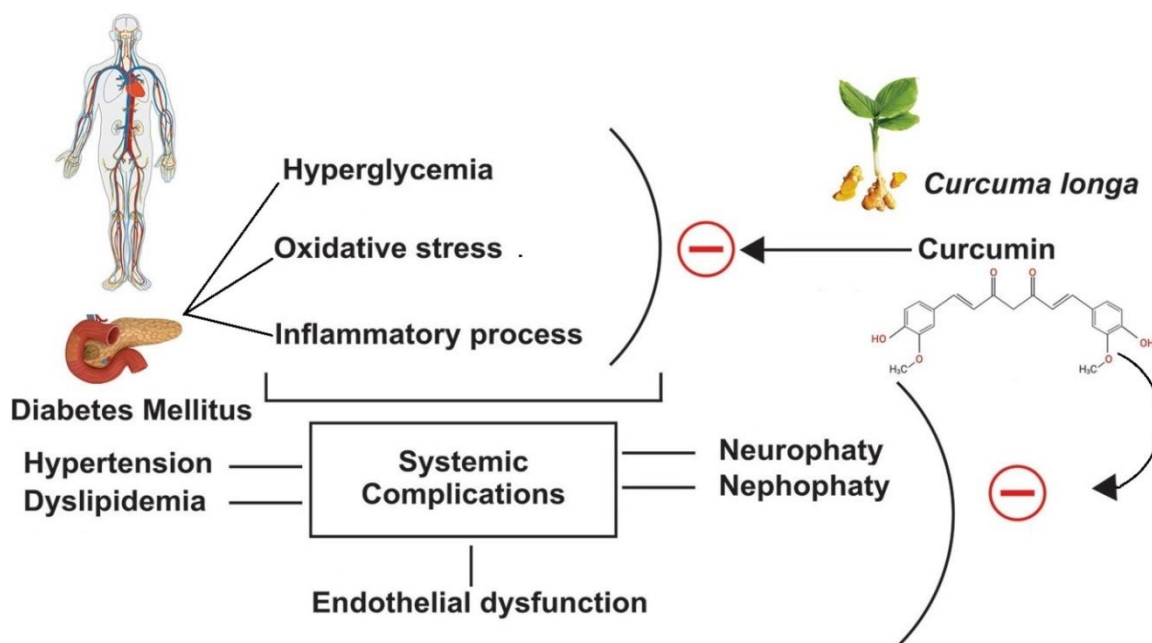


**Fig. 2.2:** Effects of curcumin.

Trial findings provided by Panahi et al. [109] showed that taking curcuminoids and piperine supplements improved hepatic and glycemic indices in type 2 diabetic individuals, but did not affect hs-CRP levels. Several measured indicators, including hs-CRP, did not respond as anticipated to the curcuminoid, which may be explained by the lack of critical information on standard-of-care treatment in this experiment. Second, randomization should have decreased the potential of bias by evenly distributing nutritional consumption and physical activity among the research groups, even though these parameters were not examined. Finally, the short trial time could be useful for evaluating curcuminoids' effectiveness in future studies.

Turmeric powder, when taken once daily for eight weeks, has beneficial effects on patients with hyperlipidemia and type 2 diabetes, according to Adab et al. [110]. Several variables, including fasting serum insulin, body mass index (BMI), triglycerides, cholesterol (LDL-c), good cholesterol (HDL-c), insulin, hemoglobin A1C, and fasting blood glucose (FBG), were assessed both before and after the intervention period. Researchers assessed the intervention's feasibility as a supplementary treatment for metabolic syndrome, atherosclerosis, and diabetes. Challenges may arise from the trial's small sample size and brief intervention period.

Researchers Adibian et al. [111] found that type 2 diabetes patients who took 1,500 mg of curcumin daily for 10 weeks reduced inflammatory markers, which may have prevented diabetic complications. The experts' consensus was that more samples, longer durations, and varying doses of curcumin might improve results.

Supplementation with nano-curcumin ameliorated and lessened the severity of DSPN in type 2 diabetic individuals in an experiment conducted by Asadi et al. [112]. There was a non-significant decrease in weight, glycemia, and body mass index after two hours in the trial. However, the authors do point out a number of limitations, such as the minimal participation rate among men, the short follow-up period, and the experiment's single dose.

Hodaei et al. [113] conducted a randomized, double-blind, placebo-controlled trial in Iran and found that individuals with NIDDM who took a high dose of curcumin daily for 10 weeks had improvements in inflammatory markers. Redox state, insulin resistance, hemoglobin A1c, and

---

blood insulin levels were unaffected by this intervention. In their study, the authors acknowledge a short duration of the intervention and a significant loss of patients.

For individuals with T2dm who had a small reduction in glomerular filtration rate (GFR), oral curcumin therapy dramatically reduced albuminuria in the Vanaie et al. [114] experiment, improving renal function and highlighting the possibility of curcumin as a viable alternative treatment. A limited sample size and a brief intervention time were identified as some of the trial's weaknesses by the authors.

Evidence suggests that people with type 2 diabetes experience reduced despair and anxiety after using nano-curcumin capsules. Also, the trial participants reported little side effects when taking curcumin [115]. Nonetheless, stress did not appear to have any major impact, and these effects were really small. The experts believed that the intervention could lead to either superior long-term effects or higher supplementing doses.

The use of nano-curcumin as a type 2 diabetes medication significantly decreased fasting levels of insulin, plasma glucose, and plasma lipids, according to findings from Shafabakhsh et al. [116]. On top of that, using nanocurcumin enhanced PBMC nitrite and antioxidant capacity levels, PPAR- $\gamma$  and LDLR gene expression, and GSH levels, while having no effect on TGF- $\beta$  gene expression or TGF- $\beta$  levels. The supplementation was found to have antioxidant and anti-inflammatory effects, according to the authors. However, they did point out that the trial had some limitations, such as not being able to measure how the administration affected other inflammation and oxidative stress biomarkers or how well participants took the nano-curcumin.

Oral nano-curcumin intervention considerably increased insulin, FBG, LDL-c, TAC, and total glutathione levels in diabetic foot ulcer patients, according to a clinical trial by Mokhtari et al. [117]. Oral administration of the intervention was also performed. In contrast, there was no change in oxidative stress, lipid profile, ulcer size, HbA1c, or inflammatory markers. The benefits of the study were highlighted, such as the fact that it was the initial assessment of nanocurcumin's effect on metabolic regulation and wound healing parameters in DFU patients. It



was justified to conduct this study since DFU patients were more likely to develop insulin resistance and cardiometabolic diseases.

Research conducted by Jun-Li Liu et al. (2013) has provided solid evidence supporting the use of "traditional" curcumin and its significance in the management of diabetes and associated conditions. Diabetes complications like insulin resistance, hyperglycemia, excessive cholesterol, islet apoptosis, and necrosis may be ameliorated by curcumin. On top of that, curcumin has the potential to reverse the harmful effects of diabetes. Despite curcumin's diversity as a natural product, clinical study results have only been reported in relation to its usage in the treatment of diabetic renal failure, microangiopathy, and retinopathy. To confirm curcumin's potential to prevent diabetes and other linked illnesses, human trials are critically needed [118].

According to research by Ahmed Abdellatif et al. (2019), for millennia, humans have used herbal remedies to alleviate the challenges related to diabetes mellitus. This study examines the effects of oral curcumin supplementation versus parenteral injection of turmeric extract on diabetic complications in animals treated with streptozocin (STZ). Both low and high doses of intraperitoneal turmeric extract were administered to STZ-induced diabetic rats, in addition to oral curcumin. Curcumin and turmeric extracts significantly raised uric acid and lowered blood sugar and creatinine levels, but not urea. Low doses improved liver enzymes; nevertheless, when doses and oral delivery rose, so did ALT and AST. Triglycerides did not decrease in the group receiving high-dose oral medication, while serum cholesterol did in all other groups. Histology investigation showed that the islet cells were protected. Following a high-dose injection, tubular structures showed minimal degradation and nearly undamaged renal corpuscles. The medication only partially protected the liver tissue [119].

According to research by Zwe-Ling Kong et al. (2019), people with diabetes who have high blood sugar usually get cardiovascular diseases (CVDs), which can be fatal. Cur, also known as curcumin, is an antioxidant with anti-inflammatory qualities that lowers the risk of CVDs. The poor absorption of curcumin rendered it mostly ineffective in clinical settings. Through the use of a streptozotocin (STZ) induced T1DM model in C57BL/6 mice, this study sought to determine if chitosan-encapsulated curcumin could protect against kidney and heart damage. The

---

results demonstrated that CEC and Cur treatments improved insulin secretion while downregulating total cholesterol and blood sugar. But there was no change in triglyceride, blood pressure, or very low-density lipoprotein cholesterol levels. An examination into histochemistry revealed that curcumin and chitosan-encapsulated curcumin alleviated renal fibrosis and left ventricular nucleus and cell enlargement, particularly following therapy with chitosan-encapsulated curcumin. In a type 1 diabetic mouse model, our results demonstrate that chitosan significantly enhances the protective effects of curcumin against renal and cardiac failure [120].

## **2.5. Potential of Resveratrol**

Chuanlin Zhu et al (2020) did research on diabetes mellitus major global health concern. It is widely widespread worldwide and is often linked to serious clinical consequences, including cardiomyopathy caused by diabetes, nephropathy, retinopathy, neuropathy, and others. Researchers in science are always searching Chinese herbal medicine for novel monomer molecules that might be used as potential medications to treat diabetes and its side effects. RSV is a polyphenol phytoalexin with a variety of physiological and biochemical effects, such as anti-inflammatory, anti-platelet, and estrogenic. Recently, RSV has drawn attention from scientists for its potential to regulate blood sugar, combat diabetes, and prevent its consequences in a variety of diabetic models. The several ways that RSV affects cellular processes appear to be the cause of these advantageous results, which establish RSV as a potentially useful drug for the management of diabetes and its sequelae. In order to serve as a guide for future study and development of RSV, we have reviewed here the mechanism that works and possible therapeutic application of RSV in both the prevention and the mitigation of various diseases throughout the past ten years [121].

A decrease in glucose absorption and utilization due to a myriad of reasons is referred to as "insulin resistance" (IR). Multiple studies have demonstrated that RSV can improve insulin sensitivity in a variety of animal models, including type 2 diabetics, hyperlipidemic mice, and obese Zucker rats. In order to drastically decrease insulin sensitivity and/or blood insulin concentration, RSV is given to animals and humans with type 2 diabetes at doses ranging from 2.5 to 400 mg/kg for 1-6 months. Human therapeutic trials have shown that by orally administering RSV (5 mg-5 g) once daily for a year, persons with diabetes can decrease blood

glucose levels and increase insulin sensitivity. Validating the increase in insulin sensitivity following RSV treatment, these results demonstrate a substantial reduction in postprandial glucose levels without an increase in insulin production. Further evidence suggests that RSV can activate sirtuin (SIRT) and AMP-dependent protein kinase (AMPK), hence resolving aberrant levels of blood glucose, insulin, and insulin-like growth factors (IGFs). Two metabolic disorders characterized by abnormalities include diabetes and obesity; SIRT1, a nucleus component, and SIRT3, a mitochondrial component, play critical regulatory roles in these diseases. By raising the ratio of NAD<sup>+</sup>/NADH, the amount of acetylation of proteins, such as p53, NF- $\kappa$ B, and fork head box protein O1 (Foxo1), can be influenced by RSV-induced activation of SIRT1 and SIRT3 (energy status sensors). Free fatty acids (FFAs) in the blood are reduced by RSV. One important factor that contributes to IR is the lipotoxicity of FFA. Red blood cell (RBC) virus can reduce reactive oxygen species (ROS) production, promote fatty acid oxidation, and prevent fatty acid synthase (FAS) damage via improving mitochondrial metabolism and stimulating SIRT1 and SIRT3. Activation of SIRT has the potential to mitigate the effects of mitochondrial malfunction, a key contributor to insulin resistance and type 2 diabetes. Research suggests that RSV triggers SIRT1 activation in  $\beta$ -cells, leading to an upregulation of mitochondrial biogenesis and a downregulation of UCP-2 production. The presence of reactive oxygen species can be protected by increased UCP-2 expression in pancreatic  $\beta$ -cells, which can potentially be an indication of stress. As a result, IR is mitigated and compensated by RES-induced downregulation of UCP-2 expression. Sun et al. shown in their in vitro investigation that SIRT1 suppresses the production of PTP1B, an important negative regulator of the insulin signaling pathways. Animals lacking PTP1B have normal glucose levels and a better insulin response than their wild-type counterparts. PTP1B antisense oligonucleotides considerably reduced PTP1B protein levels in the livers of type 2 diabetic mice. Consequently, the levels of insulin, lipids, and glucose in the mice dropped. The inhibition of PTP1B expression in both in vivo and in vitro studies suggests that RSV either enhances insulin sensitivity or prevents insulin resistance (**Figure 2.3**).

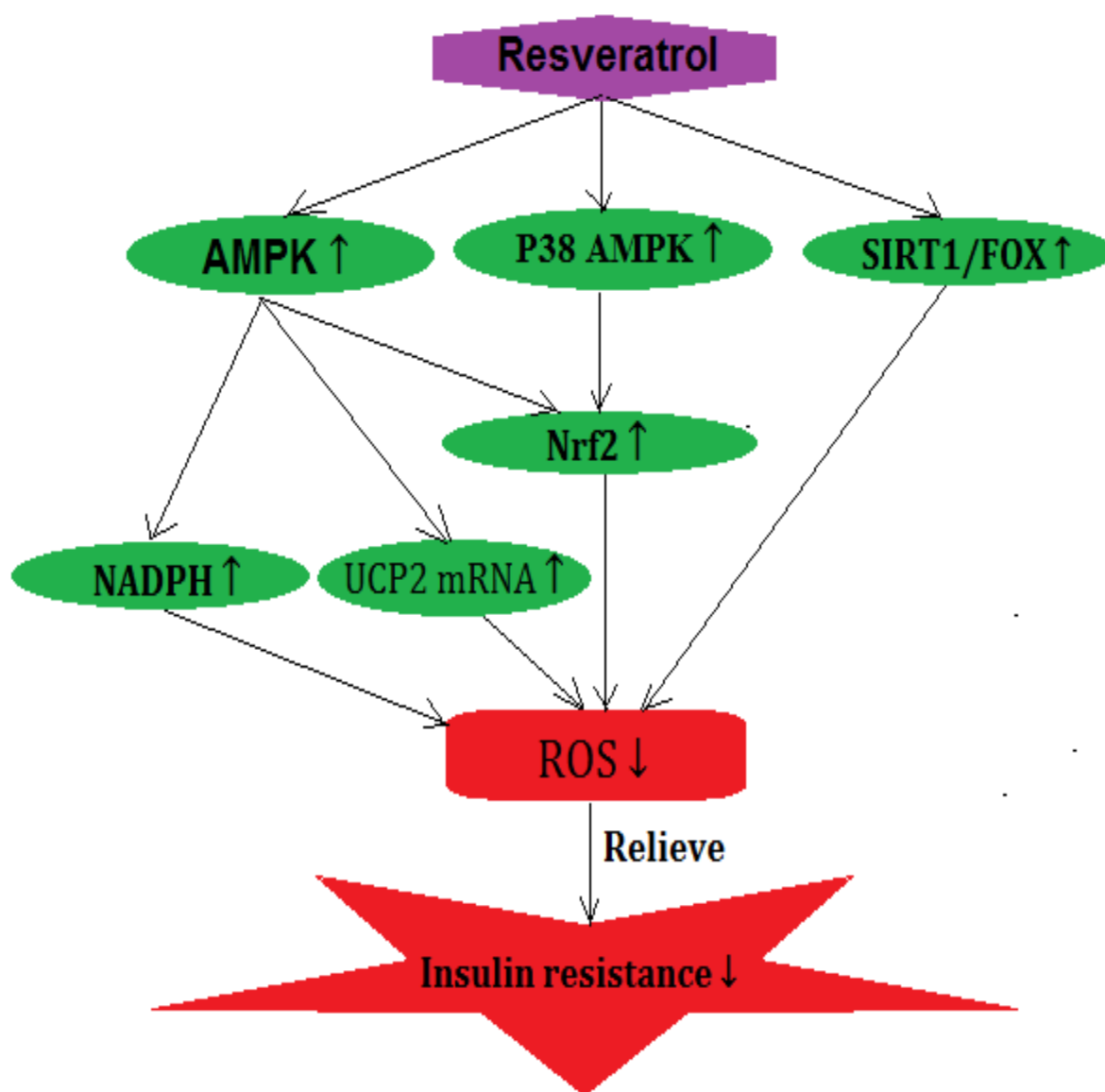


**Fig. 2.3:** Mechanism of improving insulin resistance by RSV

The main feature of type 2 diabetes is an issue with glucose metabolism. When  $\beta$ -cells are in a physiologically sound state, glucose causes a series of events that result in the release of insulin. Hence, regular glucose metabolism is crucial for steady blood sugar levels. Elevated glucose absorption by skeletal muscle is the primary mechanism by which insulin promotes glucose consumption. Nevertheless, GLUT4, an essential regulatory protein for glucose transport, has a major impact on the uptake of glucose by skeletal muscle cells. It is known that animals with diabetes express less GLUT4 protein. In the diabetic rats, it has been demonstrated that RSV (3

mg/kg for 7 days) increases the levels of both GLUT4 and GLUT2. Additionally, RSV increases GLUT4 expression, which likely explains how it improves glucose uptake or utilization in insulin-free isolated cells. It is still not apparent what the precise mechanisms are. Since acute administration of high doses of RSV promotes the phosphorylations of Akt and AMPK and enhances glucose absorption in insulin-stimulated human myotubes, a lot of recent research points to a relationship to RSV-induced PI3K activation and AMPK phosphorylation. P13 K inhibitors can surprisingly reduce hypoglycemia's impact in STZ-diabetic mice. In summary, RSV stimulates GLUT4 translocation quickly and improves activation of signal pathways that are AMPK/Akt- or PI3K/Akt-dependent, which in turn helps skeletal muscle cells absorb glucose. Additionally, Sin's group confirmed that RSV is a potentially effective anti-diabetic drug that reduces Foxo1 phosphorylation and speeds up SIRT1 deacetylase to produce a noticeable hypoglycemic effect. These effects may be essential for enhancing glucose conversion and metabolism. Reduced Foxo1 expression inhibits pyruvate dehydrogenase kinase 4 (PDK4), an enzyme that is essential to the tricarboxylic acid cycle and activates pyruvate dehydrogenase. Variations in enzyme activity within the skeletal muscle may promote glycolysis and the synthesis of glycogen (**Figure 2.4**). The studies cited earlier suggest that RSV lowers FBG levels by influencing glucose uptake and metabolism. How RSV affects glucose metabolism and insulin sensitivity in the aged needs more investigation.

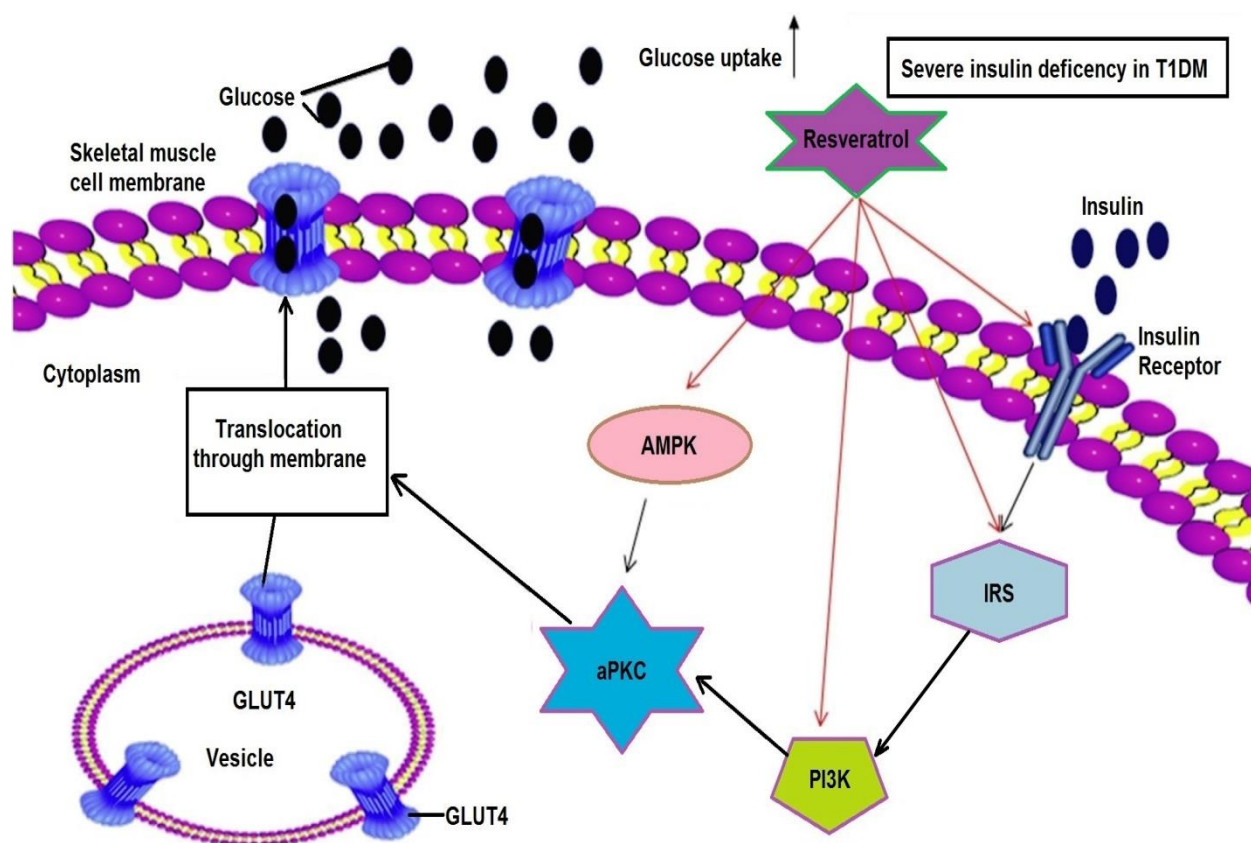


**Fig. 2.4:** Mechanism of enhancement of glucose uptake by RSV

## 2.6. Effects of resveratrol on glucose control and insulin sensitivity

In 2017, Ling Li et al. performed research on type 2 diabetes. Though the findings haven't always been dependable, resveratrol supplementation on a regular basis has been shown to improve glucose homeostasis and reverse insulin resistance in T2DM patients. Therefore, we set out to determine if resveratrol improved insulin sensitivity and glycemic control in type 2 diabetics. As of June 2017, we searched Web of Science, PubMed-Medline, Embase, and the Cochrane Library for any pertinent articles. Research including randomized controlled trials of resveratrol in the treatment of type 2 diabetes was considered. After the papers were selected, two authors worked independently to extract data and conduct qualitative assessments. The statistical analysis was conducted using RevMan and STATA tools. The included studies comprised nine randomized controlled trials with a total of 283 participants. According to a meta-analysis, resveratrol had a substantial impact on insulin concentrations and FBG levels. There was almost no change in HbA1c, low-density lipoprotein cholesterol, or high-density

lipoprotein cholesterol. Supplementing with more than 100 mg of resveratrol daily was associated with significantly lower fasting blood glucose levels compared to supplementing with less than 100 mg daily, according to subgroup analysis. To be more specific, the later dosage yielded superior benefits. Supplemental resveratrol may help with type 2 diabetes treatment, according to this meta-analysis [122].

Administration of resveratrol markedly improved insulin tolerance, insulin metabolism, and glucose metabolism in comparison to a placebo. Resveratrol improved nutrition sensing systems and reduced glucose-6-phosphatase synthesis and activity, which relieved symptoms. Among the proinflammatory cytokines found in older diabetics, resveratrol administration was found to be more effective than placebo in reducing levels of TNF- $\alpha$ , HbA1c, IL-6, and IL-1 $\beta$ . If compared to a placebo, resveratrol treatment increased glucose tolerance, stabilized lipid profiles (total cholesterol, HDL, LDL, and triglycerides), and improved renal function [123].

## **2.7 Nanomedicine for the treatment of diabetes-associated diseases**

Ying-Mei Feng et al (2021) research on two primary manifestations of cardiac failure in diabetics are cardiomyopathy and fibrosis. To improve the effectiveness of anti-diabetic medications and target profibrotic processes in cardiomyocytes specifically, a delivery mechanism is needed for therapeutic purposes. Nanoparticles (NPs) are perfect for treating diabetes because of their unique benefits, which include targeting efficiency, bioavailability, biocompatibility and low toxicity. They summarize the most recent findings about the etiology of cardiomyopathy and fibrosis in individuals with diabetes in this review and also provide an overview of how NP applications enhance the prolonged release of liraglutide and insulin after oral delivery. They present an extensive analysis of the outcomes of NP clinical trials involving diabetic patients as well as animal research examining the impact of NP-mediated anti-fibrotic therapies. All things considered, using cutting-edge NP delivery methods to treat diabetic patients' cardiomyopathy and fibrosis is a novel and promising therapeutic approach [124].

**Advantages of NPs in clinical applications**

NPs are perfect for use in vaccinations, illness diagnostics, and therapy because of a number of benefits. One important issue that impacts delivery efficiency is size. The rate at which NP is excreted from the kidneys increases with size. Large NPs are paradoxically lodged in the spleen and liver. One of the primary entrance points for NPs is endocytosis. While NPs greater than 60 nm cause receptor overconsumption, NPs between 30 and 60 nm cause robust endocytosis and less than 30nm do not cause endocytosis.

Water solubility, structural stability, targeting, and cellular absorption can all be enhanced by further conjugating electric charges, peptides, or chemical compounds during the well-controlled synthesis of NPs. The benefits of each NP for imaging and medication delivery are further enhanced by hybrid NPs like liposomes, which combine the properties of two NP types.

Alternatively, NPs can be embedded into biomaterials before administration to create a hybrid biomaterial system. During surgery, hydrogels are frequently utilized to halt bleeding from wounds. The kinetics of the drug released from NPs and the release NPs from the hydrogel are better controlled when a hydrogel and a 3D polymer structure network are combined. Additionally, the hydrogel's biodegradable quality quickens the removal of NP for detoxification [124].

**Insulin delivery through nanomicelles**

When fasting plasma glucose levels surpass 13.75 mg/dL or HbA1c levels surpass 10%, patients with type 2 diabetes who are taking two or more medications to lower glucose levels should begin subcutaneous insulin injection, according to the Study of Diabetes guidelines. Insulin glargine or a placebo was given to 12,537 individuals at random who had T2DM or impaired FBG. After 6.2 years of observation, HbA1c levels in the insulin glargine group decreased to 6.2% (95% CI, 5.8–6.8%) but they were 6.5% (95% CI, 6.0–7.1%) in the insulin free excipient group. However, the insulin glargine group saw a three-fold higher frequency of weight gain and blood sugar reduction compared to the placebo group [125]. Additional challenges to implementing insulin therapy include weight gain, cost, pain fear, and low adherence.

The most practical method of administering insulin is orally. However, rapid breakdown by digestive enzymes, poor absorption by the intestinal barrier, initial digestion of protein by



stomach's acidic pH and the intestine's basic pH significantly limit its utilization. Moreover, creating a stable structure for an insulin-loaded liposome is still a difficult technological problem due to its large molecular weight and temperature sensitivity. After decades of research, insulin-loaded NPs, whose composition, chemical groups, or particular peptide tagging can be changed as needed for the treatment of diabetes, can make oral insulin administration feasible.

A common NP conjugate is the cationic polysaccharide chitosan. Porcine insulin is conjugated with chitosan of varying diameters to maximize its entrapment efficiency. Using a 1000 kDa chitosan resulted in a 203.4 nm NP with a 75.9% insulin entrapment performance. The insulin entrapment effectiveness of NPs laden with amphiphilic lipids was 3.8 times greater (90%) than that of NPs without lipids (24%). But in just one hour, an 80% release of insulin was achieved [126].

However, metformin buildup in the liver causes lactic acidosis by delaying the removal of lactate. In a pilot research, metformin was loaded onto niosomes to enable prolonged metformin release [127]. Niosomes are created through the hydration of amphiphilic substances like cholesterol and non-ionic surfactants. Niosomes have high metformin entrapment efficiency; when negatively charged, this efficiency can reach up to 92.62%.

## **2.8 Nanomicelles**

Nanomicelles are self-assembling dispersions of colloidal particles with a hydrophobic core and a hydrophilic shell that are nanoscale, usually with particle sizes between 10 and 100 nm, according to research done by Prasun Patra et al. in 2021. Because of their size, solubility, tailored surface, or exposure to the environment, nanomicelles display distinctive or original properties. These qualities make them versatile and essential in a variety of fields, including biomedical applications. This study describes the unique properties of nanomicelles that distinguish them from other types of particles and pave the way for a variety of biological uses, such as the delivery of medications. It also emphasizes the many approaches to drug delivery and integration, their advantages and disadvantages, and how nanomicelles can encapsulate medications [128].

**Targeted Anticancer Drug Delivery through Micelles**

Yanli Zhao et al (2015) study on development of amphiphilic, reduction-responsive, intracellular copolymer micelles that are unique to cancer cells was carried out. An initiator with two heads, a disulfide linkage and a folic acid targeting unit, was used to create the copolymer with regulated molecular weight and functions. Under physiological conditions, the polymer exhibited stability by self-assembling into spherical micelles. When the intracellular reducing agent glutathione stimulated the micelles containing the anticancer medication doxorubicin, the drug was swiftly released into the surrounding milieu. Additional proof that DOX was effectively released from the ingested micelles into the cytoplasm, leading to cell death and apoptosis, was obtained from flow cytometry and confocal laser scanning microscopy studies. Presently available copolymer micelles hold potential for application in targeted cancer therapy as anticancer drug carriers [129].

# Chapter 3

## Synthesis of chitosan-curcumin conjugate

- 3.1 Synthesis of Succinyl-Curcumin conjugate
- 3.2 Synthesis of chitosan succinyl curcumin conjugated prodrug
- 3.3 Structural identification of chitosan succinyl-curcumin conjugated prodrug
  - 3.3.1 Preparation of sample for UV-vis and Fluorescence spectroscopy
  - 3.3.2 Preparation of sample for FT-IR spectrum
  - 3.3.3 Preparation of sample for  $^1\text{H}$ -NMR
- 3.4 Results and discussions
- 3.5 Conclusions

### 3.1. Synthesis of Succinyl-Curcumin conjugate

Curcumin-monosuccinate (SUC-CCMN) was made by dissolving CCMN (0.7368g, 2 mmol) and succinic anhydride (0.2001 g, 2 mmol) in 30 ml of anhydrous benzene, adding 2 ml of pyridine, and refluxing the mixture for 24 hours at 80°C to cool it down (**Figure 3.1**). The solvent was extracted from the mixture after filtering it using low pressure and temperature. Using a mobile phase of hexane-ethyl acetate (95:5) and a stationary phase of silica gel (100-200 mesh size), the residue was subsequently refined by column chromatography to produce the final product SUC-CCMN (Yield = 0.32 g, 68.31%) [130].

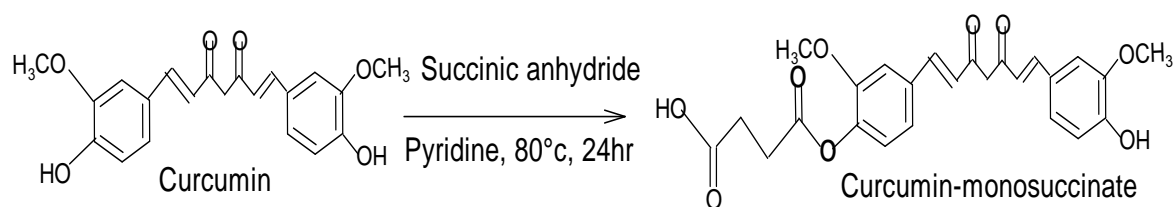


**Fig. 3.1:** Synthesis of Curcumin monosuccinate

### 3.2. Synthesis of chitosan succinyl curcumin conjugated prodrug

To synthesize chitosan di-succinyl curcumin (CHT-di(SUC-CCMN)) amphipathic prodrug conjugate, initially, in 20 ml DMSO 1.526 gm (1 mmol) carbohydrate polymer chitosan (CHT) and 0.936 mg (2 mmol) SUC-CCMN were dissolved at room temperature. After both compounds were dissolved entirely, 412 mg (2 mmol) *N,N'*-Dicyclohexylcarbodiimide (DCC) and 116 mg (1 mmol) 4-dimethylaminopyridine (DMAP) were added to the mixture while stirring continuously. This reaction was carried out in the absence of light for twenty-four hours at room temperature. The CHT-di(SUC-CCMN) conjugate was precipitated by filtering the product after the reaction was finished. The filtrate was added into a 50 ml solution containing a 1:1 (v/v) ratio of ethanol and ethyl ether to precipitate CHT-di(SUC-CCMN) conjugate. **Figure 3.2;** depicts the schematic processes for CHT-di(SUC-CCMN) synthesis.

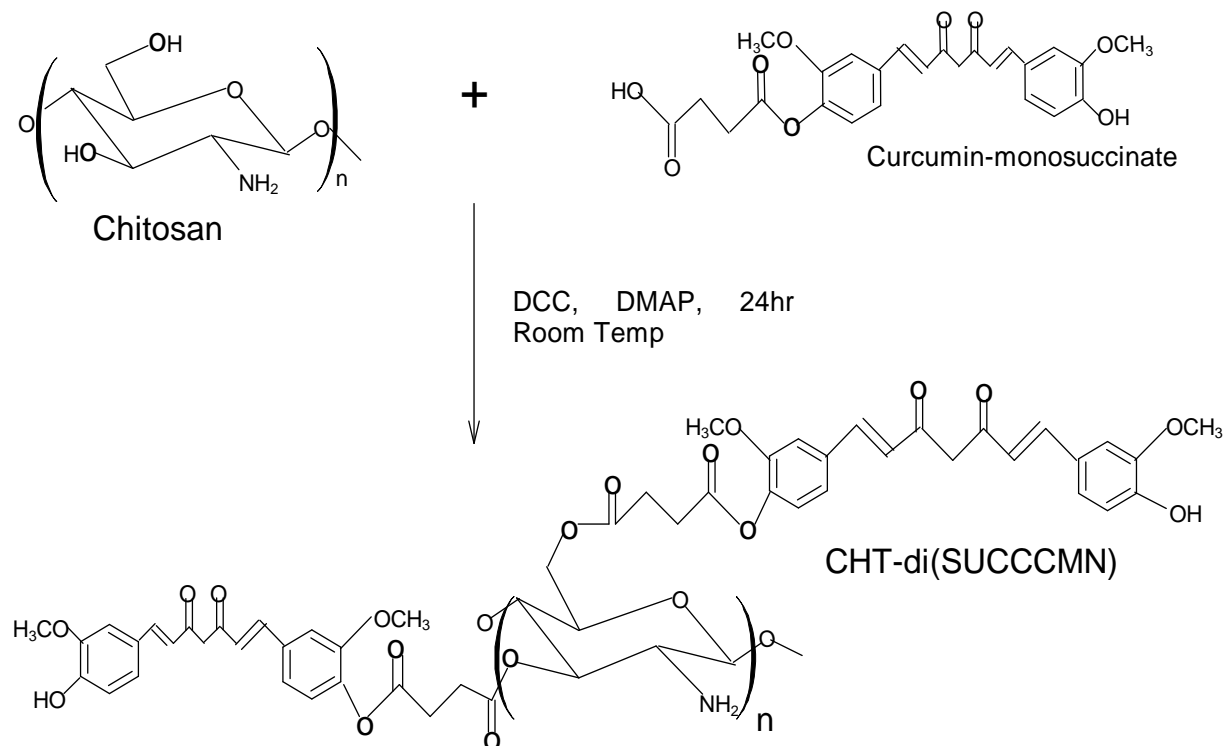


**Fig. 3.2:** Synthesis of chitosan succinyl curcumin

### 3.3. Structural identification of chitosan succinyl-curcumin conjugated prodrug

Multiple instrumental studies, such as an FTIR spectrophotometer (Shimadzu Corp No. 01988) with a spectrum range of  $4000\text{ cm}^{-1}$  to  $400\text{ cm}^{-1}$ ,  $^1\text{H-NMR}$  (Bruker-400 MHz spectrometer), and others, verified the structure of the synthesized CHT-di(SUC-CCMN). We used a fluorescence spectrophotometer (Hitachi F-4600, Japan) and a UV-vis spectrophotometer (Shimadzu, Japan) to measure the compounds' spectra from 200 to 700 nanometers. The solvent used for the analysis was DMSO- $d_6$ .

#### 3.3.1. Preparation of sample for UV-vis and Fluorescence spectroscopy

To generate concentrations of 0.5 mg/ml and 1.5 mg/ml, respectively, of CCMN and CHT-di(SUC-CCMN) conjugate, the two substances were dissolved in DMSO solutions. The mixtures were vortexed for 15 min to completely dissolve CCMN and CHT-di(SUC-CCMN), subsequently these were sonicated for 10 min, finally sample were diluted after filtration. The samples were subjected for peak absorbance spectra in UV-vis and fluorescence spectroscopy.

### 3.3.2. Preparation of sample for FT-IR spectrum

The powder form of CCMN, SUC-CCMN, CHT and CHT-di(SUC-CCMN) conjugate were taken into dehumidifier to completely remove moisture from sample. For IR spectra, FT-IR spectrophotometer (Shimadzu Corp No. 01988) was used.

### 3.3.3. Preparation of sample for $^1\text{H}$ -NMR

10 mg each of CCMN, SUC-CCMN, CHT and CHT-di(SUC-CCMN) conjugate were dissolved separately into DMSO- $d_6$  solvent, after sufficient time vortexes and sonication sample were filtered and degasified. Bruker-400 MHz spectrometers were used to get proton ( $^1\text{H}$ -NMR) spectra. The chemical shifts were recorded using parts per million (ppm) delta values, and the NMR solvent used was DMSO- $d_6$ .

## 3.4. Results and discussions

Both CCMN and CHT-di(SUC-CCMN) conjugate show peak absorbance at 427 nm (**Figure 3.3**), but conjugate shows a broader peak compared to the CCMN peak. The fluorescence emission spectral peak of CCMN and CHT-di(SUC-CCMN) shows at 550 nm and 522 nm, respectively, which help to conclude the formation of the conjugation within CHT and CCMN [131].

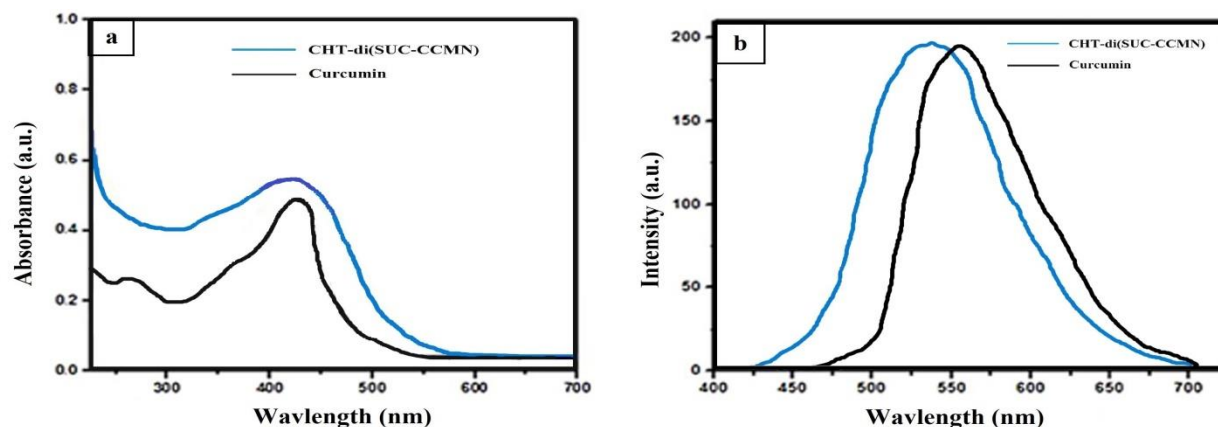


**Fig. 3.3:** (a) UV-vis and (b) Fluorescence spectroscopy of CCMN and CHT-di(SUC-CCMN)

Characteristic peaks of phenolic O-H stretching at 3507 cm<sup>-1</sup>, aromatic moiety C=C stretching at 1625 cm<sup>-1</sup>, benzene ring stretching vibrations at 1596 cm<sup>-1</sup>, C=O and C=C vibrations at 1504 cm<sup>-1</sup>, C-H bending vibrations of olefinic (>C=C<) bond at 1424 cm<sup>-1</sup>, and aromatic C-O bonding stretching vibrations at 1276 cm<sup>-1</sup> could be used to identify CCMN in its FT-IR spectrum [130,132,133].

A peak for aryl (C-H) stretching at 2942 cm<sup>-1</sup>, a peak for C=O stretching frequencies of a conjugated succinic acid moiety at 1697 cm<sup>-1</sup>, a peak for C=C of CCMN at 1627 cm<sup>-1</sup>, and a peak for stretching frequencies of the C=O and C-O (enol) groups of the CCMN moiety at 1510 cm<sup>-1</sup> and 1281 cm<sup>-1</sup> are all visible in the FT-IR spectrum of SUC-CCMN. Phenolic O-H stretching at 3505 cm<sup>-1</sup> and aryl (C-H) stretching at 2942 cm<sup>-1</sup> are also visible. The stretching frequencies of C-O-C are responsible for the peak at 1028 cm<sup>-1</sup>. Peaks at 3505 cm<sup>-1</sup>, 1697 cm<sup>-1</sup>, and 1510 cm<sup>-1</sup>, which correspond to the -OH, C=O, and C-O bands, respectively, indicate that CCMN has been successfully conjugated to SUC [130].

The CHT-di(SUC-CCMN) conjugate shows a new peak at 1735 cm<sup>-1</sup> in the FT-IR spectrum, which corresponds to the succinyl C=O group stretching frequency, and a peak at 1510 cm<sup>-1</sup> in the C-O (enol) bands stretching spectrum. Not only do CHT and SUC-CCMN show peaks, but those peaks also indicate the presence of a newly created ester link between the two compounds [132]. In the first step of the process, SUC-CCMN with a reactive carboxylic acid group is formed when succinic anhydride and CCMN react, as shown by the FTIR study. In the presence of pyridine, this acid group forms an ester bond with the hydroxyl group of CHT, resulting in the formation of CHT-di(SUC-CCMN) prodrug-polymer, as shown in the FTIR spectrum. One possible explanation for curcumin's improved solubility in CHT-di(SUC-CCMN) is that the carbonyl group (C=O) of curcumin and the hydroxyl group of chitosan create a weak hydrogen bond [134].

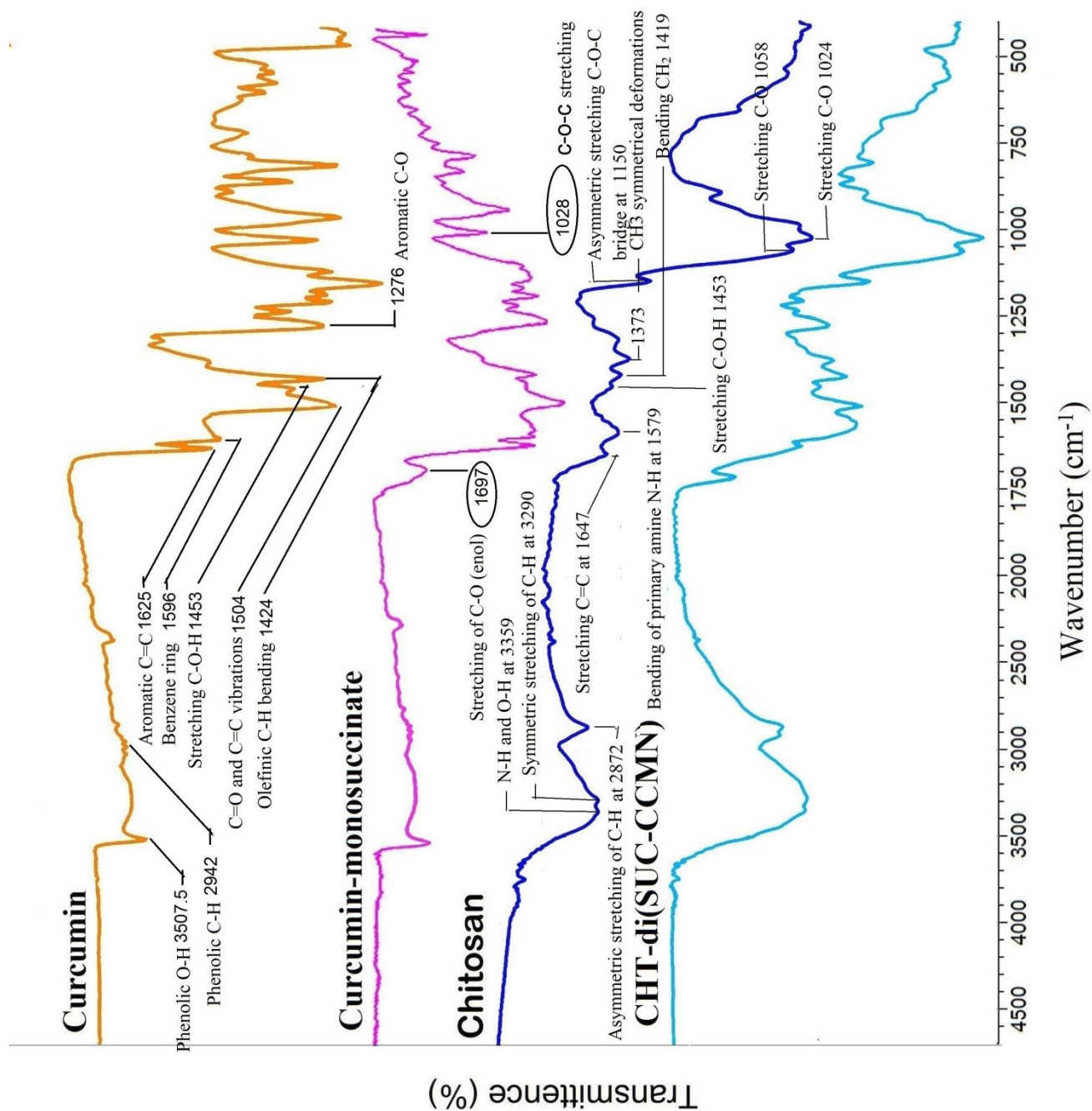


**Figure 3.4:** FT-IR Spectra of Curcumin, Curcumin-monosuccinate, Chitosan, and CHT di(SUC-CCMN)



**Table 3.1:** FT-IR spectrum Analysis

Compound	FT-IR spectrum Analysis	
Curcumin	Phenolic O-H stretching	3507 cm <sup>-1</sup>
	Phenolic C-H stretching	2942 cm <sup>-1</sup>
	Aromatic moiety C=C stretching	1625 cm <sup>-1</sup>
	Benzene ring stretching vibrations	1596 cm <sup>-1</sup>
	C=O and C=C vibrations	1504 cm <sup>-1</sup>
	Olefinic (>C=C<) C-H bending vibrations	1424 cm <sup>-1</sup>
	Stretching vibrations of the aromatic C-O	1276 cm <sup>-1</sup>
Succinyl-Curcumin	<b>Stretching phenolic of O-H</b>	<b>3505 cm<sup>-1</sup></b>
	Stretching of Aryl C-H	2942 cm <sup>-1</sup>
	<b>C=O stretching of conjugated succinic acid</b>	<b>1697cm<sup>-1</sup></b>
	Aromatic moiety C=C stretching	1627 cm <sup>-1</sup>
	<b>Stretching frequencies of C=O</b>	<b>1510cm<sup>-1</sup></b>
	Olefinic (>C=C<) C-H bending vibrations	1424 cm <sup>-1</sup>
	Stretching frequencies of C-O (enol)	1281 cm <sup>-1</sup>
	stretching frequencies of C-O-C	1028 cm <sup>-1</sup>
Chitosan	Stretching vibration of NH and OH	3359 cm <sup>-1</sup>
	Symmetric stretching of C-H	3290 cm <sup>-1</sup>
	Asymmetric stretching of C-H	2872 cm <sup>-1</sup>
	stretching vibration of C=C	1647 cm <sup>-1</sup>
	Bending vibration of the primary amine N-H	1579 cm <sup>-1</sup>
	Stretching vibration of C-O-H	1453 cm <sup>-1</sup>
	Bending vibration of CH <sub>2</sub>	1419 cm <sup>-1</sup>
	CH <sub>3</sub> symmetrical deformations	1373 cm <sup>-1</sup>
	asymmetric stretching of the C-O-C bridge	1150 cm <sup>-1</sup>
	Stretching of C-O	1058 and 1024 cm <sup>-1</sup>
Chitosan di-succinyl-curcumin (CHT-di(SUC-CCMN))	Stretching phenolic of O-H	3505 cm <sup>-1</sup>
	Stretching of Aryl C-H	2942 cm <sup>-1</sup>
	<b>stretching frequency of the C=O group</b>	<b>1735 cm<sup>-1</sup></b>
	C=O stretching of conjugated succinic acid	1697cm <sup>-1</sup>
	Aromatic moiety C=C stretching	1627 cm <sup>-1</sup>
	Olefinic (>C=C<) C-H bending vibrations	1424 cm <sup>-1</sup>
	Stretching frequencies of C-O (enol)	1281 cm <sup>-1</sup>
	stretching frequencies of C-O-C	1028 cm <sup>-1</sup>
Acetylated-Chitosan	C=O Stretching of amide (Impurity)	1645 cm <sup>-1</sup>
	C-N stretching of amide (Impurity)	1325 cm <sup>-1</sup>

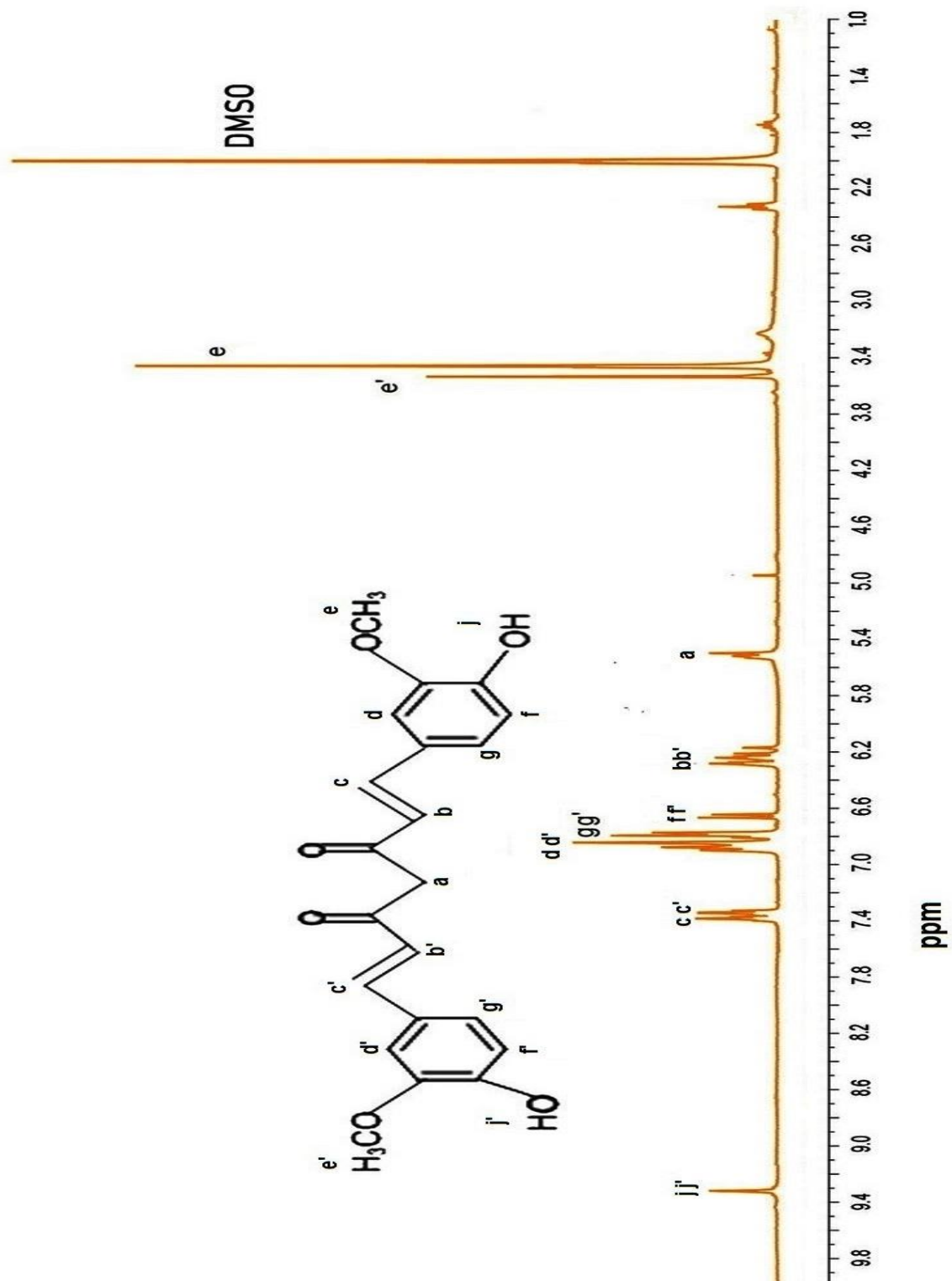
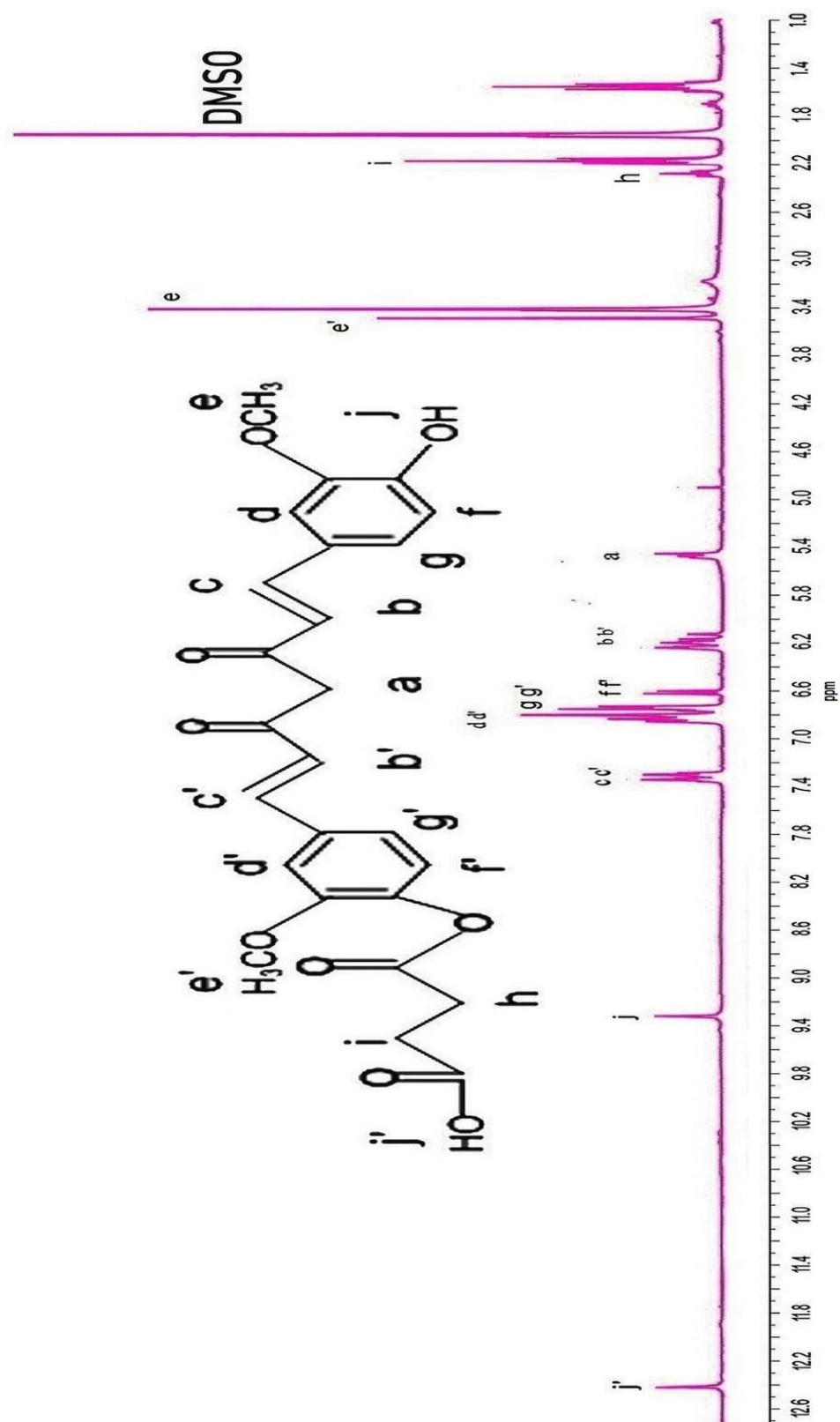
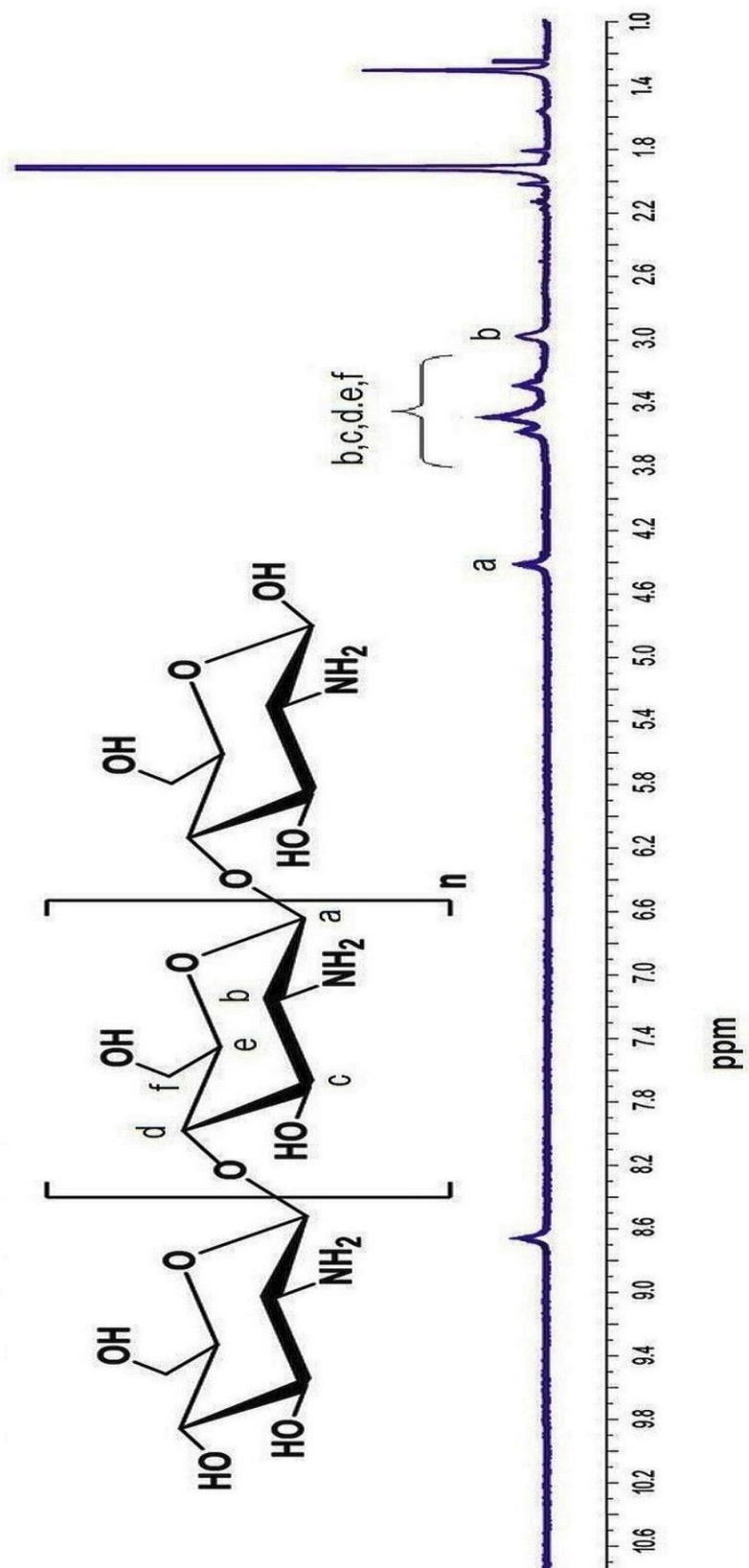


Figure 3.5:  $^1\text{H}$ -NMR of Curcumin

**Figure 3.6:**  $^1\text{H}$ -NMR of Succinyl-Curcumin

**Figure 3.7:**  $^1\text{H}$ -NMR of Chitosan

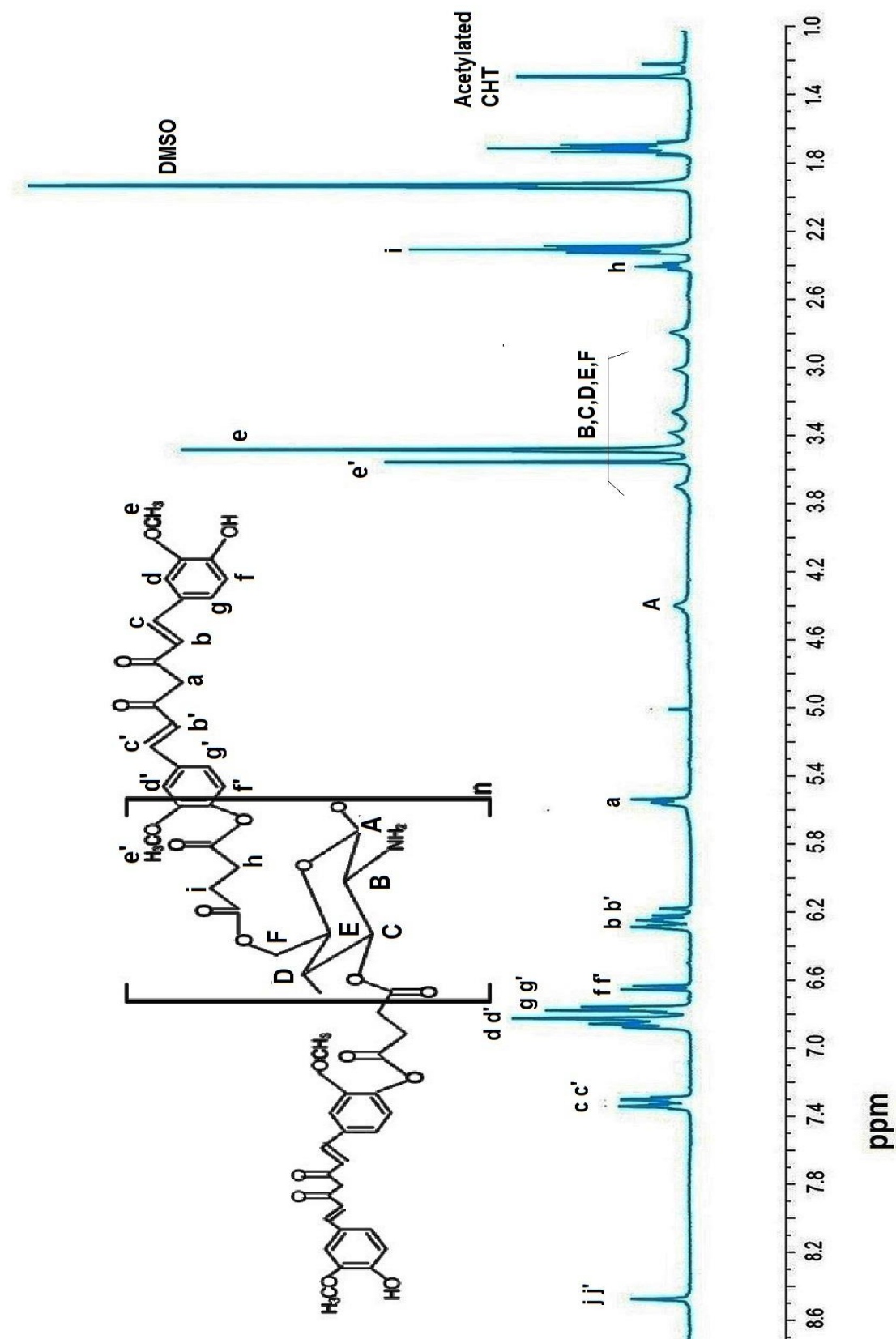
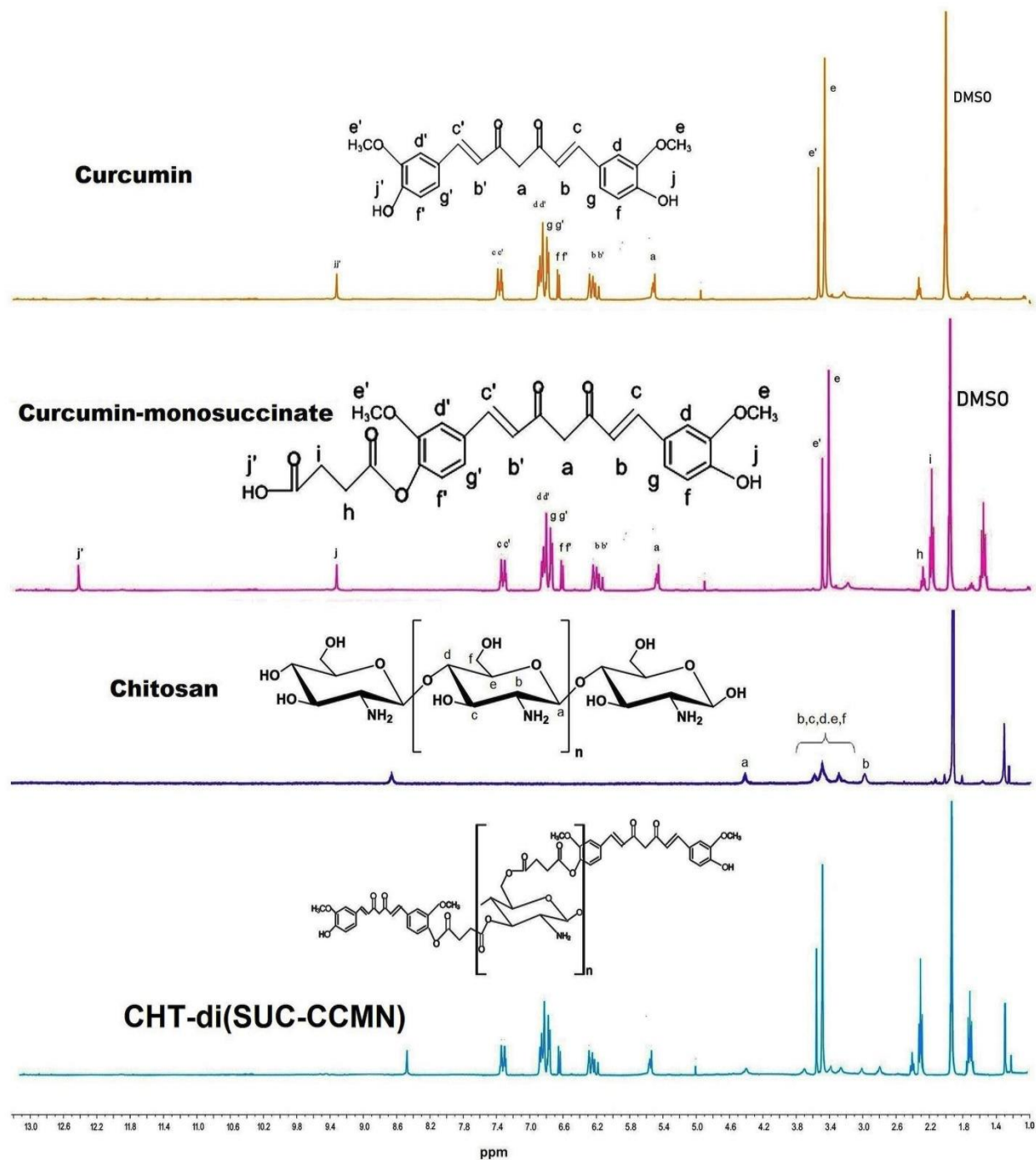


Figure 3.8:  $^1\text{H}$ -NMR of Chitosan di-succinyl curcumin



**Fig. 3.9:** <sup>1</sup>H NMR spectra of Curcumin, Curcumin-monosuccinate, Chitosan, and CHT-di(SUC-CCMN).

To assure the formation of the conjugated structure of CHT-di(SUC-CCMN), CHT, CCMN, and SUC-CCMN were initially analyzed through  $^1\text{H}$ -NMR spectroscopy. In **Figure 3.9**; it was observed that protons of CCMN show characteristic peaks between 5.4-9.4 ppm [135, 136]; CHT shows (**Figure 3.7 and 3.9**) its distinct peaks between 3.0-4.6 ppm for the protons of  $\beta(1-4)$ -D-glucosamine units [137] including peak at 1.3 ppm for the presence of acetylated chitosan impurities; SUC-CCMN shows (**Figure 3.6 and 3.9**) peak at 2.2 and 2.4 ppm for protons of  $-\text{CH}_2-\text{CH}_2-$  (Succinyl moiety) including the peaks at 9.4 and 12.5 ppm for the  $-\text{OH}$  protons of CCMN and succinyl moiety respectively in addition to peaks of CCMN (**Figure 3.5 and 3.9**). CHT-di(SUC-CCMN) conjugate exhibits its peaks (**Figure 3.8 and 3.9**) consisting of characteristic peaks of CHT (3.0-4.6ppm), CCMN (5.4-9.4ppm), and succinyl (2.0 and 2.5 ppm) moiety excluding the peaks 12.5ppm of succinyl moiety  $-\text{OH}$  proton were demonstrated the successful synthesis of desire conjugate [132, 136, 138]. Analysis of the CHT-di(SUC-CCMN) conjugate by  $^1\text{H}$ -NMR confirmed its successful synthesis. The characteristic peaks of CCMN, CHT, and SUC-CCMN were evident in their respective spectra. Notably, the conjugate's spectrum displayed peaks from all constituents except the  $-\text{OH}$  proton of the succinyl moiety. The absence of succinyl moiety  $-\text{OH}$  proton peaks 12.5ppm and the presence of all other expected peaks strongly supported the construction of the designed conjugate.

### 3.5. Conclusions

In this study, initially succinyl-curcumin was synthesized and purified through column chromatography, after purification it was reacted with chitosan to produce CHT-di(SUC-CCMN) conjugate. We used UV-vis, fluorescence, FT-IR, and  $^1\text{H}$ -NMR spectroscopy to examine curcumin, succinyl-curcumin, chitosan, and CHT-di(SUC-CCMN). The results show that the polymer chitosan and the medicine curcumin were chemically linked. It was observed that the conjugate was readily soluble in both an aqueous and an organic solvent. After conjugation, the lipophilic compound CCMN and the hydrophilic polymer CHT form an amphiphilic conjugate.



# Chapter 4

## Preparation and Characterization of Curcumin nanomicelles

- 4.1** Introduction
- 4.2** Preparation of conjugated and free curcumin containing nanomicelle (CDSCM-CCMN)
- 4.3** Determination of Drug loading and entrapment efficacy
- 4.4** CCMN release study from CDSCM-CCMN
- 4.5** Stability of CDSCM-CCMN containing CCMN in physiological conditions
- 4.6** Determination of Critical micelle concentration of CDSCM-CCMN
- 4.7** Blood compatibility
- 4.8** Characterizations of CDSCM-CCMN
  - 4.8.1 Measurement of zeta potential and hydrodynamic particle size of CDSCM-CCMN
  - 4.8.2 Differential Scanning Calorimetry
  - 4.8.3 X-Ray diffraction
  - 4.8.4 SEM, TEM and AFM
- 4.9** Results and discussions
- 4.10** Conclusions

### 4.1. Introduction

In this study, we have prepared the nano-micelles of amphipathic polymer pro-drug, initially by chemical conjugation of curcumin and chitosan via succinyl linker and subsequently dialysis of amphipathic polymer pro-drug in free CCMN containing DMSO solvent was done. Chitosan, a biopolymer known for its biocompatibility, biodegradability, and ability to form gel-like structures in acidic conditions, is utilized in drug delivery applications. Chitosan, with its glucosamine unit containing hydroxyl and amine groups, enables the conjugation of many drugs and other substances. This property can improve the drug's solubility, stability, and toxicity and facilitate the delivery of the drug to specific cells or tissues [139-141]. CCMN has several beneficial medicinal effects, such as those against viruses, inflammation, cancer, wounds, and diabetes.

However, due its inadequate aqueous solubility, rapid hydrolytic degradation and hence low bioavailability, clinical application has been greatly declined. So to overcome the CCMN associated problems and subsequently to improve therapeutic activity we follow molecular conjugation technique. The succinic anhydride was used as to form breeze between CHT and CCMN to form amphipathic polymer pro-drug conjugate. This conjugate will be converted to nanomicelles in an aqueous environment, which may aid in increasing CCMN solubility and stability.

### 4.2. Preparation of conjugated and free curcumin containing nanomicelle (CDSCM-CCMN)

By carefully combining 1 mg/ml of free CCMN-containing DMSO solution with 1 mg/ml of CHT-di(SUC-CCMN), conjugated curcumin and free curcumin containing nanomicelle were generated. After that, a dialysis bag containing the CHT-di(SUC-CCMN) and CCMN combination was immersed in double-distilled water for 24 hours, with the water being replaced every 4 hours. The molecular weight of the mixture containing dialysis membrane was 12 kDa. During the chemical process, the solvent was still present, but other components were removed via dialysis. After dialysis, the filtrate was passed through a filter with a pore size of 0.45  $\mu\text{m}$  to eliminate any bigger particles, and then it was lyophilized (**Figure 4.1**). For later use, the final micelles (CDSCM-CCMN) were kept dry and cold [142,143]. About 88.35% of CDSCM-CCMN was yielded.

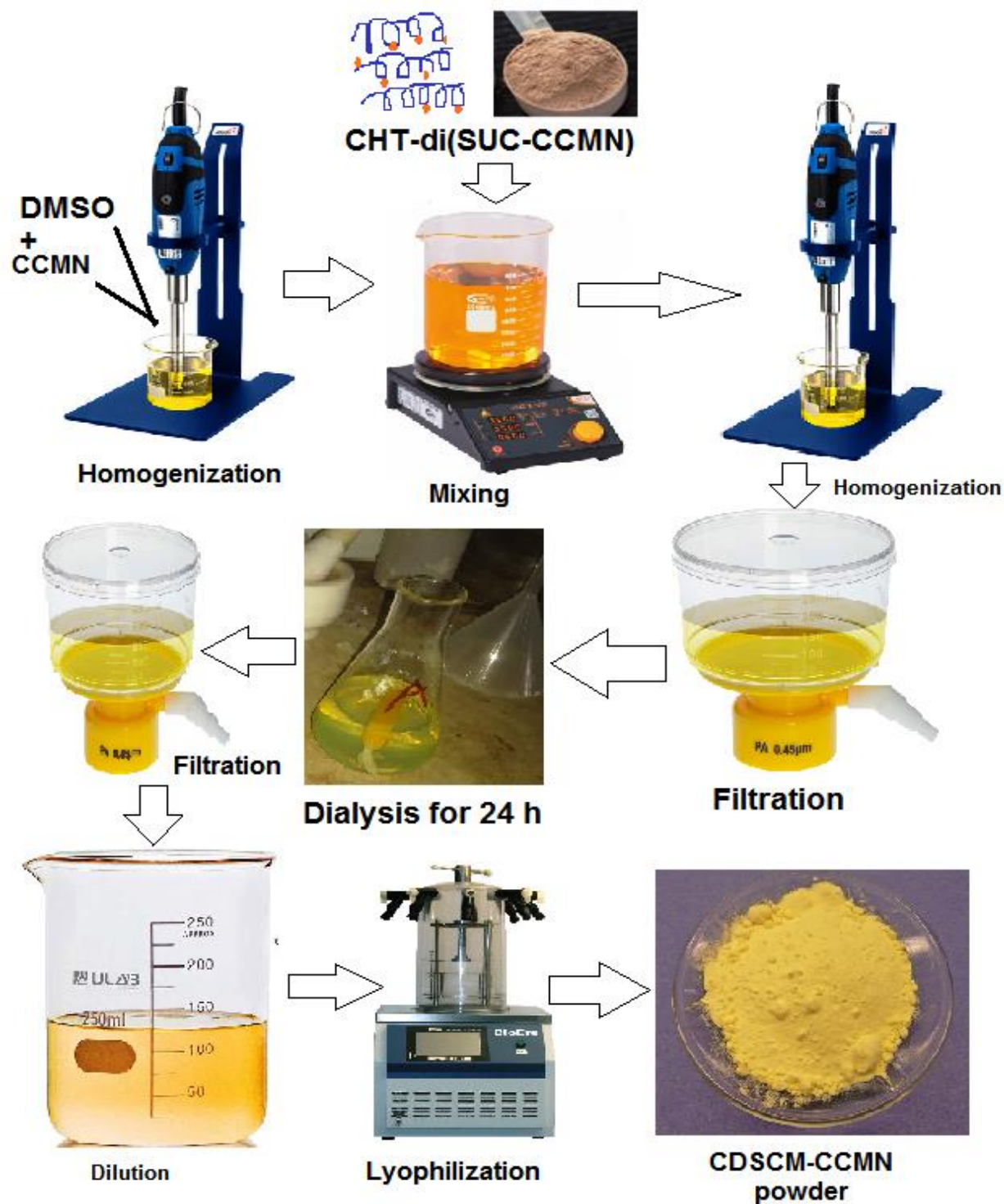


**Fig. 4.1:** Schematic presentation of CDSCM-CCMN formation

### 4.3. Determination of Drug loading and entrapment efficacy

A specified high concentration of CCMN stock solution was generated; from the stock solution, various concentrations of CCMN solution were prepared with DMSO solvent, according to the serial dilution procedure, in order to prepare a standard curve with its equation of free CCMN. **Figure 4.2;** displays the equation for the standard curve that was created by plotting the absorbance of each diluted solution against its corresponding concentration at 435 nm. The micelle's amphipathic molecular unit disappeared as CHT and CCMN separated, revealing the solution-bound micelle core components. Because of this, we were able to disrupt the micelle structure by employing powerful HCl, which facilitates the acid hydrolysis of the ester linkages between CHT and CCMN.

In order to assist the acid hydrolysis of the ester linkages that connect CHT and CCMN and enable micelle assembly, a 2 mg/ml concentration of CDSCM-CCMN was prepared with 2N HCl. The mixture was then incubated at 50°C for 1.5 hours. Methanol was added to the sample solution to make 1000 parts per million. Prior to filtering via a 0.22μ membrane, it underwent a 10-minute sonication. Centrifuged at 5000 rpm for 15 minutes followed drying the filtrate to a powder and reconstituting it with DMSO solvent. Afterwards, 10 milliliters of the supernatant was diluted. To determine the percentage of CCMN degradation in 2N HCl, a known concentration of CCMN was produced and treated as previously mentioned. Drug loading efficacy (DEE) and drug loading (DL) were examined through absorption.

$$\text{CCMN loading capacity } \left( \frac{w}{w} \% \right) = \frac{\text{Amount of CCMN}}{\text{Amount of CDSCM} - \text{CCMN}} \times 100 \quad \dots \dots \text{Eqn1}$$

### 4.4. CCMN release study from CDSCM-CCMN

In CDSCM-CCMN, one form of CCMN having in conjugated with CHT through pH-sensitive succinyl ester bonds and another free form of CCMN has in the micelle core. After acid hydrolysis breaking of CDSCM-CCMN both form of CCMN release as free form in the buffer solution. Continuous CCMN emissions from CDSCM were studied in phosphate buffer saline (PBS) at pH 5.0 and 7.4. Each PBS solution with a pH of 5.0 or 7.4 was given 10 milligrams of CDSCM-CCMN.

Each solution was transferred into a separate dialysis bag and then placed into a 90 ml beaker containing its corresponding buffer solution. Gently shaken at 37°C for seven days was the incubation temperature for them. Two milliliters (ml) of the sample were taken out of each beaker during the incubation period and replenished with the appropriate buffer at progressively longer intervals [144]. After proper dilution and filtration of withdrawn sample from both buffer solutions, they were subjected to UV-Vis spectrophotometric analysis at 427nm. The cumulative percent release of CCMN shown in **Figure 4.3**.

#### **4.5. Stability of CDSCM-CCMN containing CCMN in physiological conditions**

After an incubation time at 37°C, the stability of both free CCMN and CDSCM-CCMN containing CCMN were tested in a PBS buffer with a pH of 7.4. The absorption measurements were made using a UV-Vis spectrophotometer at 427 nm. Both compounds' absorbances were measured and visually represented as a function of time in their physiological conditions [145].

#### **4.6. Determination of Critical micelle concentration of CDSCM-CCMN**

Critical micelle concentration (CMC) signifies a concentration at which the amphiphilic polymeric compound can self-assemble into micelles in the solvent. The CMC of CDSCM-CCMN was determined by employing the self-quenching agent pyrene as the fluorescence probe in an aqueous medium, and it helps to produce fluorescence for the presence of a lipophilic part of the micelles core. Here CDSCM-CCMN at low concentration breakdown into CHT-di(SUC-CCMN) amphipathic polymer pro-drug molecule and free CCMN, but upon increasing the concentration of CDSCM-CCMN at certain concentration it again form micelle structure. In order to find the CDSCM-CCMN CMC, diluted fluorescent probe pyrene solution was vortexed with CDSCM-CCMN solutions varying in concentration from 0.004 mg/ml to 2.5 mg/ml. The mixture was left overnight to record fluorescence using a fluorescence spectrophotometer (Infinite M200, TECAN); this study was carried out at 390 nm emission [146].

#### 4.7. Blood compatibility

A hemolysis research used a blood sample from a nearby blood bank to track the hemocompatibility of CDSCM-CCMN. The blood sample was centrifuged for five minutes at 2000 rpm in order to extract the red blood cells. Three PBS buffer washes were performed on the obtained RBCs. A mixture of 10 ml PBS (pH 7.4) and 100  $\mu$ l washed RBC was used to create the stock RBC solution. A range of CDSCM-CCMN concentrations, from 0.5 to 2 mg/ml, were created using stock RBC solutions and the solutions were incubated at 37 °C for 30 minutes in order to measure the hemoglobin release from RBC by CDSCM-CCMN. Next, separate solutions should be centrifuged for five minutes at 1500 rpm to extract the supernatant for UV-Visible absorbance measurement at 541 nm [147, 148]. Distilled water was used as the positive control and PBS pH 7.4 solutions as the negative control. Using the equation below, the hemolysis percentage (Hp%) of CDSCM-CCMN was calculated:

$$Hp\% = \frac{As - An}{Ap - An} \times 100 \quad \dots \dots \dots Eqn2$$

Where As is the sample absorbance, An is the PBS buffer absorbance, and Ap is the distilled water absorbance. We took three separate readings for each parameter.

#### 4.8. Characterizations of CDSCM-CCMN

Zeta Sizer (Nano-ZS 90, Malvern Instrument, UK), field emission scanning electron microscope (FE-SEM), and HR-TEM (JEOL Japan, JEM-2100 Plus) were utilized to determine the morphology of CDSCM-CCMN.

##### 4.8.1. Measurement of zeta potential and hydrodynamic particle size of CDSCM-CCMN

Adding 10 mg of CDSCM-RSV to a 10 ml solution of 10 mM NaCl and vortexing for 10 minutes allowed us to measure the average hydrodynamic particle size and zeta potential of the nanoparticles. The mixture was passed through 0.45  $\mu$ m and 0.2  $\mu$ m filter before analysis through Zeta Sizer.

#### **4.8.2. Sample preparation for differential scanning calorimetry**

Using a differential scanning calorimeter (DSC 6000, Perkin Elmer, USA), the melting endotherms of the physical mixture, CCMN, and pure sample CDSCM-CCMN were determined. An indium standard was used to calibrate the instrument before analysis approximately 15 mg of CDSCM-CCMN, a physical combination, and CCMN, weighed exactly, were added to a 50  $\mu$ L aluminum sample pan for individual analysis. Afterwards, the pan was covered. A nitrogen gas flow rate of 50 ml/min was used to heat the sample pan from 0 to 500°C at rates of 1 and 10 °C/min, respectively. In line with the experimental plan, we adjusted the heating rate and end temperature. Using the Pyris™ Manager program (Perkin Elmer, USA), the melting endotherm of CDSCM-CCMN, physical mixture, and CCMN were recorded.

#### **4.8.3. Sample preparation for X-Ray diffraction**

The presence of CCMN crystals in the samples was assessed using X-Ray diffraction (XRD) analysis. We used a quartz standard to calibrate the XRD (Shimadzu 6000, Shimadzu Corporation, Kyoto, Japan) before we began the study. To make the surface of the glass container for examination smooth and level, the drug-polymer dispersions were evenly distributed and spread out. At room temperature, a CuK monochromatic radiation source that generated X-rays with a 40 kV production voltage and 30 mA current was used to examine the samples. A continuous  $2\theta$  range of 10-80° was scanned at a speed of two degrees per minute, with a scan step of 0.02 degrees, in order to acquire diffraction patterns of the samples.

#### **4.8.4. Sample preparation for FE-SEM, TEM and AFM**

To further understand the structure of CDSCM-CCMN, FE-SEM, TEM, and AFM were employed. The FE-SEM sample was prepared by mixing 1 milliliter of double-distilled water with 1 milligram per milliliter of lyophilized CDSCM-CCMN powder. On create the thin film; the dispersion was then applied on an aluminum sheet. After being allowed to air dry, the film was coated in gold and examined using FE-SEM.

For better morphological evaluation, Transmission Electron Microscopy (TEM) study was done. One way to create TEM samples is to use a carbon-coated copper grid and drop 0.001 mg/ml CDSCM-CCMN dispersion onto it.



Individual CDSCM-CCMN nanomicelles and groups of CDSCM-CCMN nanomicelles can be seen with the atomic force microscope (AFM), which provides three-dimensional imaging in contrast to conventional microscopy methods. After being appropriately diluted in deionized water, the nanoparticles were ultrasonicated for fifteen minutes. A stream of nitrogen was used to blow the leftover solution after 50  $\mu\text{l}$  of the dilution was applied to a cleaned substrate and incubated for ten to fifteen minutes, depending on the needed particle density. We used this general procedure on every sample.

#### 4.9. Results and discussions

The results of the UV-Vis spectrophotometric examination were discovered in terms of absorbance, and standard curve formulae were used to convert the results into terms of concentration. After calculating the data using Equation 1, it was discovered that the entrapment efficacy was  $90.84\% \pm 1.14$  w/w and the loading percent of CCMN in CDSCM-CCMN was  $36.87\% \pm 0.62$  w/w.

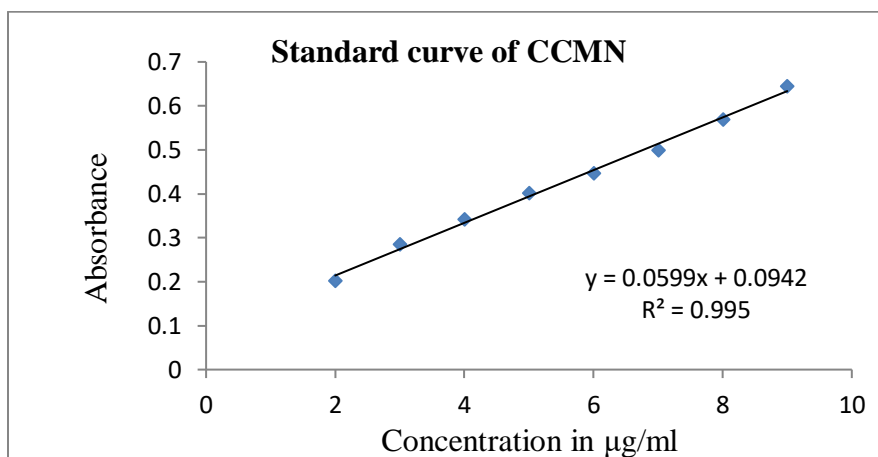


**Fig. 4.2:** Calibration curve of CCMN

As seen in **Figure 4.3**; the CCMN release pattern from CDSCMs was studied at both acidic pH 5.0 and neutral (physiological) pH 7.4. In an acidic (pH 5.0) state, 97% of CCMN was seen to be released from CDSCM-CCMN within 7 days, while 49% of CCMN was released from CDSCM-CCMN within the same time in a physiological pH 7.4 condition. The complete drug release was observed after 9 days of study in acidic pH 5.0. The higher release rate of CCMN in the acidic medium in compare to the basic medium is due to the acid-catalyzed hydrolysis of the ester linkage [149].



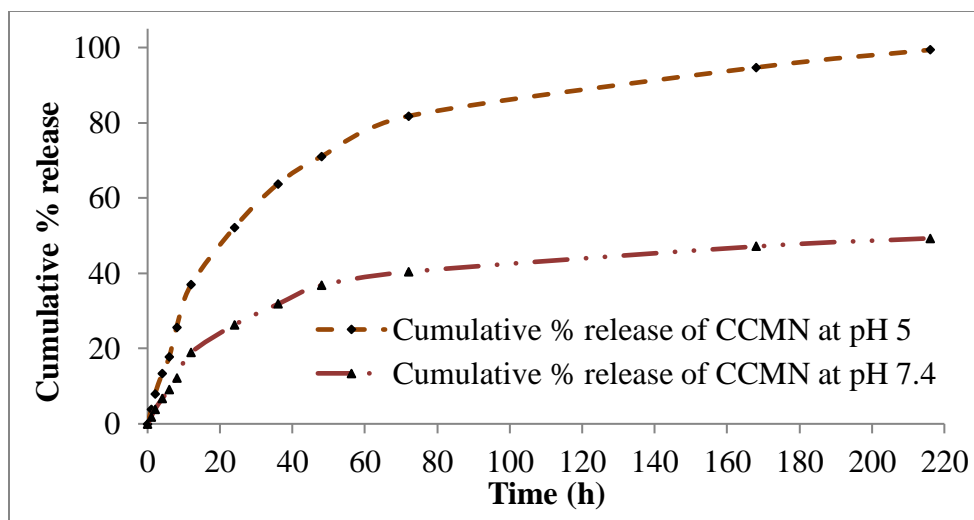


**Fig. 4.3:** CCMN release nature from CDSCM-CCMN

The percentage remaining to degrade was calculated and presented in **Figure 4.4**. It was observed that free CCMN was about to degrade entirely after 8h, while more than 90% of CCMN in CDSCM-CCMN was still present at the same time. It was found that conjugated CCMN exist in CDSCM-CCMN are much more stable than free CCMN. So nanomicelles developed by conjugation of CCMN with CHT significantly improve CCMN stability.

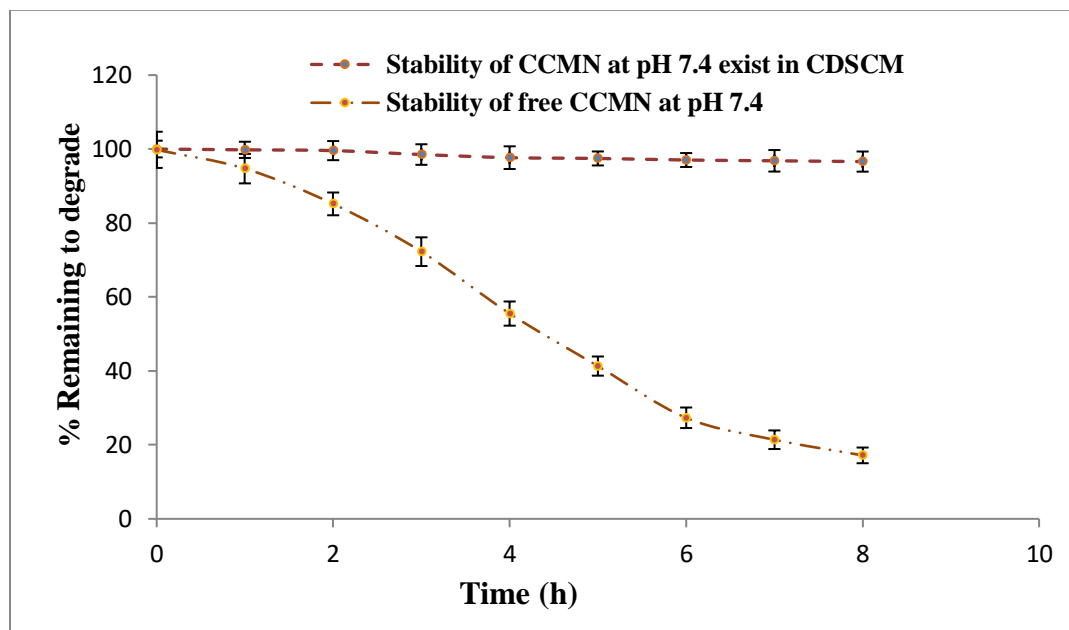


**Fig. 4.4:** Stability of CDSCM-CCMN containing CCMN

The intensity ratio of pyrene's (I335/I332) peaks depends on the medium's polarity [150,151]. The fluorescence intensity changed rapidly when pyrene transited from hydrophilic media to the lipophilic core of CDSCM-CCMN. Plotting of logarithm concentration of CDSCM-CCMN vs. intensity ratio constructs two straight lines intersecting at a point known as CMC was 0.4836 mg/ml (**Figure 4.5**). Lower CMC values signify its stability, prolonging blood circulation, and accessible to the targeting of the drug [152].

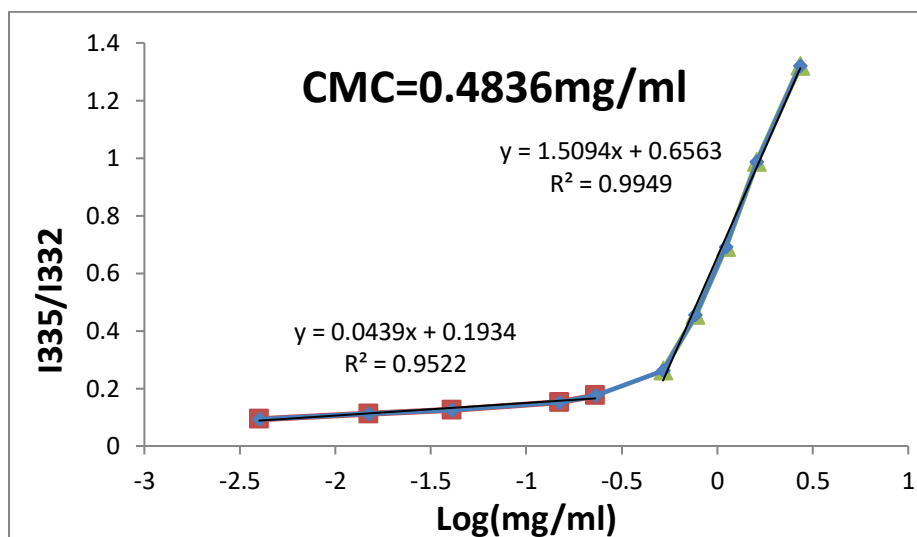


**Fig. 4.5:** Determination of Critical Micelle Concentration of CDSCM-CCMN

After sufficient time of incubation of CDSCM-CCMN with RBC, it was observed that around 2.0 % of hemoglobin was released at the highest concentration of CDSCM-CCMN (2 mg/ml), as shown in **Figure 4.6**. This signifies that the nano-formulation CDSCM-CCMN was compatible with RBC and blood, so it can be applicable through intravenous administration.

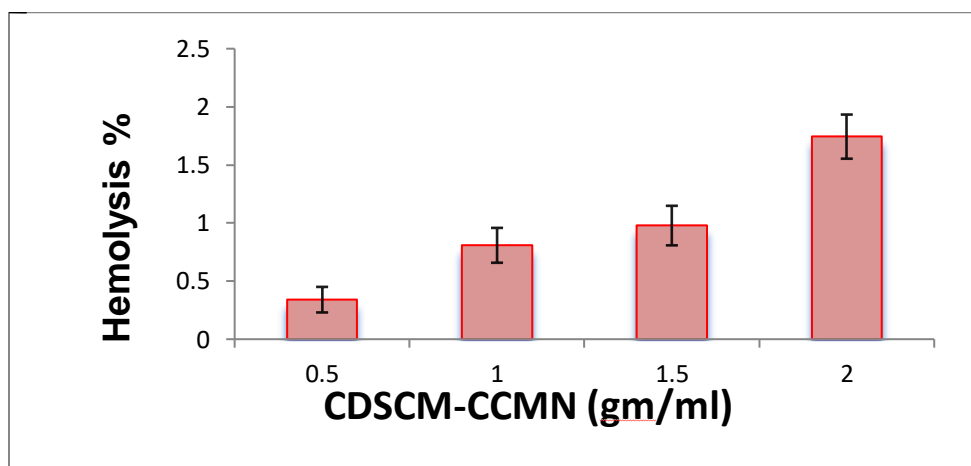


**Fig. 4.6:** Hemolysis of CDSCM-CCMN

The zeta potential and hydrodynamic particle size of the CDSCM-CCMN were determined by means of dynamic light scattering (DLS). **Figure 4.7;** displays the hydrodynamic particle size distribution of CDSCM-CCMN, while **Figure 4.8;** displays the zeta potential. The zeta potential of CDSCM-CCMN was around -19.72 mV, indicating a strong negative charge, while the average hydrodynamic particle size was approximately  $109.7 \pm 17.9$  nm. It was found that the polydispersity index of the micelle was 0.19, which signifies the homogeneity of micelle size. This negative charge is caused by the presence of unbound hydroxyl (-OH) groups in the glucosamine units of the CHT exist on the surface of CDSCM-CCMN. This accumulation of hydroxyl groups results in the formation of a highly negatively charged CDSCM-CCMN surface. This negative charge serves to maintain the micelle's stability. Higher negative surface charges repel each CDSCM-CCMN from the other, thereby reducing nanomicelle accumulation [153].

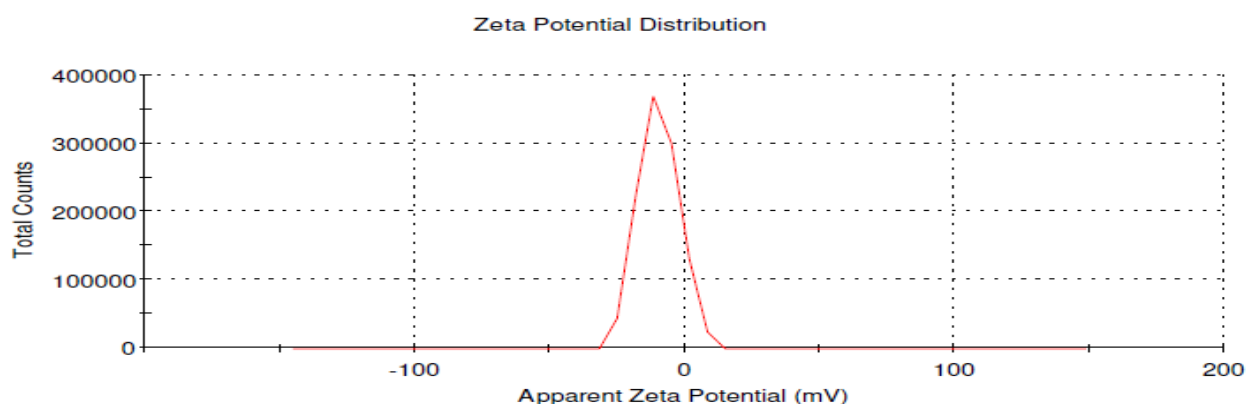


**Fig. 4.7:** Zeta Potential of CDSCM-CCMN

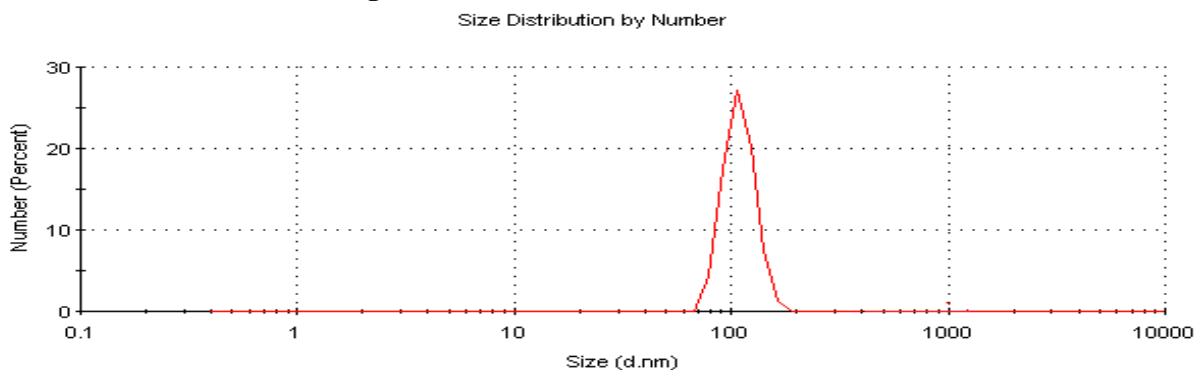


**Fig. 4.8:** Hydrodynamic particle size of CDSCM-CCMN

**Figure 4.9;** depicted the differential scanning calorimetry (DSC) thermograms of the physical mixture, pure CCMN and CDSCM-CCMN. Around 183°C, when the CCMN melting point is

found, the clear endothermic peak of CCMN emerged. Less intensely, the drug endothermic peak also observed about 180°C on the physical mixture curve. In the physical mixture, each peak matched its intrinsic melting point. The CCMN and physical mixture showed some similarities to the free CCMN, so it concluded that the physical mixture system was only blended and components are crystalline. As a result, the presence of the CCMN melting peak in the physical mixture may also indicate that the system did not form an amorphous state. Totally disappearance of CCMN peak in the thermograms of CDSCM-CCMN, it indicated that the polymer nanomicelle was amorphous and evenly distributed throughout the micelle. According to the DSC data, CCMN was effectively distributed throughout the micelle and was present in an amorphous form. Therefore, no amorphous state formed in this system due to the presence of the CCMN melting peak (less intense) in the physical mixture.

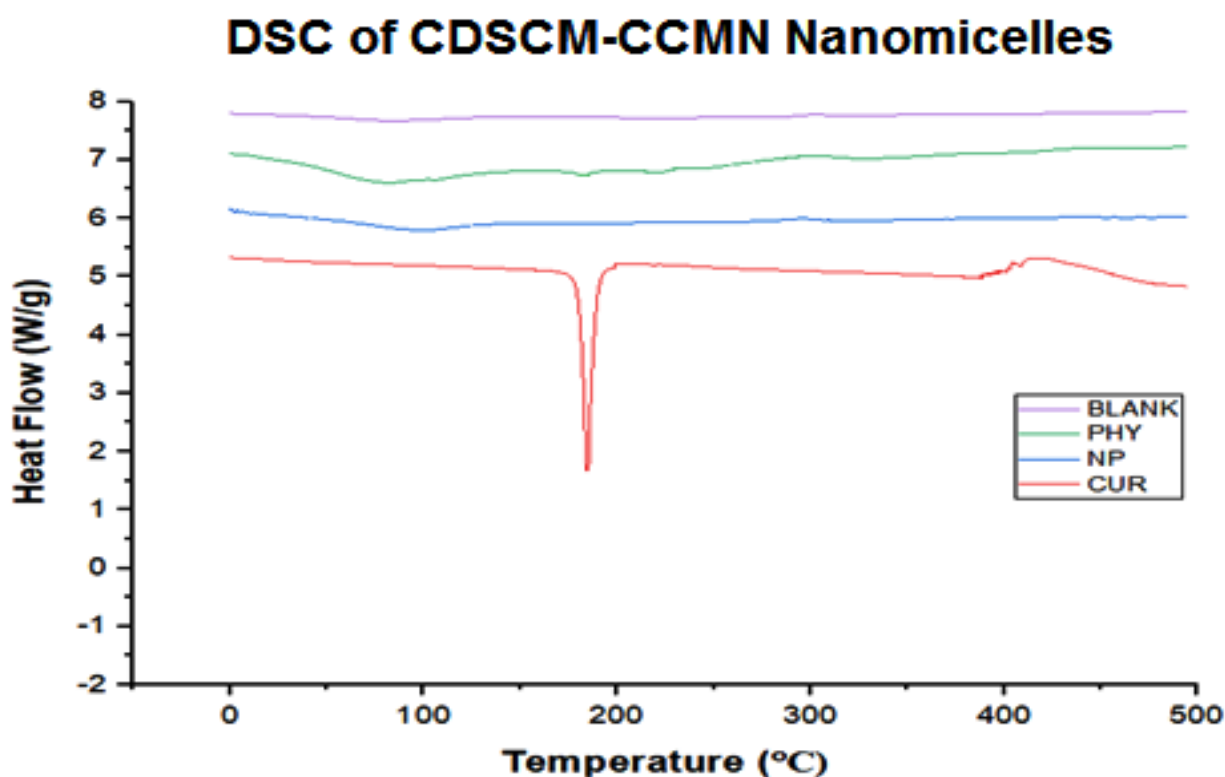


**Figure 4.9:** DSC thermogram of CDSCM-CCMN (NP), Physical mixture and CCMN

**Fig. 4.10;** displayed the XRD patterns of CDSCM-CCMN, physical mixtures, and pure CCMN. The remarkable crystallinity of CCMN can be explained by the multiple extremely sharp peaks shown in the XRD spectrogram. Curcumin's distinctive peaks could also be seen, albeit less

clearly, in the physical mixture's diffraction pattern. In the XRD spectrogram, the physical mixture had some, but not all of the distinctive peaks of CCMN appeared because of the high concentration of carriers relative to CCMN. These findings showed that there was still some CCMN in the physical combination in the crystalline form. The CDSCM-CCMN showed a significant difference from those of pure CCMN and the physical mixture; the CCMN peaks entirely vanished, indicating the presence of an amorphous state of CCMN in the CDSCM-CCMN.

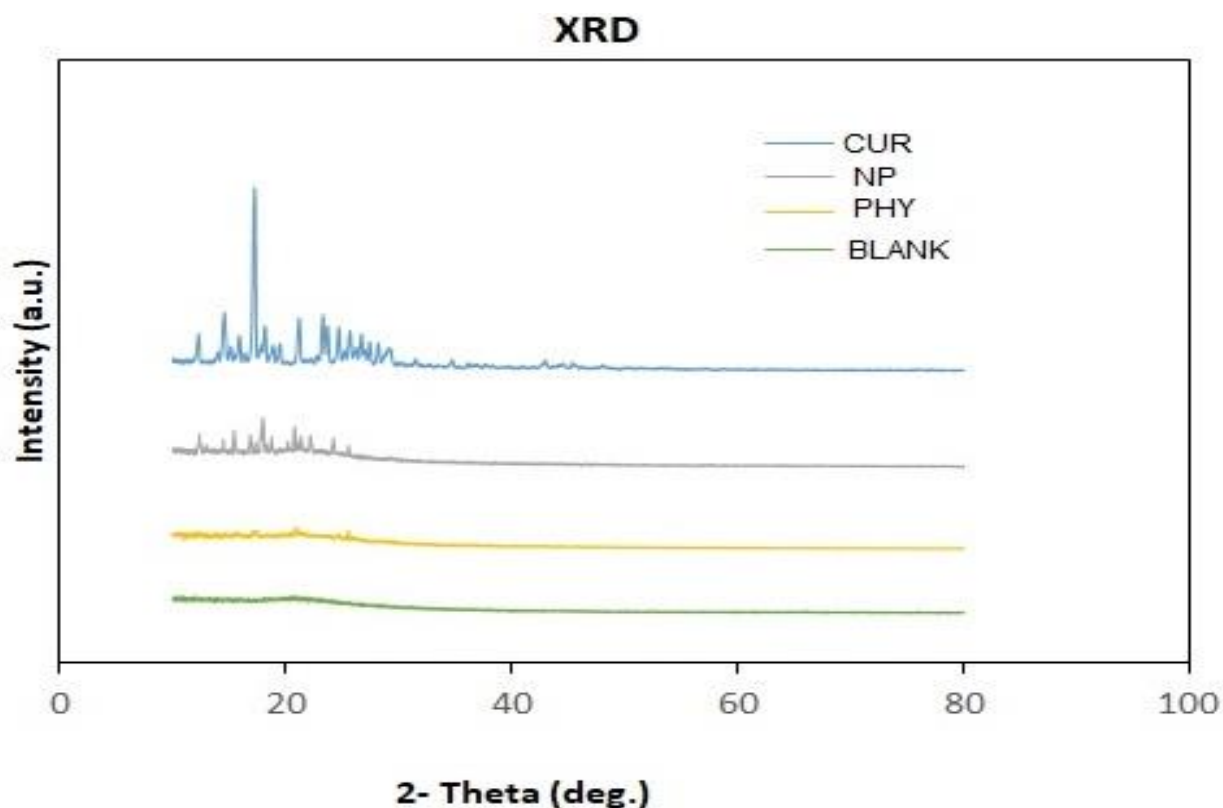


**Fig. 4.10:** XRD of CDSCM-CCMN (NP), Physical mixture and CCMN.

From the image as shown in **Figure 4.11**; it indicates that CDSCM-CCMN was roughly spherical and mostly uniform in size. The shape of the particle is distinguishable.

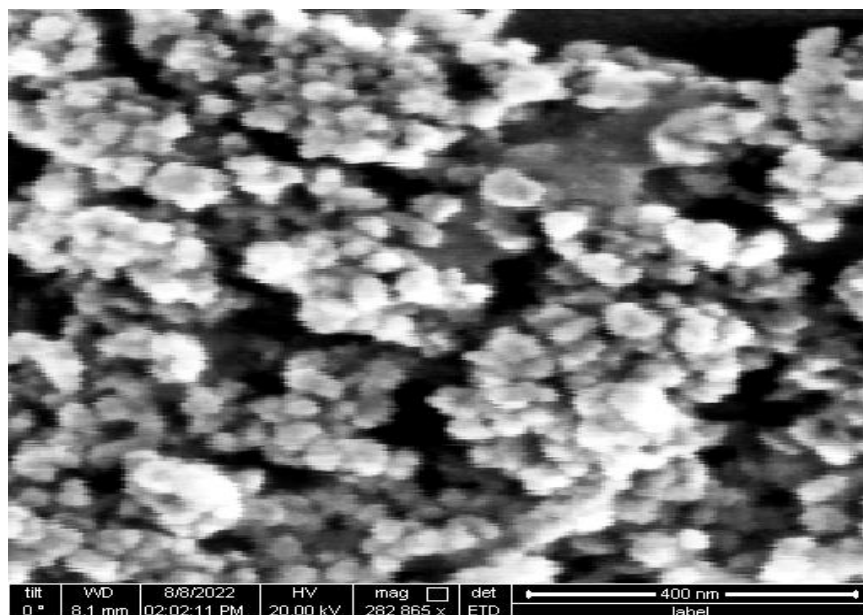


**Fig. 4.11:** FE-SEM of CDSCM-CCMN

The TEM image as shown in **Figure 4.12**; it shows that the CDSCM-CCMN was spherical in shape and within the size range of 50-150 nm.

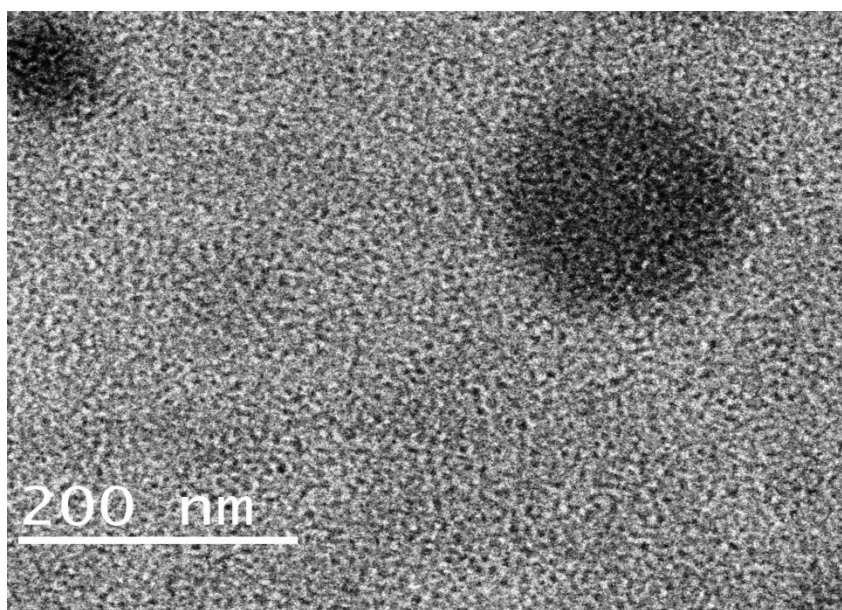


**Fig. 4.12:** TEM of CDSCM-CCMN

In this investigation, the nanomicelles were detected in each AFM measurement by setting the scan area with less than 20 nm/pixel resolution. Even if we see nanomicelles in this state,



measuring their sizes is unaffected. The thermal noise method was used to calibrate the cantilever's spring constant before any data was taken. Following this, automated particle analysis and cross-sectional line profiling were used to study the nanoparticles' area-equivalent diameter and height, correspondingly. The average diameters of the CDSCM-CCMN nanomicelles in an aqueous solution were satisfactorily quantified by AFM cross-sectional line profiling (**Figure 4.13 and 4.14**). Our research clarifies the need for standardizing AFM to assess the dimensions and morphology of nanomicelles.

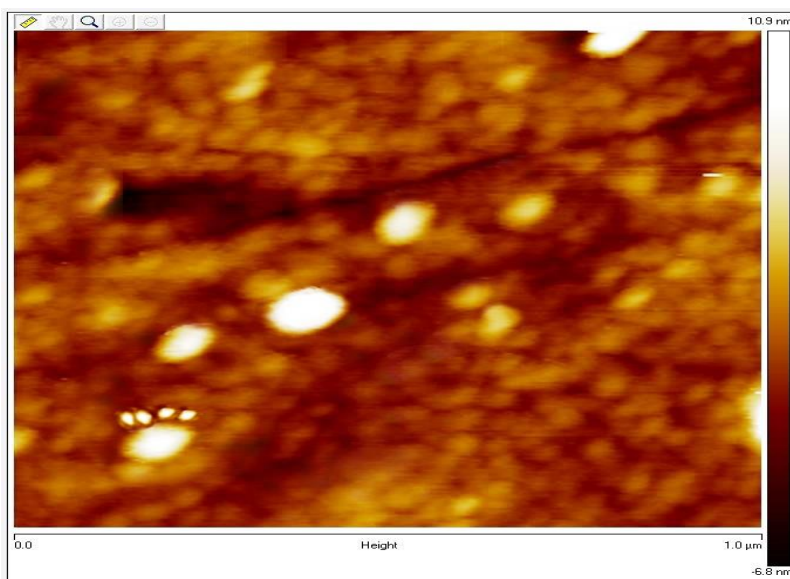


**Figure 4.13:** 2d AFM of CDSCM-CCMN

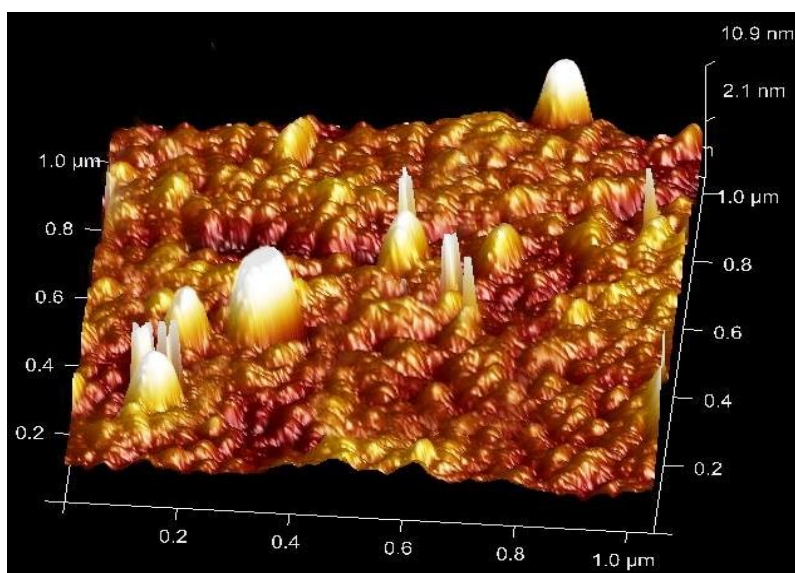


**Fig. 4.14:** 3d AFM of CDSCM-CCMN

#### 4.10. Conclusions

The CMC at which amphiphilic conjugate self-assembled into a micelle was 0.4836 mg/mL in an aqueous medium. Because of the low CMC value, the nanomicelles indicate stability, extending blood circulation and making the medicine more accessible for targeting. When incubated with RBC at the maximum concentration of CDSCM-CCMN, about 2.0% hemoglobin was liberated. This indicates that our CDSCM-CCMN nano-formulation was compatible with RBC and blood, indicating that these nanomicelles can be administered intravenously as well. Using a Zeta Sizer, the hydrodynamic size range of the micelles was found to be  $109.7 \pm 17.9$  nm. The micelle's polydispersity index, which measures the homogeneity of micelle size, was determined to be 0.19. These indicate that micelles did not aggregated and form a suitable dispersion in an aqueous media. The micelle's zeta potential of -19.72 mV indicates that its surface was significantly negatively charged, which may aid in the micelles' capacity to resist one another, in the aqueous medium, and improve stability. The morphological assessment of CDSC-CCMN micelles was evaluated microscopically where we used FE-SEM, TEM, and AFM. The thin layer of lyophilized CDSCM-CCMN powder was seen to be virtually spherical and aggregated in the SEM image. But in order to make things clear, these micelles are examined under a TEM, and it was found that particle sizes were between 50 to 150 nm and were spherical. Imaging of CDSCM-CCMN micelles by AFM technique proved its roughly spherical and moderately uniform shape. This shows how the prepared nanomicelles' hydrodynamic size was similar. Better homogeneous biodistribution will take place as a result of the morphological assessment of the nanomicelles, which offers a clear understanding of the size and form of the nanomicelles and was appropriate for in vivo characterization.



# Chapter 5

## Preparation and characterization of curcumin-resveratrol nanomicelles

- 5.1** Introduction
- 5.2** Preparation of conjugated curcumin and free resveratrol containing nanomicelles (CDSCM-RSV)
- 5.3** Determination of Critical micelle concentration of CDSCM-RSV
- 5.4** Blood compatibility
- 5.5** Characterizations of CDSCM-RSV
  - 5.5.1 Measurement of zeta potential and hydrodynamic particle size of CDSCM-CCMN
  - 5.5.2 Differential Scanning Calorimetry
  - 5.5.3 X-Ray diffraction
  - 5.5.4 SEM, TEM and AFM
- 5.6** Results and discussions
- 5.7** Conclusions

### 5.1. Introduction

In this study, first we have prepared the nanomicelles of amphipathic polymer prodrug by chemical conjugation of curcumin with chitosan via succinyl linker and subsequently dialysis of synthesized amphipathic polymer prodrug in free RSV containing DMSO solvent. Chitosan, a biopolymer known for its biocompatibility, biodegradability, and ability to form gel-like structures in acidic conditions, was utilized in drug delivery applications. Chitosan, with its glucosamine unit containing hydroxyl and amine groups, enables the conjugation of many drugs and other substances. This property can improve the drug's solubility, stability, and toxicity and facilitate the delivery of the drug to specific cells or tissues [139,140,141]. The therapeutic characteristics of CCMN are diverse and extensive, encompassing anti-inflammatory, anti-cancer, wound-healing, antioxidant, and antidiabetic effects. Unfortunately, its low bioavailability, rapid hydrolytic breakdown, and poor water solubility have greatly reduced its therapeutic utility. To add to its list of medicinal benefits, resveratrol fights cancer, inflammation, and type 2 diabetes by acting as an antioxidant and reducing free radical damage. Red grapes, gigantic knotweed, and a plethora of other plant parts may contain it. However, due to its poor water solubility and bioavailability, it is not as useful in therapeutic applications.

In order to address issues with the solubility and bioavailability of both medications while also achieving synergistic therapeutic effects against diabetes, we have created nanomicelles that are loaded with free form resveratrol (in the form of an amphipathic polymer prodrug in the micelle core) and conjugated form CCMN.

The succinic anhydride was used to form bridge between CHT and CCMN to form amphipathic polymer prodrug conjugate. From these conjugates, nanomicelle was prepared in an aqueous environment that can help to increasing the aqueous solubility of CCMN and RSV as well as to improve therapeutic activity.

### 5.2. Preparation of conjugated curcumin and free resveratrol containing nanomicelles (CDSCM-RSV)

For the preparation of conjugated CCMN and free RSV containing nanomicelle, 1 mg/ml CHT-di(SUC-CCMN) solution was prepared with 1mg/ml free RSV containing DMSO by proper mixing. The next step was to combine CHT-di(SUC-CCMN) with RSV in a dialysis bag (Mol.Wt 12 kDa). The bag was then immersed in water (deionized) for 24 hours, with the water

being replaced every 4 hours. Dialysis was used to remove additional components, while the solvent was still present in the chemical process. After dialysis, the filtrate was passed through a filter with a pore size of 0.45  $\mu\text{m}$  to eliminate any bigger particles, and then it was lyophilized.

The CDSCM-RSV schematic preparation process is shown in **Figure 5.1**; below. For later use, the finished micelles (CDSCM-RSV) were kept dry and cold [142,143]. About 87.78% of CDSCM-RSV was yielded.

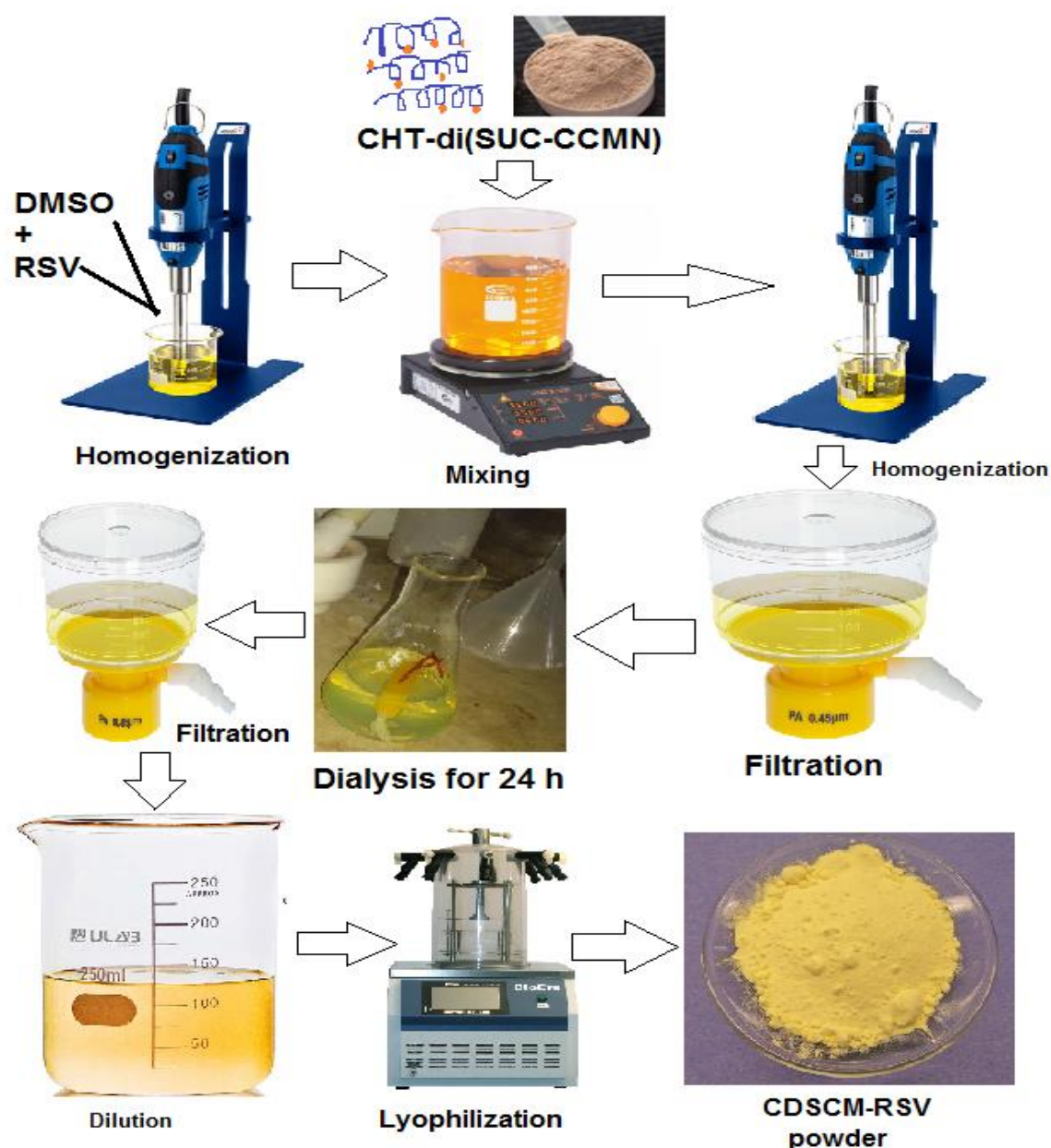


**Fig. 5.1:** Schematic presentation of CDSCM-RSV formation

### 5.3. Determination of Critical micelle concentration of CDSCM-RSV

CMC signifies a concentration at which the amphiphilic polymeric compound can self-assemble into micelles in the solvent. The CMC of CDSCM-RSV was determined by employing the self-quenching agent pyrene as the fluorescence probe in an aqueous medium, and it helps to produce fluorescence for the presence of a lipophilic part of the micelles core. Here CDSCM-RSV at low concentration breakdown into CHT-di(SUC-CCMN) amphipathic polymer pro-drug molecule and free resveratrol, but upon increasing the concentration of CDSCM-RSV at certain concentration it again form micelle structure. A diluted fluorescent probe pyrene solution was vortexed with CDSCM-RSV solutions ranging in concentration from 0.004 mg/ml to 2.5 mg/ml in order to ascertain the CMC of CDSCM-RSV. The mixture was left overnight to record fluorescence using a fluorescence spectrophotometer (Infinite M200, TECAN); this study was carried out at 390 nm emission [146].

### 5.4. Blood compatibility

A hemolysis investigation used a blood sample from a nearby blood bank to track the hemocompatibility of CDSCM-RSV. The blood sample was centrifuged for five minutes at 2000 rpm in order to extract the red blood cells. Three PBS buffer washes were performed on the obtained RBCs. A mixture of 10 ml PBS (pH 7.4) and 100 µl washed RBC was used to create the stock RBC solution. In order to quantify the hemoglobin release from RBC by CDSCM-RSV, stock RBC solutions were used to create CDSCM-RSV at concentrations ranging from 0.5 to 2 mg/ml. The samples were then incubated at 37 °C for 30 minutes. Next, separate solutions should be centrifuged for five minutes at 1500 rpm to extract the supernatant for UV-visible absorbance measurement at 541 nm [147,148]. Distilled water was used as the positive control and PBS pH 7.4 solutions as the negative control. Using the equation below, the hemolysis percentage (Hp%) of CDSCM-RSV was calculated:

$$Hp\% = \frac{As - An}{Ap - An} \times 100 \quad \dots \dots \dots Eqn2$$

Where As is the sample absorbance, An is the PBS buffer absorbance, and Ap is the distilled water absorbance. We took three separate readings for each parameter.

## **5.5. Characterizations of CDSCM-RSV**

To study the structure of CDSCM-RSV, scientists used a Zeta Sizer (Nano-ZS 90, Malvern Instrument, UK), a FE-SEM Quanta 200, and HR-TEM from JEOL Japan, JEM-2100 Plus.

### **5.5.1. Measurement of zeta potential and hydrodynamic particle size of CDSCM-RSV**

Adding 10 mg of CDSCM-RSV to a 10 ml solution of 10 mM NaCl and vortexing for 10 minutes allowed us to measure the average hydrodynamic particle size and zeta potential of the nanoparticles.

### **5.5.2. Differential Scanning Calorimetry**

The melting endotherm of the physical mixture, RSV, CCMN, and pure sample CDSCM-RSV was determined using a differential scanning calorimeter (DSC 6000, Perkin Elmer, USA). Indium standard was used to calibrate the device prior to analysis. For each individual analysis, a 50  $\mu$ L aluminum sample pan was loaded with 15 mg of CDSCM-RSV, physical mixture, CCMN, and RSV. Each component was meticulously weighed before sealing. Nitrogen gas flowed over the sample was 50 ml/min to heat the sample pan from 0 to 500°C, with rates ranging from 1 to 10 °C/min. In order to follow the experimental design, we adjusted the heating rate and end heating temperature. The melting endotherm changes of CDSCM-RSV, physical mixture, CCMN, and RSV were documented using Perkin Elmer, USA and its related software.

### **5.5.3. X-Ray diffraction**

An X-Ray diffraction (XRD) study was carried out to determine whether the samples contained CCMN and RSV crystals. We used a quartz standard to calibrate the XRD (Shimadzu 6000, Shimadzu Corporation, Kyoto, Japan) before we began the study. To make the surface of the glass container for examination smooth and level, the drug-polymer dispersions were evenly distributed and spread out. At room temperature, radiation source that generated X-Rays with a 40 kV production voltage and 30 mA current was used to examine the samples. A continuous 2 $\theta$  range of 10-80° was scanned at a speed of two degrees per minute, with a scan step of 0.02 degrees, in order to acquire diffraction patterns of the samples.

#### **5.5.4. Sample preparation for FE-SEM, TEM and AFM**

FE-SEM, TEM, and AFM were also used to determine the morphology of CDSCM-RSV. The lyophilized CDSCM-RSV powder and 1 milliliter of double-distilled water were mixed to make the SEM sample. On create the thin film; the dispersion was then applied on an aluminum sheet. After being allowed to air dry, the film was coated in gold and examined using a FE-SEM. For better morphological evaluation, Transmission Electron Microscopy (TEM) study was done. To produce the TEM samples, a carbon-coated copper grid was sprinkled with a drop of 0.001 mg/ml CDSCM-RSV.

Individual CDSCM-RSV nanomicelles and groups of CDSCM-RSV nanomicelles can be seen with the atomic force microscope (AFM), which provides two-dimensional and three-dimensional imaging in contrast to conventional microscopy methods. After being appropriately diluted in deionized water, the nanoparticles were ultrasonicated for fifteen minutes. A stream of nitrogen was used to blow the leftover solution after 50  $\mu$ l of the dilution was applied to a cleaned substrate and incubated for ten to fifteen minutes, depending on the needed particle density. We used this general procedure on every sample.

#### **5.6. Results and Discussions**

The intensity ratio of pyrene's (I335/I332) peaks depends on the medium's polarity [150,151]. The fluorescence intensity changed rapidly when pyrene transited from hydrophilic media to the lipophilic core of CDSCM-RSV. Plotting of logarithm concentration of CDSCM-RSV vs. intensity ratio constructs two straight lines intersecting at a point known as CMC was 0.4644 mg/ml (**Figure 5.2**). Lower CMC values signify its stability, prolonging blood circulation, and accessible to the targeting of the drug [152].

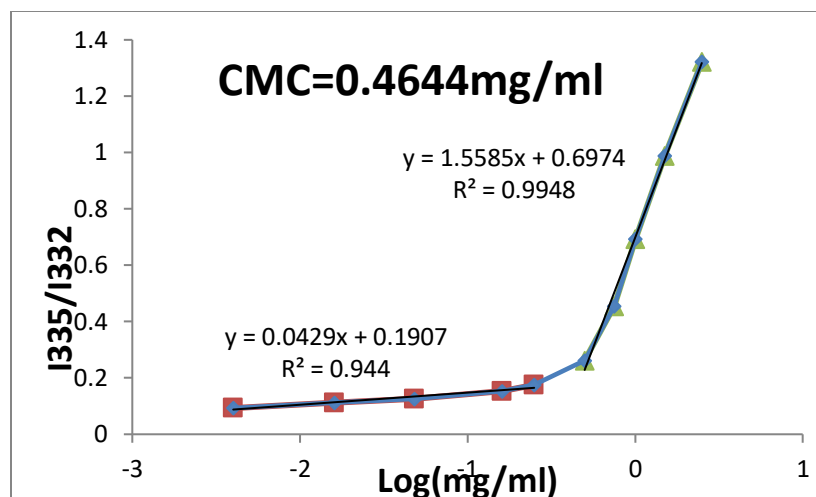


**Fig. 5.2:** Determination of Critical Micelle Concentration of CDSCM-RSV

Hemocompatibility is an important criterion to evaluate compatibility in terms of hemoglobin release from RBC by drug-loaded nanoparticles for the safety and biocompatibility of nano-drug formulation. Drugs associated with nanoparticles can damage the RBC partially or fully. A hemolytic study determined the percentage of hemoglobin released from RBC. After the interaction between CDSCM-RSV and RBCs, it could release hemoglobin from the damaged RBCs. The absorbance of hemoglobin was determined using a UV-visible spectrophotometer and expressed as a percentage. After sufficient time of incubation of CDSCM-RSV with RBC, it was observed that around 2.5% of hemoglobin was released at the highest concentration of CDSCM-RSV (2 mg/ml), as shown in **Figure 5.3**. This signifies that our nano-formulation of CDSCM-RSV is compatible with RBC and blood, so these nanomicelles are also applicable in intravenous administration.

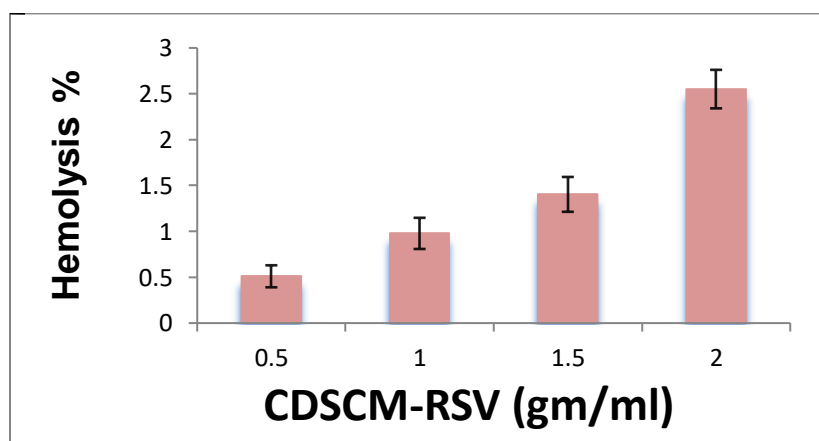


**Fig. 5.3:** Hemolysis of CDSCM-RSV

To determine the hydrodynamic particle size and zeta potential of the CDSCM-RSV, dynamic light scattering (DLS) was used. **Figure 5.4;** displays the hydrodynamic particle size distribution of CDSCM-RSV, while Figure 5.5 displays the zeta potential. With a zeta potential of approximately -32.84 mV and an average hydrodynamic particle size of  $56.12 \pm 15.2$  nm, CDSCM-RSV was clearly negatively charged. This negative charge was caused by the presence of unbound hydroxyl (-OH) groups in the glucosamine units of the CHT exist on the surface of CDSCM-RSV. This accumulation of hydroxyl groups results in the formation of a highly negatively charged CDSCM-RSV surface. This negative charge serves to maintain the micelle's stability. Higher negative surface charges repel each CDSCM-RSV from the other, thereby reducing nanomicelle accumulation [153].

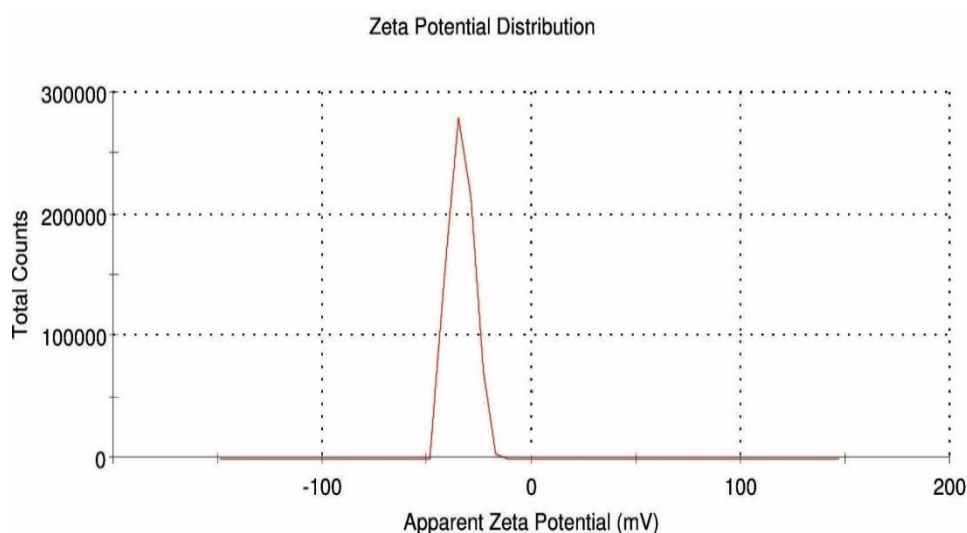


**Fig. 5.4:** Zeta Potential of CDSCM-RSV



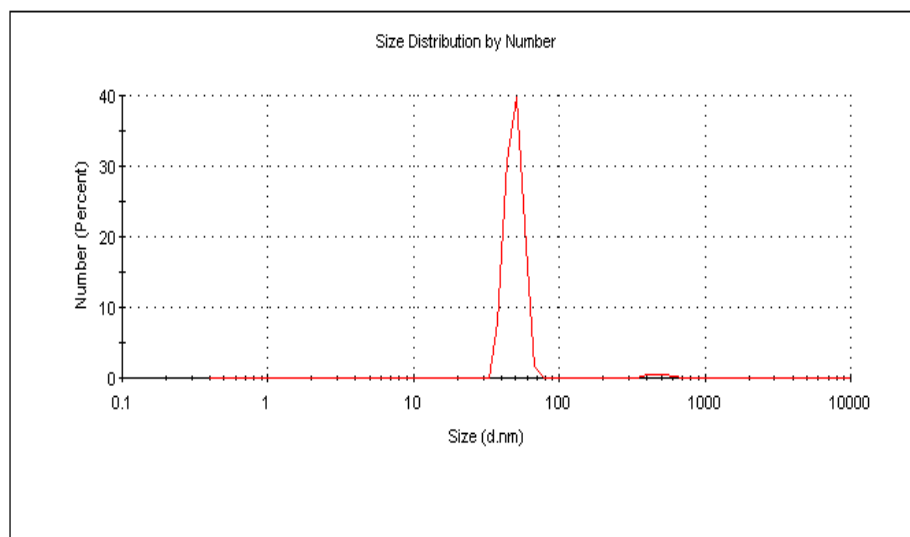


**Fig. 5.5:** Hydrodynamic particle size of CDSCM-RSV

**Figure 5.6;** displayed the differential scanning calorimetry (DSC) thermograms of the CDSCM-RSV, Physical mixture, CCMN, and RSV. Around 183°C, when the CCMN melting point is found, the clear endothermic peak of CCMN emerged. Similarly around 432°C, when resveratrol melting point was found, the clear endothermic peak of RSV emerged. Less intensely, the drug endothermic peak also observed about 180°C and 430°C on the physical mixture curve. In the physical mixture, each peak matched its intrinsic melting point. The CCMN, RSV and physical mixture showed some similarities to the free CCMN and free RSV, so it concluded that the physical mixture system was only blended and that both components are crystalline. As a result, the presence of the CCMN and RSV melting peaks in the physical mixture may also indicate that the system did not form an amorphous state. The total disappearance of CCMN and RSV in the thermograms of CDSCM-RSV indicated that the polymer nanomicelle was amorphous and evenly distributed throughout the micelle. According to the DSC data, CCMN and RSV were effectively distributed throughout the micelle and were present in an amorphous form. Therefore, it's possible that no amorphous state formed in this system due to the presence of the CCMN and RSV melting peak in the physical mixture.

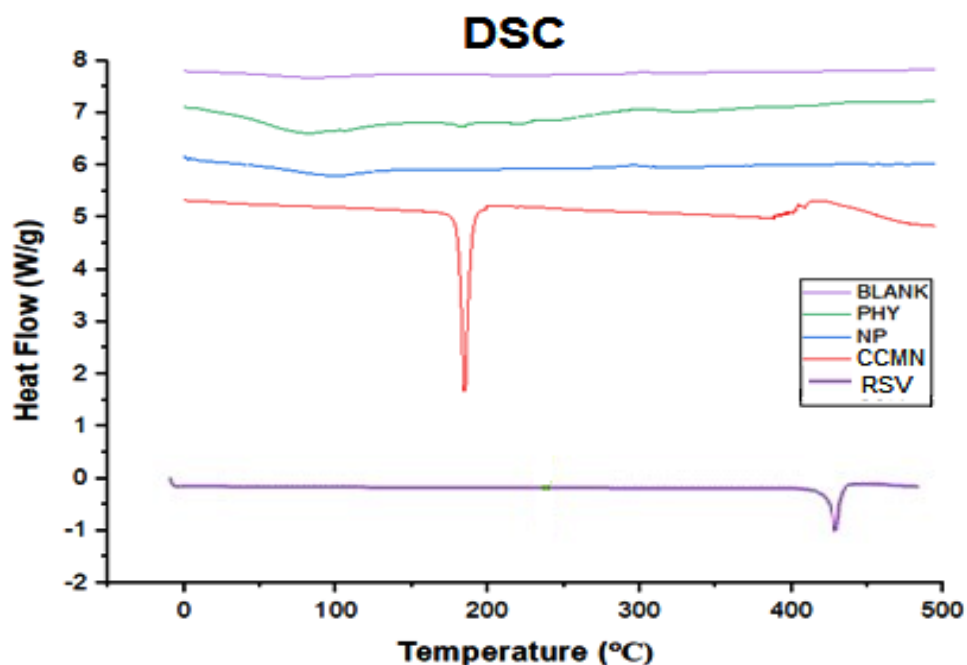


**Fig. 5.6:** DSC thermogram of CDSCM-RSV (NP), Physical mixture, CCMN, and RSV

**Figure 5.7;** displayed the XRD patterns of CDSCM-RSV, physical mixtures, CCMN and pure RSV. The remarkable crystallinity of CCMN, RSV can be explained by the multiple extremely sharp peaks shown in the XRD spectrogram. RSV and Curcumin's distinctive peaks could also be seen, albeit less clearly, in the physical mixture's diffraction pattern. The physical mixture had some, but not all, of the distinctive peaks of CCMN and RSV because of the high concentration of carriers relative to CCMN and RSV. These findings showed that there was still some CCMN and RSV in the physical combination in the crystalline form. The CDSCM-RSV showed a significant difference from those of pure CCMN, RSV and the physical mixture; the CCMN and RSV peaks entirely vanished, indicating the presence of an amorphous state of CCMN and RSV in the CDSCM-RSV.

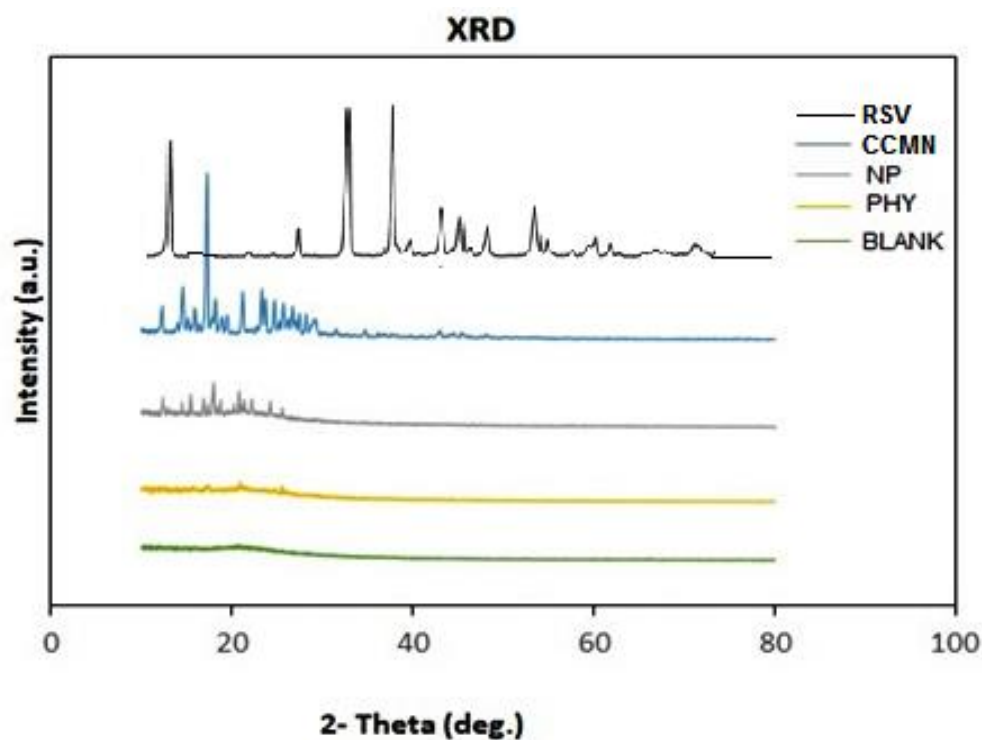


**Fig. 5.7:** XRD of CDSCM-RSV (NP), Physical mixture, CCMN and RSV.

**Figure 5.8;** indicates that CDSCM-RSV was roughly spherical and mostly uniform in size. The shape of the particle is distinguishable.

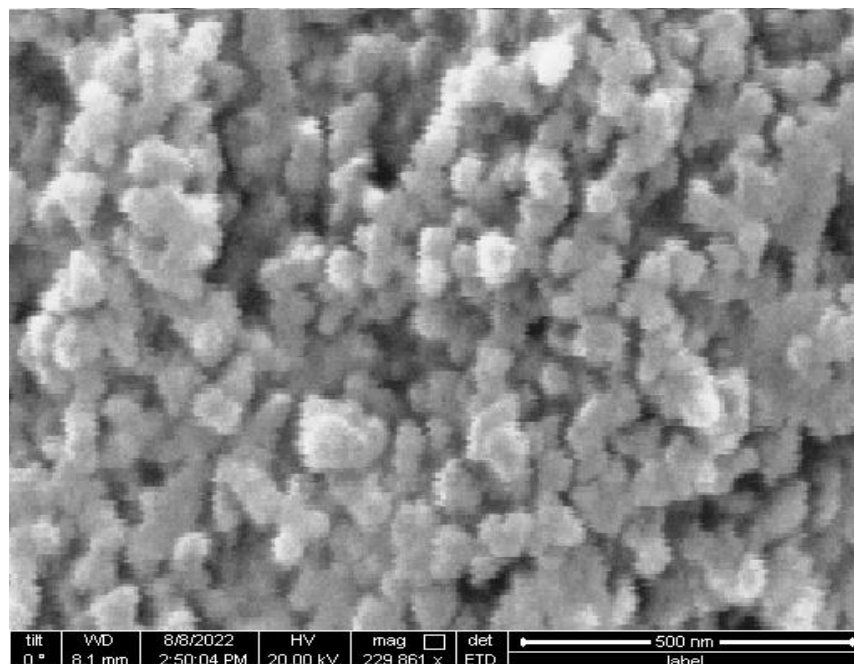


**Fig. 5.8:** FE-SEM of CDSCM-CCMN

**Figure 5.9;** shows that the CDSCM-CCMN was spherical in shape and within the size range of 80-100 nm.

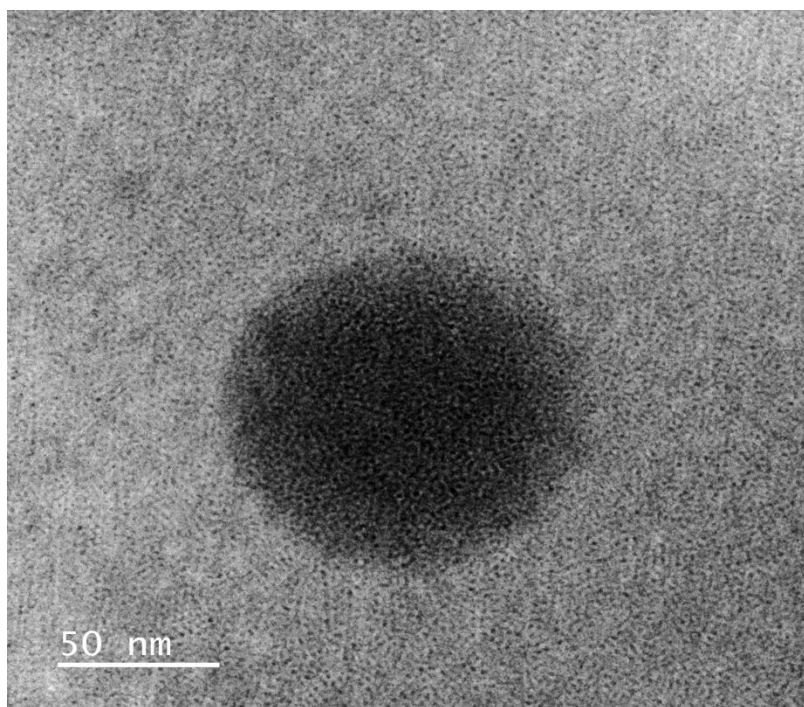


**Fig. 5.9:** TEM of CDSCM-RSV

In this work used less than 20 nm/pixel resolution for the scan in order to identify the CDSCM-RSV nanomicelle in each AFM measurement. As long as we observe nanomicelles in this form, there is no appreciable effect on the measurement of their diameters. The thermal noise method was used to calibrate the cantilever's spring constant before any data was taken. Following this, computerized particle characterization and cross-sectional line profiling were used to study the nanoparticles' area-equivalent diameter and height, correspondingly. The average sizes of the nanomicelles in an aqueous solution were satisfactorily quantified by AFM cross-sectional line profiling (**Figure 5.10** and **5.11**). Our research clarifies the need for standardizing AFM to assess the dimensions and morphology of nanomicelles.

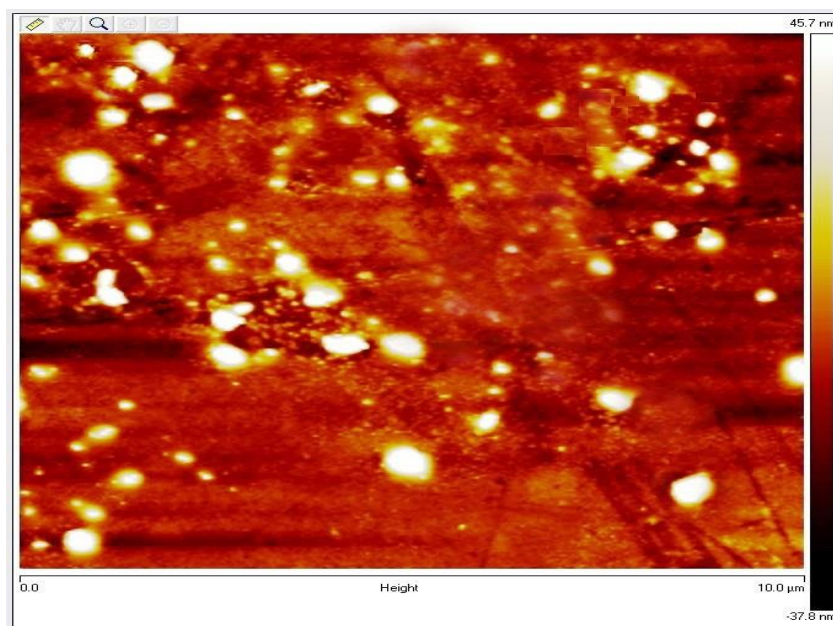


**Fig. 5.10:** 2d AFM of CDSCM-RSV

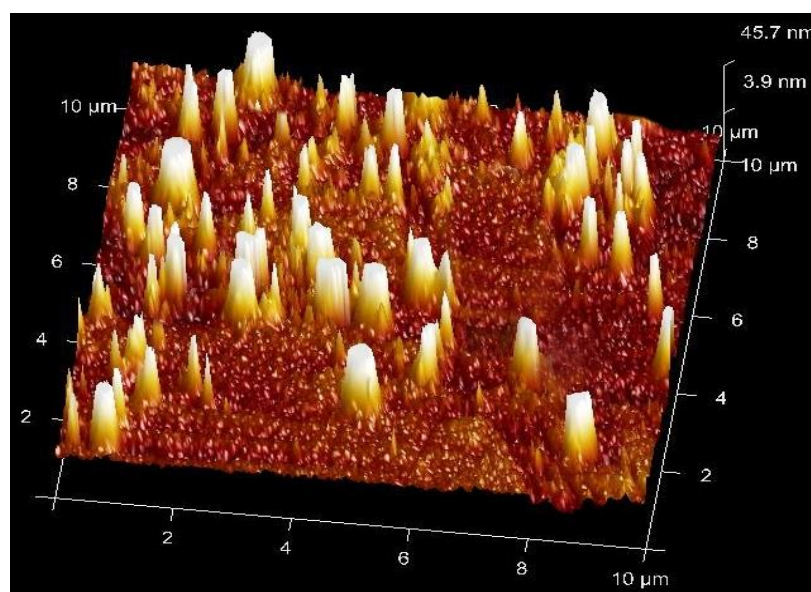


**Fig. 5.11:** 3d AFM of CDSCM-RSV

### 5.7. Conclusions

The CMC at which amphiphilic conjugate self-assembled into a micelle was 0.4644 mg/mL in an aqueous medium. Because of the low CMC value, the nanomicelles indicate stability, extending blood circulation and making the medicine more accessible for targeting. When incubated with RBC at the highest dose of CDSCM-RSV, approximately 2.5% hemoglobin was released. This



indicates that our CDSCM-RSV nano-formulation was compatible with RBC and blood, meaning that intravenous delivery of these nanomicelles was also feasible. Using a Zeta Sizer, the hydrodynamic size range of the micelles was found to be  $56.12 \pm 15.2$  nm. The micelle's polydispersity index, which measures the homogeneity of micelle size, was determined to be 0.18. These indicate that micelles did not aggregated and form a suitable dispersion in an aqueous media. The micelle's zeta potential of -32.84 mV indicates that its surface was significantly negatively charged, which may aid in the micelles' capacity to resist one another, in the aqueous medium, and improve stability. The morphological assessment of CDSC-CCMN micelles was evaluated microscopically where we used FE-SEM, TEM, and AFM. The thin layer of lyophilized CDSCM-RSV powder was observed to be virtually spherical and aggregated in the SEM image. But in order to make things clear, these micelles were examined under a TEM, and it was found that particle sizes were between to 80-100 nm and were spherical. Imaging of CDSCM-RSV micelles by AFM technique proved its roughly spherical and moderately uniform shape. This shows how the prepared nanomicelles' hydrodynamic size was similar. Better homogeneous biodistribution will take place as a result of the morphological assessment of the nanomicelles, which offers a clear understanding of the size and form of the nanomicelles and was appropriate for in vivo characterization.

# Chapter 6

## HPLC method development for estimation of curcumin and resveratrol

- 6.1** Introduction
- 6.2** Materials and methods
  - 6.2.1 Chemicals and reagents
  - 6.2.2 Instrumentation and chromatographic conditions
  - 6.2.3 Preparation of calibration standards and sample solution
  - 6.2.4 Method validation
  - 6.2.5 In-vitro release study of CCMN and RSV from nanomicelle
  - 6.2.6 Stability of CDSCM-RSV containing CCMN and RSV in physiological pH
- 6.3** Data analysis
- 6.4** Results and discussions
- 6.5** Conclusions

## 6.1. Introduction

In the CDSCM-RSV nanoparticle, RSV exists in the nanomicelle core and CCMN exist in the micelle forming amphipathic polymer pro-drug conjugate. It was very difficult to estimate free form of RSV and conjugated form of CCMN from CDSCM-RSV simultaneously. There were very few HPLC techniques available for estimating CCMN and RSV free forms simultaneously, but none were available for estimating both medications in two distinct forms from nanomicelles at the same time. Therefore, for the simultaneous determination of both medicines from nanomicelles, an accurate, precise, fast, and reliable RP-HPLC approach was needed. Our research primarily focuses on developing and validating the RP-HPLC method for measuring curcumin and resveratrol from nanomicelles simultaneously. It was discovered that 254 nm is the common wavelength, or the isosbestic point [154], at which both medications exhibit maximal absorption.

## 6.2. MATERIALS AND METHODS

### 6.2.1. Chemicals and reagents

Sigma-Aldrich Chemicals Company of St. Louis, Missouri, USA, supplied the rat plasma and resveratrol (purity > 99%). The low molecular weight chitosan, succinic anhydride, dimethyl sulfoxide (DMSO), and curcumin (purity>99%) were supplied by TCI Chemical (India) Pvt. Ltd. We obtained water, acetic acid glacial, methanol, ammonium acetate, orthophosphoric acid analytical grade, and acetonitrile (ACN) HPLC grade from Merck Specialities Pvt. Ltd. in Mumbai, India. A Millex syringe with a 0.45µm pore size is used to filter the sample solution.

### 6.2.2. Instrumentation and chromatographic conditions

The HPLC system included an Agilent injector (G1329B), a PDA detector (G13150), Version 1.5 software (Lab solution), and an Agilent 1260-infinity (Minneapolis, MN) solvent supply pump with a 20 µl capacity. Chromatographic separation was accomplished using a Phenomenex Gemini (250 mm X 4.6 mm i.d., 5 µm particle, C18 reversed-phase) column. The proportions of the components in the mobile phase were adjusted through multiple trials. The optimal parameters for the analysis were a 1:1 ratio of acetonitrile to water (0.5 % ortho phosphoric acid, pH 4.6), with a mobile phase flow rate of 1.0 ml/min for a run period of 20 min. The sample injection volume was 10µl, and the column temperature was 25°C. The test sample and mobile phase were filtered through a 0.45 µm membrane filter and sonicated for 20 minutes before being used. Through the use of a UV–Vis spectrophotometer (Shimazu, Japan), the separate peak



absorption spectra of CCMN and RSV were superimposed to determine the isosbestic wavelength, or the common peak absorbance of both medications. The absorption spectra curves were found to cross at 254 nm for both. As a result, 254 nm was chosen as the isosbestic detecting wavelength.

### **6.2.3. PREPARATION OF CALIBRATION STANDARDS AND SAMPLE SOLUTION**

#### **6.2.3.1. Preparation of RSV standard**

The material was transferred quantitatively into a 100 ml volumetric flask after being properly weighed to 10 mg of RSV. Eighty milliliters of ethanol was added, mixed well, and then added to obtain a solution with a concentration of one hundred micrograms per milliliter. Working standard solutions with concentration ranges of 0.1-32 µg/ml were prepared using a mobile phase and progressive dilution. The solutions were all kept at 4°C until they were ready to be used.

#### **6.2.3.2. Preparation of CCMN standard**

To conduct the quantitative analysis, a 100 ml volumetric flask was filled with 10 mg of accurately weighted CCMN. To attain a concentration of 100 µg/ml, the flask was filled with methanol after 80 ml of it was added and well mixed by shaking. Standard working solutions in the concentration range of 0.1-64 µg/ml were generated by diluting with mobile phase, just like RSV. The solutions were all kept at 4°C until they were ready to be used.

#### **6.2.3.3. Preparation of sample solution**

To investigate the loading efficiency and drug loading, nanomicelles were prepared using 2N HCl and incubated at 50°C for 1.5 hours, at a concentration of 2 mg/ml. It was carried out to hydrolyze ester linkages, which are present between CHT and CCMN, using acid. Methanol was added to the sample solution to make 1000 parts per million. Prior to filtering via a 0.22µ membrane, it underwent a 10-minute sonication. The filtrate was evaporated to get dry powder, which was subsequently reconstituted with the mobile phase solution. After centrifuging the mixture at 5000 rpm for 15 minutes, the 10 ml solution was made from the 1.0 ml supernatant. To determine the percentage of CCMN and RSV degradation in 2N HCl, a known quantity of both substances (1:1) was synthesized and subjected to the following procedures. Within two

hours, RP-HPLC analysis was performed on every sample to look into drug loading efficacy (DLE) and drug loading (DL) [155–156].

#### **6.2.4. Method validation**

The validation of the simultaneous estimation of CCMN and RSV in nano-micelles is conducted in accordance with the International Conference on Harmonization (ICH) requirements as outlined in Q2(R1). The guidelines include selectivity, linearity, system suitability, resilience, accuracy, precision, and limit of detection (LOD and limit of quantification, or LOQ) [157].

##### **6.2.4.1. Selectivity**

The aim of this investigation was to distinguish distinct drug peaks and remove any other substances present in the nano-micelle. Standard medications, standard medication mixtures, and nano-micelle sample solutions were all independently examined using HPLC equipment.  $R_s$  (resolution) need to be more than 1.5 in order to confirm the method's selectivity [158].

##### **6.2.4.2. System suitability**

In order to determine if the system was suitable, a 1:1 combination of CCMN and RSV in methanol was prepared at a concentration of 01  $\mu\text{g/ml}$ . After six separate HPLC analyses at varying intervals, the following parameters were recorded: area under the curve (AUC), resolution ( $R_s$ ), retention time ( $t_R$ ), tailing factor ( $T_f$ ), and net theoretical plate number ( $N$ ). Statistical metrics such as standard deviation (SD) and relative standard deviation (RSD) were determined using the computer data. Appropriateness of the system is defined as an RSD value lower than 2%.

##### **6.2.4.3. CCMN and RSV calibration solutions preparation for linearity assessment**

In order to create a calibration standard solution with strengths of 02  $\mu\text{g/ml}$ , 04  $\mu\text{g/ml}$ , 06  $\mu\text{g/ml}$ , 08  $\mu\text{g/ml}$ , 16  $\mu\text{g/ml}$ , and 32  $\mu\text{g/ml}$  for CCMN and 01  $\mu\text{g/ml}$ , 02  $\mu\text{g/ml}$ , 04  $\mu\text{g/ml}$ , 08  $\mu\text{g/ml}$ , 12  $\mu\text{g/ml}$ , and 16  $\mu\text{g/ml}$  for RSV, respectively, the stock solutions of CCMN and RSV in methanol were prepared separately and diluted by mobile phase. Everybody went through a 0.22  $\mu$  filter prior to being injected into the HPLC apparatus. In order to assess the linearity of both drugs, the

regression correlation coefficient (R<sup>2</sup>) was calculated by visually plotting the resulting peak regions against the strengths of CCMN and RSV, respectively [159,160].

#### 6.2.4.4. Sensitivity

In order to determine the test's sensitivity, LOD and LOQ were computed. The terms LOD and LOQ indicate the relative amounts of less that our developed HPLC technology can detect and measure, respectively. The data from the calibration curve was transformed into the standard deviation ( $\sigma$ ) and slope (S) of linear regression for CCMN and RSV using statistical computations [158]. The following equation was used to compute LOD and LOQ.

$$LOD = \frac{3.3\sigma}{S} \dots\dots Eq1$$

$$LOQ = \frac{10\sigma}{S} \dots\dots Eq2$$

In this context,  $\sigma$  represents the response standard error and S denotes the calibration curve's slope.

#### 6.2.4.5. Accuracy and precision

The ICH Q2(R1) rules state that accuracy is defined as the degree to which results are comparable to one another or to actual values, and precision as the degree to which results are similar to actual values. Three concentrations of CCMN (02 $\mu$ g/ml, 04 $\mu$ g/ml, and 08 $\mu$ g/ml) and RSV (02 $\mu$ g/ml, 04 $\mu$ g/ml, and 08 $\mu$ g/ml) were generated from standard solution for the accuracy and precision assessment. Under the same experimental conditions, all of those were examined in triplicate using an HPLC system both on the same day (intra-day) and over the course of three successive days (inter-day). For accurate and precise measurement, the recorded peak responses of the intra- and inter-day chromatograms were statistically computed. We have computed the mean, SD, and percentage RSD statistically [161,162].

#### 6.2.4.6. Robustness

When small deliberate changes to chromatographic conditions, such as flow rate, pH, and composition, do not significantly alter the expected results or the repeatability of the results is not affected, the developed method is regarded as robust. From the data received from the

chromatographic analysis after making small adjustments to the parameters, the RSD was computed. For the chromatographic method to be considered robust, it should remain below 2%.

#### **6.2.5. In-vitro release study of CCMN and RSV from nanomicelles**

We looked at the cumulative releases of RSV and CCMN from nanomicelles in PBS buffers with pH 5.0 and 7.4. Separately, 10 milliliters of pH 5.0 and 7.4 PBS buffer solutions were mixed with a set amount of nanomicelles (10 mg). Each of the solutions was placed into a different dialysis bag and then into a 90 ml buffer solution. Those were incubated at 37°C with gentle shaking for nine days. Two milliliters (ml) of the sample were taken out of each beaker during the incubation period and replenished with the appropriate buffer at progressively longer intervals [163]. The developed RP-HPLC method was used to examine the samples in order to determine the percent cumulative drug release [156].

#### **6.2.6. Stability of CDSCM-RSV containing CCMN and RSV in physiological pH**

The stability of free CCMN, free RSV and CDSCM-RSV containing CCMN and RSV were analyzed in PBS buffer pH 7.4 for a specific incubation period at 37°C. Accurately weighted a fixed quantity of free CCMN, free RSV and CDSCM-RSV were dissolved in PBS buffer pH 7.4, sample were withdrawn in a fixed interval up to a certain period and replace with PBS buffer pH 7.4. The entire samples were analyzed through our developed chromatographic method. The concentrations of free CCMN, free RSV and CDSCM-RSV containing CCMN and RSV were measured in terms of AUC and plotted against time.

### **6.3. Data analysis**

All of the data were statistically analyzed by Excel Microsoft INC USA to find the equation of the calibration curve, the least square ( $R^2$ ), the standard deviation, the mean, the relative standard deviation, and the mean.

## **6.4. RESULTS AND DISCUSSION**

### **6.4.1. Finding of common maximum absorbance wavelength**

Methanol solutions with concentrations of 05 µg/ml of CCMN and 10 µg/ml of RSV were subjected to spectral analysis. Absorption spectra in the 200-400 nm range were recorded and

displayed for both medications. In this case, the crossover point of the two drugs' absorption spectra occurs at 254 nm, which is also their isosbestic wavelength (shared maximum absorbance wavelength), as shown in **Figure 6.1**.

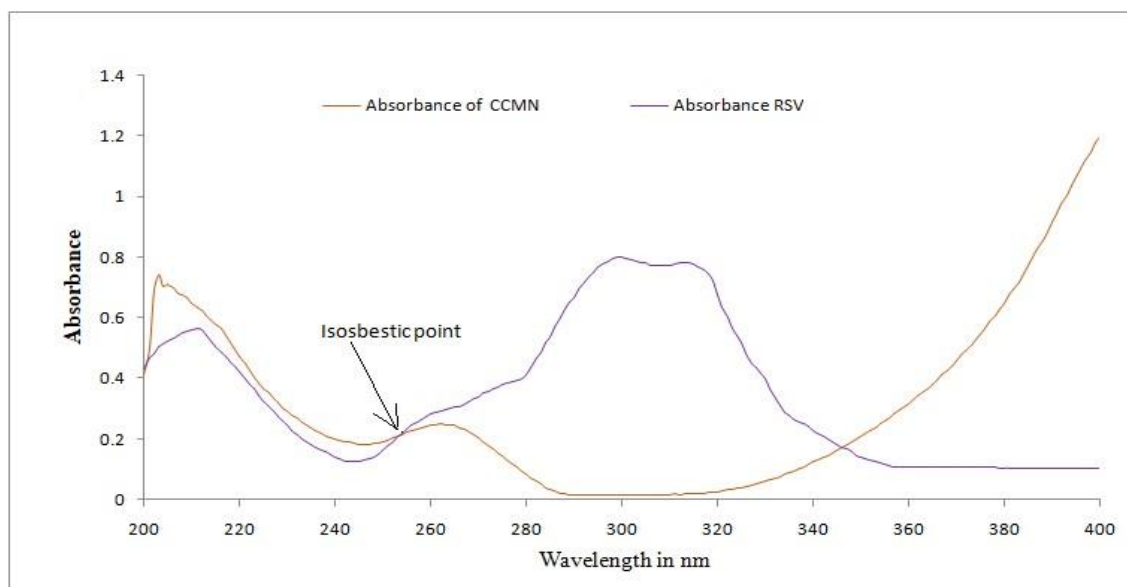


**Fig. 6.1:** Superimposition UV spectrum of CCMN and RSV

#### 6.4.2. Optimization of chromatographic parameters

Numerous investigations were conducted in order to optimize the mobile phase's flow rate, pH, column temperature, and ratios of its constituent parts, which include water, acetonitrile, and orthophosphoric acid. Following multiple trials, the pH of the mobile phase was set to 4.6, the flow rate was optimized to 1.0 ml/min, the column temperature was set to 25 °C, and the water-to-acetonitrile ratio was 1:1. Prior to using the composition mentioned above as the mobile phase, we tried using a different ratio of water to methanol as the mobile phase, but the outcomes were not good. The simultaneous estimation of CCMN and RSV was performed at a fixed isosbestic wavelength of 254 nm. The chromatograms of the two standard drugs, as displayed in **Figure 6.2**; when mixed under optimal chromatographic conditions showed distinct, acute sharp peaks, with retention times of 8.15 min for RSV and 11.41 min for CCMN, respectively. The same chromatographic conditions were used for the independent analysis of the two medicines, the results of which are displayed in **Figure 6.3 and 6.4**. Higher theoretical plate counts, lower equivalent theoretical plate heights, and lower tailing factors are indicative of the chromatographic results that meet HPLC analysis acceptance standards.

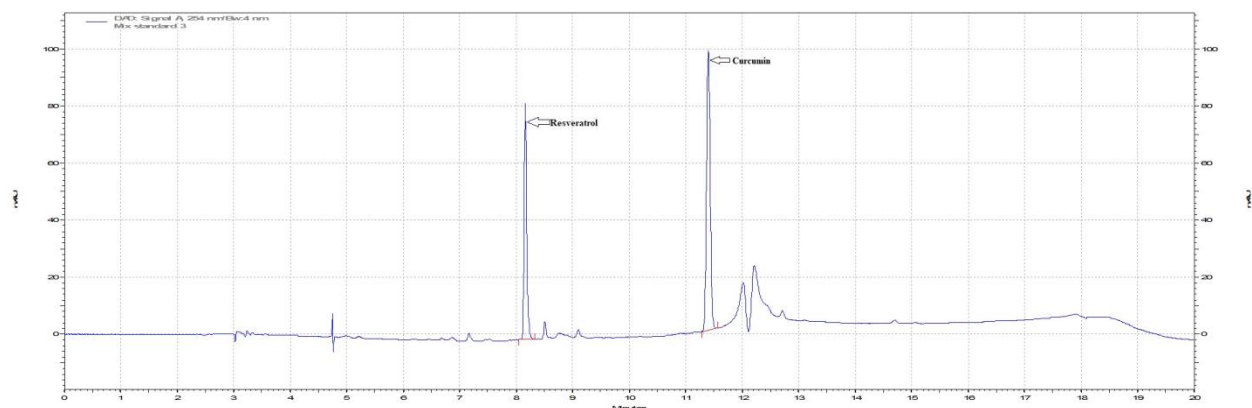


**Fig. 6.2:** RP-HPLC chromatogram of resveratrol and curcumin standard

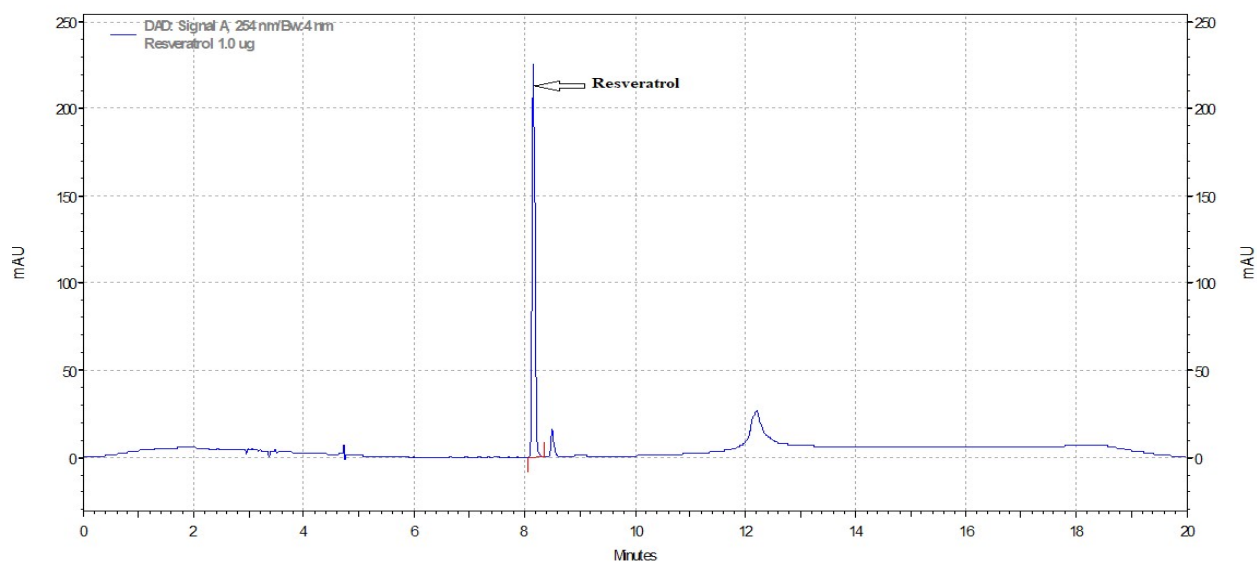


**Fig. 6.3:** RP-HPLC chromatogram of resveratrol standard ( $t_R$ -8.15 min)

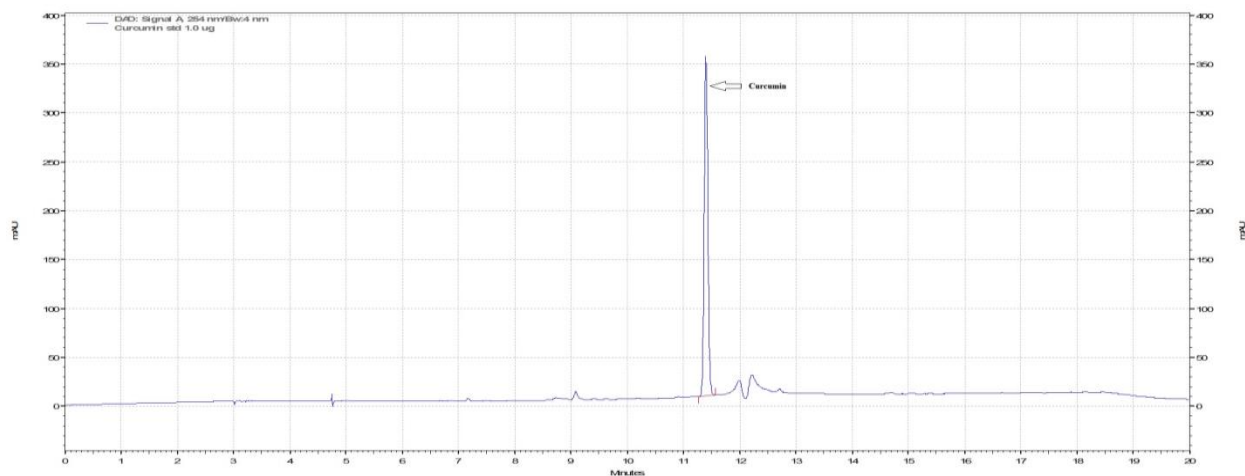


**Fig. 6.4:** RP-HPLC chromatogram of Curcumin standard ( $t_R$ -11.41 min)

### 6.4.3. Method Validation

We adhere to the ICH guidelines specified in Q2(R1) for the validation of the RP-HPLC method.

#### 6.4.3.1. System suitability test

To test the developed procedure's compatibility with the system, the CCMN and RSV solution mixture was injected into the HPLC column six times. Both CCMN and RSV had analytical values of 01 µg/ml in the mixture. Retention time, theoretical plate count, area under curve, tailing factor, and resolution were among the metrics obtained to evaluate system adequacy (**Table 6.1**). Our created method meets all requirements set out by ICH and USP since the RSD values of all metrics were less than 2%. The peaks of the medications were entirely separated, as the mean resolution for both drugs was  $7.360 \pm 0.117$ . Consequently, the RP-HPLC technology that we have developed is both effective and very suited [164].

**Table 6.1: System suitability of the developed method**

Sample	$t_R$		NTP		AUC		$T_f$		Rs
	RSV	CCMN	RSV	CCMN	RSV	CCMN	RSV	CCMN	
1	8.109	11.381	8085	8270	109456	174443	1.108	1.158	7.479
2	8.105	11.317	7987	8207	109237	173806	1.126	1.211	7.342
3	8.281	11.404	7894	8181	109975	174378	1.142	1.201	7.138
4	8.169	11.408	7913	8102	109981	173800	1.139	1.184	7.403
5	8.167	11.405	7992	8064	109635	174049	1.131	1.214	7.401
6	8.165	11.401	7882	8188	109579	174202	1.148	1.198	7.397
Average	8.166	11.386	7958.833	8168.667	109644	174113	1.132	1.194	7.360
S.D	0.064	0.035	77.484	74.382	293	277	0.014	0.021	0.117
R.S.D (%)	0.778	0.309	0.974	0.911	0.267	0.159	1.260	1.736	1.591

n=6;  $t_R$ : Retention time, NTP: Number of theoretical plate, AUC: Area under the curve,  $T_f$ : Tailing factor, Rs: Resolution

#### 6.4.3.2. Linearity, range and sensitivity

Figures 6.5 and 6.6 in MS-Excel show the area under the curve (AUC) for different concentrations of the two drugs plotted against their concentrations. An independent analysis was conducted on six distinct concentrations of CCMN (0.002mg/ml, 0.004mg/ml, 0.006mg/ml, 0.008mg/ml, .016mg/ml, and 0.032mg/ml) and RSV (0.001mg/ml, 0.002mg/ml, 0.004mg/ml, 0.008mg/ml, 0.012mg/ml, and 0.016mg/ml). The linearity ranges for CCMN and RSV were found to be 2-32 µg/ml and 1-16 µg/ml, respectively, according to the data. At  $y = 171178.89x + 19619.91$  and  $y = 108179.53x + 6862.02$ , respectively, were the CCMN and RSV calibration curves. Both CCMN and RSV had correlation coefficients ( $R^2$ ) very near to 1, which indicates linearity, with values of 0.99987 and 0.99992, respectively. The sensitivity of the test was

ascertained by computing the LOD and LOQ. 0.284939359  $\mu\text{g/ml}$  was the limit of detection (LOD) for CCMN, followed by 0.863452604  $\mu\text{g/ml}$  for LOQ. And 0.12463075  $\mu\text{g/ml}$  was the limit of detection (LOD) for RSV, while 0.37766894  $\mu\text{g/ml}$  was the limit of quantification (LOQ). It was concluded from the LOD and LOQ data that the created approach is extremely sensitive, yielding measurable results at less than 0.87  $\mu\text{g/ml}$  for CCMN and less than 0.38  $\mu\text{g/ml}$  for RSV. The data presented above is summarized in **Table 6.2**.

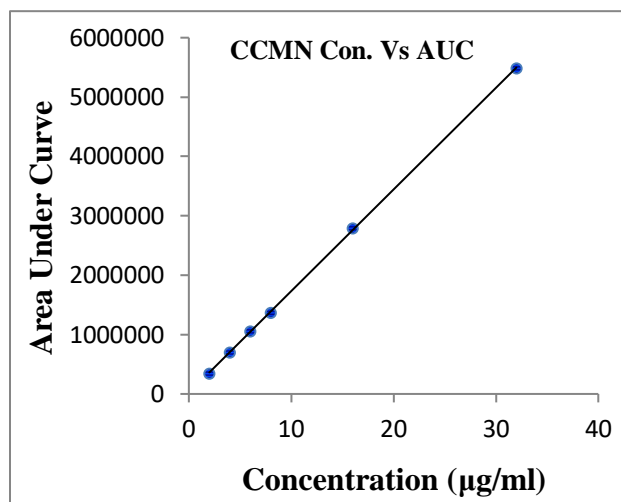


Figure 6.5: Calibration curve of CCMN

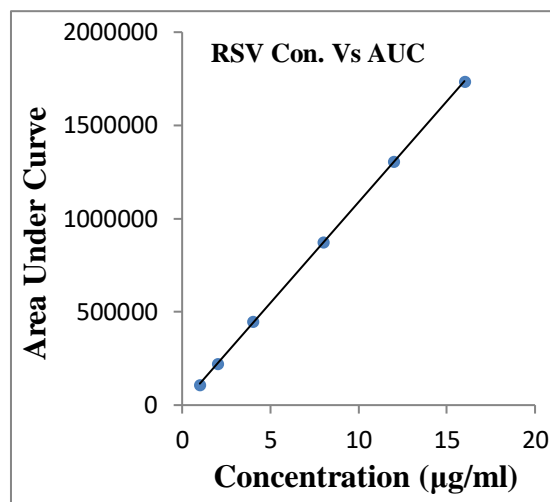


Figure 6.6: Calibration curve of RSV

**Table 6.2: Validation parameters for curcumin and resveratrol**

Parameter	CCMN	RSV
Linearity range ( $\mu\text{g/ml}$ )	2.00-32.00	1.00-16.00
Linear equation	$Y = 171178.89 X + 19619.91$	$Y = 108179.53X + 6862.02$
Correlation coefficient of ( $R^2$ )	0.99987	0.99992
Slope	171178.89	108179.53
Intercept	19619.91	6862.02
Standard error ( $\sigma$ )	14780.48582	4085.60492
LOD <sup>#</sup> ( $\mu\text{g/ml}$ )	0.284939359	0.12463075
LOQ <sup>\$</sup> ( $\mu\text{g/ml}$ )	0.863452604	0.37766894

Every value is regarded as mean  $\pm$ SD, with n = 6; <sup>#</sup> Calculated from Eq1, <sup>\$</sup> Calculated from Eq2

#### 6.4.3.3. Accuracy and precision

In order to conduct research with a high degree of accuracy and precision, three separate concentrations of RSV and CCMN were prepared: 0.002Mg/ml, 0.004Mg/ml, and 0.008Mg/ml. These complete samples were examined both intra- and inter-day in accordance with ICH recommendations [157]. The outcomes of the analysis were condensed into **Tables 6.3, 6.4,** and



**6.5.** The results of the HPLC analysis were statistically computed to determine the percent recovery and percent RSD. The percentage accuracy of the CCMN's intra-day and inter-day recovery was  $100.041 \pm 0.22\%$  and  $99.75 \pm 0.42\%$ , respectively. The corresponding values for RSV were  $100.041 \pm 0.21\%$  and  $100.14 \pm 0.29\%$ , respectively, and these values indicate the accuracy acceptance criterion. Similarly, the CCMN's intra-day and intra-day% RSDs were  $0.44 \pm 0.28$  and  $0.28 \pm 0.02$ , respectively. The precision acceptance standards were indicated by the respective RSV values of  $0.24 \pm 0.05$  and  $0.32 \pm 0.19$ , respectively. Our proposed approach is more reliable than other ways because it achieves a percent RSD of accuracy and precision below 0.5 percent, which is below the guidelines for acceptance criteria [165].

**Table 6.3:** Summary of intra-day and inter-day precision and accuracy of the method

Type of analysis	Nominal Strength in ( $\mu\text{g/ml}$ )	Mean Strength found, $\mu\text{g/ml}$		Mean Accuracy %		RSD% (Precision)	
		CCMN	RSV	CCMN	RSV	CCMN	RSV
Intra-day	2	$2.003 \pm 0.015$	$1.997 \pm 0.006$	100.166667	99.833333	0.7625	0.2892
	4	$4.007 \pm 0.012$	$4.010 \pm 0.010$	100.166667	100.25	0.2882	0.2494
	8	$7.983 \pm 0.021$	$8.003 \pm 0.015$	99.7916667	100.0417	0.2608	0.1909
Inter-day	2	$1.987 \pm 0.006$	$1.997 \pm 0.006$	99.3333333	99.833333	0.2906	0.2892
	4	$4.007 \pm 0.012$	$4.017 \pm 0.021$	100.166667	100.4167	0.2882	0.5183
	8	$7.980 \pm 0.020$	$8.013 \pm 0.012$	99.75	100.1667	0.2506	0.1441

Each value is shown as mean  $\pm$ SD,  $n = 3$ . The intra-day and inter-day percentage RSD of CCMN was  $0.44 \pm 0.28$  and  $0.28 \pm 0.02$ , the intra-day and inter-day percentage RSD of RSV was  $0.24 \pm 0.05\%$  and  $0.32 \pm 0.19\%$ , respectively, and the intra-day and inter-day accuracy of CCMN was  $100.041 \pm 0.22\%$  and  $99.75 \pm 0.42\%$ ; the intra-day and inter-day accuracy of RSV was  $100.041 \pm 0.21$  and  $100.14 \pm 0.29$ ; and so on.

**Table 6.4:** Intra-day analysis results of CCMN and RSV

Conc.	Intra-day analysis of CCMN				Intra-day analysis of RSV				Intra-day % Accuracy	
	Found	Mean	SD	RSD%	Found	Mean	SD	RSD%	CCMN	RSV
2	1.99	2.0033	0.0153	0.7624	1.99	1.9967	0.0058	0.2892	100.1667	99.3333
	2				2					
	2.02				2					
4	4	4.0067	0.0115	0.2882	4.01	4.01	0.01	0.2494	100.1667	100.25
	4.02				4.02					
	4				4					
8	7.96	7.9833	0.0208	0.2608	7.99	8.0033	0.0153	0.1909	99.7917	100.0417
	7.99				8					
	8				8.02					

Every value is regarded as mean  $\pm$ SD, with  $n = 3$ .

**Table 6.5:** Inter-day analysis results of CCMN and RSV

Conc.	Day	Inter-day analysis of CCMN				Inter-day analysis of RSV				Inter-day % Accuracy	
		Found	Mean	SD	RSD%	Found	Mean	SD	RSD%	CMN	RSV
2	Day-1	1.98	1.9867	0.0058	0.2906	1.99	1.99667	0.0058	0.2892	99.3333	99.8333
	Day-2	1.99				2					
	Day-3	1.99				2					
4	Day-1	4	4.0067	0.0115	0.2882	4.04	4.0167	0.0208	0.5183	100.1667	100.4167
	Day-2	4.02				4.01					
	Day-3	4				4					
8	Day-1	8	7.98	0.02	0.2506	8.02	8.0133	0.0115	0.1441	99.75	100.1667
	Day-2	7.96				8					
	Day-3	7.98				8.02					

Every value is regarded as mean  $\pm$ SD, with n = 3.

#### 6.4.3.4. Robustness

Different concentrations of CCMN and RSV were prepared for low-, medium-, and high-quality control (LQC, MQC, and HQC, respectively). The concentrations for CCMN were 0.001mg/ml, 0.016mg/ml, and 0.032mg/ml, whereas for RSV they were 0.001mg/ml, 0.008mg/ml, and 0.016mg/ml. Changing the concentration levels and retention durations of the assay was done by observing the effects of small changes to the chromatographic parameters, including pH ( $4.6 \pm 0.2$ ), wavelength ( $254 \pm 2\text{nm}$ ), flow rate ( $1 \pm 0.1\text{ ml/min}$ ), and mobile phase composition. The results show that it meets all of the standards set out by the USP and the ICH (**Figure 6.5** and **Figure 6.6**). With retention duration and test RSD values below 2%, our developed technique meets the robustness acceptance condition.

**Table 6.6:** Summary of robustness of method

Variables	Value	Strength	CCMN								RSV							
			RT	RT(mean)	SD of RT	%RSD of RT	Assay %	Assay %(mean)	SD of Assay %	%RSD of Assay	RT	RT(mean)	SD of RT	%RSD of RT	Assay %	Assay %(mean)	SD of Assay %	%RSD of Assay
Flow rate  (pH=4.6, Water:CAN= 50:50, Wavelength= 254)	0.9	LQC	11.85	11.847	0.0153	0.1289	100.41	99.797	0.6531	0.6544	8.64	8.573	0.0586	0.6835	100.85	99.840	0.8822	0.8836
		MQC	11.86				99.87				8.53				99.45			
		HQC	11.83				99.11				8.55				99.22			
	1	LQC	11.45	11.413	0.0351	0.3077	99.49	99.950	0.4927	0.4930	8.18	8.153	0.0306	0.3747	99.17	99.863	0.6008	0.6016
		MQC	11.41				99.89				8.12				100.23			
		HQC	11.38				100.47				8.16				100.19			
	1.1	LQC	11.08	11.023	0.0551	0.4996	100.41	99.907	0.7136	0.7143	7.91	7.817	0.0950	1.2159	99.41	100.117	0.6574	0.6566
		MQC	11.02				100.22				7.82				100.71			
		HQC	10.97				99.09				7.72				100.23			
pH  (Flow rate= 01ml/min Water:CAN= 50:50, Wavelength= 254)	4.4	LQC	11.18	11.110	0.0700	0.6301	100.48	100.097	0.7077	0.7070	7.98	7.943	0.0321	0.4047	100.11	99.807	0.2793	0.2799
		MQC	11.04				99.28				7.93				99.56			
		HQC	11.11				100.53				7.92				99.75			
	4.6	LQC	11.45	11.413	0.0351	0.3077	99.49	99.950	0.4927	0.4930	8.18	8.153	0.0306	0.3747	99.17	99.863	0.6008	0.6016
		MQC	11.41				99.89				8.12				100.23			
		HQC	11.38				100.47				8.16				100.19			
	4.8	LQC	11.71	11.607	0.1106	0.9529	99.79	99.787	0.6250	0.6263	8.38	8.307	0.0666	0.8016	99.48	99.580	0.2088	0.2097
		MQC	11.62				99.16				8.25				99.82			
		HQC	11.49				100.41				8.29				99.44			
Composition (Water:ACN)  (Flow rate= 01ml/min, pH=4.6 Wavelength= 254)	50:50	LQC	11.45	11.413	0.0351	0.3077	99.49	99.950	0.4927	0.4930	8.18	8.153	0.0306	0.3747	99.17	99.863	0.6008	0.6016
		MQC	11.41				99.89				8.12				100.23			
		HQC	11.38				100.47				8.16				100.19			
	55:45	LQC	11.27	11.210	0.0600	0.5352	100.75	99.803	0.8259	0.8275	8.11	7.997	0.1266	1.5834	99.74	99.870	0.1253	0.1255
		MQC	11.21				99.23				8.02				99.88			
		HQC	11.15				99.43				7.86				99.99			
	60:40	LQC	10.89	10.817	0.0702	0.6493	99.14	99.563	0.9395	0.9436	7.83	7.867	0.0404	0.5137	100.01	100.287	0.3958	0.3946
		MQC	10.81				100.64				7.91				100.11			
		HQC	10.75				98.91				7.86				100.74			
Detection wavelength  (Flow rate= 01ml/min (pH=4.6, Water:CAN= 50:50))	252	LQC	11.5	11.423	0.0709	0.6211	99.97	99.660	0.5543	0.5562	8.28	8.203	0.0681	0.8298	99.94	99.937	0.1050	0.1051
		MQC	11.36				99.99				8.15				100.04			
		HQC	11.41				99.02				8.18				99.83			
	254	LQC	11.45	11.413	0.0351	0.3077	99.49	99.950	0.4927	0.4930	8.18	8.153	0.0306	0.3747	99.17	99.863	0.6008	0.6016
		MQC	11.41				99.89				8.12				100.23			
		HQC	11.38				100.47				8.16				100.19			
	256	LQC	11.46	11.413	0.0503	0.4410	100.42	99.793	0.6742	0.6756	8.25	8.163	0.0757	0.9275	99.05	99.650	0.6940	0.6964
		MQC	11.42				99.88				8.11				100.41			
		HQC	11.36				99.08				8.13				99.49			

All the values are considered as mean  $\pm$ SD, n=3**6.4.4. Drug loading and entrapment efficacy**

The amphipathic molecular unit of the micelle vanished after CHT and CCMN separated, exposing the micelle core materials to the solution. This allowed us to break the micelle architecture using strong HCl, which aids in acid hydrolyzing ester bonds that exist between

CHT and CCMN. Prior to our established RP-HPLC analysis, a blank sample and a known concentration of CCMN and RSV mixture solution were similarly treated. Using standard curve formulae, the results of the HPLC analysis were translated from terms of AUC to terms of concentration. After computing the total sample's results (**Figure 6.7, 6.8, and 6.9**), it was discovered that the percentage of CCMN loaded into the nano-micelle was  $26.52 \pm 0.67$  w/w, with an entrapment efficacy of  $93.72\% \pm 1.02$  w/w; likewise, the percentage of RSV loaded into the nano-micelle core was  $14.56 \pm 0.18$  w/w, with an entrapment efficacy of  $98.72\% \pm 0.12$  w/w. RSV exists in free form while CCMN exists in conjugated form in the nano-micelles. Conjugated and free pharmaceuticals are extremely difficult to measure concurrently from nanomicelles using HPLC analysis or any other type of examination. There are many studies [163,146,132,131] on drug conjugates where the therapeutic qualities were assessed more thoroughly, however there aren't many that describe how conjugated drugs are estimated. Numerous research studies on drug administration by micelle are available [165,166,167]. In most situations, pharmaceuticals are entrapped in the micelle core, and this may be easily estimated using chromatographic or UV-Vis spectroscopy methods. For the first time, we created an analytical technique to concurrently estimate two medicines in two different molecular forms—conjugated and free—from a nano-micelle. Here, we also took into account the influence of % deterioration while estimating the medication. We simultaneously measured the conjugated CCMN and free RSV using our own RP-HPLC technique.

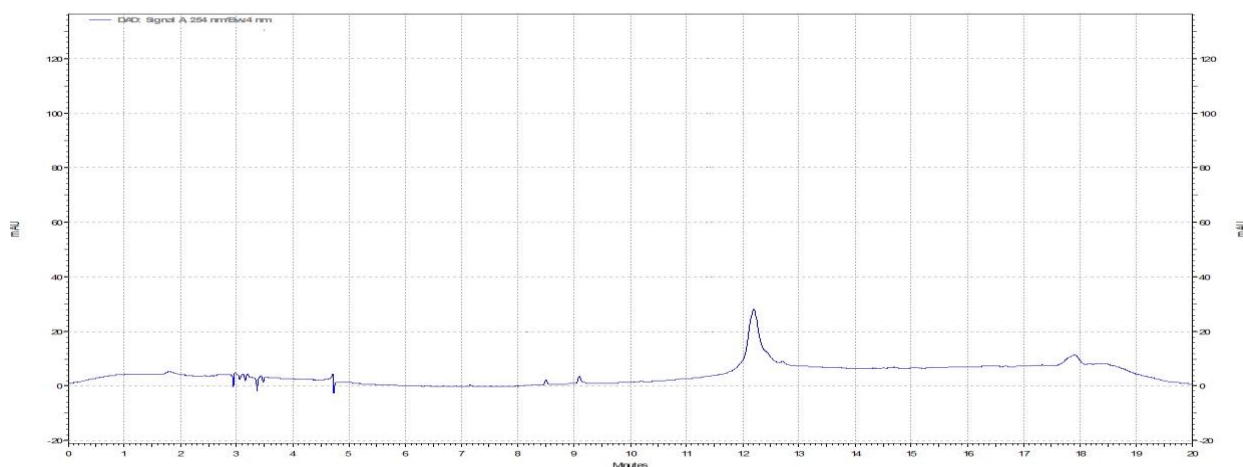


**Fig. 6.7:** A blank sample RP-HPLC chromatogram

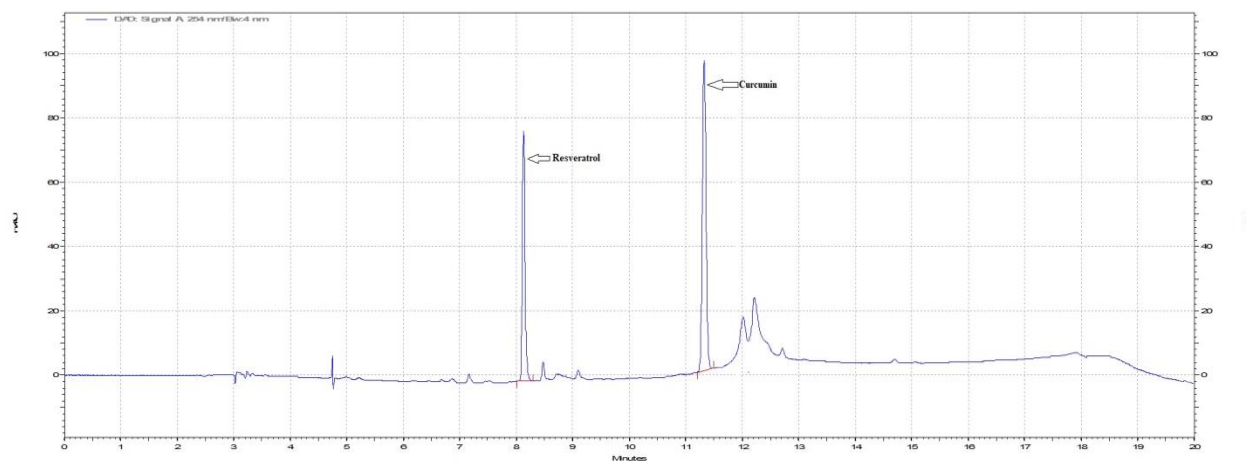


**Fig. 6.8:** RP-HPLC chromatogram of CCMN and RSV treated with 2N HCl

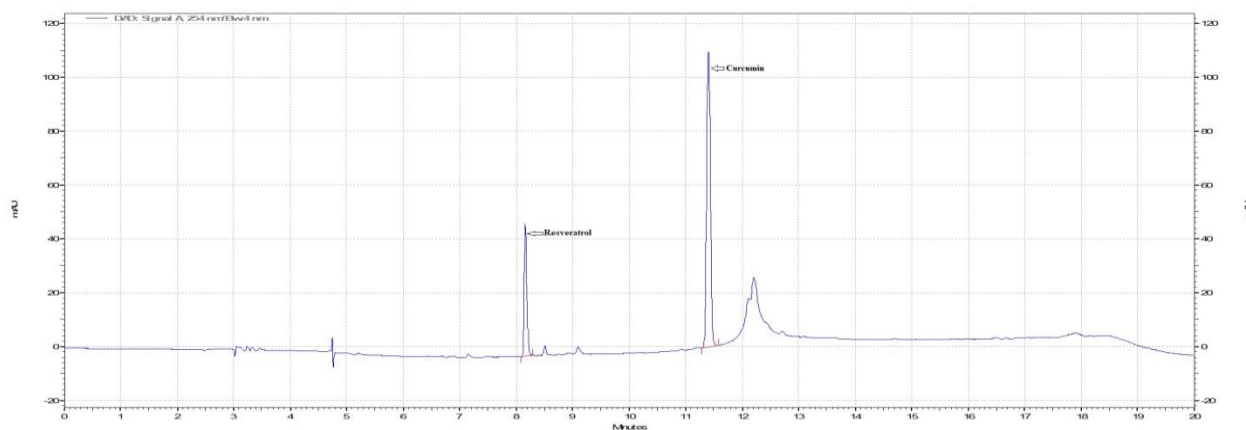


**Fig. 6.9:** Nano-micelle sample RP-HPLC chromatogram

#### 6.4.5. Cumulative drug release

By using the dialysis method, the cumulative releases of CCMN and RSV from nanomicelles were observed in phosphate buffer pH 5.0 and pH 7.4. As a result, the percentage of CCMN and RSV degradation in the same environment at the same time interval was assessed. Samples were removed from each tank at varying intervals, for a maximum of nine days, and RP-HPLC analysis was performed. More than 50% of the medications remained in the nanomicelles to be released within 7 days at pH 7.4, while over 90% of the pharmaceuticals (CCMN and RSV) were found to be released from the nano-micelle within 7 days at pH 5.0. Additionally, it was noted that after nine days, all of the medications were released at pH 5.0, but over 47% of the medications were still inside the nanomicelles and needed to be released at pH 7.4 (**Figure 6.10** and **Table 6.7**). Using standard curve formulae, the results of the HPLC analysis were translated

from terms of AUC to terms of concentration. We also take into account the effect of drug degradation percentage over the course of the cumulative drug release trial. Here, using the RP-HPLC approach, we were able to see the release pattern of both medications from nanomicelles, something that was not achievable using UV-Vis spectroscopy.

**Table 6.7:** Cumulative percent release results of CCMN and RSV in pH 5.0 and pH 7.4

Time (h)	CCMN release at pH 5		RSV release at pH 5		CCMN release at pH 7.4		RSV release at pH 7.4	
	AUC	Cumulative % release	AUC	Cumulative % release	AUC	Cumulative % release	AUC	Cumulative % release
0	0	0	0	0	0	0	0	0
1	358414	3.769869498	101224	2.995439719	188414	1.878225477	51224	1.408232817
2	714708	7.772164751	154809	4.726403754	364708	3.858687091	74809	2.171000641
4	1094689	12.07767875	264901	8.268143893	604689	6.567430986	134901	4.100138568
6	1544679	17.20448682	374699	11.83549901	808679	8.902395035	194699	6.039019405
8	2144794	24.0518553	514684	16.39596886	1084794	12.06261549	264684	8.320260136
12	3077681	34.66886027	757771	24.27375985	1597681	17.88819743	377771	11.99195284
24	4498705	50.82132605	1458697	46.76242114	2398705	26.97704189	758697	24.20186223
36	5499347	62.45418959	2099436	67.56300091	2799347	31.6998411	1149436	36.84419852
48	6229891	71.19293147	2389891	77.44751409	3129891	35.68721829	1309881	42.30008701
72	7049983	81.00939236	2686874	87.63145545	3509983	40.2627125	1386874	45.15779557
168	8291286	95.60405613	2997987	98.35821618	4001286	46.1179809	1487987	48.80561351
216	8610021	100.0711363	3020131	100.0106652	4284421	49.71156665	1580131	52.20081573

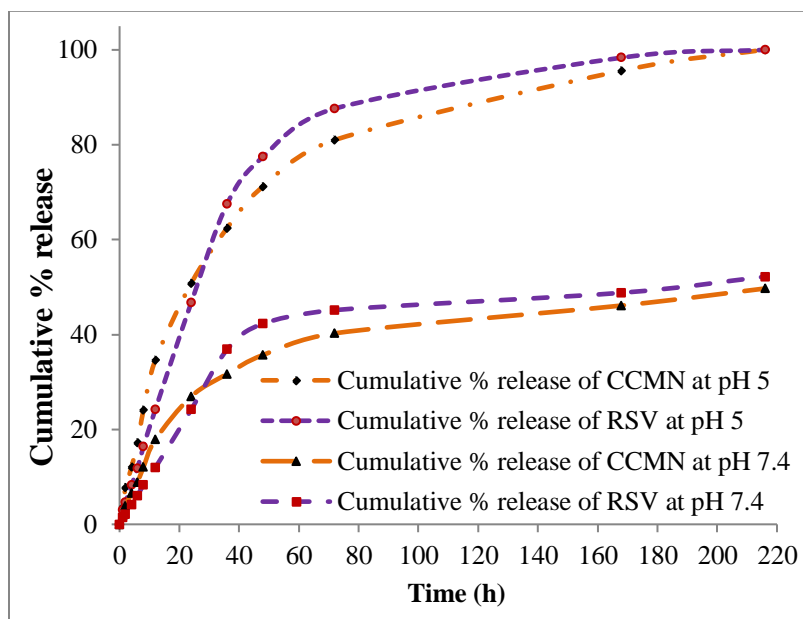


**Fig. 6.10:** Cumulative percent release pattern of CCMN and RSV in pH 5.0 and pH 7.4

#### 6.4.6. Stability of CDSCM-RSV containing CCMN and RSV in physiological pH

The proportion that is still prone to degradation was computed and displayed in **Figure 6.11**. Over 90% of CCMN in CDSCM-RSV was still present at the same time as free CCMN was predicted to completely decay after 8 hours. Conjugated CCMN was discovered to be significantly more stable than free CCMN in CDSCM-RSV. Thus, CCMN stability is greatly increased by the nanomicelles created through conjugating CCMN with CHT.

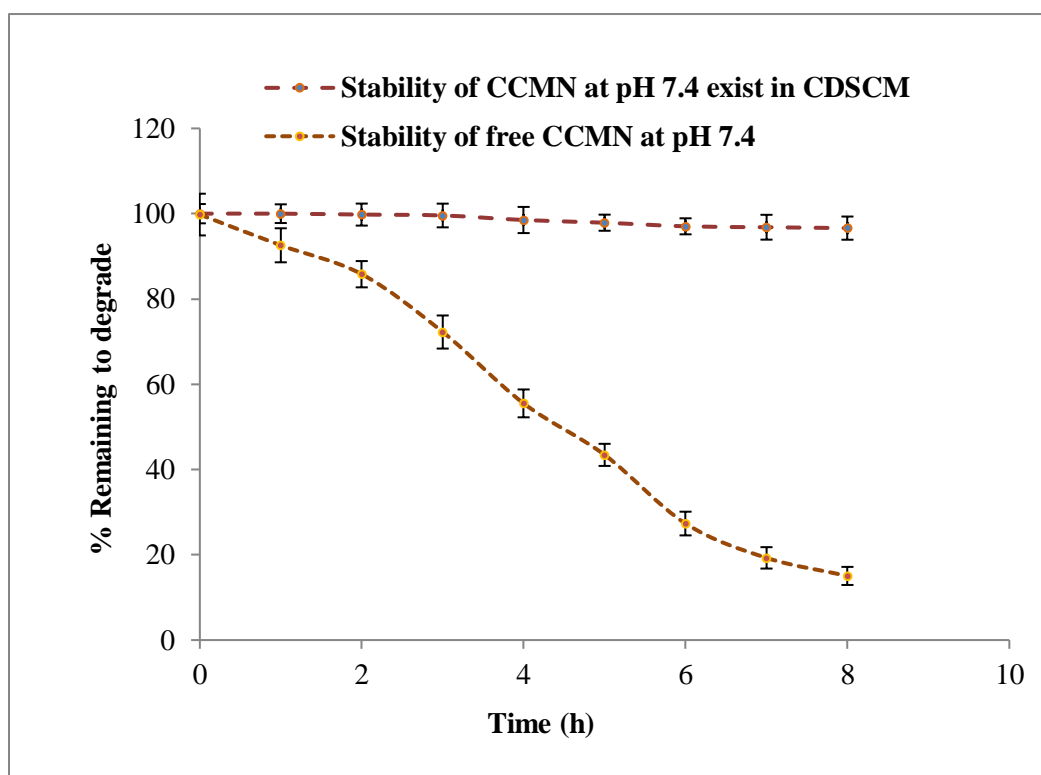


**Fig. 6.11:** Stability study of CDSCM-RSV containing CCMN at pH 7.4

The percentage of RSV left to deteriorate was computed and displayed in Figure 6.12. Over 90% of RSV in CDSCM-RSV was still present at the same time as free RSV was predicted to completely deteriorate after 8 hours. RSV with CDSCM-RSV was discovered to be significantly more stable than free RSV. Thus, conjugation-developed nanomicelles greatly increase RSV stability (**Figure 6.12**).

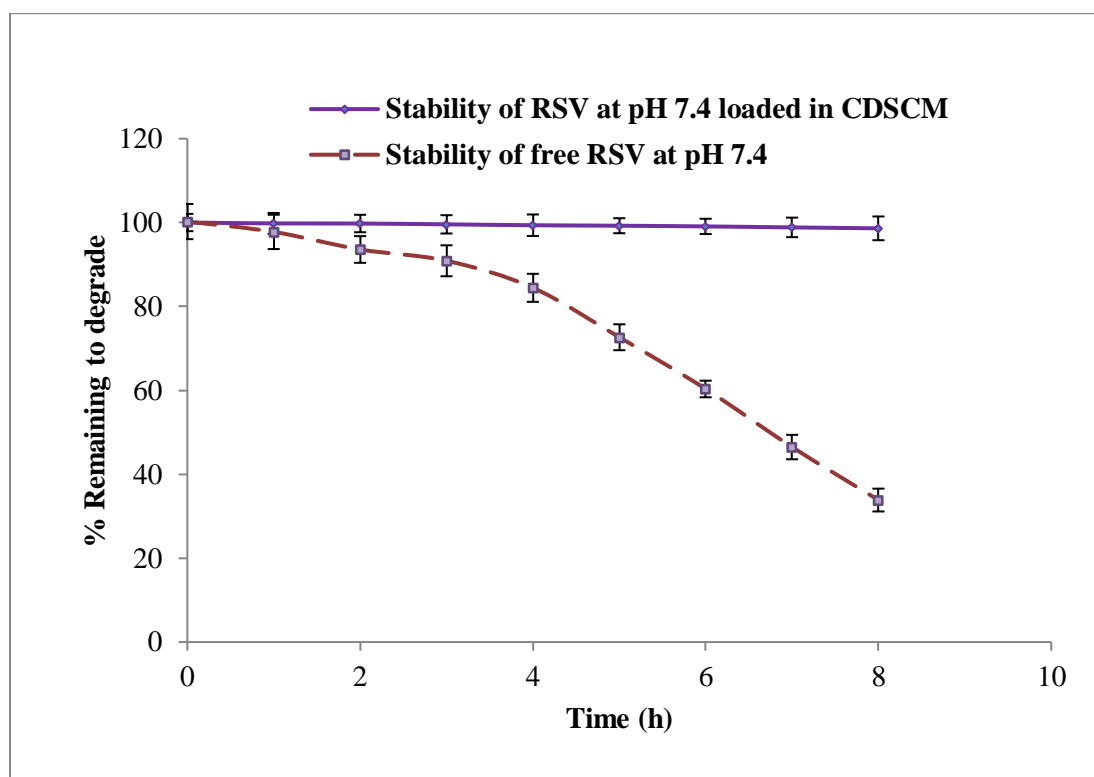


**Fig. 6.12:** Stability study of CDSCM-RSV containing RSV at pH 7.4

## 6.5. Conclusions

Our developed RP-HPLC method was used to analyze the free form of resveratrol and the conjugated form of curcumin present in the CDSCM-RSV nanomicelle concurrently. Following ICH Q2(R1) guidelines, the devised RP-HPLC technique was validated. It was discovered that our developed approach demonstrated its precision criteria, linearity, robustness, and compatibility for the system. The chromatogram revealed that the drug-arousing peaks from the nanomicelle extract and the drug-arousing peaks from the mixture of medicines at known concentrations were entirely separated and well-resolved. The resolution of peaks was significantly impacted by insignificant interactions from other drugs. There was no such compound in our established approach, which resulted in a longer column lifetime, compromised column integrity, and required a great deal of time to remove from the column.



# Chapter 7

## ***In-vivo* study of CDSCM-CCMN and CDSCM-RSV as antidiabetic nanoformulation**

- 7.1 Introduction
- 7.2 Experimental animals
- 7.3 Experiment design for *In-vivo* study
  - 7.3.1 Induction of Type-II diabetes mellitus
  - 7.3.2 Sampling of blood to estimate FBG level
  - 7.3.3 Measurement of body weight
  - 7.3.4 Analysis of biochemical parameters level
  - 7.3.5 Carbohydrate metabolizing enzymes estimation
- 7.4 Histopathology of pancreas
- 7.5 Statistical analysis
- 7.6 Results and discussions
- 7.7 Conclusions

### 7.1. Introduction

We have developed two types of nanomicelles (CDSCM-CCMN, CDSCM-RSV), one consist single drug CCMN as conjugated and free form, another consist two drugs CCMN and RSV as conjugated and free form respectively, both were subjected to *in-vivo* evaluation as antidiabetic derivative and compared their potential with standard drug Glybenclamide. The powder form of nanomicelle was administered to male Balb/C mice through oral gavages. Initially all the animals were examined thoroughly, underweight, skin infected and aggressive animal were discarded and selected animal were acclimatized in animal house. In regular basis body weight and fasting blood glucose (FBG) levels of all the animals was measured. There are many biochemical parameters that signify diabetic animals but FBG level is the main biochemical parameter which directly correlate the diabetic animals. Other biochemical parameters which were evaluated in our study were Serum glutamate oxaloacetic transaminase (SGOT), serum glutamate pyruvic transaminase (SGPT), serum uric acid, hemoglobin A1c (HbA1c), and lipid profile components like high density lipoid (HDL), low density lipid (LDL), serum triglycerides, total serum cholesterol, and lysosomal enzymes like alkaline phosphatase (ALP) and acid phosphatase (ACP) hexokinase (HK), glucose-6-phosphate dehydrogenase (G6PD), and lactate dehydrogenase (LDH).

### 7.2. Experimental animals

For the *in vivo* antidiabetic study, 6 weeks old male Balb/C mice [168,169] weigh about 25-30g, obtained from Chakraborty Enterprises (North 24 Parganas PIN-743312 West Bengal), registered breeders. Before start of experiments, they were kept for 7 days to adjust standard laboratory conditions with a standard diet according to protocols. After administration of streptozotocine (Diabetic inducer) they were kept for 3days for molding. In the molding period if FBG level increased more than 200mg/dL was considered as diabetic animal and treatment was started immediately. The start day of treatment was considered as zero days and treatment stop in 21<sup>st</sup> days (**Figure 7.1 & 7.2**). This experiment followed the guidelines of the "Institutional Animal Ethics Committee", Jadavpur University, India, throughout the study, followed the National Institute of Health (NIH) recommendations.

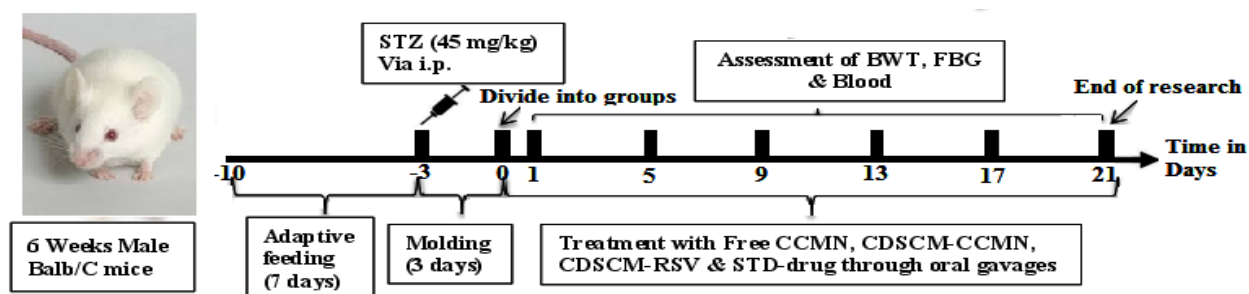


Fig. 7.1: Experimental protocol

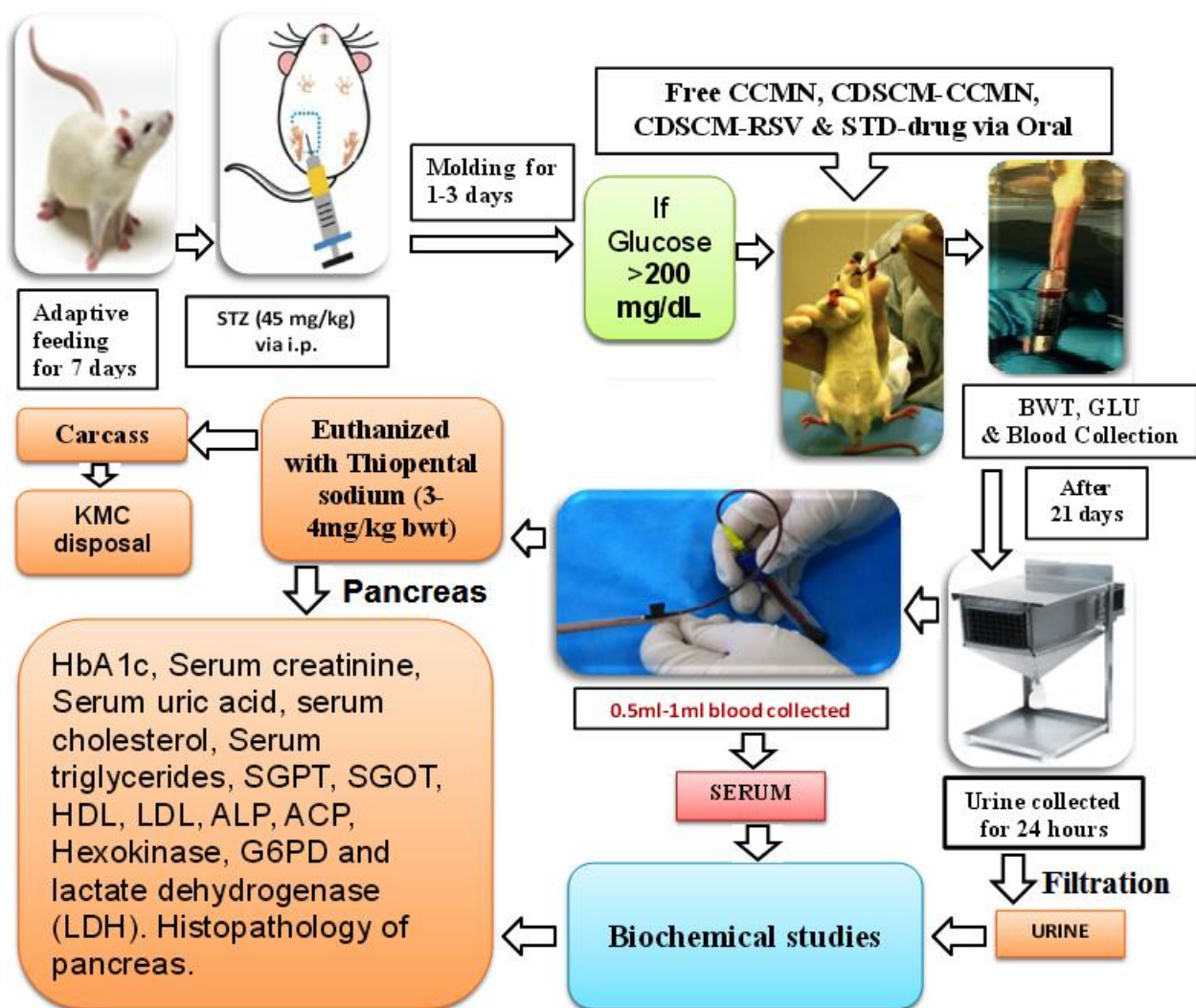


Fig. 7.2: Schematic testing protocol

### 7.3. Experiment design for *In-vivo* study

Thirty animals in total were caught and distributed equally into five groups. **Group I:** Regular diets high in fat were given to non-diabetic control animals (NDc). **Group II:** A single dosage of a diabetes inducer was administered together with a usual meal heavy in fat. **Group III:** Diabetic Control Free CCMN (Dc-F-CCMN), which was treated orally with free CCMN at a dose of 100 mg/kg body weight for 21 days after receiving a typical meal heavy in fat and a single dose of diabetic inducer. **Group IV:** Diabetic control drug-nanoparticle (Dc-M-CCMN) was administered oral CDSCM-CCMN corresponding to 100 mg/kg CCMN payload for 21 days after receiving a typical meal heavy in fat and a single dose of diabetic inducer. **Group V:** Diabetic control drug-containing nanoparticle (Dc-M-RSV) was administered oral CDSCM-RSV corresponding to 100 mg/kg CCMN and RSV accumulated payload for 21 days after receiving a typical meal heavy in fat and a single dose of diabetic inducer. **Group VI:** Diabetic control standard drug (Dc-SD), which received a high fat-containing regular diet with a single dose of diabetic inducer and treated orally with 2 mg/kg b.w. glibenclamide for 21 days.

**Table 7.1:** Group division of animals for treatment

Groups	No. of animals	Treatment used
<b>Group I:</b> Non-diabetic control animals (NDc)	6	High fat diet (HFD) + Saline solution
<b>Group II:</b> Diabetic control (Dc)	6	HFD + STZ
<b>Group III:</b> DC free CCMN (Dc-F-CCMN)	6	HFD + STZ + Free CCMN (100 mg/kg b.w.)
<b>Group IV:</b> DC receiving CDSCM-CCMN (Dc-M-CCMN)	6	HFD + STZ + CDSCM-CCMN (100 mg/kg b.w. CCMN equivalent )
<b>Group V:</b> DC receiving CDSCM-RSV (Dc-M-RSV)	6	HFD + STZ + CDSCM-RSV (100 mg/kg b.w. CCMN & RSV accumulated equivalent )
<b>Group VI:</b> DC standard drug (Dc-SD)	6	HFD + STZ + Glybenclamide (2 mg/kg b.w.)

### **7.3.1. Induction of Type-II diabetes mellitus**

A single intraperitoneal injection of 45 mg/kg b.w. of STZ and 110 mg/kg b.w. of nicotinamide were administered to overnight-fasting mice to induce Type-II diabetes mellitus [170,171,172]. It was necessary to dissolve the STZ solution in a saline solution and a citrate buffer with a pH of 4.5 as part of the separate preparation process. Group I, which consisted of animals without diabetes, was administered saline injections instead of STZ. An Accu-Check glucometer, made by Roche Diagnostics, was used to measure the FBG levels of all the animals. When animals' FBG levels were higher than 200 mg/dl for three consecutive days after receiving the STZ injection, they were categorized as diabetic. The trial was terminated for animals that were determined not to have diabetes when their blood glucose levels were below 145 mg/dl.

### **7.3.2. Sampling of blood to estimate FBG level**

Blood samples were collected by pricking the tail and then gently milking it with warm water to evaluate the FBG level of each animal. The direction of milking was from the body side to the tail tip to enhance bleeding. One drop of blood was placed on a strip of the accu-check glucometer to check blood glucose levels, and it was done in duplicate to ensure the consistency of glucometer readings [173].

### **7.3.3. Measurement of body weight**

The weight of every animal in every group was recorded every four days. There was documentation of the weight variation. Additionally, the weight of each animal's liver was documented after 21 days.

### **7.3.4. Analysis of biochemical parameters level**

On the 21st day of the trial, all animals had their blood drawn via heart puncture under a light anesthetic for the biochemical examination. In a cooled centrifuge, blood samples were centrifuged for 15 minutes at 4000 rpm. The serums were properly balanced and kept for further examination at -80°C. SGOT, SGPT, serum uric acid, HbA1c, and lipid profile components like HDL, LDL, serum triglycerides, total serum cholesterol, and lysosomal enzymes like ALP and ACP were measured using auto-analyzer (USA) and ELIZA kits [173,174].

### **7.3.5. Carbohydrate metabolizing enzymes estimation**

To estimate the level of HK, G6PD, and LDH parameters in the pancreas, liver, and kidney, all animals were euthanized with thiopental sodium after 21 days of treatment. The 0.3 g of tissues were chopped up and mixed with 3 ml of 0.01M Tris-HCL before being centrifuged at 10,000 rpm for 20 minutes at 4°C. We used the appropriate colorimetric test kits for HK, G6PD, and LDH [174,175] to treat the supernatants.

### **7.4. Histopathology of pancreas**

After the pancreas carefully removed, the blood was removed by washing in distilled water. After that, it was cut into pieces and kept for histopathological research in a 10% neutral buffered formalin solution. These organs' tissues were dehydrated in alcohol, cleaned with xylene, and then placed in paraffin. The tissue of the pancreas was sectioned into sections about 5µm (five micrometers) thick using a microtome from paraffin blocks. The sections were then inspected under a light microscope (photograph amplified by approximately 400 times), mounted in neutral dibutylphthalate polystyrene xylene (DPX) media, and stained with hematoxylin and eosin.

### **7.5. Statistical analysis**

For the statistical analysis, all the readings were taken more than two times, standard deviation (SD) was calculated from obtained data, and the actual value of the readings was represented as mean  $\pm$  SD, where it possible. One-way analysis of variance (ANOVA) with a P-value  $< 0.05$  was utilized for the statistical processing of the obtained results in order to determine which groups or categories had significant changes compared to other statistical tools, such as the student t-test. Different software like Origin Pro 9.0 and GraphPad Prism 6.0 are used for the graphical representation of statistically processed data.

### **7.6. Results and discussions**

Following three days of inducing diabetes, it was noted that  $284 \pm 9$  mg/dL of FBG was present in the majority of the animals. Exclusion from the study was made for animals with fasting blood glucose levels  $\leq 200$  mg/dL, and these animals should be categorized as diabetic. Group II mice gradually lost weight once diabetes developed (**Figure 7.5**), whereas group III animals gained

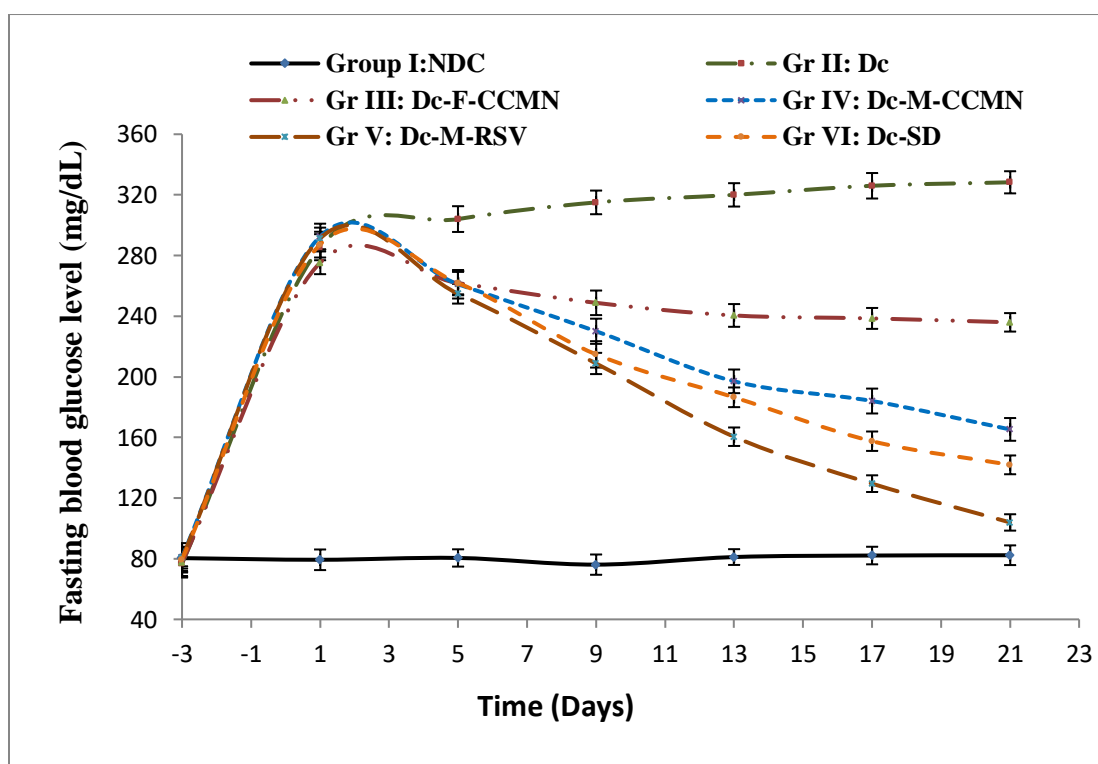
just a small amount of weight. When comparing the body weight of group IV (the group receiving CDSCM-CCMN) and group V (the group receiving CDSCM-RSV) to group VI (the diabetic control group getting conventional medication), a significant increase was noted. The aforementioned results underscore the importance of establishing a connection between diabetes and body weight, as well as the potential role of CDSCM-CCMN and CDSCM-RSV in mitigating the changes in body weight associated with diabetes.

Every four days, the FBG level of the animals was measured after they had fasted overnight. In group II, the FBG level increased gradually (**Figure 7.3**), whereas in groups III, IV, and V, the FBG level decreased gradually. The non-diabetic control group I has no significant change in FBG levels. The reduction of FBG level in CDSCM-RSV recipients group IV was significantly more than the standard drug recipient group V. Following 21 days of therapy, the greatest drop in blood glucose levels was seen in group V CDSCM-RSV users (**Figure 7.4**).

The changes in FBG concentrations reflect the effect of interventions on glucose metabolism. The observed reduction in FBG levels across groups IV and V provides evidence of the potential efficacy of these therapies in managing diabetes. The observed difference in the rate of FBG level reduction between group V (the group receiving the CDSCM-RSV treatment) and group VI (standard drug glibenclamide) may be attributed to the unique mechanism of action of CDSCM-RSV. The promise of dual drug containing nanomicelles as a viable technique for glucose control in diabetes treatment is demonstrated by the faster rate of decline in FBG levels in the CDSCM-RSV group (IV) compared to the traditional drug group (VI).

**Table 7.2:** Fasting blood glucose level (mg/dL) at the treatment

Test Day	Gr I: NDc	Gr II: Dc	Gr III: Dc-F-CCMN	Gr IV: Dc-M-CCMN	Gr V: Dc-M-RSV	Gr VI: Dc-SD
-3	80.4±5.4	76.7±9.1	77.4±8.8	81.1±9.2	80.5±7.0	79.4±8.5
1	79.3±6.8	285.5±8.6	275.2±7.5	292.5±8.5	291.2±7.2	287.2±8.5
5	80.5±5.7	304.05±8.0	261.8±8.0	261.05±9.4	254.8±6.5	261.8±7.4
9	76.1±6.7	315.05±8.1	248.8±8.1	230.05±8.3	208.8±7.0	214.8±8.7
13	81.1±5.2	320.02±7.7	240.48±7.5	197.02±7.8	160.48±6.1	186.48±6.5
17	82.1±5.8	326.02±8.4	238.52±6.9	184.02±8.2	129.52±5.5	157.52±6.4
21	82.3±6.5	328.3±7.3	235.93±6.1	165.3±7.5	103.93±5.4	141.93±6.2

**Fig. 7.3:** Fasting blood glucose level assessment



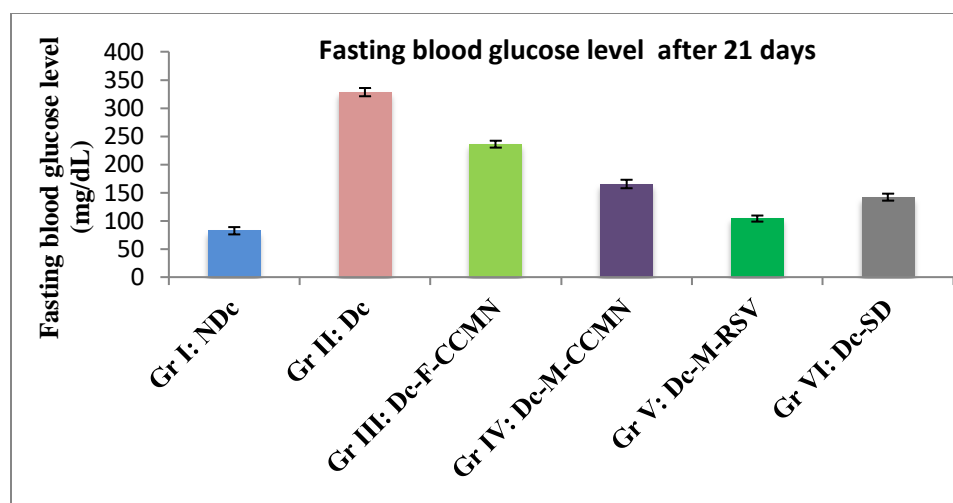


**Fig. 7.4:** Fasting blood glucose level after 21 days

Over the course of the investigation, the diabetic control group-II, which was not receiving treatment—saw a notable decrease in body weight. This body weight reduction could have been caused by a decrease in feed intake, an increase in catabolic processes (such as proteolysis, lipolysis, glycogenolysis, and metabolic pathway disruption), muscle atrophy, and tissue protein loss [176–179]. Gaining body weight was one indicator of recovery in the diabetic mice treated with CDSCM-RSV and CDSCM-CCMN [180]. The liver is the body's primary metabolic organ and is essential to maintaining lipid and glucose balance. The liver's increased accumulation of lipids and cholesterol may be the reason for the notable increases in liver weight.

**Table 7.3: Body weight and liver weight assessment**

Test Day	Gr I: NDc	Gr II: Dc	Gr III: Dc-F-CCMN	Gr IV: Dc-M-CCMN	Gr V: Dc-M-RSV	Gr VI: Dc-SD
1st Day	28.87±0.40	30.68±0.60	28.87±0.85	27.82±0.40	28.57±0.30	27.37±0.75
5th Day	29.47±0.60	30.08±0.55	28.72±1.00	28.57±0.60	29.92±0.45	28.12±0.90
9th Day	30.08±0.70	29.62±1.20	27.82±1.05	29.17±0.65	31.28±0.70	29.02±0.90
13th Day	30.68±0.95	28.57±0.85	27.37±1.10	29.77±0.90	31.73±1.00	30.08±1.00
17th Day	31.13±0.50	27.82±0.75	27.07±1.10	30.38±0.45	32.03±0.50	30.83±0.95
21st Day	31.58±0.50	26.77±1.00	26.92±0.70	30.23±0.55	32.33±0.55	31.28±0.60
Wt. of the liver at 21st Day	1.30±0.10	1.58±0.15	1.48±1.0	1.30±0.20	1.42±0.05	1.44±0.05

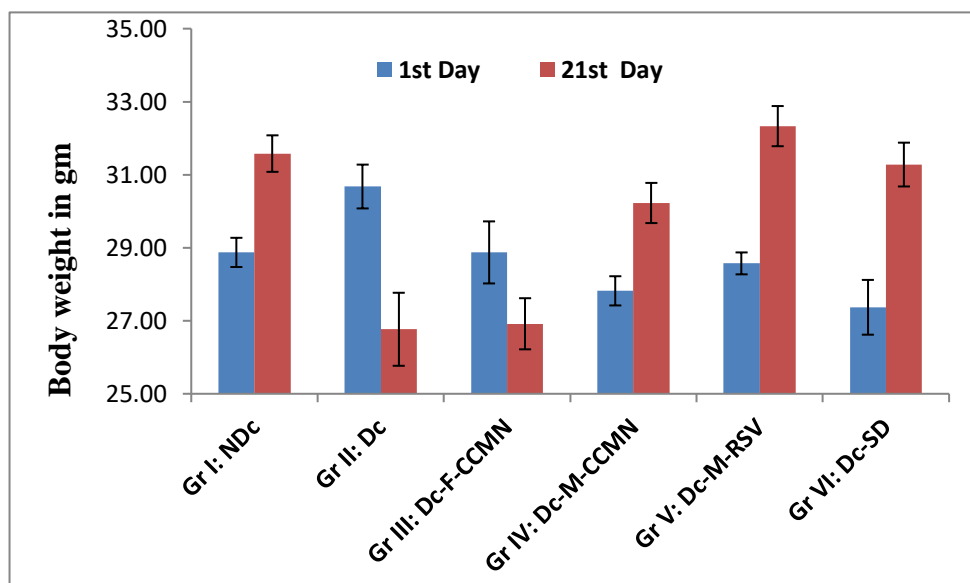


**Fig. 7.5:** Body weight variation

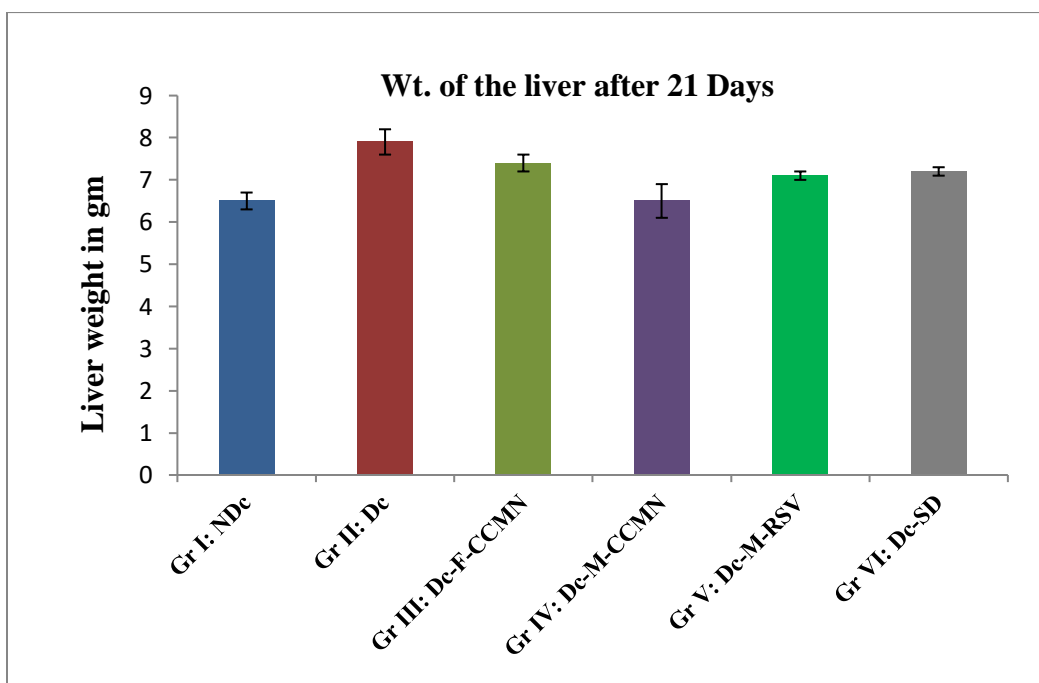


**Fig. 7.6:** Comparison of liver weight after 21 days

**Table 7.4: Study of biochemical parameters after 21 days**

Parameter	Gr I: NDc	Gr II: Dc	Gr III: Dc-F-CCMN	Gr IV: Dc-M-CCMN	Gr V: Dc-M-RSV	Gr VI: Dc-SD
<b>HbA1c (%)</b>	5.70 ± 0.23	12.03 ± 0.3	9.55 ± 0.22	7.01 ± 0.3	5.74 ± 0.20	6.19 ± 0.16
<b>Serum creatinine (mg/dL)</b>	0.81±0.05	1.51±0.04	1.11±0.03	1.09±0.03	1.01±0.04	1.17±0.04
<b>Serum uric acid (mg/dL)</b>	4.1±0.4	6.3± 0.2	5.1±0.3	5.7± 0.3	4.63±0.2	5.5±0.5
<b>Serum cholesterol (mg/dL)</b>	83.0±1.1	157±1.7	140±1.2	130±1.8	91±0.9	124±2.1
<b>Serum triglycerides (mg/dL)</b>	90.0±1.1	156.2±1.9	141.7±2.2	128.9±2.7	95±1.4	111±3.1
<b>SGPT (IU/L)</b>	70.0±1.0	170.6±3.86	152.6±3.86	110.6±3.86	72.0±1.0	80.0±1.0
<b>SGOT (IU/L)</b>	121.2±2.3	255.2±4.3	220.2±2.3	181.2±2.3	136.2±2.3	140.2±2.3
<b>HDL cholesterol (mg/dL)</b>	51.0±1.2	32±2.1	35.5±1.4	37±1.8	44.5±1.5	43.1±1.4
<b>LDL cholesterol (mg/dL)</b>	21±1.2	88.8±2.4	82.1±1.5	70.2±2.4	33.5±1.5	61.8±1.6
<b>ALP (IU/L)</b>	170.0±1.5	233± 3.0	228±2.5	223± 3.0	185±2.2	211±2.1
<b>Hexokinase (U/ml)</b>	1.65±0.11	1.25±0.03	1.26±0.12	1.29±0.04	1.47±0.21	1.34±0.32
<b>G6PD(U/ml)</b>	22.61±1.42	95.43±2.07	72.61±2.52	61.83±2.87	34.98±2.84	58.81±1.82
<b>LDH(U/ml)</b>	13.63±0.7	26.76±1.4	24.8±0.8	20.46±1.8	15.8±0.8	17.7±1.02

Since HbA1c provides a reliable assessment of chronic hyperglycemia and is linked to the risk of long-term diabetic issues, it is currently considered the test of choice for the management of chronic diabetes. In diabetics, blood glucose levels rise, and the way the glucose molecule binds to hemoglobin depends on its concentration. Hemoglobin that has been bonded to glucose, or glycated, is known as HbA1c, and it indicates an individual's average blood glucose level. The

blood becomes glycated with the hemoglobin. The fact that the HbA1c levels and blood glucose levels are directly correlated is significant.

The consistency of high FBG levels in the animals indicates high glycated hemoglobin (HbA1c). After 21 days; the HbA1c levels of animals in group IV treated with CDSCM-RSV were lower (**Table 7.4 and Figure 7.7**). This decrease in HbA1c reflects the improved blood sugar management made possible by the administration of CDSCM-RSV.

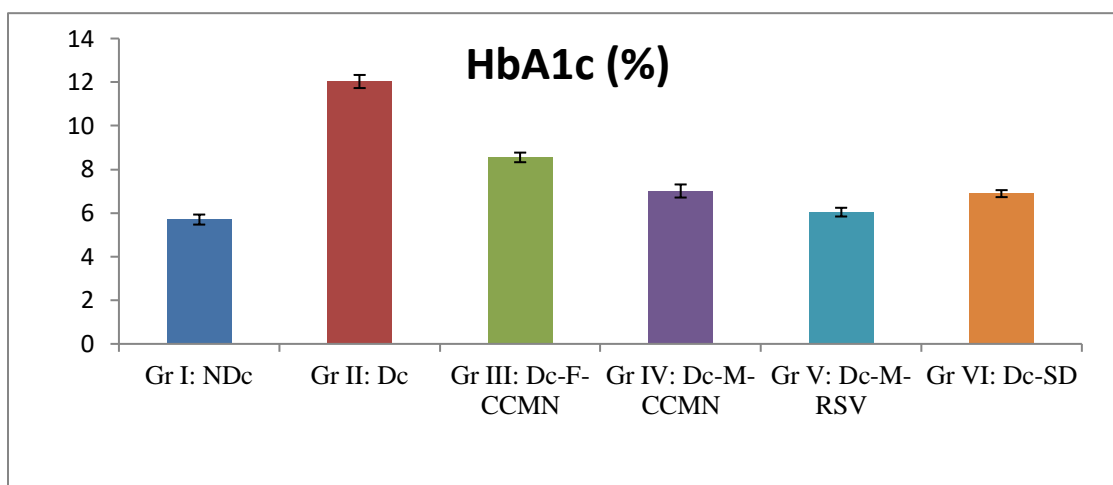


**Fig. 7.7:** Glycated hemoglobin (HbA1c) after 21 days of treatment

In order to evaluate hepatic function, one looks at ALP, SGPT, and SGOT levels. However, because creatinine and serum uric acid have comparable values, the idea of evaluating renal function has been proposed. The impaired kidney function was demonstrated by the increased concentrations of urea and creatinine in the blood serum of the diabetic control group-II and the free curcumin group-III mice. When compared to the first control group, all of the rats given "STZ" to induce diabetes showed elevated serum creatinine and urea levels (**Table 7.4 and Figure 7.8**). Kidney damage due to "STZ," aberrant glucose levels, or glycosylated protein levels might account for this observation [181]. Even after being treated with CDSCM-RSV, CDSCM-CCMN, and conventional medications, the diabetic mice's kidneys demonstrated a protective effect, allowing them to eliminate waste products from the blood more effectively.

The blood of diabetic mice showed elevated levels of triglycerides and cholesterol as well as a decrease in HDL (**Table 7.4 and Figure 7.8**), which suggested that the mice may have been predisposed to cardiovascular disorders [182]. This is usually caused by low insulin levels,

which trigger the lipase enzyme to hydrolyze stored triglycerides, releasing a high amount of glycerol and fatty acids into the bloodstream. Fatty acid synthesis into cholesterol and phospholipids may be facilitated by the elevated blood fatty acid level [180, 183]. Free fatty acid (FFA) mobilization from peripheral fat depots increased, leading to a greater blood lipid level in the diabetic patient. The mice treated with CDSCM-RSV and CDSCM-CCMN showed much reduced levels of LDL, triglycerides, and cholesterol in their serum, while the mice treated with "STZ" had much greater levels of HDL (Table 7.4 and Figure 7.8, 7.9).

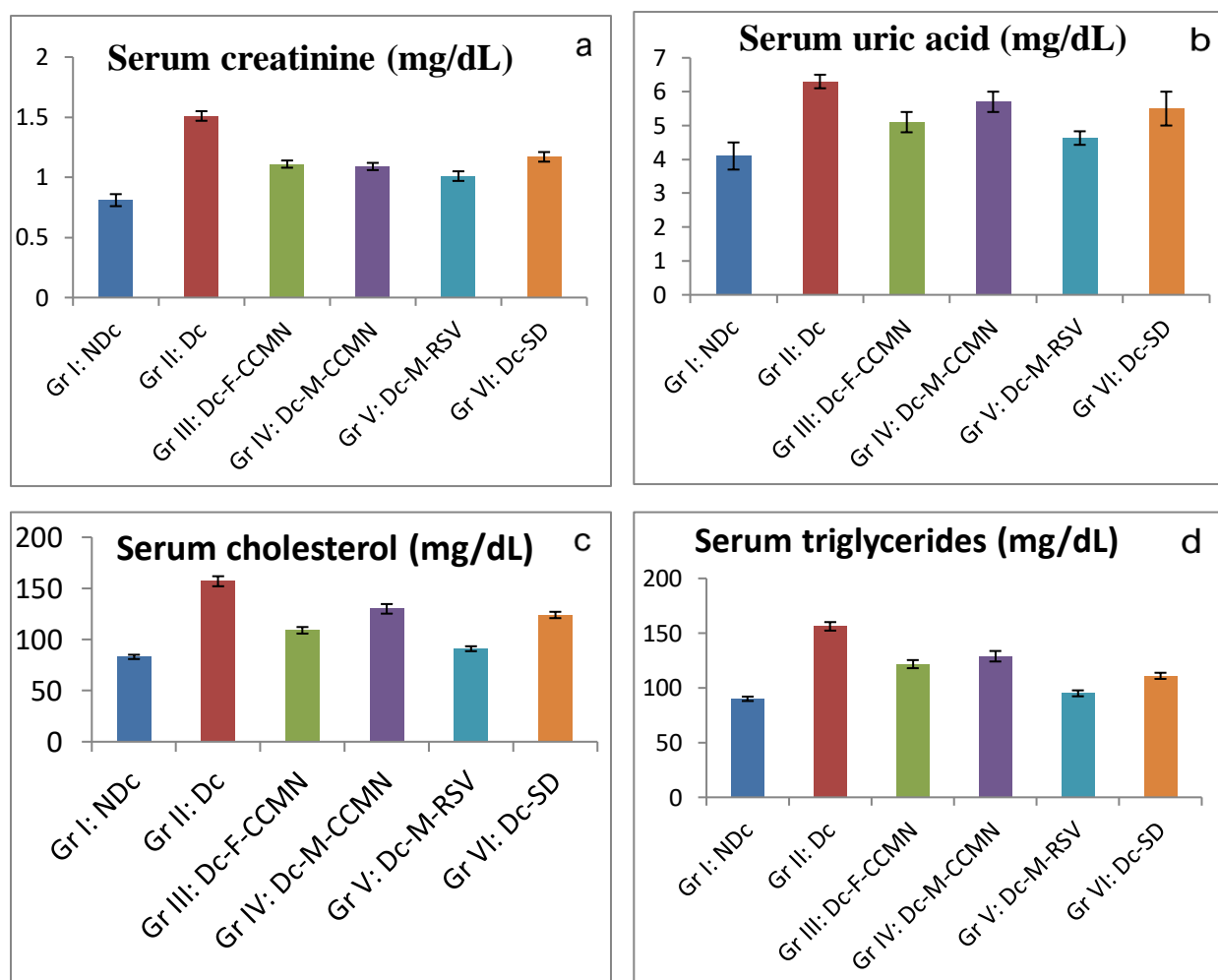


**Fig. 7.8:** Level of (a) Serum creatinine, (b) Serum uric acid, (c) Serum cholesterol, (d) Serum triglycerides

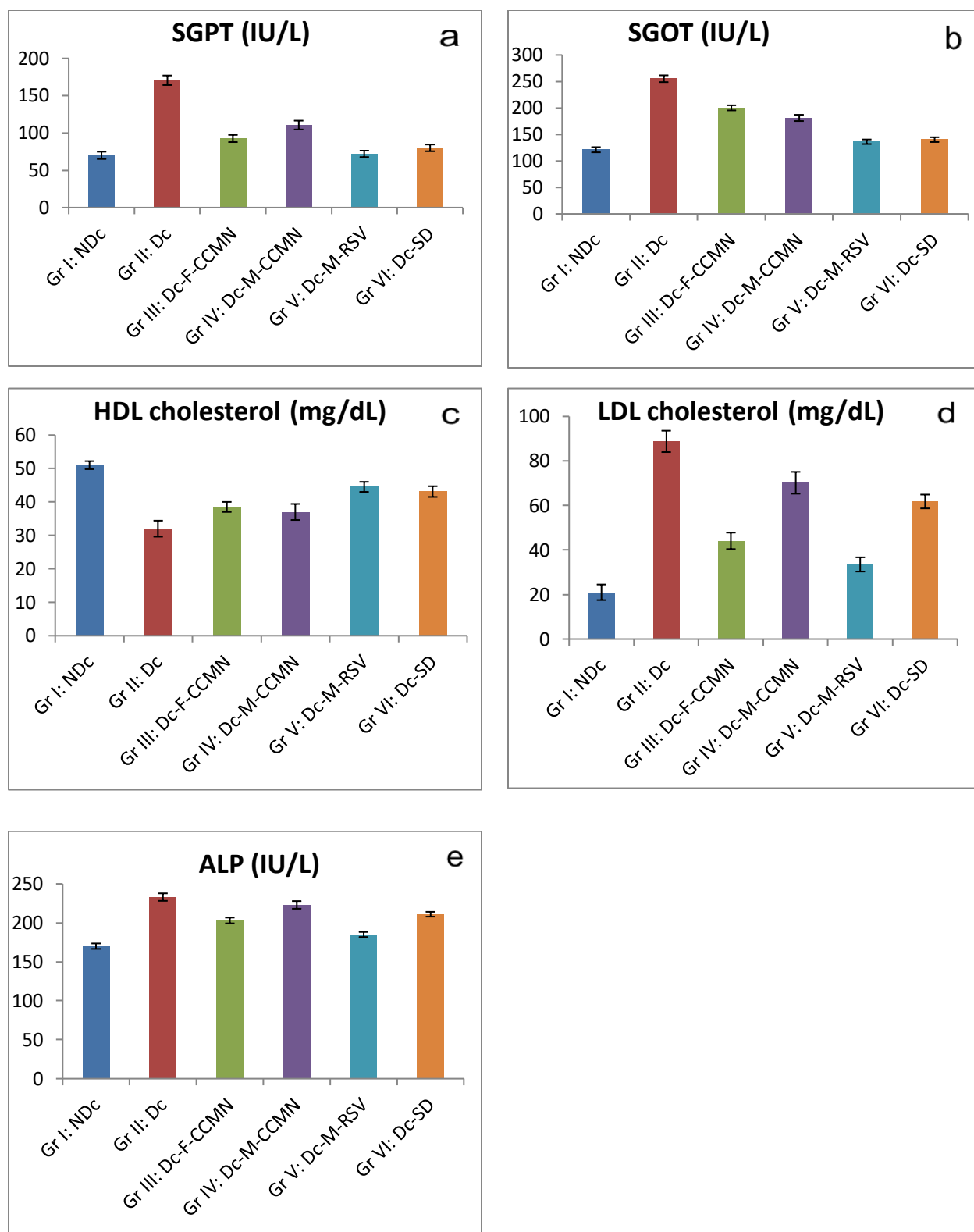


**Fig. 7.9:** Level of (a) SGPT, (b) SGOT, (c) HDL cholesterol, (d) LDL cholesterol, (e) ALP

The hexokinase (HK) that phosphorylates glucose during the glycolysis process was analyzed. Increases in hepatic hexokinase can enhance the liver's ability to store glycogen by increasing blood glucose utilization. Among diabetes biomarkers, hepatic HK is very sensitive to changes in the glycolytic pathway. A decrease in glucose-6-phosphate dehydrogenase (G6PD) activity was linked to diabetes mellitus. The production of reducing equivalents like NADH and NADPH, as well as the hexose monophosphate pathway (HMP), were also impacted by this [184]. While HK and G6PD activity decreased in diabetic control group II and diabetic control free CCMN group III, respectively, they increased in groups IV and V treated with CDSCM-CCMN and CDSCM-RSV, respectively (**Table 7.4 and Figure 7.10**). This indicates that the activity of the enzymes HK and G6PD responsible for metabolizing carbohydrates was enhanced by CDSCM-RSV and CDSCM-CCMN.

The cytosolic enzyme lactate dehydrogenase (LDH) catalyzes the anaerobic glycolysis process, which transforms pyruvate into lactate. Lactate is then transformed into glucose through glucogenic flux. When LDH levels are high, it throws off glucose metabolism and causes insulin secretion problems in diabetes [185]. Lipase activity was shown to be significantly enhanced in both the diabetic control group II and the free CCMN diabetic control group III that were given free curcumin in this study. Diabetes is associated with increased LDH activity because it impairs glucose-stimulated insulin production. The CDSCM-CCMN and CDSCM-RSV treated groups showed a considerable suppression of LDH activity (**Table 7.4 and Figure 7.10**). The positive benefits of the nanomicelle were demonstrated by the decrease of LDH activity.

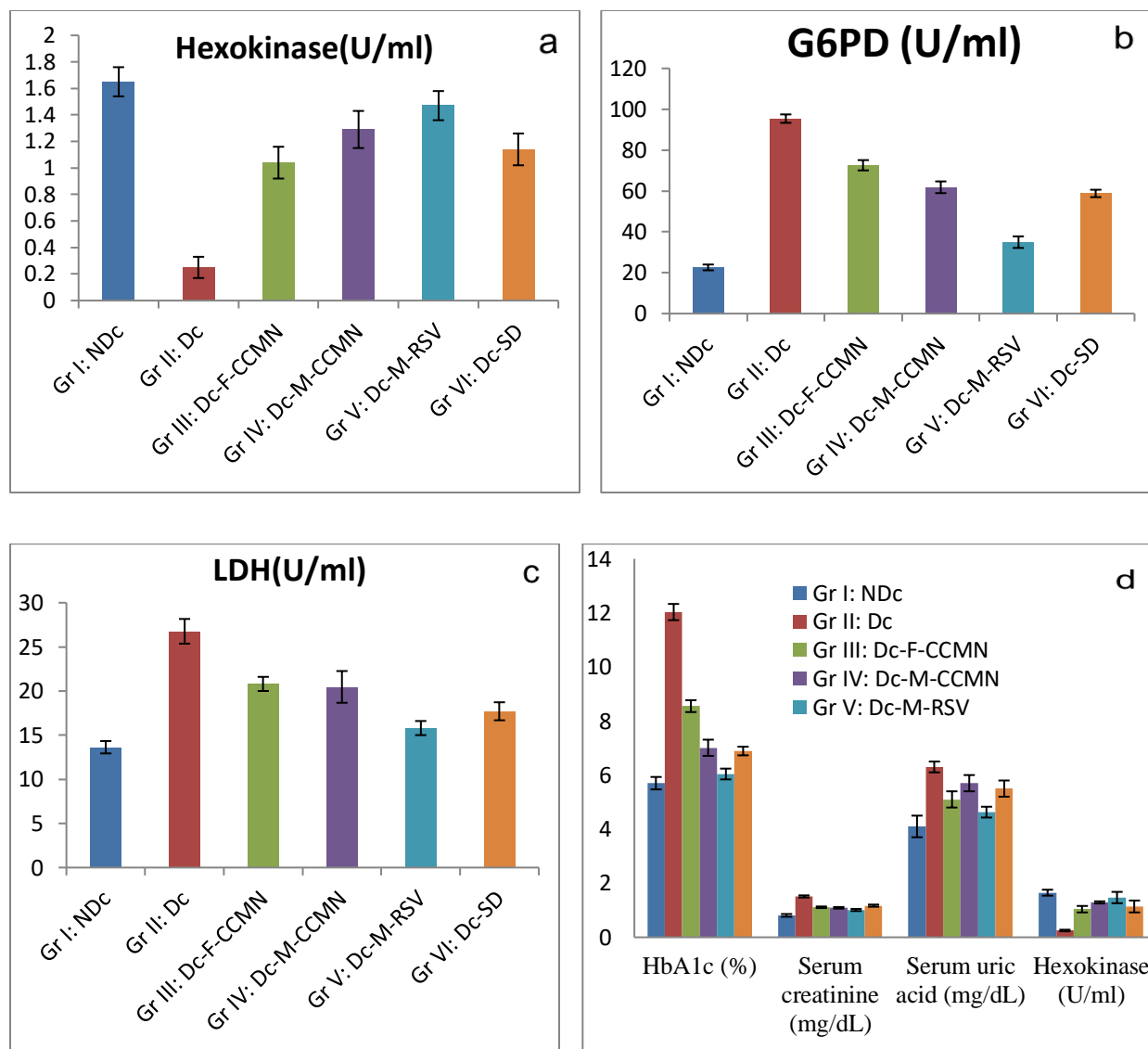


**Fig. 7.10:** Level of (a) Hexokinase, (b) G6PD, (c) HDL cholesterol, (d) LDH, (e) Inter group comparison of HbA1c, Serum creatinine, Serum uric acid, hexokinase



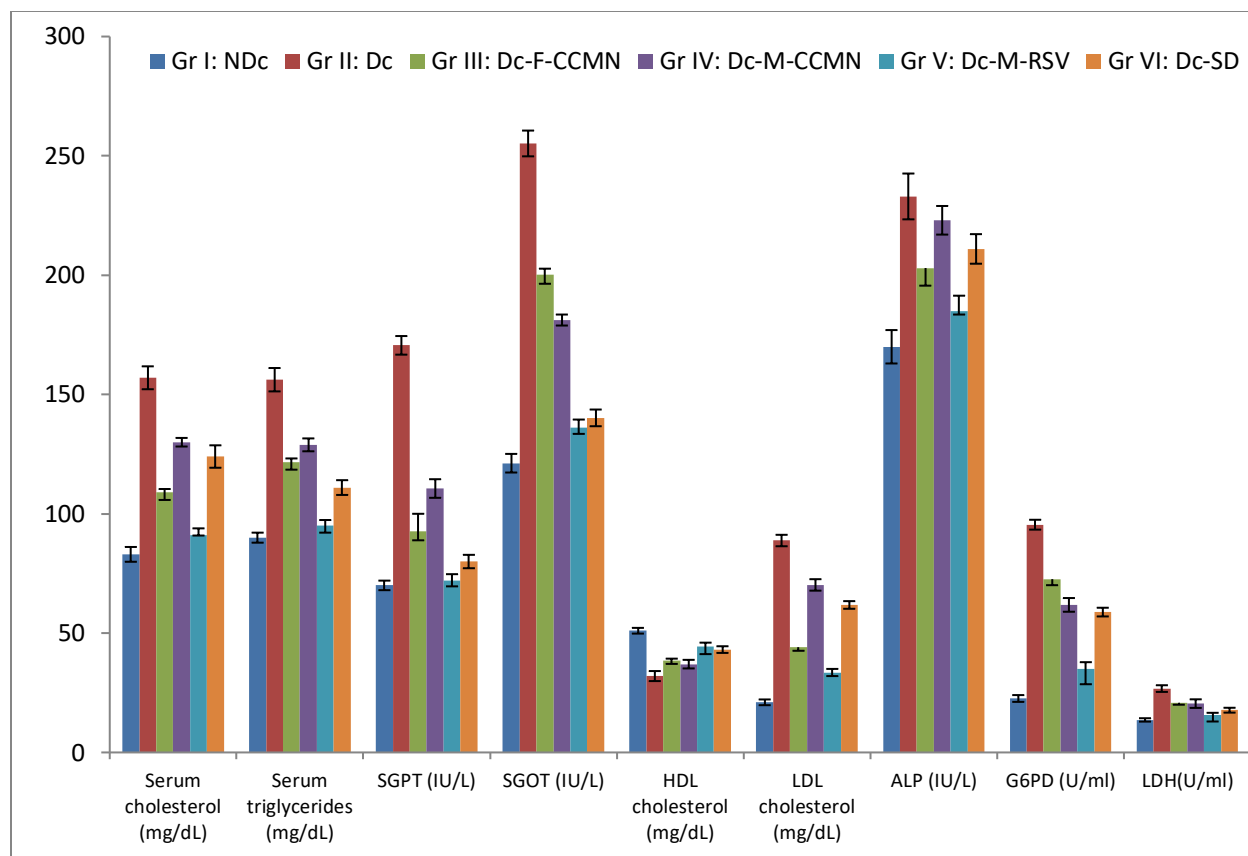


**Fig. 7.11:** Inter group comparison of Serum cholesterol, Serum triglycerides, SGOT, HDL cholesterol, LDL cholesterol, ALP, G6PD and HDL

During hyperglycemia, glucose autoxidation increased the generation of free radicals, which may cause organ damage [186, 187, 188]. Histopathology data (**Figure 7.12**) demonstrated that "STZ" caused a particular kind of necrosis in the pancreatic tissues of the positive control group II. Pancreas structures, endoplasmic reticulum, acinus, and  $\beta$  cells in the Langerhans islet are all typical in normal mice. Induced diabetes in mice via "STZ" treatment results in aberrant architecture, endoplasmic reticulum damage, aberrant acini, and  $\beta$  cells. On the other hand, both CDSCM-CCMN and CDSCM-RSV treated mice showed less dimensional changes in their islets and minor damage to their islets of Langerhans.



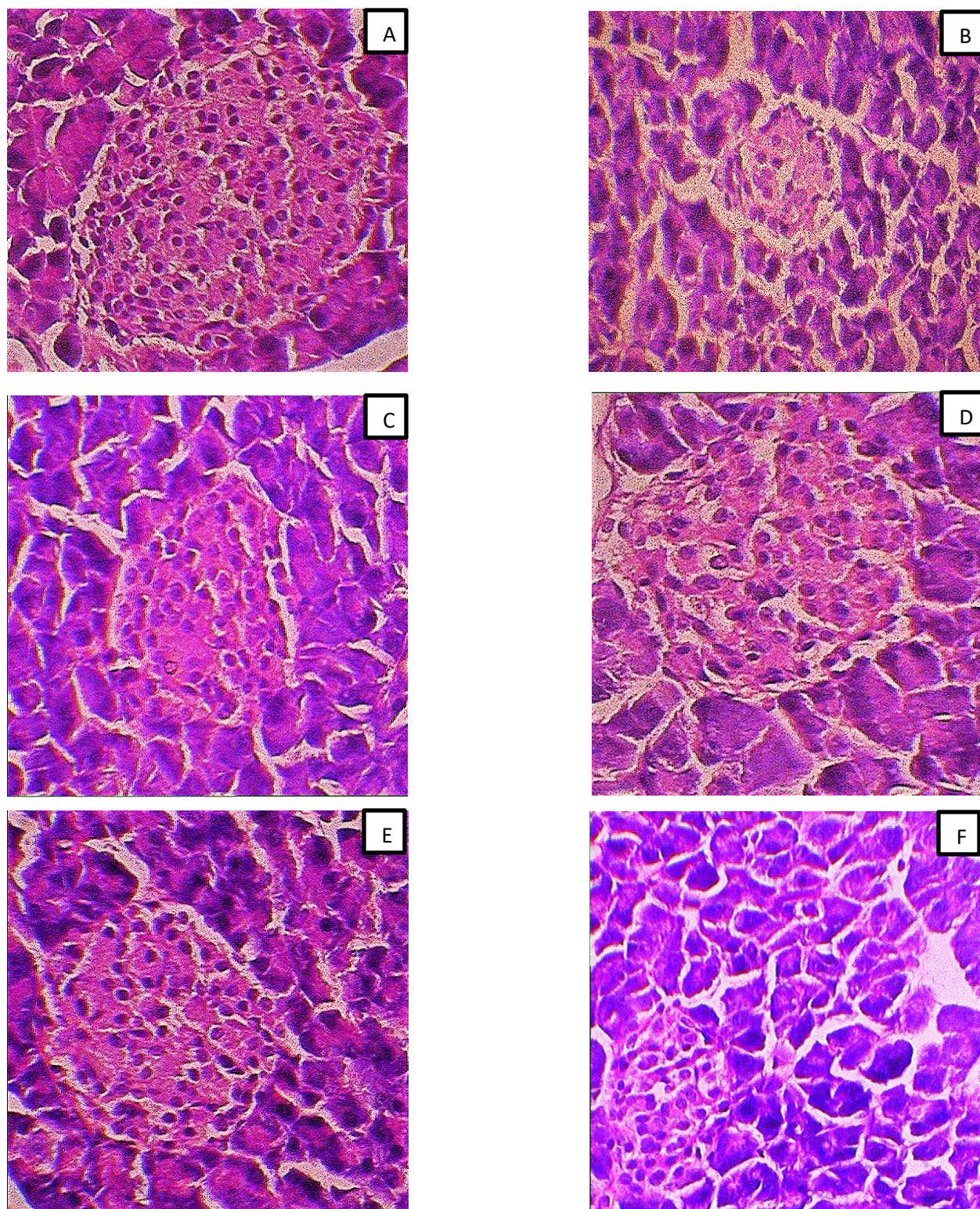


**Fig. 7.12:** Histopathology of pancreas of (A) Normal Gr-I: NDc, (B) STZ Gr-II: Dc, (C) Free drug Gr-III: Dc-F-CCMN, (D) Nanoparticle Gr-IV:Dc-M-CCMN, (E) Nanoparticle Gr-V:Dc-M-RSV and (F) Standard drug Gr-VI: Dc-SD animals



### 7.7. Conclusion

As a result, our research's conclusions showed that newly developed and unique CDSCM-CCMN and CDSCM-RSV nanomicelles were effective in controlling diabetes, and that the lipid profile and blood glucose levels of the treated mice significantly decreased. Both nanomicelles produced outcomes that were compared to those of glibenclamide. The therapeutic efficacy of pure free form curcumin was also compared to that of glibenclamide, albeit with a few disadvantages.

The ability of animals treated with both CDSCM-CCMN and CDSCM-RSV to lower FBG levels was considerably greater than that of animals treated with unbound CCMN and the standard medication glibenclamide; additionally, the animals treated with both drugs combined showed the highest ability to lower FBG levels.

Interestingly, the effects of CDSCM-CCMN and CDSCM-RSV on body weight in diabetic-induced animals were found to be less severe than those of free CCMN and the conventional drug. The difference suggests that CDSCM-CCMN and CDSCM-RSV may have a more targeted and potent effect on glucose regulation, potentially allowing for a more targeted method of treating elevated FBG levels. In addition, the consistent elevation of FBG levels in these animals suggests the presence of an elevated amount of HbA1c, highlighting the chronic nature of the diabetic condition under study [189, 190]. After 21 days, HbA1c levels were significantly reduced in animals treated with CDSCM-RSV, according to this research. This correlation can be explained by the direct relationship between skeletal muscle mass and creatinine levels, where creatinine levels progressively increase as body weight decreases, increasing the risk of type II diabetes [191]. Notably, the creatinine levels of CDSCM-CCMN and CDSCM-RSV treated animals were substantially lower than those of CCMN-free and standard-drug-treated animals. Notably, treatment with CDSCM-RSV increased hexokinase enzyme levels, which may have improved glucose metabolism. G6PD is an additional enzyme associated with type II diabetes.

Nevertheless, administration of CDSCM-RSV reduced blood glucose-6-phosphate dehydrogenase levels, suggesting a restoration of metabolic equilibrium. Several metabolic disorders involving enzymes such as hexokinase, G6PD, LDH, SGPT, SGOT, and ALP, which exhibit altered concentrations in tissues and blood, are associated with Type II diabetes.

Compared to other interventions, the CDSCM-RSV treatment substantially restores blood enzyme levels (**Figure 7.11**). The histopathological indices indicate that CDSCM-RSV restore normal architecture of pancreas tissue more efficiently than other diabetic groups. The above results could indicate that CDSCM-RSV restores the normal metabolic process in group V more efficiently than in other diabetic groups.

# Chapter 8

## Summary and conclusions

- 8.1 Introduction**
- 8.2 Chapter 2:** Review of Literature
- 8.3 Chapter 3:** Synthesis of chitosan-curcumin conjugate
- 8.4 Chapter 4:** Preparation and Characterization of Curcumin nanomicelles
- 8.5 Chapter 5:** Preparation and characterization of curcumin-resveratrol nanomicelle
- 8.6 Chapter 6:** HPLC method development for estimation of curcumin and resveratrol
- 8.7 Chapter 7:** *In-vivo* study of CDSCM-CCMN and CDSCM-RSV as antidiabetic nanoformulation
- 8.8 Conclusion**

## 8.1. Introduction

A chronic metabolic disease that has a terrible effect on quality of life, diabetes affects millions of people across the globe. Diabetes treatment frequently has issues with choosing the right medication, determining its dosage, and managing unintended side effects. Compounds derived from a variety of plants have been used for centuries, some of which have been shown to have strong antidiabetic effects. The most effective and widely researched multifunctional polyphenolic compounds are resveratrol and curcumin. However, clinical applicability has significantly decreased due to their low bioavailability, fast hydrolytic breakdown, and poor water solubility.

Our team has created nanomicelles containing both resveratrol (RSV) and curcumin (CCMN) to combat diabetes by concurrently resolving issues with solubility and bioavailability. Our study on **“*In Vitro* and *In Vivo* Characterization and Evaluation of Some naturally Occurring Small Molecules Based Nanoformulation for Diabetes Management”** has been summarized under the following aspect:

- **Chapter 2:** Review of Literature
- **Chapter 3:** Synthesis of chitosan-curcumin conjugate
- **Chapter 4:** Preparation and Characterization of curcumin nanomicelles
- **Chapter 5:** Preparation and characterization of curcumin-resveratrol nanomicelles
- **Chapter 6:** HPLC method development for estimation of curcumin and resveratrol
- **Chapter 7:** *In-vivo* study of CDSCM-CCMN and CDSCM-RSV as antidiabetic nanoformulation

## 8.2. Chapter 2: Review of Literature

In this chapter of the thesis summarized the information regarding diabetes mellitus. The etiology, case and disease mechanism of T1DM, T2DM and other forms of DM are summarized. Socioeconomic condition, knowledge about disease and awareness of diabetes can largely influence of DM. Adequate knowledge regarding disease's etiology, ideal measurements, complications, follow-up and management through lifestyle modifications, drug treatment can control the prevalence of acute severe condition of the disease. From statistical assessment of

Diabetic on certain population, it was found that 75.67% used oral hypoglycemic drugs exclusively; 24.32% used insulin in addition to oral hypoglycemic agents; and 14.86% sought advice from a dietician. T1DM which is the insulin depended diabetes mellitus can manage by glucose monitoring and insulin delivery whereas T2DM which is the noninsulin depended diabetes mellitus can control by prevention of insulin resistance, increasing the release of insulin or by prevention of other associated secondary causes.

Among the many physiological and pharmacological effects of curcumin—a bioactive component of *Curcuma longa*—are its anti-inflammatory, anticancer, nerve-protecting, and anti-diabetic actions. Although its precise dosage is still unknown, curcumin offers a low-cost, safe substitute for the current therapeutic approach for this condition. Resveratrol is a polyphenol phytoalexin with a variety of physiological and biochemical effects, such as anti-inflammatory, anti-platelet, and estrogenic. Recently, RSV has drawn attention from scientists for its potential to regulate blood sugar, combat diabetes, and prevent its consequences in a variety of diabetic models. In this chapter we show the molecular mechanism of resveratrol, how it prevent insulin resistance and enhance glucose uptake.

Nanoparticles are perfect for treating diabetes because of their unique benefits, which include targeting efficiency, bioavailability, biocompatibility and low toxicity. Colloidal particles self-assemble into nanomicelles, which typically have a lipophilic core and a hydrophilic shell and a diameter ranging from 10 to 100 nm. Whether it's their size, solubility, surface tailoring, or environmental exposure, nanomicelles exhibit its unique features. These characteristics render them multipurpose and indispensable in different domains, including biomedical applications.

### **8.3. Chapter 3: Synthesis of chitosan-curcumin conjugate**

In this chapter of thesis enucleate conjugation of drug with polymer to improve the aqueous solubility of drug, improve optimum drug release in controlled manner, improve therapeutic efficacy, minimize the side effects and improved patient compliances. To synthesize chitosan-curcumin conjugate, initially curcumin was reacted with succinic anhydride in the presence of pyridine to produce curcumin monosuccinate (%Yield was 68.31). The reaction was carried out at 80°C in one atmospheric pressure for 36 hours. After completion of reaction it was purified by column chromatography. Again curcumin monosuccinate was reacted with chitosan in DMSO solvent in the presence of *N, N'*-Dicyclohexylcarbodiimide and 4-dimethylaminopyridine to

produce chitosan succinyl curcumin conjugate (chitosan di-succinyl curcumin i.e., CHT-di(SUC-CCMN)). It was purified through column chromatography and recrystallized with 1:1 ratio solvent of ethanol and ethyl ether.

Peak absorbance is seen at 427 nm for both curcumin and the CHT-di(SUC-CCMN) conjugate; however, the conjugate peak is wider than the curcumin peak. The synthesis of the chitosan-curcumin conjugate is concluded by the fluorescence emission spectrum peak of curcumin at 550 nm and that of CHT-di(SUC-CCMN) at 522 nm.

The FTIR analysis demonstrates that the procedure begins with the reaction of CCMN and succinic anhydride, which results in the formation of SUC-CCMN with a reactive carboxylic acid group. The FTIR spectra show that this acid group forms an ester bond with the hydroxyl group of CHT when pyridine is present, which results in the creation of the prodrug CHT-di(SUC-CCMN).

Analysis of the CHT-di(SUC-CCMN) conjugate by <sup>1</sup>H-NMR confirmed its successful synthesis. The characteristic peaks of CCMN, CHT, and SUC-CCMN were evident in their respective spectra. Notably, the conjugate's spectrum displayed peaks from all constituents except the -OH proton of the succinyl moiety. Absence of succinyl -OH peak and the presence of all other expected peaks strongly supported the construction of the designed conjugate.

#### **8.4. Chapter 4: Preparation and Characterization of curcumin nanomicelles**

In this chapter of thesis explain preparation and characterization of nanomicelle which contain conjugated and free form of curcumin. The curcumin nanomicelle (CDSCM-CCMN) was prepared through dialysis process and it was passed through 0.45 µm filter to separate larger size particle. After lyophilization of the filtrate the powder form of the micelle was subjected for characterization and *in-vitro* analysis. The percent of yield was about 88.35. To know the entrapment efficacy of curcumin, the micelle's architecture was destroyed by treating it with concentrated HCl. The results showed that the entrapment efficacy was about 90.84% ± 01.14 w/w and the percent loading of CCMN in CDSCM-CCMN was approximately 36.87 % ± 0.62 w/w.

It was observed that 97 % of CCMN was released in pH 5.0 medium, whereas 49% of CCMN was released in pH 7.4 (physiological) medium from CDSCM-CCMN within 7 days. The complete drug release was observed after 9 days of study in acidic pH 5.0



It was observed that at physiological fluid (pH 7.4) free CCMN was about to degrade entirely within 8h, while more than 90 % of CCMN in CDSCM-CCMN was still present at the same time. It was found that conjugated CCMN exist in CDSCM-CCMN are much more stable than free CCMN. So nanomicelles developed by conjugation of CCMN with CHT significantly improve CCMN stability.

Very low critical micelle concentration (0.4836 mg/ml) of CDSCM-CCMN signify its stability, prolonging blood circulation, and accessible to the targeting of the drug.

Figure 4.6 illustrates that after giving CDSCM-CCMN enough time to incubate with RBC, approximately 2.0% of hemoglobin was released at the maximum concentration of CDSCM-CCMN (2 mg/ml). This signifies that the nano-formulation CDSCM-CCMN was compatible with RBC and blood, so it can applicable through intravenous administration.

The average hydrodynamic particle size of CDSCM-CCMN was about  $109.7 \pm 17.9$  nm and zeta potential was about -19.72 mV, which indicating its pronounced negative charge. This negative charge is caused by the presence of unbound hydroxyl (-OH) groups in the glucosamine units of the CHT exist on the surface of CDSCM-CCMN. This accumulation of hydroxyl groups results in the formation of a highly negatively charged CDSCM-CCMN surface. This negative charge serves to maintain the micelle's stability. Higher negative surface charges repel each CDSCM-CCMN from the other, thereby reducing nanomicelle accumulation.

Totally disappearance of CCMN peak in the thermograms of CDSCM-CCMN, it indicated that the polymer nanomicelle was amorphous and evenly distributed throughout the micelle. According to the DSC data, CCMN was effectively distributed throughout the micelle and was present in an amorphous form. Therefore, it's possible that no amorphous state formed in this system due to the presence of the CCMN melting peak (less intense) in the physical mixture.

In the XRD spectrogram, the physical mixture had some, but not all of the distinctive peaks of CCMN appeared because of the high concentration of carriers relative to CCMN. These findings showed that there was still some CCMN in the physical combination in the crystalline form.

According to the FE-SEM picture seen in **Figure 4.11**; CDSCM-CCMN was primarily uniform in size and fairly spherical. The particles might be distinguished by their shapes. According to **Figure 4.12's** TEM picture, the CDSCM-CCMN was spherical in shape and fell between 50 to 150 nm in size. The average diameters of the CDSCM-CCMN nanomicelles in an aqueous solution were satisfactorily quantified by AFM cross-sectional line profiling (**Figure 4.13** and **4.14**).

### **8.5. Chapter 5: Preparation and characterization of curcumin-resveratrol nanomicelles**

As in chapter 4, I have generated and analyzed nanomicelles that contain conjugated form of curcumin and free forms of resveratrol. The curcumin-resveratrol nanomicelle (CDSCM-RSV) was prepared through dialysis process and it was passed through 0.45  $\mu\text{m}$  filter to separate larger size particle. After lyophilization of the filtrate the powder form of the micelle was subjected for morphological characterization and blood compatibility.

The critical micelle concentration of CDSCM-RSV was found to be approximately 0.4644 mg/ml, indicating its stability, ability to extend blood circulation, and accessibility to the drug's target.

As illustrated in **Figure 5.3**; it was found that approximately 2.5% of hemoglobin was released at the maximum concentration of CDSCM-RSV (2 mg/ml) following an adequate amount of time for incubation with RBC. This signifies that the nanoformulation CDSCM-RSV was compatible with RBC and blood, so it can applicable through intravenous administration also.

With a zeta potential of approximately -32.84 mV and an average hydrodynamic particle size of  $56.12 \pm 15.2$  nm, CDSCM-RSV was clearly negatively charged. This negative charge is caused by the presence of unbound hydroxyl (-OH) groups in the glucosamine units of the CHT which exist on the surface of CDSCM-RSV nanomicelles. This accumulation of hydroxyl groups results in the formation of a highly negatively charged CDSCM-RSV surface. This negative charge serves to maintain the micelle's stability. Higher negative surface charges repel each CDSCM-RSV from the other, thereby reducing nanomicelle accumulation.

Totally disappearance of CCMN and RSV peaks in the thermograms of CDSCM-RSV (NP) (**Figure 5.6**), it indicates that the polymer nanomicelle was amorphous and evenly distributed throughout the micelle. According to the DSC data, CCMN and RSV were effectively distributed throughout the micelle and were present in an amorphous form. Therefore, it's possible that no amorphous state formed in this system due to the presence of the CCMN's and RSV's less intense melting peak in the physical mixture.

In the XRD spectrogram, the physical mixture had some, but not all of the distinctive peaks of CCMN and RSV appeared because of the high concentration of carriers relative to CCMN and RSV. These findings showed that there was still some CCMN and RSV in the physical combination in the crystalline form.

According to the FE-SEM picture displayed in **Figure 5.8**; CDSCM-RSV was primarily uniform in size and fairly spherical. The shape of the particles was distinguishable. **Figure 5.9**; displays a transmission electron micrograph (TEM) of the CDSCM-RSV, which reveals that it was round and had a size between 80 to 100 nm. Using AFM cross-sectional line profiling, the average diameters of the CDSCM-RSV nanomicelles in an aqueous solution were quantified, and the results were satisfactory (**Figure 5.10** and **5.11**).

## 8.6. Chapter 6: HPLC method development for estimation of curcumin and resveratrol

In order to measure resveratrol and curcumin from CDSCM-RSV at the same time, this chapter details the process of developing the RP-HPLC method. In CDSCM-RSV, curcumin and resveratrol were found in the conjugated and free forms, respectively. It was discovered that the isosbestic point, or common wavelength at which both medications exhibit maximum absorption, is 254 nm. In an optimal chromatographic setting, the combined chromatogram of the two reference medications showed distinct peaks with retention times of 8.15 minutes for RSV and 11.41 minutes for CCMN.

**Table 6.1** summarizes the results of the evaluations of several characteristics that were used to assess the system's appropriateness. These criteria included retention time, number of theoretical plates, and area under the curve, tailing factor, and resolution. The peaks of both medications were entirely distinct, as their average resolution was  $7.360 \pm 0.117$ . In accordance

with USP and ICH standards, our devised method has an RSD value of less than 2% for all other parameters.

The results indicated that the CCMN and RSV had linearity ranges of 2-32  $\mu\text{g/ml}$  and 1-16  $\mu\text{g/ml}$ , respectively. Their calibration curves were  $y = 171178.89x + 19619.91$  and  $y = 108179.53x + 6862.02$ , and their correlation coefficient values ( $R^2$ ) were 0.99987 and 0.99992, respectively. These values were very close to 1, which indicates that the data met the linearity requirements.

The percentage accuracy for the CCMN's intra-day and inter-day recovery was  $100.041 \pm 0.22\%$  and  $99.75 \pm 0.42\%$ , respectively. The corresponding values for the RSV were  $100.041 \pm 0.21\%$  and  $100.14 \pm 0.29\%$ , respectively. These values were extremely close to 100, indicating that the accuracy met the acceptance standards. The intra-day and intra-day percentage RSD of CCMN were  $0.44 \pm 0.28$  and  $0.28 \pm 0.02$ , respectively, while the RSV values were  $0.24 \pm 0.05$  and  $0.32 \pm 0.19$ , respectively. The RSD values of both medications in the intra-day and inter-day analysis were less than 2%, indicating the precision acceptability criterion.

To see how minor adjustments to chromatographic parameters, such as pH ( $4.6 \pm 0.2$ ), wavelength ( $254 \pm 2\text{nm}$ ), flow rate ( $1 \pm 0.1\text{ ml/min}$ ), and mobile phase composition, affected assay at various concentration levels and retention times. All of the data indicate compliance with USP guidelines and the ICH acceptance requirements (**Table 6.6**). The fact that the retention duration and assay RSD values were less than 2% indicates that our devised method satisfies the robustness approval criteria.

The results showed that the percent loading of RSV in the CDSCM-RSV core was  $14.56 \pm 0.18\text{ w/w}$  and the percent loading of CCMN was  $26.52 \pm 0.67\text{ w/w}$  with an entrapment efficacy of  $93.72\% \pm 1.02\text{ w/w}$ .

More than 50% of the medications remained in the nanomicelles to be released within 7 days at pH 7.4, while over 90% of the pharmaceuticals (CCMN and RSV) were found to be released from the nanomicelle within 7 days at pH 5.0. Additionally, it was noted that after nine days, all of the medications were released at pH 5.0, but over 47% of the medications were still inside the nanomicelles and needed to be released at pH 7.4 (**Figure 6.10** and **Table 6.7**).

It was observed that free CCMN was about to degrade entirely after 8h, while more than 90% of CCMN in CDSCM-RSV was still present at the same time, so the conjugated CCMN exist in CDSCM-RSV was much more stable than free CCMN (**Figure 6.11**). It was also

observed that free RSV was about to degrade entirely after 8h, while more than 90% of RSV in CDSCM-RSV was still present at the same time (**Figure 6.12**). CDSCM-RSV containing CCMN and RSV were much more stable than corresponding free form. So nanomicelles developed by conjugation technology significantly improve CCMN and RSV stability.

### **8.7. Chapter 7: *In-vivo* study of CDSCM-CCMN and CDSCM-RSV as antidiabetic nanoformulation**

In this chapter of thesis *in-vivo* antidiabetic activity of newly develop CDSCM-CCMN and CDSCM-RSV nanomicelles was shown. The ability of animals treated with both CDSCM-CCMN and CDSCM-RSV to lower FBG levels was considerably greater than that of animals treated with unbound CCMN and the standard medication glibenclamide; additionally, the animals treated with both drugs combined showed the highest ability to lower FBG levels.

Interestingly, the effects of CDSCM-CCMN and CDSCM-RSV on body weight in diabetic-induced animals were found to be less severe than those of free CCMN and the conventional drug.

The difference in different biochemical parameters that suggests CDSCM-CCMN and CDSCM-RSV may have a more targeted and potent effect on glucose regulation. In addition, the consistent elevation of FBG levels in these animals suggests the presence of an elevated amount of glycated hemoglobin (HbA1c), highlighting the chronic nature of the diabetic condition under study [189, 190]. After 21 days, HbA1c levels were significantly reduced in animals treated with CDSCM-RSV, according to this research. This correlation can be explained by the direct relationship between skeletal muscle mass and creatinine levels, where creatinine levels progressively increase as body weight decreases, increasing the risk of type II diabetes [191]. Notably, the creatinine levels of CDSCM-CCMN and CDSCM-RSV treated animals were substantially lower than those of free CCMN and standard-drug-treated animals. Notably, treatment with CDSCM-RSV increased hexokinase enzyme levels, which may have improved glucose metabolism. G6PD is an additional enzyme associated with type II diabetes. Administration of CDSCM-RSV reduced blood G6PD levels, suggesting a restoration of metabolic equilibrium. Several metabolic disorders involving enzymes such as hexokinase, G6PD, LDH, SGPT, SGOT, and ALP, which exhibit altered concentrations in tissues and blood,

are associated with Type II diabetes. Compared to other interventions, the CDSCM-RSV treatment substantially restores blood enzyme levels. The above results could indicate that CDSCM-RSV restores the normal metabolic process in CDSCM-RSV treated group animals (Group V) more efficiently than in other diabetic groups.

### **8.8. Conclusion**

The polymer drug conjugated amphipathic prodrug, overcome solubility and bioavailability problems; and simultaneously achieve synergistic therapeutic effects against diabetes, not only that but also nanomicelles formulation strategy put extra input in stability and controlled release of drugs.

Novel ways that completely utilize the progress of nanotechnology in the battle against the increasing incidence of diabetes are anticipated to emerge soon, utilizing a combination of curcumin and resveratrol as a medication.

**References**

1. Sembulingam K, Sembulingam P. Essentials of Medical Physiology: Endocrine functions of pancreas; 6<sup>th</sup> ed. JP Medical Ltd. 2012:415-424.
2. Davidson MB, Harmel AP, Mathur R. Davidson's Principles and Practice of Medicine. In: Pearson ER, McCrimmon RJ. Diabetes mellitus; 23<sup>rd</sup> ed. Elsevier. 2018:719-762
3. Melmed S, Auchus RJ, Goldfine AB, Rosen CJ, Kopp PA. WILLIAMS Textbook of Endocrinology. In: Bush JB, Polonsky KS, Burant CF. Type 2 Diabetes Mellitus; 12<sup>th</sup> ed. Elsevier. 2011:1361-1427
4. Cheng AL, Hsu CH, Lin JK, et al. Phase I clinical trial of curcumin, a chemopreventive agent, in patients with high-risk or pre-malignant lesions. *Anticancer Res.* 2001;21(4B):2895-2900.
5. Sharma RA, Euden SA, Platton SL, Cooke DN, Shafayat A, Hewitt HR, Marczylo TH, Morgan B, Hemingway D, Plummer SM, et al. Phase I clinical trial of oral curcumin biomarkers of systemic activity and compliance. *Clin. Cancer Res.* 2004, 10, 6847–6854, doi:10.1158/1078-0432.CCR-04-0744.
6. I–food, C.; Services, H. CFR - Code of Federal Regulations Title 21 CFR - Code of Federal Regulations Title 21 Tariq Al-Jallad CFR - Code of Federal Regulations Title 21 Tariq Al-Jallad. *U.S. Food Drug Adm.* 2014, 5–6.
7. Shehzad A, Khan S.; Shehzad O, Lee YS. Curcumin Therapeutic Promises and Bioavailability in Colorectal Cancer. *Drugs of Today* 2010, 46, 523–532.
8. Anand P, Thomas SG, Kunnumakkara AB, Sundaram C, Harikumar KB, Sung B, Tharakan ST, Misra K, Priyadarsini IK, Rajasekharan KN, et al. Biological activities of curcumin and its analogues (congeners) made by man and mother nature. *Biochem. Pharmacol.* 2008, 76, 1590–1611, doi:10.1016/j.bcp.2008.08.008.
9. Kouhpeikar H, Butler AE, Bamian F, Barreto GE, Majeed M, Sahebkar A. Curcumin as a therapeutic agent in leukemia. *J Cell Physiol.* 2019; 234(8):12404-12414. doi: 10.1002/jcp.28072. Epub 2019 Jan 4. PMID: 30609023.
10. Fu YS, Chen TH, Weng L, Huang L, Lai D, Weng CF. Pharmacological properties and underlying mechanisms of curcumin and prospects in medicinal potential. *Biomed. Pharmacother.* 2021;141:111888.

11. Parsamanesh N, Moossavi M, Bahrami A, Butler AE, Sahebkar A. Therapeutic potential of curcumin in diabetic complications. *Pharmacol Res.* 2018; 136:181–193
12. Abdollahi E, Momtazi AA, Johnston TP, Sahebkar A. Therapeutic effects of curcumin in inflammatory and immune-mediated diseases: a nature-made jack-of-all-trades? *J Cell Physiol* 2018; 233(2):830–848.
13. Poolsup N, Suksomboon N, Kurnianta PDM, Deawjaroen K. Effects of curcumin on glycemic control and lipid profile in prediabetes and type 2 diabetes mellitus: a systematic review and meta-analysis. *PLoS One.* 2019; 14(4):e0215840. <https://doi.org/10.1371/journal.pone.0215840>
14. Liu X, Zhang W, Wang L, Wang S, Yu Y, Chen S et al. Male patients with diabetes undergoing coronary artery bypass grafting have increased major adverse cerebral and cardiovascular events. *Interact Cardiovasc Thorac Surg.* 2019;28(4):607–612
15. Aziz MTA, El-Asmar MF, El-Ibrashy IN, Rezq AM, Al-Malki AL, Wassef MA et al. Effect of novel water soluble curcumin derivative on experimental type-1 diabetes mellitus (short term study). *Diabetol Metab Syndr.* 2012; 4(1):30. <https://doi.org/10.1186/1758-5996-4-30>
16. Zheng J, Cheng J, Zheng S, Feng Q, Xiao X. Curcumin, a polyphenolic curcuminoid with its protective effects and molecular mechanisms in diabetes and diabetic cardiomyopathy. *Front Pharmacol.* 2018; 9:472. <https://doi.org/10.3389/fphar.2018.00472>
17. Wojcik M, Krawczyk M, Wojcik P, Cytryk K, Wozniak LA. Molecular mechanisms underlying curcumin-mediated therapeutic effects in type 2 diabetes and cancer. *Oxidative Med Cell Longev.* 2018:9698258. <https://doi.org/10.1155/2018/9698258>
18. Weisberg S, Leibel R, Tortoriello D. Proteasome inhibitors, including curcumin, improve pancreatic  $\beta$ -cell function and insulin sensitivity in diabetic mice. *Nutr Diabetes.* 2016; 4:e205–e205
19. Soleimani V, Sahebkar A, Hosseinzadeh H. Turmeric (*Curcuma longa*) and its major constituent (curcumin) as nontoxic and safe substances: Review. *Phytother Res.* 2018; 32(6):985–995. <https://doi.org/10.1002/ptr.6054>.
20. Zhang LX, Li CX, Kakar MU, Khan MS, Wu PF, Amir RM, Dai DF, Naveed M, Li QY, Saeed M, Shen JQ, Rajput SA, Li JH. Resveratrol (RV): A pharmacological review and



- call for further research, *Biomedicine & Pharmacotherapy*, 2021;143,112164, <https://doi.org/10.1016/j.biopha.2021.112164>
21. Marques FZ, Markus MA, Morris BJ. Resveratrol: cellular actions of a potent natural chemical that confers a diversity of health benefits. *Int J Biochem Cell Biol.* 2009; 41(11):2125-2128. doi: 10.1016/j.biocel.2009.06.003.
22. Baur JA, Sinclair DA. Therapeutic potential of resveratrol: the in vivo evidence. *Nat. Rev. Drug Discovery.* 2006; 5:493–506.
23. Richard JL. Coronary risk factors - the french paradox. *Arch. Mal. CoeurVaiss.*, 1987; 80: 17-21.
24. Fuhrman B, Lavy A, Aviram M. Consumption of red wine with meals reduces the susceptibility of human plasma and low-density-lipoprotein to lipid-peroxidation. *Am J Clin Nutr.* 1995;61(3):549-554.
25. Kopp P, Resveratrol, a phytoestrogen found in red wine. A possible explanation for the conundrum of the 'French paradox'? *Eur J Endocrinol.* 1998; 138(6):619-620.
26. Bertelli AAA, Das DK. Grapes wines resveratrol and heart health. *J Cardiovasc Pharmacol.* 2009;54(6):468-476.
27. Jang MS, Cai EN, Udeani GO, Slowing KV, Thomas CF, Beecher CWW, Fong HHS, Farnsworth NR, Kinghorn AD, Mehta RG, Moon RC, Pezzuto JM. Cancer chemopreventive activity of resveratrol, a natural product derived from grapes. *Science.* 1997;275(5297):218-220.
28. Dore S. Unique properties of polyphenol stilbenes in the brain: More than direct antioxidant actions; Gene/protein regulatory activity. *Neurosignals.* 2005;14(1-2):61-70.
29. Shakibaei M, Csaki C, Nebrich S, Mobasheri A. Resveratrol suppresses interleukin-1 beta-induced inflammatory signaling and apoptosis in human articular chondrocytes: Potential for use as a novel nutraceutical for the treatment of osteoarthritis. *Biochem Pharmacol.* 2008;76(11):1426-1439.
30. Delmas D, Lançon A, Colin D, Jannin B, Latruffe N. Resveratrol as a chemopreventive agent: a promising molecule for fighting cancer. *Curr Drug Targets.* 2006;7(4):423-442. doi:10.2174/138945006776359331

- 
31. Joe AK, Liu H, Suzui M, Vural ME, Xiao D, Weinstein IB. Resveratrol induces growth inhibition, S-phase arrest, apoptosis, and changes in biomarker expression in several human cancer cell lines. *Clin Cancer Res.* 2002;8(3):893-903.
  32. Harikumar KB, Aggarwal BB. Resveratrol: a multitargeted agent for age-associated chronic diseases. *Cell Cycle.* 2008;7(8):1020-1035. doi:10.4161/cc.7.8.5740
  33. Parker JA, Arango M, Abderrahmane S, et al. Resveratrol rescues mutant polyglutamine cytotoxicity in nematode and mammalian neurons [published correction appears in *Nat Genet.* 2005 May;37(5):555]. *Nat Genet.* 2005;37(4):349-350. doi:10.1038/ng1534
  34. Hung LM, Chen JK, Huang SS, Lee RS, Su MJ. Cardioprotective effect of resveratrol, a natural antioxidant derived from grapes. *Cardiovasc Res.* 2000;47(3):549-555. doi:10.1016/s0008-6363(00)00102-4
  35. Baur JA, Sinclair DA. Therapeutic potential of resveratrol: the in vivo evidence. *Nat Rev Drug Discov.* 2006;5(6):493-506. doi:10.1038/nrd2060
  36. Burns J, Yokota T, Ashihara H, Lean ME, Crozier A. Plant foods and herbal sources of resveratrol. *J Agric Food Chem.* 2002;50(11):3337-3340. doi:10.1021/jf0112973
  37. Sobolev VS, Cole RJ. trans-resveratrol content in commercial peanuts and peanut products. *J Agric Food Chem.* 1999;47(4):1435-1439. doi:10.1021/jf9809885
  38. Counet C, Callemien D, Collin S. Chocolate and cocoa: New sources of trans-resveratrol and trans-piceid. *Food Chem.* 2006;98(4):649-657.
  39. Hurst WJ, Glinski JA, Miller KB, Apgar J, Davey MH, Stuart DA. Survey of the trans-resveratrol and trans-piceid content of cocoa-containing and chocolate products. *J Agric Food Chem.* 2008;56(18):8374-8378. doi:10.1021/jf801297w
  40. Wang Y, Catana F, Yang Y, Roderick R, van Breemen RB. An LC-MS method for analyzing total resveratrol in grape juice, cranberry juice, and in wine. *J Agric Food Chem.* 2002;50(3):431-435. doi:10.1021/jf010812u
  41. Itzkowitz SH, Yio X. Inflammation and cancer IV. Colorectal cancer in inflammatory bowel disease: the role of inflammation. *Am J Physiol Gastrointest Liver Physiol.* 2004;287(1):G7-G17. doi:10.1152/ajpgi.00079.2004
  42. Stojanović S, Sprinz H, Brede O. Efficiency and mechanism of the antioxidant action of trans-resveratrol and its analogues in the radical liposome oxidation. *Arch Biochem Biophys.* 2001;391(1):79-89. doi:10.1006/abbi.2001.2388
-

- 
43. Szewczuk LM, Forti L, Stivala LA, Penning TM. Resveratrol is a peroxidase-mediated inactivator of COX-1 but not COX-2: a mechanistic approach to the design of COX-1 selective agents. *J Biol Chem*. 2004;279(21):22727-22737. doi:10.1074/jbc.M314302200
  44. Sgambato A, Ardito R, Faraglia B, Boninsegna A, Wolf FI, Cittadini A. Resveratrol, a natural phenolic compound, inhibits cell proliferation and prevents oxidative DNA damage. *Mutat Res*. 2001;496(1-2):171-180. doi:10.1016/s1383-5718(01)00232-7
  45. Fontecave M, Lepoivre M, Elleingand E, Gerez C, Guittet O. Resveratrol, a remarkable inhibitor of ribonucleotide reductase. *FEBS Lett*. 1998;421(3):277-279. doi:10.1016/s0014-5793(97)01572-x
  46. Locatelli GA, Savio M, Forti L, et al. Inhibition of mammalian DNA polymerases by resveratrol: mechanism and structural determinants. *Biochem J*. 2005;389(Pt 2):259-268. doi:10.1042/BJ20050094
  47. Stewart JR, Ward NE, Ioannides CG, O'Brian CA. Resveratrol preferentially inhibits protein kinase C-catalyzed phosphorylation of a cofactor-independent, arginine-rich protein substrate by a novel mechanism. *Biochemistry*. 1999;38(40):13244-13251. doi:10.1021/bi990875u
  48. Goswami SK, Das DK. Resveratrol and chemoprevention. *Cancer Lett*. 2009;284(1):1-6. doi:10.1016/j.canlet.2009.01.041
  49. Rubiolo JA, Mithieux G, Vega FV. Resveratrol protects primary rat hepatocytes against oxidative stress damage: activation of the Nrf2 transcription factor and augmented activities of antioxidant enzymes. *Eur J Pharmacol*. 2008;591(1-3):66-72. doi:10.1016/j.ejphar.2008.06.067
  50. Saiko P, Szakmary A, Jaeger W, Szekeres T. Resveratrol and its analogs: defense against cancer, coronary disease and neurodegenerative maladies or just a fad?. *Mutat Res*. 2008;658(1-2):68-94. doi:10.1016/j.mrrev.2007.08.004
  51. Boscolo P, del Signore A, Sabbioni E, et al. Effects of resveratrol on lymphocyte proliferation and cytokine release. *Ann Clin Lab Sci*. 2003;33(2):226-231.
  52. Anekonda TS. Resveratrol--a boon for treating Alzheimer's disease?. *Brain Res Rev*. 2006;52(2):316-326. doi:10.1016/j.brainresrev.2006.04.004
-

- 
53. Marambaud P, Zhao H, Davies P. Resveratrol promotes clearance of Alzheimer's disease amyloid-beta peptides. *J Biol Chem.* 2005;280(45):37377-37382. doi:10.1074/jbc.M508246200
54. Olas B, Wachowicz B, Szewczuk J, Saluk-Juszczak J, Kaca W. The effect of resveratrol on the platelet secretory process induced by endotoxin and thrombin. *Microbios.* 2001;105(410):7-13.
55. Szkudelska K, Szkudelski T. Resveratrol, obesity and diabetes. *Eur J Pharmacol.* 2010;635(1-3):1-8. doi:10.1016/j.ejphar.2010.02.054
56. Palsamy P, Subramanian S. Modulatory effects of resveratrol on attenuating the key enzymes activities of carbohydrate metabolism in streptozotocin-nicotinamide-induced diabetic rats. *Chem Biol Interact.* 2009;179(2-3):356-362. doi:10.1016/j.cbi.2008.11.008
57. Milovanovic M, Arsenijevic A, Milovanovic J, Kanjevac T, Arsenijevic N. Nanoparticles in Antiviral Therapy. *Antimicrobial Nanoarchitectonics.* 2017:383–410. doi: 10.1016/B978-0-323-52733-0.00014-8. Epub 2017 Jun 30. PMCID: PMC7173505.
58. Kataoka K, Kwon GS, Yokoyama M, Okano T, Sakurai Y. Block copolymer micelles as vehicles for drug delivery. *J. Controll Release.* 1993;24(1-3):119–132.
59. Matsumura Y, Maeda H. A new concept for macromolecular therapeutics in cancer chemotherapy: mechanism of tumoritropic accumulation of proteins and the antitumor agent smancs. *Cancer Res.* 1986;46(12 Pt 1):6387-6392.
60. Nagayama S, Ogawara K, Fukuoka Y, Higaki K, Kimura T. Time-dependent changes in opsonin amount associated on nanoparticles alter their hepatic uptake characteristics. *Int J Pharm.* 2007;342(1-2):215-221. doi:10.1016/j.ijpharm.2007.04.036
61. Vega-Villa KR, Takemoto JK, Yáñez JA, Remsberg CM, Forrest ML, Davies NM. Clinical toxicities of nanocarrier systems. *Adv Drug Deliv Rev.* 2008;60(8):929-938. doi:10.1016/j.addr.2007.11.007
62. Ning YM, He K, Dagher R, et al. Liposomal doxorubicin in combination with bortezomib for relapsed or refractory multiple myeloma. *Oncology (Williston Park).* 2007;21(12): 1503–1508.
63. Ogawara K, Un K, Minato K, Tanaka K, Higaki K, Kimura T. Determinants for in vivo anti-tumor effects of PEG liposomal doxorubicin: importance of vascular permeability within tumors. *Int J Pharm.* 2008;359(1-2):234-240. doi:10.1016/j.ijpharm.2008.03.025
-

- 
64. Maeda H, Wu J, Sawa T, Matsumura Y, Hori K. Tumor vascular permeability and the EPR effect in macromolecular therapeutics: a review. *J Control Release*. 2000;65(1-2):271-284. doi:10.1016/s0168-3659(99)00248-5
65. Schroeder A, Heller DA, Winslow MM, et al. Treating metastatic cancer with nanotechnology. *Nat Rev Cancer*. 2011;12(1):39-50. doi:10.1038/nrc3180
66. Chauhan VP, Stylianopoulos T, Martin JD, et al. Normalization of tumour blood vessels improves the delivery of nanomedicines in a size-dependent manner. *Nat Nanotechnol*. 2012;7(6):383-388. Published 2012 Apr 8. doi:10.1038/nnano.2012.45
67. Trivedi R, Kompella UB. Nanomicellar formulations for sustained drug delivery: strategies and underlying principles. *Nanomedicine (Lond)*. 2010;5(3):485-505. doi:10.2217/nnm.10.10
68. Determan MD, Cox JP, Mallapragada SK. Drug release from pH-responsive thermogelling pentablock copolymers. *J Biomed Mater Res A*. 2007;81(2):326-333. doi:10.1002/jbm.a.30991
69. Qiu L, Zhang J, Yan M, Jin Y, Zhu K. Reverse self-assemblies based on amphiphilic polyphosphazenes for encapsulation of water-soluble molecules. *Nanotechnol*. 2007;18(47):475602.
70. Melo EP, Aires-Barros MR, Cabral JM. Reverse micelles and protein biotechnology. *Biotechnol Annu Rev*. 2001;7:87-129. doi:10.1016/s1387-2656(01)07034-x
71. Torchilin VP. Micellar nanocarriers: pharmaceutical perspectives. *Pharm Res*. 2007;24(1):1-16. doi:10.1007/s11095-006-9132-0
72. Koo OM, Rubinstein I, Onyuksel H. Camptothecin in sterically stabilized phospholipid micelles: a novel nanomedicine. *Nanomedicine*. 2005;1(1):77-84. doi:10.1016/j.nano.2004.11.002
73. Xu W, Ling P, Zhang T. Polymeric micelles, a promising drug delivery system to enhance bioavailability of poorly water-soluble drugs. *J Drug Deliv*. 2013;2013:340315. doi:10.1155/2013/340315
74. Hsu CH, Kuo SW, Chen JK, Ko FH, Liao CS, Chang FC. Self-assembly behavior of A-B diblock and C-D random copolymer mixtures in the solution state through mediated hydrogen bonding. *Langmuir*. 2008;24(15):7727-7734. doi:10.1021/la703960g
-

- 
75. Kuo S-W, Tung P-H, Lai C-L, Jeong K-U, Chang F-C. Supramolecular micellization of diblock copolymer mixtures mediated by hydrogen bonding for the observation of separated coil and chain aggregation in common solvents. *Macromol Rapid Commun.* 2008;29(3):229–233.
76. Yoncheva K, Calleja P, Agüeros M, et al. Stabilized micelles as delivery vehicles for paclitaxel. *Int J Pharm.* 2012;436(1-2):258-264. doi:10.1016/j.ijpharm.2012.06.030
77. Lee ES, Shin HJ, Na K, Bae YH. Poly(L-histidine)-PEG block copolymer micelles and pH-induced destabilization. *J Control Release.* 2003;90(3):363-374. doi:10.1016/s0168-3659(03)00205-0
78. Bromberg L. Polymeric micelles in oral chemotherapy. *J Control Release.* 2008;128(2):99-112. doi:10.1016/j.jconrel.2008.01.018
79. Lee ES, Na K, Bae YH. Polymeric micelle for tumor pH and folate-mediated targeting. *J Control Release.* 2003;91(1-2):103-113. doi:10.1016/s0168-3659(03)00239-6
80. Tang BC, Dawson M, Lai SK, et al. Biodegradable polymer nanoparticles that rapidly penetrate the human mucus barrier. *Proc Natl Acad Sci U S A.* 2009;106(46):19268-19273. doi:10.1073/pnas.0905998106
81. Smart JD. The basics and underlying mechanisms of mucoadhesion. *Adv Drug Deliv Rev.* 2005;57(11):1556-1568. doi:10.1016/j.addr.2005.07.001
82. Ponchel G, Irache J. Specific and non-specific bioadhesive particulate systems for oral delivery to the gastrointestinal tract. *Adv Drug Deliv Rev.* 1998;34(2-3):191-219. doi:10.1016/s0169-409x(98)00040-4
83. Crater JS, Carrier RL. Barrier properties of gastrointestinal mucus to nanoparticle transport. *Macromol Biosci.* 2010;10(12):1473-1483. doi:10.1002/mabi.201000137
84. Sammalkorpi M, Karttunen M, Haataja M. Ionic surfactant aggregates in saline solutions: sodium dodecyl sulfate (SDS) in the presence of excess sodium chloride (NaCl) or calcium chloride (CaCl<sub>2</sub>). *J Phys Chem B.* 2009;113(17):5863-5870. doi:10.1021/jp901228v
85. Chiappetta DA, Hocht C, Taira C, Sosnik A. Oral pharmacokinetics of the anti-HIV efavirenz encapsulated within polymeric micelles. *Biomaterials.* 2011;32(9):2379-2387. doi:10.1016/j.biomaterials.2010.11.082
-

- 
86. Ahn J, Miura Y, Yamada N, et al. Antibody fragment-conjugated polymeric micelles incorporating platinum drugs for targeted therapy of pancreatic cancer. *Biomaterials*. 2015;39:23-30. doi:10.1016/j.biomaterials.2014.10.069
  87. Trinh HM, Joseph M, Cholkar K, Mitra R, Mitra AK. Nanomicelles in diagnosis and drug delivery. In *Emerging Nanotechnologies for Diagnostics, Drug Delivery and Medical Devices*, Elsevier. 2017;45-58.
  88. Kim D, Lee ES, Park K, Kwon IC, Bae YH. Doxorubicin loaded pH-sensitive micelle: antitumoral efficacy against ovarian A2780/DOXR tumor. *Pharm Res*. 2008;25(9):2074-2082. doi:10.1007/s11095-008-9603-6
  89. Bae Y, Nishiyama N, Fukushima S, Koyama H, Yasuhiro M, Kataoka K. Preparation and biological characterization of polymeric micelle drug carriers with intracellular pH-triggered drug release property: tumor permeability, controlled subcellular drug distribution, and enhanced in vivo antitumor efficacy. *Bioconjug Chem*. 2005;16(1):122-130. doi:10.1021/bc0498166
  90. Singh R, Lillard JW Jr. Nanoparticle-based targeted drug delivery. *Exp Mol Pathol*. 2009;86(3):215-223. doi:10.1016/j.yexmp.2008.12.004
  91. Bae Y, Kataoka K. Intelligent polymeric micelles from functional poly(ethylene glycol)-poly(amino acid) block copolymers. *Adv Drug Deliv Rev*. 2009;61(10):768-784. doi:10.1016/j.addr.2009.04.016
  92. Rapoport N. Physical stimuli-responsive polymeric micelles for anti- cancer drug delivery. *Prog Polym Sci*. 2007;32(8-9):962–990.
  93. Torchilin V. Tumor delivery of macromolecular drugs based on the EPR effect. *Adv Drug Deliv Rev*. 2011;63(3):131-135. doi:10.1016/j.addr.2010.03.011
  94. Kim TY, Kim DW, Chung JY, et al. Phase I and pharmacokinetic study of Genexol-PM, a cremophor-free, polymeric micelle-formulated paclitaxel, in patients with advanced malignancies. *Clin Cancer Res*. 2004;10(11):3708-3716. doi:10.1158/1078-0432.CCR-03-0655
  95. Gong J, Chen M, Zheng Y, Wang S, Wang Y. Polymeric micelles drug delivery system in oncology. *J Control Release*. 2012;159(3):312-323. doi:10.1016/j.jconrel.2011.12.012
-



- 
96. Oerlemans C, Bult W, Bos M, Storm G, Nijssen JF, Hennink WE. Polymeric micelles in anticancer therapy: targeting, imaging and triggered release. *Pharm Res.* 2010;27(12):2569-2589. doi:10.1007/s11095-010-0233-4
  97. Civiale C, Licciardi M, Cavallaro G, Giammona G, Mazzone MG. Polyhydroxyethylaspartamide-based micelles for ocular drug delivery. *Int J Pharm.* 2009;378(1-2):177-186. doi:10.1016/j.ijpharm.2009.05.028
  98. Patel A, Cholkar K, Agrahari V, Mitra AK. Ocular drug delivery systems: An overview. *World J Pharmacol.* 2013;2(2):47-64. doi:10.5497/wjp.v2.i2.47
  99. Vadlapudi AD, Mitra AK. Nanomicelles: an emerging platform for drug delivery to the eye. *Ther Deliv.* 2013;4(1):1-3. doi:10.4155/tde.12.122
  100. Fireman S, Toledano O, Neimann K, Loboda N, Dayan N. A look at emerging delivery systems for topical drug products. *Dermatol Ther.* 2011;24(5):477-488. doi:10.1111/j.1529-8019.2012.01464.x
  101. Makhmalzade BS, Chavoshy F. Polymeric micelles as cutaneous drug delivery system in normal skin and dermatological disorders. *J Adv Pharm Technol Res.* 2018;9(1):2-8. doi:10.4103/japtr.JAPTR\_314\_17
  102. Thabit MF. Awareness Regarding Diabetes Mellitus and Its' Complications in Type 2 Diabetic Patients. *Al-Kindy Col. Med. J.* 2013;9(2):25-28.
  103. Foma MA, Saidu Y, Omoleke SA, Jafali J. Awareness of diabetes mellitus among diabetic patients in the Gambia: a strong case for health education and promotion. *BMC Public Health.* 2013;13:1124. doi: 10.1186/1471-2458-13-1124.
  104. Dussa K, Parimalakrishnan S, Sahay R. Assessment of diabetes knowledge using diabetes knowledge questionnaire among people with type 2 diabetes mellitus. *Asian J Pharm Clin Res* 2015;8(2):254-256.
  105. Deshmukh, CD, Jain A. Diabetes Mellitus: A Review. *Int J Pure App. Biosci.* 2015; 3(3):224-230.
  106. Schmitt A, Gahr A, Hermanns N, Kulzer B, Huber J, Haak T. The Diabetes Self-Management Questionnaire (DSMQ): development and evaluation of an instrument to assess diabetes self-care activities associated with glycaemic control. *Health Qual Life Outcomes.* 2013;11:138. doi:10.1186/1477-7525-11-138
-



- 
107. Brew-Sam N, Chhabra M, Parkinson A, et al. Experiences of young people and their caregivers of using technology to manage type 1 diabetes mellitus: systematic literature review and narrative synthesis. *JMIR Diabetes*. 2021;6(1):e20973. doi:10.2196/20973
  108. Marton LT, Pescinini-E-Salzedas LM, Camargo MEC, et al. The effects of curcumin on diabetes mellitus: a systematic review. *Front Endocrinol (Lausanne)*. 2021;12:669448. doi:10.3389/fendo.2021.669448
  109. Panahi Y, Khalili N, Sahebi E, et al. Effects of curcuminoids plus piperine on glycemic, hepatic and inflammatory biomarkers in patients with type 2 diabetes mellitus: a randomized double-blind placebo-controlled trial. *Drug Res (Stuttg)*. 2018;68(7):403-409. doi:10.1055/s-0044-101752
  110. Adab Z, Eghtesadi S, Vafa MR, et al. Effect of turmeric on glycemic status, lipid profile, hs-CRP, and total antioxidant capacity in hyperlipidemic type 2 diabetes mellitus patients. *Phytother Res*. 2019;33(4):1173-1181. doi:10.1002/ptr.6312
  111. Adibian M, Hodaei H, Nikpayam O, Sohrab G, Hekmatdoost A, Hedayati M. The effects of curcumin supplementation on high-sensitivity C-reactive protein, serum adiponectin, and lipid profile in patients with type 2 diabetes: A randomized, double-blind, placebo-controlled trial. *Phytother Res*. 2019;33(5):1374-1383. doi:10.1002/ptr.6328
  112. Asadi S, Gholami MS, Siassi F, Qorbani M, Khamoshian K, Sotoudeh G. Nano curcumin supplementation reduced the severity of diabetic sensorimotor polyneuropathy in patients with type 2 diabetes mellitus: A randomized double-blind placebo- controlled clinical trial. *Complement Ther Med*. 2019;43:253-260. doi:10.1016/j.ctim.2019.02.014
  113. Hodaei H, Adibian M, Nikpayam O, Hedayati M, Sohrab G. The effect of curcumin supplementation on anthropometric indices, insulin resistance and oxidative stress in patients with type 2 diabetes: a randomized, double-blind clinical trial. *Diabetol Metab Syndr*. 2019;11:41. Published 2019 May 27. doi:10.1186/s13098-019-0437-7
  114. Vanaie A, Shahidi S, Iraj B, et al. Curcumin as a major active component of turmeric attenuates proteinuria in patients with overt diabetic nephropathy. *J Res Med Sci*. 2019;24:77. doi:10.4103/jrms.JRMS\_1055\_18
  115. Asadi S, Gholami MS, Siassi F, Qorbani M, Sotoudeh G. Beneficial effects of nano-curcumin supplement on depression and anxiety in diabetic patients with peripheral
-

- neuropathy: A randomized, double-blind, placebo-controlled clinical trial. *Phytother Res.* 2020;34(4):896-903. doi:10.1002/ptr.6571
116. Shafabakhsh R, Asemi Z, Reiner Z, Soleimani A, Aghadavod E, Bahmani F. The effects of nano-curcumin on metabolic status in patients with diabetes on hemodialysis, a randomized, double blind, placebo-controlled trial. *Iran J Kidney Dis.* 2020;14(4):290-299.
117. Mokhtari M, Razzaghi R, Momen-Heravi M. The effects of curcumin intake on wound healing and metabolic status in patients with diabetic foot ulcer: A randomized, double-blind, placebo-controlled trial. *Phytother Res.* 2021;35(4):2099-2107. doi:10.1002/ptr.6957
118. Zhang DW, Fu M, Gao SH, Liu JL. Curcumin and diabetes: a systematic review. *Evid Based Complement Alternat Med.* 2013;2013:636053. doi:10.1155/2013/636053
119. Essa R, El Sadek AM, Baset ME, et al. Effects of Turmeric (*Curcuma longa*) Extract in streptozocin-induced diabetic model. *J Food Biochem.* 2019;43(9):e12988. doi:10.1111/jfbc.12988
120. Sudirman S, Lai CS, Yan YL, Yeh HI, Kong ZL. Histological evidence of chitosan-encapsulated curcumin suppresses heart and kidney damages on streptozotocin-induced type-1 diabetes in mice model. *Sci Rep.* 2019;9(1):15233. doi:10.1038/s41598-019-51821-6
121. Huang DD, Shi G, Jiang Y, Yao C, Zhu C. A review on the potential of Resveratrol in prevention and therapy of diabetes and diabetic complications. *Biomed Pharmacother.* 2020;125:109767. doi:10.1016/j.biopha.2019.109767
122. Zhu X, Wu C, Qiu S, Yuan X, Li L. Effects of resveratrol on glucose control and insulin sensitivity in subjects with type 2 diabetes: systematic review and meta-analysis. *Nutr Metab (Lond).* 2017;14:60. doi:10.1186/s12986-017-0217-z
123. Ma N, Zhang Y. Effects of resveratrol therapy on glucose metabolism, insulin resistance, inflammation, and renal function in the elderly patients with type 2 diabetes mellitus: A randomized controlled clinical trial protocol. *Medicine (Baltimore).* 2022;101(32):e30049. doi:10.1097/MD.00000000000030049

- 
124. Luo XM, Yan C, Feng YM. Nanomedicine for the treatment of diabetes-associated cardiovascular diseases and fibrosis. *Adv Drug Deliv Rev.* 2021;172:234-248. doi:10.1016/j.addr.2021.01.004
  125. ORIGIN Trial Investigators, Gerstein HC, Bosch J, et al. Basal insulin and cardiovascular and other outcomes in dysglycemia. *N Engl J Med.* 2012;367(4):319-328. doi:10.1056/NEJMoa1203858
  126. García-Díaz M, Foged C, Nielsen HM. Improved insulin loading in poly(lactic-co-glycolic) acid (PLGA) nanoparticles upon self-assembly with lipids. *Int J Pharm.* 2015;482(1-2):84-91. doi:10.1016/j.ijpharm.2014.11.047
  127. Hasan AA, Madkor H, Wageh S. Formulation and evaluation of metformin hydrochloride-loaded niosomes as controlled release drug delivery system. *Drug Deliv.* 2013;20(3-4):120-126. doi:10.3109/10717544.2013.779332
  128. Bose A, Roy Burman D, Sikdar B, Patra P. Nanomicelles: Types, properties and applications in drug delivery. *IET Nanobiotechnol.* 2021;15(1):19-27. doi:10.1049/nbt2.12018
  129. Zhang Y, Qu Q, Li M, Zhao Y. Intracellular Reduction-Responsive Sheddable Copolymer Micelles for Targeted Anticancer Drug Delivery. *Asian J Org Chem.* 2015;4(3):226–232. doi:10.1002/ajoc.201402146.
  130. Jain S, Jain R, Das M, Agrawal AK, Thanki K, Kushwah V. Combinatorial bio-conjugation of gemcitabine and curcumin enables dual drug delivery with synergistic anticancer efficacy and reduced toxicity, *RSC Adv.* 2014;4:29193–29201. <https://pubs.rsc.org/en/content/articlehtml/2014/ra/c4ra04237a>
  131. Sarika PR, James NR, Kumar PR, Raj DK, Kumary TV. Gum arabic-curcumin conjugate micelles with enhanced loading for curcumin delivery to hepatocarcinoma cells. *Carbohydr Polym.* 2015;134:167-174. doi:10.1016/j.carbpol.2015.07.068
  132. Sauraj, Kumar SU, Kumar V, Priyadarshi R, Gopinath P, Negi YS. pH-responsive prodrug nanoparticles based on xylan-curcumin conjugate for the efficient delivery of curcumin in cancer therapy. *Carbohydr Polym.* 2018;188:252-259. doi:10.1016/j.carbpol.2018.02.006
  133. Wang J, Jiang JZ, Chen W, Bai ZW. Synthesis and characterization of chitosan alkyl urea. *Carbohydr Polym.* 2016;145:78-85. DOI: 10.1016/j.carbpol.2016.03.022
-

- 
134. Ponnusamy C, Sugumaran A, Krishnaswami V, Palanichamy R, Velayutham R, Natesan S. Development and evaluation of polyvinylpyrrolidone k90 and poloxamer 407 self-assembled nanomicelles: enhanced topical ocular delivery of artemisinin. *Polymers (Basel)*. 2021;13(18):3038. doi:10.3390/polym13183038
  135. Praveen A, Prasad D, Mishra S, Nagarajan S, Chaudhari SR. Facile NMR approach for profiling curcuminoids present in turmeric. *Food Chem.* 2021;341(Pt2):128646. doi:10.1016/j.foodchem.2020.128646
  136. Waghela BN, Sharma A, Dhumale S, Pandey SM, Pathak C. Curcumin conjugated with PLGA potentiates sustainability, anti-proliferative activity and apoptosis in human colon carcinoma cells. *PLoS One*. 2015;10(2):e0117526. Published 2015 Feb 18. doi:10.1371/journal.pone.0117526
  137. Hansen NML, Plackett D. Synthesis and characterization of birch wood xylan succinoylated in 1-n-butyl-3-methylimidazolium chloride. *Polym Chem.* 2011;2:2010–2020. <https://doi.org/10.1039/c1py00086a>
  138. Huo M, Zhang Y, Zhou J, Zou A, Yu D, Wu Y, Li J, Li H. Synthesis and characterization of low-toxic amphiphilic chitosan derivatives and their application as micelle carrier for antitumor drug. *Int J Pharm.* 2010;394(1-2):162-173. doi:10.1016/j.ijpharm.2010.05.001
  139. Aranaz I, Alcántara AR, Civera MC, et al. Chitosan: an overview of its properties and applications. *Polymers (Basel)*. 2021;13(19):3256. Published 2021 Sep 24. doi:10.3390/polym13193256
  140. Sharifi-Rad J, Quispe C, Butnariu M, Rotariu LS, Sytar O, Sestito S et al. Chitosan nanoparticles as a promising tool in nanomedicine with particular emphasis on oncological treatment. *Cancer Cell Int.* 2021;21(1):318. doi: 10.1186/s12935-021-02025-4
  141. Dastidar DG, Saha S, Dutta G, Abat S, Guha N, Ghosh D. Surface functionalization of porous chitosan microsphere with silver nanoparticle and carbon dot. *Mater Res Express.* 2020;7:015031. <https://doi.org/10.1088/2053-1591/ab637f>
  142. Li M, Gao M, Fu Y, et al. Acetal-linked polymeric prodrug micelles for enhanced curcumin delivery. *Colloids Surf B Biointerfaces.* 2016;140:11-18. doi:10.1016/j.colsurfb.2015.12.025
-

- 
143. Junyaprasert VB, Thummarati P. Innovative design of targeted nanoparticles: polymer-drug conjugates for enhanced cancer therapy. *Pharmaceutics*. 2023;15(9):2216. Published 2023 Aug 27. doi:10.3390/pharmaceutics15092216
  144. Sauraj, Kumar SU, Gopinath P, Negi YS. Synthesis and bio-evaluation of xylan-5-fluorouracil-1-acetic acid conjugates as prodrugs for colon cancer treatment. *Carbohydr Polym*. 2017;157:1442-1450. doi:10.1016/j.carbpol.2016.09.096
  145. Dey S, Sreenivasan K. Conjugation of curcumin onto alginate enhances aqueous solubility and stability of curcumin. *Carbohydr Polym*. 2014;99:499-507. doi:10.1016/j.carbpol.2013.08.067
  146. Raveendran R, Pillai CKS, Bhuvaneshwar GS, Sharma CP. Enhanced cytotoxicity and cellular internalization of hemocompatible curcumin loaded pluronic linolenate micelles in cancer cells. *J. Nanopharmaceutics Drug Deliv*. 2014;2:36–51. <https://doi.org/10.1166/jnd.2014.1046>
  147. Lale SV, Kumar A, Prasad S, Bharti AC, Koul V. Folic acid and trastuzumab functionalized redox responsive polymersomes for intracellular doxorubicin delivery in breast cancer. *Biomacromolecules*. 2015;16(6):1736-1752. doi:10.1021/acs.biomac.5b00244
  148. Ponnusamy C, Sugumaran A, Krishnaswami V, Kandasamy R, Natesan S. Design and development of artemisinin and dexamethasone loaded topical nanodispersion for the effective treatment of age-related macular degeneration. *IET Nanobiotechnol*. 2019;13(8):868-874. doi:10.1049/iet-nbt.2019.0130
  149. Parekh VJ, Rathod VK, Pandit AB. Substrate hydrolysis: Methods, mechanism, and industrial applications of substrate hydrolysis, in: *compr. Biotechnol. Second Ed., Academic Press*. 2011: pp. 104–118. <https://doi.org/10.1016/B978-0-08-088504-9.00094-5>
  150. Sahu A, Bora U, Kasoju N, Goswami P. Synthesis of novel biodegradable and self-assembling methoxy poly(ethylene glycol)-palmitate nanocarrier for curcumin delivery to cancer cells. *Acta Biomater*. 2008;4(6):1752-1761. doi:10.1016/j.actbio.2008.04.021
  151. Li H, Hu D, Liang F, Huang X, Zhu Q. Influence factors on the critical micelle concentration determination using pyrene as a probe and a simple method of preparing
-

- samples. *R Soc Open Sci.* 2020;7(3):192092. Published 2020 Mar 4. doi:10.1098/rsos.192092
152. Zhang X, Huang Y, Li S. Nanomicellar carriers for targeted delivery of anticancer agents. *Ther Deliv.* 2014;5(1):53-68. doi:10.4155/tde.13.135
153. Liu YX, Liu KF, Li CX, Wang LY, Liu J, He J, Lei J, Liu X. Self-assembled nanoparticles based on a carboxymethylcellulose-ursolic acid conjugate for anticancer combination therapy. *RSC Adv.* 2017;7:36256–36268. doi.org/10.1039/c7ra05913b
154. Arayne MS, Sultana N, Tabassum A. RP-LC simultaneous quantitation of co-administered drugs for (non-insulin-dependent) diabetic mellitus induced dyslipidemia in active pharmaceutical ingredient, pharmaceutical formulations and human serum with UV-detector. *Clin Chim Acta.* 2013;425:54-61. doi: 10.1016/j.cca.2013.06.020
155. Li H, Zhao X, Ma Y, Zhai G, Li L, Lou H. Enhancement of gastrointestinal absorption of quercetin by solid lipid nanoparticles. *J Control Release.* 2009;133(3):238-44. doi: 10.1016/j.jconrel.2008.10.00287
156. Chaudhari VS, Borkar RM, Murty US, Banerjee S. Analytical method development and validation of reverse-phase high-performance liquid chromatography (RP-HPLC) method for simultaneous quantifications of quercetin and piperine in dual-drug loaded nanostructured lipid carriers. *J Pharm Biomed Anal.* 2020;186:113325. doi: 10.1016/j.jpba.2020.113325
157. ICH. Validation of analytical procedures: text and methodology. In: International Conference on Harmonisation. Vol. Q2(R1). Geneva, Geneva; 2005.
158. González AG, Herrador MA. A practical guide to analytical method validation, including measurement uncertainty and accuracy profiles. *Trends in Anal Chem.* 2007;26:227-238.
159. AOAC, official methods of analysis of AOAC international. *J AOAC Int*, (Gaithersburg, MD, USA), Guidelines for Standard Method Performance Requirements. 2012:9.
160. Thomas A, Varkey J. Development and validation of a new RP HPLC analytical method for the determination of etodolac succinic acid co-crystals in spiked rabbit plasma. *Int J Curr Pharm Sci.* 2023;15(2):59-63. doi: 10.22159/ijcpr.2023v15i2.2098.
161. Khursheed R, Singh SK, Kapoor B, Gulati M, Wadhwa S, Gupta S. Development and validation of RP-HPLC method for simultaneous determination of curcumin and

- quercetin in extracts, marketed formulations, and self-nanoemulsifying drug delivery system. *Re: GEN Open*. 2021;1(1):43-52. doi: 10.1089/regen.2021.0021.
162. Ahmad S, Khabiya P, Au T, Raheman BA. Quality by design approach to develop stability indicating reversed-phase high-performance liquid chromatography method development for ambroxol. *Asian J Pharm Clin Res*. 2021;14(12):44-9. doi: 10.22159/ajpcr.2021.v14i12.42939.
163. Sauraj, Kumar SU, Gopinath P, Negi YS. Synthesis and bio-evaluation of xylan-5-fluorouracil-1-acetic acid conjugates as prodrugs for colon cancer treatment. *Carbohydr Polym*. 2017;157:1442-1450. doi:10.1016/j.carbpol.2016.09.096
164. USP. Chromatography USP. In: National formulary 37, *Pharmacopeial convention inc*. Vol. 621. USA; 2009.
165. Nasr M, Abdel Rahman MH. Simultaneous determination of curcumin and resveratrol in lipidic nanoemulsion formulation and rat plasma using HPLC: optimization and application to real samples. *J AOAC Int*. 2019;102(4):1095-1101. doi:10.5740/jaoacint.18-0269
166. Yusuf H, Wijiani N, Rahmawati RA, Primaharinastiti R, Rijal MAS, Isadiartuti D. Analytical method for the determination of curcumin entrapped in polymeric micellar powder using HPLC. *J Basic Clin Physiol Pharmacol*. 2021;32(4):867-873. doi:10.1515/jbcpp-2020-0491
167. Prasad HK, Hariprasad R, Habibur Rahman SMH. Method development and validation for the simultaneous estimation of resveratrol and quercetin in bulk and pharmaceutical dosage form by RP-HPLC. *J Pharm Sci Res*. 2019;11(12):3777-81.
168. Shafiee F, Khoshvishkaie E, Davoodi A, Dashti Kalantar A, Bakhshi Jouybari H, Ataee R. The determination of blood glucose lowering and metabolic effects of *Mespilus germanica* L. Hydroacetic extract on streptozocin-induced diabetic balb/c mice. *Medicines (Basel)*. 2018;5(1):1 doi:10.3390/medicines5010001
169. Wahab M, Bhatti A, John P. Evaluation of antidiabetic activity of biogenic silver nanoparticles using *thymus serpyllum* on streptozotocin-induced diabetic balb/c mice. *Polymers (Basel)*. 2022;14(15):3138. doi:10.3390/polym14153138
170. Cruz PL, Moraes-Silva IC, Ribeiro AA, Marchi JF, Melo TMD, Santos F, Silva MB, Strunz CMC, Caldini EG. Nicotinamide attenuates streptozotocin-induced diabetes



- complications and increases survival rate in rats: role of autonomic nervous system. *BMC Endocr Disord.* 2021;21(1):133. doi:10.1186/s12902-021-00795-6
171. Rathore P, Mahor A, Jain S, Haque A, Kesharwani P. Formulation development, *in vitro* and *in vivo* evaluation of chitosan engineered nanoparticles for ocular delivery of insulin. *RSC Adv.* 2020;10(71):43629-43639. doi:10.1039/d0ra07640f
  172. Chandirasegaran G, Elanchezhiyan C, Ghosh K. Effects of berberine chloride on the liver of streptozotocin-induced diabetes in albino wistar rats. *Biomed Pharmacother.* 2018;99:227-236. doi:10.1016/j.biopha.2018.01.007
  173. Akbar MU, Zia KM, Akash MSH, Nazir A, Zuber M, Ibrahim M. In-vivo anti-diabetic and wound healing potential of chitosan/alginate/maltodextrin/pluronic-based mixed polymeric micelles: Curcumin therapeutic potential. *Int J Biol Macromol.* 2018;120(Pt B):2418-2430. doi:10.1016/j.ijbiomac.2018.09.010
  174. El-Far YM, Zakaria MM, Gabr MM, El Gayar AM, Eissa LA, El-Sherbiny IM. Nanoformulated natural therapeutics for management of streptozotocin-induced diabetes: potential use of curcumin nanoformulation. *Nanomedicine (Lond).* 2017;12(14):1689-1711. doi:10.2217/nmm-2017-0106
  175. Elsadek MF, Ahmed BM. Effect of sakuranin on carbohydrate-metabolizing enzyme activity modifications in streptozotocin-nicotinamide-induced diabetic wistar rats. *Saudi J Biol Sci.* 2022;29(3):1402-1406. doi:10.1016/j.sjbs.2021.11.035
  176. Prabhakar PK, Doble M. A target based therapeutic approach towards diabetes mellitus using medicinal plants. *Curr Diabetes Rev.* 2008;4(4):291-308. doi:10.2174/157339908786241124
  177. al-Shamaony L, al-Khazraji SM, Twaij HA. Hypoglycaemic effect of Artemisia herba alba. II. Effect of a valuable extract on some blood parameters in diabetic animals. *J Ethnopharmacol.* 1994;43(3):167-171. doi:10.1016/0378-8741(94)90038-8
  178. Griesmacher A, Kindhauser M, Andert SE, Schreiner W, Toma C, Knoebl P, Pietschmann P, Prager R, Schnack C, Schemthaler G. Enhanced serum levels of thiobarbituric-acid-reactive substances in diabetes mellitus. *Am J Med.* 1995;98:469-475.
  179. Koenig RJ, Peterson CM, Jones RL, Saudek C, Lehrman M, Cerami A. Correlation of glucose regulation and hemoglobin A1c in diabetes mellitus. *N Engl J Med.* 1976;295(8):417-420. doi:10.1056/NEJM197608192950804



- 
180. Swanston-Flatt SK, Day C, Bailey CJ, Flatt PR. Traditional plant treatments for diabetes. Studies in normal and streptozotocin diabetic mice. *Diabetologia*. 1990;33(8):462-464. doi:10.1007/BF00405106
  181. Lal SS, Sukla Y, Singh A, Andriyas EA, Lall AM. Hyperuricemia, high serum urea and hypoproteinemia are the risk factor for diabetes. *Asian J Med Sci*. 2009;1:33- 34.
  182. Jouad H, Lemhadri A, Maghrani M, Zeggwagh NA, Eddouks M. Cholesterol-lowering activity of the aqueous extract of *Spergularia purpurea* in normal and recent-onset diabetic rats. *J Ethnopharmacol*. 2003;87:43-49.
  183. Cho SY, Park JY, Park EM, Choi MS, Lee MK, Jeon SM, Jang MK, Kim MJ, Park YB. Alternation of hepatic antioxidant enzyme activities and lipid profile in streptozotocin-induced diabetic rats by supplementation of dandelion water extract. *Clinica Chimica Acta*. 2002;317(1-2):109-117. DOI: 10.1016/s0009-8981(01)00762-8
  184. Pari L, Suman S. Efficacy of Naingin on hepatic enzymes of carbohydrate metabolism in STZ-Nicotinamide induced Type 2 diabetes rats. *Int J Pharm. Biol.Archi*. 2010; 1(2): 280-286.
  185. Prasath GS, Subramanian SP. Modulatory effects of fisetin, a bioflavonoid, on hyperglycemia by attenuating the key enzymes of carbohydrate metabolism in hepatic and renal tissues in streptozotocin-induced diabetic rats. *Eur J Pharmacol*. 2011;668(3):492-496. doi:10.1016/j.ejphar.2011.07.021
  186. Baynes JW, Thorpe SR. Current Opinion in Endocrinology. *Diabetes and Obesity*. 1996;3:277-284.
  187. Grattagliano I, Bonfrate L, Diogo CV, Wang HH, Wang DQ, Portincasa P. Biochemical mechanisms in drug-induced liver injury: certainties and doubts. *World J Gastroenterol*. 2009;15(39):4865-4876. doi:10.3748/wjg.15.4865
  188. Trautwein C, Koch A. Mechanisms of acute liver failure. *Liver Immunology*. 2013;373-388. Published 2013 Oct 29. doi:10.1007/978-3-319-02096-9\_25
  189. Chao G, Zhu Y, Chen L. Role and risk factors of glycosylated hemoglobin levels in early disease screening. *J. Diabetes Res*. 2021;1-8. 10.1155/2021/6626587.
  190. Sherwani SI, Khan HA, Ekhzaimy A, Masood A, Sakharkar MK. Significance of HbA1c test in diagnosis and prognosis of diabetic patients. *Biomark Insights*. 2016;11:95-104. Published 2016 Jul 3. doi:10.4137/BMI.S38440
-

191. Harita N, Hayashi T, Sato KK, Nakamura Y, Yoneda T, Endo G, Kambe H. Lower serum creatinine is a new risk factor of type 2 diabetes: The Kansai Healthcare Study. *Diabetes Care*. 2009;32(3):424-426. doi:10.2337/dc08-1265

## RP-HPLC METHOD DEVELOPMENT AND VALIDATION FOR SIMULTANEOUS ESTIMATION OF CURCUMIN AND RESVERATROL IN NANO-MICELLE: DUAL DRUG DUAL FORM SIMULTANEOUS ESTIMATION

S. K. MOSIUR RAHAMAN<sup>a</sup>, ATANU CHANDRA<sup>b</sup>, RANU BISWAS<sup>\*b</sup>

<sup>a</sup>Laboratory of Nanomedicine, Division of Pharmaceutical Biotechnology, Department of Pharmaceutical Technology, Jadavpur University, Kolkata-700032, West Bengal, India. <sup>b</sup>Department of Pharmaceutical Technology, Jadavpur University, Kolkata-700032, West Bengal, India. <sup>c</sup>Emami Limited, Deputy Manager-R and D-Analytical, Kolkata-700056, West Bengal, India

\*Corresponding author: Ranu Biswas; \*Email: rbiswas.pharmacy@jadavpuruniversity.in

Received: 31 Dec 2023, Revised and Accepted: 13 Feb 2024

### ABSTRACT

**Objective:** To develop a reverse-phase high-performance liquid chromatography (RP-HPLC) method for simultaneous estimation of conjugated form of Curcumin (CCMN) and free form of Resveratrol (RSV) in nano-micelle.

**Methods:** The conjugation of lipophilic CCMN and hydrophilic Chitosan (CHT) through succinyl linker produce amphipathic molecule that can self-assemble into RSV solution to form micelle. Here RSV exists in micelle core as free form and CCMN with micelle backbone as conjugated form. So it required to estimate conjugated drug and free drug simultaneously from nano-micelle. We developed a RP-HPLC method, utilized C18 column, follow flow rate of mobile phase 1.0 ml/min, which consist of acetonitrile with water (0.5% *Ortho* Phosphoric acid, pH 4.6) in the ratio of 1:1 for 20 min. Injection volume was 10µl and column temperature 25 °C. Isosbestic detection of both drugs was at 254 nm.

**Results:** The retention time of RSV and CCMN were at 8.15 min and 11.41 min respectively, completely distinguished sharp peak of CCMN and RSV developed with resolution 7.360±0.117, wide range of linearity with correlation coefficient value ( $R^2$ ) of CCMN and RSV were 0.99987 and 0.99992 respectively and recovery value of CCMN and RSV were 100.041±0.22 % and 100.041±0.21 % respectively. The RSD (relative standard deviation) for accuracy, precision and robustness of the method was found to be less than 2%.

**Conclusion:** The develop method for simultaneous estimation of conjugated CCMN and free form of RSV in the nano-micelle formulation was consider to be accurate, precise, robust and sensitive.

**Keywords:** Nano-micelle, Amphipathic, RP-HPLC, Estimation, Validation

© 2024 The Authors. Published by Innovare Academic Sciences Pvt Ltd. This is an open access article under the CC BY license (<https://creativecommons.org/licenses/by/4.0/>)  
DOI: <https://dx.doi.org/10.22159/ijap.2024v16i3.50276> Journal homepage: <https://innovareacademics.in/journals/index.php/ijap>

### INTRODUCTION

Polyphenolic phyto compounds are gaining enormous demand in the treatment of different diseases and ailments of human beings in different countries because of wide safety margin, easy availability and low costs

[1-3]. The polyphenolic phytoconstituent CCMN chemically known as 1, 7-bis (4-hydroxy-3-methoxyphenyl)-1, 6-heptadiene-3, 5-dione occurs in *Curcuma longa* Linn having diverse therapeutic activity like anti-viral, anti-inflammatory, anti-cancer, antioxidant, wound healing and anti-diabetic [4-6], proved by *in vitro* and *in vivo* studies [7].

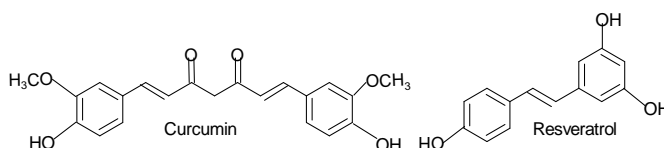


Fig. 1: Structure of curcumin and resveratrol

The polyphenolic phytoconstituent RSV, also known as phytoalexin, chemically known as 3,5,4'-trihydroxy-trans-stilbene found in red grapes skin, giant knotweed, blueberries, mulberries, eucalyptus and many more having anticancer, anti-inflammatory, antioxidant and type-2 anti-diabetic activity. It diminishes the progress of neurodegenerative disorders and enhances the lifespan of the SIRT1 gene [8-10].

Both drugs have many common therapeutic activities against different diseases. Hence, simultaneous administration of both drugs can produce their synergistic effect against inflammation, oxidative stress and diabetes. Unfortunately, both drugs have very little aqueous solubility and bioavailability. The very slow absorption and fast metabolism of CCMN impose minimal use despite its enormous therapeutic potential. RSV has less bioavailability, faster metabolism and rapid elimination, which arouse delivery problems.

To overcome those problems and simultaneously achieve synergistic therapeutic effects against diabetes, we have developed nano-

micelles loaded with two drugs (CCMN and RSV). To construct an amphipathic molecule, here hydrophilic polymer CHT is conjugated with lipophilic polyphenolic compound CCMN via succinyl linker. This amphipathic molecule self-assembled to form micelle in the RSV solution; after completion of micelle formation by dialysis process entire mixture was passed through 0.45µm filter paper to get nano-size micelle. RSV exists in the nano-micelle core while the amphipathic molecule structure consists of CCMN.

There are very few HPLC methods available for the simultaneous estimation of CCMN and RSV but no HPLC method available for simultaneous estimation of both drugs of two different forms from nano-micelle. Hence, an accurate, precise, rapid and robust RP-HPLC method is required for simultaneous estimation of both drugs from nano-micelles. Our studies focus on the development and validation of the RP-HPLC method for simultaneous estimation of CCMN and RSV from nano-micelles. The common wavelength where both drugs

show maximum absorbance, known as the isosbestic point [11] was found to be 254 nm.

## MATERIALS AND METHODS

### Chemicals and reagents

Resveratrol (purity>99 %) and rat plasma were procured from Sigma Aldrich chemicals company (St. Louis, Missouri, United States). Curcumin (purity>99 %), Chitosan (low molecular weight), succinic anhydride and dimethyl sulfoxide (DMSO) were purchased from TCI Chemical (India) Pvt. Ltd. HPLC grade acetonitrile (ACN), water, glacial acetic acid, methanol, ammonium acetate and analytical grade *Ortho* Phosphoric were purchased from Merck Specialities Pvt. Ltd., Mumbai, India. Sample solution passes through a 0.45µm pore size Millex syringe.

### Preparation and characterization of nano-micelle

Initially amphipathic molecule was synthesized by conjugation of CCMN and CHT through succinyl linker. For the preparation of nano-micelle, 1 mg/ml solution of amphipathic molecule were prepared with 1 mg/ml RSV containing DMSO solution by proper mixing. This mixture was taken into a dialysis bag (Mol. Wt12 kDa), placed into double distilled water for 24 h, and replaced the water in 4 h intervals. Amphipathic molecules were self-assembled in the dialysis bag. During dialysis process unbound-free drugs and other substance were eliminated. After completion of dialysis, it was passed through a filter of 0.45 µm pore size to avoid the large particles and then lyophilized the product. The final nano-micelles were stored in a cool and dry place for further use [12, 13]. The yield of nano-micelles was approximately 88%.

### Instrumentation and chromatographic conditions

The HPLC system used was Agilent 1260-infinity (Minneapolis, MN), solvent delivery pump equipped with 20 µl, loop and agilent sample injector (G1329B), and photodiode array (PDA) detector (G13150) using Lab Solution software (Version 1.5). Chromatographic separation was accomplished using Phenomenex Gemini (250 mm X 4.6 mm i.d., 5 µm particle, C18 reversed-phase) Column. The constituents of mobile phase and their ratio were optimized after many trials. The optimized condition of analysis was that the flow rate of mobile phase 1.0 ml/min for run time 20 min, which consist of acetonitrile with water (0.5% *Ortho* Phosphoric acid, pH 4.6) in the ratio of 1:1. Sample injection volume was 10µl and column temperature was 25 °C Before utilization of both mobile phase and test sample those were sonicated for 20 min and filtered through 0.45µm membrane filter. The isosbestic wavelength, which is the common peak absorbance of both drugs, was determined by superimposition of individual peak absorption spectra of CCMN and RSV of the range of 200 nm to 400 nm (UV-vis spectrophotometer, Shimadzu, Japan) and it was found that both absorption spectra curve cross at 254 nm. The isosbestic detection wavelength was fixed at 254 nm.

### Preparation of calibration standards and sample solution

#### Preparation of RSV standard

Quantitatively, 10 mg of RSV was transferred quantitatively into a 100 ml volumetric flask after being accurately weighted. 80 ml of ethanol was added dissolved well, and the volume was made up with ethanol to obtain a solution of 100 µg/ml. The working standard solution with a concentration range of 0.1-32µg/ml was prepared by serial dilution with a mobile phase. Before use all those solution were kept at 4 °C

#### Preparation of CCMN standard

Accurately weighted 10 mg CCMN was transferred quantitatively into a 100 ml volumetric flask. 80 ml of methanol was added, shaken well to dissolve and the volume was made up with methanol to get a concentration 100 µg/ml. In a similar way like RSV the working standard solution in the concentration range of 0.1-64µg/ml was prepared by dilution with mobile phase. Before use all those solutions were kept at 4 °C

### Preparation of sample solution for investigation of drugs loading and loading efficacy

A concentration of 2 mg/ml of nano-micelle was prepared with 2N HCl, incubated for 1.5 h at 50 °C for acid hydrolysis of ester bonds exist in between CHT and CCMN. The sample solution was diluted with methanol to produce 1000 ppm. Before filtration through 0.22µm membrane, it was sonicated for 10 min. Filtrate was evaporated to produce dry powder then re-constituted with mobile phase solution centrifuge the solution for 15 min at 5000rpm and then 1.0 ml supernatant was diluted to 10 ml. A known concentration of CCMN and RSV (1:1 ratio) was prepared and treated as above (to know percent degradation of CCMN and RSV in 2N HCl). All the samples were subjected to RP-HPLC analysis within 2 h to investigate drug loading efficacy (DEE) and drug loading (DL) [14-17].

### Method validation

For the validation of simultaneous estimation of CCMN and RSV in nano-micelle, we follow the guideline of International Conference on Harmonisation (ICH) stated in Q2(R1). The guideline includes selectivity, system suitability, linearity, limit of detection (LOD), limit of quantification (LOQ), accuracy, precision, and robustness [18].

#### Selectivity

The objective of this study is to clearly separate peaks of drugs and eliminate other substance involve in the nano-micelle. Through HPLC systems separately analyzed standard drugs, standard drugs mixture, nano-micelle sample solution, and nano-micelle free sample solution. For the method selectivity confirmation, Rs (resolution) should be >1.5 [19].

#### System suitability

To evaluate system suitability, a mixture (1:1 ratio) of CCMN and RSV at a concentration of 01 µg/ml in methanol was prepared. It was analyzed six times through HPLC with different time interval and noted down area under the curve or peak area (AUC), numbers of theoretical plate (N), retention time (t<sub>R</sub>), tailing factor (T<sub>f</sub>) and resolution (R<sub>s</sub>). The data generated was calculated to obtain statistical values such as standard deviation (SD) relative standard deviation (RSD). The acceptance limit for system suitability RSD value should be less than 2%.

### CCMN and RSV calibration solutions preparation for linearity assessment

Separately 01 mg/ml stock solution of CCMN and RSV in methanol were prepared and diluted by mobile phase to produce calibration standard solution of strength 02µg/ml, 04µg/ml, 06µg/ml, 08µg/ml, 16µg/ml and 32µg/ml for CCMN and 01µg/ml, 02µg/ml, 04µg/ml, 08µg/ml, 12µg/ml and 16µg/ml for RSV. Before injection to HPLC system, all were passed through 0.22µ filter. The obtained peak areas were graphically plotted against the corresponding strength of CCMN and RSV to obtain the regression correlation coefficient (R<sup>2</sup>) [20, 21] for the linearity assessment of both drugs.

#### Sensitivity

LOD and LOQ were calculated to know the sensitivity of test. LOD signify how much less quantity our developed HPLC analysis can sense and LOQ signify how much less quantity our developed HPLC analysis can quantify. Standard deviation (σ) and slope (S) of linear regression for CCMN and RSV were obtained from data generated in calibration curve by statistical calculation [19]. Based on the equation below, LOD and LOQ were calculated.

$$LOD = \frac{3.3\sigma}{S} \dots \dots \dots \text{Eq1}$$

$$LOQ = \frac{10\sigma}{S} \dots \dots \dots \text{Eq2}$$

Where σ = the standard error of the response, S = the slope of the calibration curve.

#### Accuracy and precision

As per the guide line of ICH Q2(R1) accuracy is the closeness of obtained results to the actual value and precision is the closeness of obtained results among each other or it may be define as

repeatability of obtained results. For the accuracy and precision assessment three concentration of CCMN (02µg/ml, 04µg/ml and 08µg/ml) and RSV (02µg/ml, 04µg/ml and 08µg/ml) were prepared from standard solution. All those were analyzed through HPLC system in triplicate within same day (Intra-day) and in three consecutive days (inter-day), follow the same experimental condition for all. The measured peak responses of chromatogram of intra-day and inter-day were statistically calculated for accuracy and precision measurement. Statistically, we have calculated mean, SD, and % RSD [22-26].

### Robustness

The develop method consider to be a robust method when minor intentional change of chromatographic condition like flow rate, pH, and composition unaffected the reproducibility of results or no significant change occur in expected results. The chromatographic analysis data obtained after small changes in parameters were analyzed to calculate RSD, which should remain less than 2% for the chromatographic method to be robust.

### In vitro release study of CCMN and RSV from nano-micelle

The cumulative releases of CCMN and RSV from nano-micelle were studied in PBS buffer pH 5.0 and 7.4. Separately a fixed quantity of nano-micelle (10 mg) was dispersed in 10 ml of PBS buffer pH 5.0

and 7.4 solutions. All those solutions were taken into two separate dialysis bags and transferred it into 90 ml respective buffers solution. Those were incubated at 37 °C for 9 d with moderate shaking. During the incubation period, with an increasing time interval, 2 ml of the sample was withdrawn from each beaker and replaced with the respective buffer [27]. The samples were investigated to investigate percent cumulative drug release [14-17] using the developed RP-HPLC method.

### Data analysis

All the data were statistically analyzed as required to obtain the least square ( $R^2$ ), standard deviation, mean, relative standard deviation and equation of the calibration curve by Excel Microsoft INC USA.

## RESULTS AND DISCUSSION

### Finding of common maximum absorbance wavelength

The spectral analyses of CCMN and RSV at concentration 05µg/ml and 10µg/ml solutions were done respectively in methanol. The absorption spectra in the range of 200 nm to 400 nm of both drugs were recorded and plotted. Here the superimposition of two different absorption spectra crosses to each other at wavelength 254 nm, which is the common maximum absorbance wavelength (isosbestic wavelength) of both drugs shown in fig. 2.

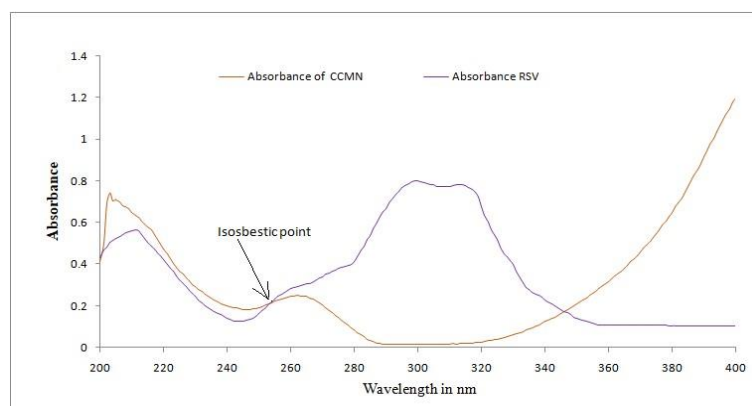


Fig. 2: Superimposition UV spectrum of CCMN and RSV

### Optimization of chromatographic parameters

Extensive analyses were done to optimize various parameters like the flow rate of the mobile phase, pH of the mobile phase, column temperature, ratios of the mobile phase components like acetonitrile, *Ortho* Phosphoric acid and water. After many trials, it was optimized that the flow rate of the mobile phase was 1.0 ml/min, pH of the mobile phase was 4.6, Column temperature was 25 °C ratio of water and 0.5% *Ortho* Phosphoric acid (pH 4.6) containing acetonitrile was 1:1. Before utilization of above composition as mobile phase, we utilize water and methanol at a different ratio as a mobile phase but the results were not

satisfactory. For the simultaneous estimation of CCMN and RSV, the isosbestic wavelength 254 nm was fixed.

Under optimized chromatographic conditions, the chromatogram of the mixture of both standard drugs showed distinctly separated acute sharp peaks with retention times of 8.15 min and 11.41 min for RSV and CCMN, respectively in simultaneous analysis fig. 3. Both drugs were analyzed separately under the same chromatographic condition also; chromatograms were shown in fig. 4 and fig. 5. The chromatographic results execute a higher number of theoretical plate, lesser height of equivalent theoretical plate and lesser tailing factor; those signify the acceptance criteria of HPLC analysis.

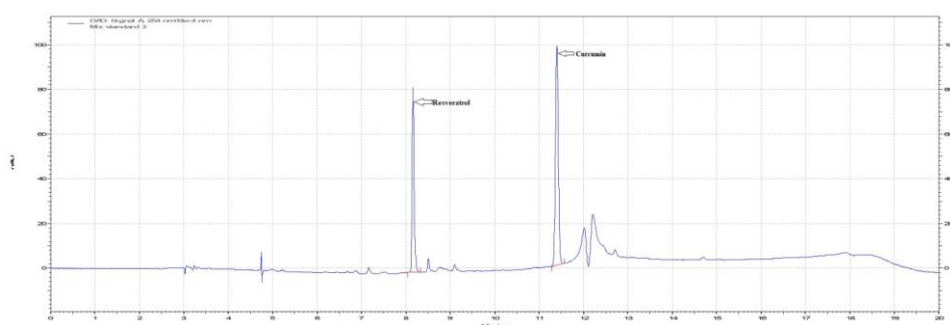
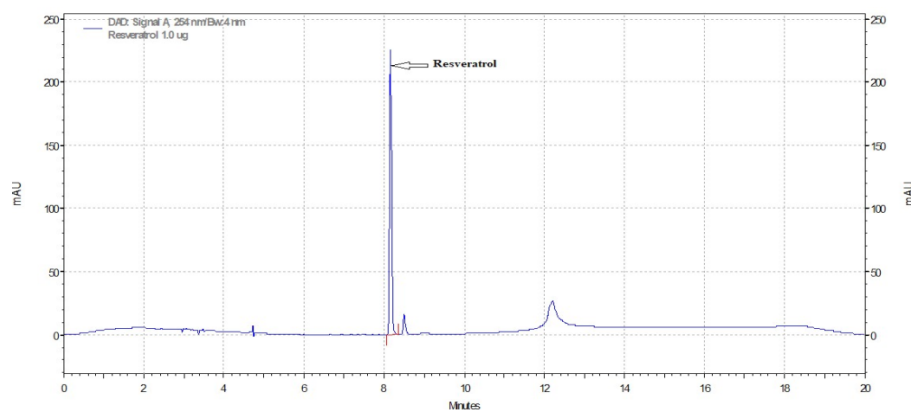
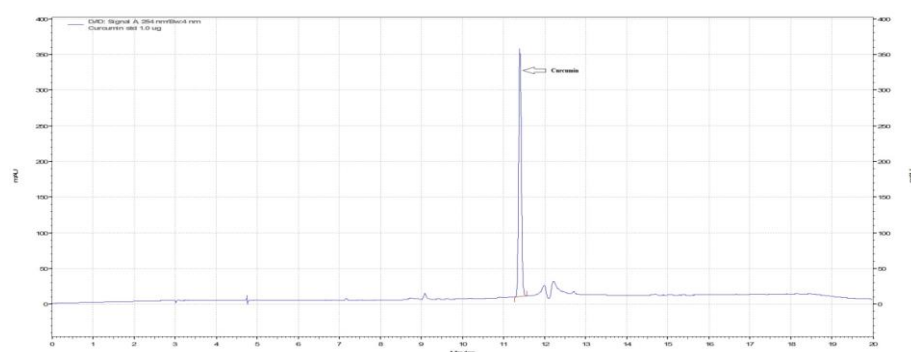


Fig. 3: RP-HPLC chromatogram of resveratrol and curcumin standard

Fig. 4: RP-HPLC chromatogram of resveratrol standard ( $t_R$ -8.15 min)Fig. 5: RP-HPLC chromatogram of curcumin standard ( $t_R$ -11.41 min)

### Method validation

For the RP-HPLC method validation we follow the guideline of ICH stated in Q2(R1).

### System suitability test

The mixture of CCMN and RSV solution was injected in the HPLC column six times to analyze the system suitability of the developed method. The analyzing concentration of CCMN and RSV in the

mixture was 01  $\mu\text{g/ml}$  each. To analyze system suitability, different parameters like retention time, number of theoretical plates, area under the curve, tailing factor and resolution were determined (table 1). The average resolution of both drugs was  $7.360 \pm 0.117$  which signifies the complete separation of peak of the drugs and the RSD value of all parameters was less than 2% which signifies that our developed method fulfils the requirements of ICH guideline as well as USP guideline. So our developed RP-HPLC method is very suitable and highly effective [28].

Table 1: System suitability of the developed method

Sample	t <sub>R</sub>		N	AUC		T <sub>f</sub>	Rs		
	RSV	CCMN		RSV	CCMN		RSV	CCMN	
1	8.109	11.381	8085	8270	109456	174443	1.108	1.158	7.479
2	8.105	11.317	7987	8207	109237	173806	1.126	1.211	7.342
3	8.281	11.404	7894	8181	109975	174378	1.142	1.201	7.138
4	8.169	11.408	7913	8102	109981	173800	1.139	1.184	7.403
5	8.167	11.405	7992	8064	109635	174049	1.131	1.214	7.401
6	8.165	11.401	7882	8188	109579	174202	1.148	1.198	7.397
Average	8.166	11.386	7958.833	8168.667	109644	174113	1.132	1.194	7.360
SD	0.064	0.035	77.484	74.382	293	277	0.014	0.021	0.117
RSD (%)	0.778	0.309	0.974	0.911	0.267	0.159	1.260	1.736	1.591

$n=6$ ;  $t_R$ : Retention time, N: Number of theoretical plate, AUC: Area under the curve,  $T_f$ : Tailing factor, Rs: Resolution

### Linearity, range and sensitivity

Six different concentration of CCMN (02 $\mu\text{g/ml}$ , 04 $\mu\text{g/ml}$ , 06 $\mu\text{g/ml}$ , 08 $\mu\text{g/ml}$ , 16 $\mu\text{g/ml}$  and 32 $\mu\text{g/ml}$ ) and RSV (01 $\mu\text{g/ml}$ , 02 $\mu\text{g/ml}$ , 04 $\mu\text{g/ml}$ , 08 $\mu\text{g/ml}$ , 12 $\mu\text{g/ml}$  and 16 $\mu\text{g/ml}$ ) were analyzed separately and AUC of different concentration of both compound were plotted against their respective concentration in MS-Excel fig. 6a and 6b. It was found that the linearity range of CCMN was 2-32  $\mu\text{g/ml}$  and RSV was 1-16  $\mu\text{g/ml}$ ,

equation of calibration curve were  $Y = 171178.89X + 19619.91$  for CCMN and  $Y = 108179.53X + 6862.02$  for RSV, the correlation coefficient value ( $R^2$ ) of CCMN and RSV were 0.99987 and 0.99992 respectively, very near to 1, that signify the criteria of linearity. To know the sensitivity of the test LOD and LOQ were calculated. LOD and LOQ of CCMN were 0.284939359  $\mu\text{g/ml}$  and 0.863452604  $\mu\text{g/ml}$ , respectively. LOD and LOQ of RSV were 0.12463075  $\mu\text{g/ml}$  and 0.37766894  $\mu\text{g/ml}$ , respectively. From LOD and LOQ results it was concluded that the developed method

is very sensitive, <01 µg/ml solution of CCMN and <0.37766894 µg/ml solution of RSV can be quantified. All the above data is summarized in table 2.

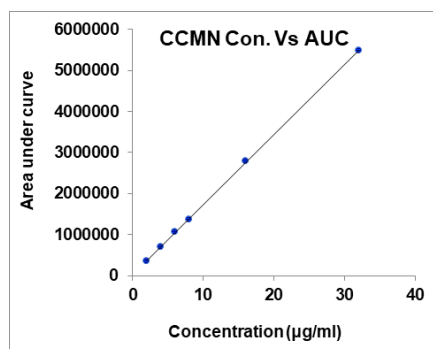


Fig. 6a: Calibration curve of CCMN

#### Accuracy and precision

Three different concentrations of CCMN (02 µg/ml, 04 µg/ml and 08 µg/ml) and RSV (02 µg/ml, 04 µg/ml and 08 µg/ml) were prepared for accuracy and precision study. Those entire samples were analyzed in intra-day and inter-day as per the guidelines of ICH [18]. The analysis results were summarized in tables 3, 4, and 5. HPLC analysis data obtained were statistically calculated to analyze %RSD

and percent recovery. The intra-day and inter-day recovery (percent accuracy) of CCMN were 100.041±0.22 % and 99.75±0.42 %, respectively, in correspondence to RSV were 100.041±0.21 % and 100.14±0.29 %, respectively, it signifies the acceptance criteria of accuracy. Similarly, intra-day and intra-day % RSD of CCMN were 0.44±0.28 and 0.28±0.02 respectively, in correspondence to RSV were 0.24±0.05 and 0.32±0.19 respectively, it signifies the acceptance criteria of precision. As per the guideline of acceptance criteria, the percent RSD of accuracy and precision should be below 2% but our method achieves below 0.5 % in this regard, so our developed method has more reliability than other methods [29].

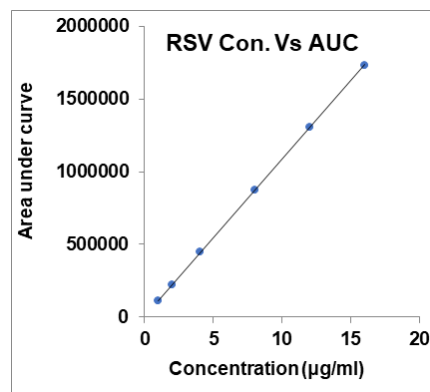


Fig. 6b: Calibration curve of RSV

Table 2: Validation parameters for curcumin and resveratrol

Parameter	CCMN	RSV
Linearity range (µg/ml)	2.00-32.00	1.00-16.00
Linear equation	$Y = 171178.89X + 19619.91$	$Y = 108179.53X + 6862.02$
Correlation coefficient of ( $R^2$ )	0.99987	0.99992
Slope	171178.89	108179.53
Intercept	19619.91	6862.02
Standard error ( $\sigma$ )	14780.48582	4085.60492
LOD (µg/ml)	0.284939359 <sup>#</sup>	0.12463075 <sup>#</sup>
LOQ (µg/ml)	0.863452604 <sup>\$</sup>	0.37766894 <sup>\$</sup>

All the values are considered as mean±SD, n=6; <sup>#</sup>Calculated from Eq1, <sup>\$</sup>Calculated from Eq2

Table 3: Summary of intra-day and inter-day precision and accuracy of the method

Type of analysis	Nominal strength in (µg/ml)	Mean strength found, µg/ml		Mean Accuracy %		RSD% (Precision)	
		CCMN	RSV	CCMN	RSV	CCMN	RSV
Intra-day	2	2.003±0.015	1.997±0.006	100.166667	99.833333	0.7625	0.2892
	4	4.007±0.012	4.010±0.010	100.166667	100.25	0.2882	0.2494
	8	7.983±0.021	8.003±0.015	99.7916667	100.0417	0.2608	0.1909
Inter-day	2	1.987±0.006	1.997±0.006	99.3333333	99.833333	0.2906	0.2892
	4	4.007±0.012	4.017±0.021	100.166667	100.4167	0.2882	0.5183
	8	7.980±0.020	8.013±0.012	99.75	100.1667	0.2506	0.1441

Intra-day and inter-day accuracy of CCMN were 100.041±0.22 % and 99.75±0.42 %; Intra-day and inter-day accuracy of RSV were 100.041±0.21 % and 100.14±0.29 %; Intra-day and inter-day % RSD of CCMN were 0.44±0.28 and 0.28±0.02; Intra-day and inter-day % RSD of RSV were 0.24±0.05 % and 0.32±0.19 % respectively; All the values are presented as mean±SD, n=3.

Table 4: Intra-day analysis results of CCMN and RSV

Conc.	Intra-day analysis of CCMN				Intra-day analysis of RSV				Intra-day % accuracy	
	Found	Mean	SD	RSD%	Found	Mean	SD	RSD%	CCMN	RSV
2	1.99	2.0033	0.0153	0.7624	1.99	1.9967	0.0058	0.2892	100.1667	99.3333
	2				2					
	2.02				2					
4	4	4.0067	0.0115	0.2882	4.01	4.01	0.01	0.2494	100.1667	100.25
	4.02				4.02					
	4				4					
8	7.96	7.9833	0.0208	0.2608	7.99	8.0033	0.0153	0.1909	99.7917	100.0417
	7.99				8					
	8				8.02					

All the values are considered as mean±SD, n=3



Table 5: Inter-day analysis results of CCMN and RSV

Conc.	Day	Inter-day analysis of CCMN				Inter-day analysis of RSV				Inter-day % Accuracy	
		Found	Mean	SD	RSD%	Found	Mean	SD	RSD%	CCMN	RSV
2	Day-1	1.98	1.9867	0.0058	0.2906	1.99	1.99667	0.0058	0.2892	99.3333	99.8333
	Day-2	1.99				2					
	Day-3	1.99				2					
4	Day-1	4	4.0067	0.0115	0.2882	4.04	4.0167	0.0208	0.5183	100.1667	100.4167
	Day-2	4.02				4.01					
	Day-3	4				4					
8	Day-1	8	7.98	0.02	0.2506	8.02	8.0133	0.0115	0.1441	99.75	100.1667
	Day-2	7.96				8					
	Day-3	7.98				8.02					

All the values are considered as mean $\pm$ SD, n=3

### Robustness

Different concentrations of CCMN and RSV were prepared like LQC, MQC and HQC (i.e., Low, Medium and high-quality control) for CCMN those were 01 $\mu$ g/ml, 16 $\mu$ g/ml and 32  $\mu$ g/ml, respectively, for RSV which were 01 $\mu$ g/ml, 08 $\mu$ g/ml and 16  $\mu$ g/ml respectively. Minor changes in chromatographic conditions like flow rate (1 $\pm$ 0.1

ml/min), pH (4.6 $\pm$ 0.2) wavelength (254 $\pm$ 2 nm), and composition of mobile phase were done to observe the effect in terms of retention time and assay at different concentration levels. All the results signify the acceptance criteria of ICH as well as USP guidelines table 6. RSD values of retention time and assay were less than 2% which proves that our developed method fulfills the acceptance criteria of robustness.

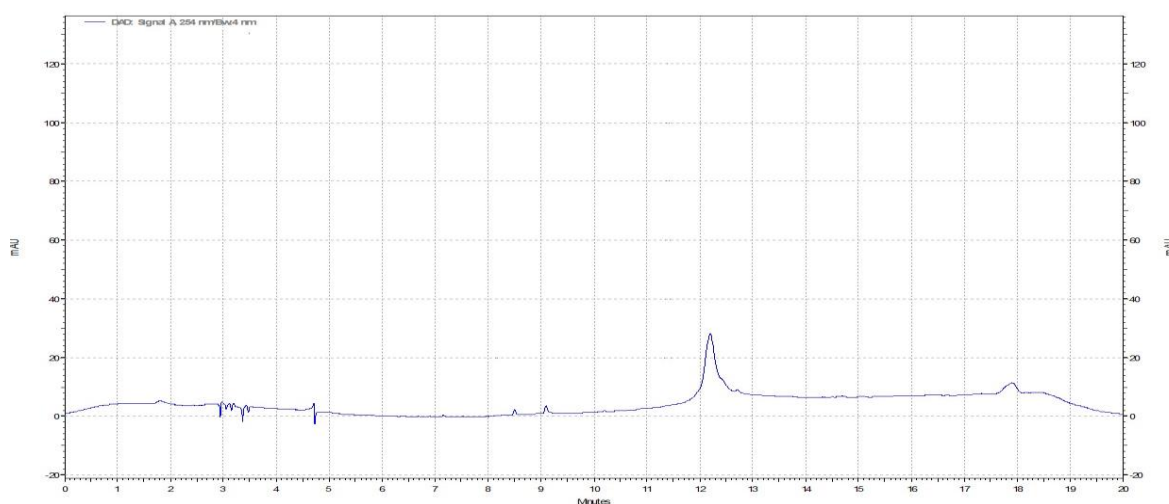


Fig. 7: A blank sample RP-HPLC chromatogram

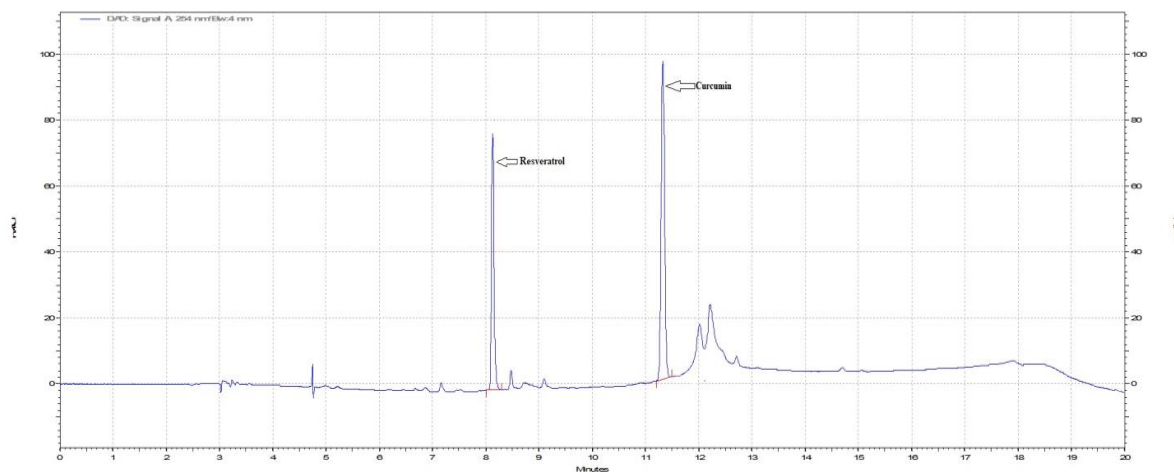


Fig. 8: RP-HPLC chromatogram of CCMN and RSV treated with 2N HCl



Table 6: Summary of robustness of method

Variables	Value	Strength	CCMN								RSV							
			RT	RT (mean)	SD of RT	%RSD of RT	Assay %	Assay % (mean)	SD of assay %	% RSD of assay	RT	RT (mean)	SD of RT	%RSD of RT	Assay %	Assay % (mean)	SD of assay %	%RSD of assay
Flow rate (pH=4.6, Water: CAN= 50:50, Wavelength h= 254)	0.9	LQC	11.85	11.847	0.0153	0.1289	100.41	99.797	0.6531	0.6544	8.64	8.573	0.0586	0.6835	100.85	99.840	0.8822	0.8836
		MQC	11.86				99.87				8.53				99.45			
		HQC	11.83				99.11				8.55				99.22			
	1	LQC	11.45	11.413	0.0351	0.3077	99.49	99.950	0.4927	0.4930	8.18	8.153	0.0306	0.3747	99.17	99.863	0.6008	0.6016
		MQC	11.41				99.89				8.12				100.23			
		HQC	11.38				100.47				8.16				100.19			
	1.1	LQC	11.08	11.023	0.0551	0.4996	100.41	99.907	0.7136	0.7143	7.91	7.817	0.0950	1.2159	99.41	100.117	0.6574	0.6566
		MQC	11.02				100.22				7.82				100.71			
		HQC	10.97				99.09				7.72				100.23			
pH (Flow rate= 01 ml/min, Water: CAN= 50:50, Wavelength h= 254)	4.4	LQC	11.18	11.110	0.0700	0.6301	100.48	100.097	0.7077	0.7070	7.98	7.943	0.0321	0.4047	100.11	99.807	0.2793	0.2799
		MQC	11.04				99.28				7.93				99.56			
		HQC	11.11				100.53				7.92				99.75			
	4.6	LQC	11.45	11.413	0.0351	0.3077	99.49	99.950	0.4927	0.4930	8.18	8.153	0.0306	0.3747	99.17	99.863	0.6008	0.6016
		MQC	11.41				99.89				8.12				100.23			
		HQC	11.38				100.47				8.16				100.19			
	4.8	LQC	11.71	11.607	0.1106	0.9529	99.79	99.787	0.6250	0.6263	8.38	8.307	0.0666	0.8016	99.48	99.580	0.2088	0.2097
		MQC	11.62				99.16				8.25				99.82			
		HQC	11.49				100.41				8.29				99.44			
Composition (Water: ACN) (Flow rate= 01 ml/min, pH=4.6 Wavelength h= 254)	50:50	LQC	11.45	11.413	0.0351	0.3077	99.49	99.950	0.4927	0.4930	8.18	8.153	0.0306	0.3747	99.17	99.863	0.6008	0.6016
		MQC	11.41				99.89				8.12				100.23			
		HQC	11.38				100.47				8.16				100.19			
	55:45	LQC	11.27	11.210	0.0600	0.5352	100.75	99.803	0.8259	0.8275	8.11	7.997	0.1266	1.5834	99.74	99.870	0.1253	0.1255
		MQC	11.21				99.23				8.02				99.88			
		HQC	11.15				99.43				7.86				99.99			
	60:40	LQC	10.89	10.817	0.0702	0.6493	99.14	99.563	0.9395	0.9436	7.83	7.867	0.0404	0.5137	100.01	100.287	0.3958	0.3946
		MQC	10.81				100.64				7.91				100.11			
		HQC	10.75				98.91				7.86				100.74			
Detection wavelength (Flow rate= 01 ml/min (pH=4.6, Water: CAN= 50:50)	252	LQC	11.5	11.423	0.0709	0.6211	99.97	99.660	0.5543	0.5562	8.28	8.203	0.0681	0.8298	99.94	99.937	0.1050	0.1051
		MQC	11.36				99.99				8.15				100.04			
		HQC	11.41				99.02				8.18				99.83			
	254	LQC	11.45	11.413	0.0351	0.3077	99.49	99.950	0.4927	0.4930	8.18	8.153	0.0306	0.3747	99.17	99.863	0.6008	0.6016
		MQC	11.41				99.89				8.12				100.23			
		HQC	11.38				100.47				8.16				100.19			
	256	LQC	11.46	11.413	0.0503	0.4410	100.42	99.793	0.6742	0.6756	8.25	8.163	0.0757	0.9275	99.05	99.650	0.6940	0.6964
		MQC	11.42				99.88				8.11				100.41			
		HQC	11.36				99.08				8.13				99.49			

All the values are considered as mean±SD, n=3

### Drug loading and entrapment efficacy

To break the micelle architected we utilized concentrated HCl that helps to acid hydrolyze ester bonds that exist between CHT and CCMN, the amphipathic molecular unit of the micelle disappeared after separation of CHT and CCMN and consequently, micelle core materials were exposed to the solution. Similarly, a known concentration of CCMN and RSV mixture solution and a blank sample were treated in the same way before being subjected to our developed RP-HPLC analysis. From HPLC analysis, the results were found in terms of AUC and it was converted in terms of concentration through standard curve equations. The obtained results of the entire sample (fig. 7, 8 and 9) were calculated and it was found that the percent loading of CCMN in nano-micelle was  $26.52 \pm 0.67$  w/w and entrapment efficacy was  $93.72 \pm 1.02$  w/w, the percent loading of RSV in nano-micelle core was  $14.56 \pm 0.18$  w/w and entrapment efficacy was  $98.72 \pm 0.12$  w/w.

In the nano-micelles, CCMN exists in conjugated form and RSV exists in free form. It is very difficult to estimate conjugated drugs and free drugs simultaneously from nano-micelle by HPLC analysis or by any other method of analysis. A lot of papers [27, 30-34] are available on drug conjugates where therapeutic properties were being evaluated with more emphasis, but very few papers are available which explain the estimation of conjugated drug. There are many research articles are available [29, 35, 36] on drug delivery through micelle, where drugs are entrapped in a micelle core in most cases and it is easy to estimate either by UV-Vis Spectroscopy or by chromatographic method. First time we developed an analytical method to estimate dual drugs of dual molecular form (conjugated and free) simultaneously from nano-micelle. Here we also considered the impact of percent degradation during the estimation of drugs. The conjugated CCMN and free RSV were measured simultaneously through our developed RP-HPLC method.

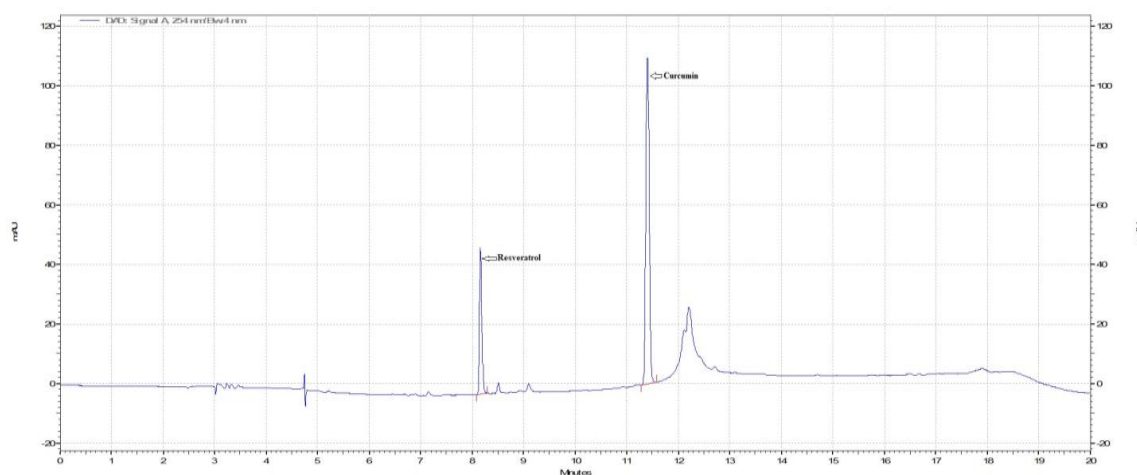


Fig. 9: Nano-micelle sample RP-HPLC chromatogram

### Cumulative drug release

The cumulative releases of CCMN and RSV from nano-micelles were observed in phosphate buffer pH 5.0 and pH 7.4 through the dialysis method and consequently, the percent degradation of CCMN and RSV in the same environment at the same time interval was evaluated. In different time intervals, up to 9 d samples were taken from each vessel and subjected to RP-HPLC analysis. It was observed that more than 90% of drugs (CCMN and RSV) were released from the nano-micelle within 7 d at pH 5.0, whereas more than 50% of the drugs remained in

the nano-micelles to be released within 7 d at pH 7.4. It was also observed that after 9 d 100% of drugs were released at pH 5.0, whereas more than 45% of the drugs remained in the nano-micelles to be released at pH 7.4. Fig. 10 and table 6. From HPLC analysis the results were found in terms of AUC and it was converted in terms of concentration through standard curve equations. During the cumulative drug release study we also consider the impact of percent degradation of drugs throughout the study. Here we observed and compared the selected drug release pattern simultaneously from nano-micelle, which couldn't be possible in UV-Vis spectroscopy.

Table 7: Cumulative percent release results of CCMN and RSV in pH 5.0 and pH 7.4

Time (h)	CCMN release at pH 5		RSV release at pH 5		CCMN release at pH 7.4		RSV release at pH 7.4	
	AUC	Cumulative % release	AUC	Cumulative % release	AUC	Cumulative % release	AUC	Cumulative % release
0	0	0	0	0	0	0	0	0
1	358414	3.769869498	101224	2.995439719	188414	1.878225477	51224	1.408232817
2	714708	7.772164751	154809	4.726403754	364708	3.858687091	74809	2.171000641
4	1094689	12.07767875	264901	8.268143893	604689	6.567430986	134901	4.100138568
6	1544679	17.20448682	374699	11.83549901	808679	8.902395035	194699	6.039019405
8	2144794	24.0518553	514684	16.39596886	1084794	12.06261549	264684	8.320260136
12	3077681	34.66886027	757771	24.27375985	1597681	17.88819743	377771	11.99195284
24	4498705	50.82132605	1458697	46.76242114	2398705	26.97704189	758697	24.20186223
36	5499347	62.45418959	2099436	67.56300091	2799347	31.6998411	1149436	36.84419852
48	6229891	71.19293147	2389891	77.44751409	3129891	35.68721829	1309881	42.30008701
72	7049983	81.00939236	2686874	87.63145545	3509983	40.2627125	1386874	45.15779557
168	8291286	95.60405613	2997987	98.35821618	4001286	46.1179809	1487987	48.80561351
216	8610021	100.0711363	3020131	100.0106652	4284421	49.71156665	1580131	52.20081573

All the values are considered as mean  $\pm$  SD, n=3

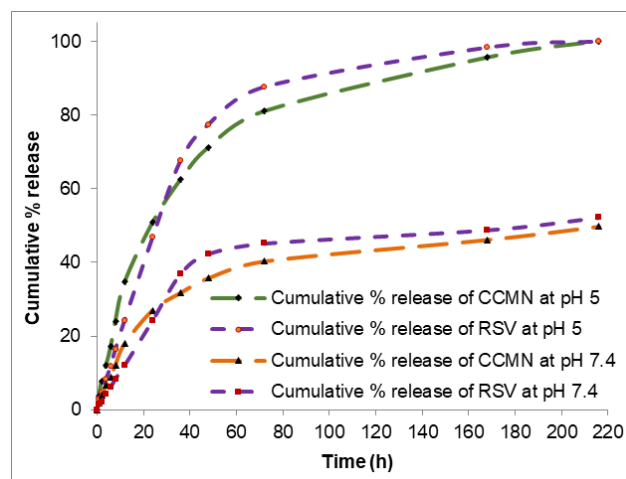


Fig. 10: Cumulative percent release pattern of CCMN and RSV in pH 5.0 and pH 7.4

## CONCLUSION

Conjugated curcumin and free form of resveratrol that exist in nano-micelle were evaluated simultaneously by developing and validating the RP-HPLC method. As per the guideline of ICH Q2(R1), the developed RP-HPLC method was validated. It was found that our develop method proved its robustness, accuracy, linearity, system suitability and criteria of precision. From the chromatogram, it was found that the peaks of drugs arouse from nano-micelle extract and peaks of drugs arouse from known concentration drugs mixture were well resolved and completely separated. There were negligible interferences of other substances in the resolution of peaks. In our development method, there was no such compound which took a huge time to eliminate from the column, reduced column lifetime and disturbed the integrity of column.

## ACKNOWLEDGMENT

The authors would like to thank Jadavpur University, Departments of Chemistry and Pharmaceutical Technology for technical assistance and expertise and also thank to Emami Limited for technical assistance and expertise.

## FUNDING

Self-funding

## AUTHORS CONTRIBUTIONS

All authors have contributed equally.

## CONFLICTS OF INTERESTS

The authors have declared no conflict of interest.

## REFERENCES

- Rathod NB, Elabed N, Punia S, Ozogul F, Kim SK, Rocha JM. Recent developments in polyphenol applications on human health: a review with current knowledge. *Plants (Basel)*. 2023;12(6):1217. doi: 10.3390/plants12061217, PMID 36986905.
- Haque A, Brazeau D, Amin AR. Perspectives on natural compounds in chemoprevention and treatment of cancer: an update with new promising compounds. *Eur J Cancer*. 2021;149:165-83. doi: 10.1016/j.ejca.2021.03.009, PMID 33865202.
- Patra JK, Das G, Fraceto LF, Campos EVR, Rodriguez Torres MDP, Acosta Torres LS. Nano-based drug delivery systems: recent developments and future prospects. *J Nanobiotechnology*. 2018;16(1):71. doi: 10.1186/s12951-018-0392-8, PMID 30231877.
- Kouhpeikar H, Butler AE, Bamian F, Barreto GE, Majeed M, Sahebkar A. Curcumin as a therapeutic agent in leukemia. *J Cell Physiol*. 2019;234(8):12404-14. doi: 10.1002/jcp.28072, PMID 30609023.
- Krishnamurthy G, Deepti Roy L, Kumar J, Gour P, Arland SE, Rehman N. Design, preparation, and *in silico* study of novel curcumin-biphenyl carbonitrile conjugate as novel anticancer drug molecules. *Int J App Pharm*. 2023;15(4):143-59. doi: 10.22159/ijap.2023v15i4.45811.
- Raju SK, Karunakaran A, Kumar S, Sekar P, Murugesan M, Karthikeyan M. Biogenic synthesis of copper nanoparticles and their biological applications: an overview. *Int J Pharm Pharm Sci*. 2022;14(3):8-26. doi: 10.22159/ijpps.2022v14i3.43842, doi: 10.22159/ijpps.2022v14i3.43842.
- Fu YS, Chen TH, Weng L, Huang L, Lai D, Weng CF. Pharmacological properties and underlying mechanisms of curcumin and prospects in medicinal potential. *Biomed Pharmacother*. 2021;141:111888. doi: 10.1016/j.biopha.2021.111888, PMID 34237598.
- Meng X, Zhou J, Zhao CN, Gan RY, Li HB. Health benefits and molecular mechanisms of resveratrol: a narrative review. *Foods*. 2020;9(3):340-67. doi: 10.3390/foods9030340, PMID 32183376.
- Zhang LX, Li CX, Kakar MU, Khan MS, Wu PF, Amir RM. Resveratrol (RV): a pharmacological review and call for further research. *Biomed Pharmacother*. 2021;143:112164. doi: 10.1016/j.biopha.2021.112164, PMID 34649335.
- Resveratrol RG. Multiple activities on the biological functionality of the cell. R. C Gupta, editor. *Nutraceuticals*. Cambridge: Academic Press; 2016. p. 453-64.
- Arayne MS, Sultana N, Tabassum A. RP-LC simultaneous quantitation of co-administered drugs for (non-insulin-dependent) diabetic mellitus induced dyslipidemia in active pharmaceutical ingredient, pharmaceutical formulations and human serum with UV-detector. *Clin Chim Acta*. 2013;425:54-61. doi: 10.1016/j.cca.2013.06.020, PMID 23838368.
- Li M, Gao M, Fu Y, Chen C, Meng X, Fan A. Acetal-linked polymeric prodrug micelles for enhanced curcumin delivery. *Colloids Surf B Biointerfaces*. 2016;140:11-8. doi: 10.1016/j.colsurfb.2015.12.025, PMID 26731193.
- Zhu WT, Liu SY, Wu L, Xu HL, Wang J, Ni GX. Delivery of curcumin by directed self-assembled micelles enhances the therapeutic treatment of non-small-cell lung cancer. *Int J Nanomedicine*. 2017;12:2621-34. doi: 10.2147/IJN.S128921, PMID 28435247.
- Banerjee S, Roy S, Bhaumik KN, Pillai J. Mechanisms of the effectiveness of lipid nanoparticle formulations loaded with anti-tubercular drugs combinations toward overcoming drug bioavailability in tuberculosis. *J Drug Target*. 2020;28(1):55-69. doi: 10.1080/1061186X.2019.1613409, PMID 31035816.
- Banerjee S, Roy S, Nath Bhaumik K, Kshetrapal P, Pillai J. Comparative study of oral lipid nanoparticle formulations (LNFs) for chemical stabilization of antitubercular drugs: physicochemical and cellular evaluation. *Artif Cells Nanomed Biotechnol*. 2018;46Suppl1:540-58. doi: 10.1080/21691401.2018.1431648, PMID 29373927.

16. Li H, Zhao X, Ma Y, Zhai G, Li L, Lou H. Enhancement of gastrointestinal absorption of quercetin by solid lipid nanoparticles. *J Control Release*. 2009;133(3):238-44. doi: 10.1016/j.jconrel.2008.10.002, PMID 18951932.
17. Chaudhari VS, Borkar RM, Murty US, Banerjee S. Analytical method development and validation of reverse-phase high-performance liquid chromatography (RP-HPLC) method for simultaneous quantifications of quercetin and piperine in dual-drug loaded nanostructured lipid carriers. *J Pharm Biomed Anal*. 2020;186:113325. doi: 10.1016/j.jpba.2020.113325, PMID 32380356.
18. ICH. Validation of analytical procedures: text and methodology. In: International Conference on Harmonisation. Vol. Q2(R1). Geneva, Geneva; 2005.
19. Gustavo Gonzalez A, Angeles Herrador M. A practical guide to analytical method validation, including measurement uncertainty and accuracy profiles. *TrAC Trends Anal Chem*. 2007;26(3):227-38. doi: 10.1016/j.trac.2007.01.009.
20. AOAC, official methods of analysis of AOAC international. *J AOAC Int*, (Gaithersburg, MD, USA), Guidelines for Standard Method Performance Requirements. 2012:9.
21. Thomas A, Varkey J. Development and validation of a new RP HPLC analytical method for the determination of etodolac succinic acid co-crystals in spiked rabbit plasma. *Int J Curr Pharm Sci*. 2023;15(2):59-63. doi: 10.22159/ijcpr.2023v15i2.2098.
22. Khursheed R, Singh SK, Kapoor B, Gulati M, Wadhwa S, Gupta S. Development and validation of RP-HPLC method for simultaneous determination of curcumin and quercetin in extracts, marketed formulations, and self-nanoemulsifying drug delivery system. *Re: GEN Open*. 2021;1(1):43-52. doi: 10.1089/regen.2021.0021.
23. Bhutia GT, De AK, Bera T. Validation, stability studies, and simultaneous estimation of co-encapsulated curcumin, epigallocatechin gallate nanoformulation by RP-HPLC method. *Int J Appl Pharm*. 2022;14(6):186-95.
24. De AK, Bera T. Analytical method development, validation and stability studies by RP-HPLC method for simultaneous estimation of andrographolide and curcumin in co-encapsulated nanostructured lipid carrier drug delivery system. *Int J App Pharm*. 2021;13(5):73-86. doi: 10.22159/ijap.2021v13i5.42181.
25. Kumar AKH, Sudha V, Vijayakumar A, Padmapriyadarsini C. Simultaneous method for the estimation of bedaquiline and delamanid in human plasma using high-performance liquid chromatography. *Int J Pharm Pharm Sci*. 2021;13(6):36-40. doi: 10.22159/ijpps.2021v13i6.40853.
26. Ahmad S, Khabiya P, Au T, Raheman Bakhshi A. Quality by design approach to develop stability indicating reversed-phase high-performance liquid chromatography method development for ambroxol. *Asian J Pharm Clin Res*. 2021;14(12):44-9. doi: 10.22159/ajpcr.2021.v14i12.42939.
27. Sauraj, Kumar SU, Gopinath P, Negi YS. Synthesis and bio-evaluation of xylan-5-fluorouracil-1-acetic acid conjugates as prodrugs for colon cancer treatment. *Carbohydr Polym*. 2017;157:1442-50. doi: 10.1016/j.carbpol.2016.09.096, PMID 27987854.
28. USP. Chromatography USP. In: National formulary 37, Pharmacopeial convention inc. Vol. 621. USA; 2009.
29. Nasr M, Abdel Rahman MH. Simultaneous determination of curcumin and resveratrol in lipidic nanoemulsion formulation and rat plasma using HPLC: Optimization and application to real samples. *J AOAC Int*. 2019;102(4):1095-101. doi: 10.5740/jaoacint.18-0269, PMID 30651158.
30. Dey S, Sreenivasan K. Conjugation of curcumin onto alginate enhances aqueous solubility and stability of curcumin. *Carbohydr Polym*. 2014;99:499-507. doi: 10.1016/j.carbpol.2013.08.067, PMID 24274536.
31. Sauraj, Kumar SU, Kumar V, Priyadarshi R, Gopinath P, Negi YS. pH-responsive prodrug nanoparticles based on xylan-curcumin conjugate for the efficient delivery of curcumin in cancer therapy. *Carbohydr Polym*. 2018;188:252-9. doi: 10.1016/j.carbpol.2018.02.006, PMID 29525163.
32. Sarika PR, James NR, Kumar PRA, Raj DK, Kumary TV. Gum arabic-curcumin conjugate micelles with enhanced loading for curcumin delivery to hepatocarcinoma cells. *Carbohydr Polym*. 2015;134:167-74. doi: 10.1016/j.carbpol.2015.07.068, PMID 26428113.
33. Yang R, Zhang S, Kong D, Gao X, Zhao Y, Wang Z. Biodegradable polymer-curcumin conjugate micelles enhance the loading and delivery of low-potency curcumin. *Pharm Res*. 2012;29(12):3512-25. doi: 10.1007/s11095-012-0848-8, PMID 22961588.
34. Tian C, Asghar S, Xu Y, Chen Z, Zhang J, Ping Q. Tween 80-modified hyaluronic acid-ss-curcumin micelles for targeting glioma: synthesis, characterization and their *in vitro* evaluation. *Int J Biol Macromol*. 2018;120(B):2579-88. doi: 10.1016/j.ijbiomac.2018.09.034, PMID 30195608.
35. Yusuf H, Wijiani N, Rahmawati RA, Primaharinastiti R, Rijal MAS, Isadiartuti D. Analytical method for the determination of curcumin entrapped in polymeric micellar powder using HPLC. *J Basic Clin Physiol Pharmacol*. 2021;32(4):867-73. doi: 10.1515/jbcpp-2020-0491, PMID 34214361.
36. Prasad HK, Hariprasad R, Habibur Rahman SMH. Method development and validation for the simultaneous estimation of resveratrol and quercetin in bulk and pharmaceutical dosage form by RP-HPLC. *J Pharm Sci Res*. 2019;11(12):3777-81.

Scientific paper

# Succinyl Curcumin Conjugated Chitosan Polymer-Prodrug Nanomicelles: A Potential Treatment for Type-II Diabetes in Diabetic Balb/C Mice

Sk Mosiur Rahaman,<sup>1</sup> Gouranga Dutta,<sup>2</sup> Ranu Biswas,<sup>1,\*</sup> Abimanyu Sugumaran,<sup>3,\*</sup> Mohamed M. Salem,<sup>4</sup> Mohammed Gamal,<sup>5,\*</sup> Mohamed Abdelrahman<sup>6</sup> and Mounir M. Salem-Bekhit<sup>7</sup>

<sup>1</sup> Department of Pharmaceutical Technology, Jadavpur University, Kolkata 700032, West Bengal, India;

<sup>2</sup> Department of Pharmaceutics, SRM College of Pharmacy, SRM Institute of Science and Technology, Kattankulathur 603203, Tamilnadu, India;

<sup>3</sup> Department of Pharmaceutical Sciences, Assam University (A Central University), Silchar 788011, Assam, India;

<sup>4</sup> College of Medicine, Huazhong University of Science and Technology, China;

<sup>5</sup> Pharmaceutical Analytical Chemistry Department, Faculty of Pharmacy, Beni-Suef University, AlshaheedShehata Ahmad Hegazy St., 62514, Beni-Suef, Egypt;

<sup>6</sup> Clinical Pharmacy Department, College of Pharmacy, Al-Mustaqbal University, Babylon, 51001, Iraq;

<sup>7</sup> Department of Pharmaceutics, College of Pharmacy, King Saud University, PO Box 2457, Riyadh 11451, Saudi Arabia.

\* Corresponding author: E-mail: [abimanyu.s@aus.ac.in](mailto:abimanyu.s@aus.ac.in); [rbiswas.pharmacy@jadavpuruniversity.in](mailto:rbiswas.pharmacy@jadavpuruniversity.in); [mgamalm3000@yahoo.com](mailto:mgamalm3000@yahoo.com)

Received: 02-05-2024

## Abstract

Diabetes mellitus is a chronic metabolic disorder marked by elevated blood sugar levels, leading to organ dysfunction. Curcumin, derived from turmeric, exhibits promise in managing type II diabetes. Amphipathic polymer prodrugs were synthesized by conjugating curcumin with chitosan through succinic anhydride. Nanomicelles, formed via dialysis of amphipathic polymer prodrug, were spherical with an average hydrodynamic size of 57 nm. *In vitro* release studies revealed 97% curcumin release at pH 5 in 7 days. A 21-day experiment on diabetic mice compared nano micelles, standard drugs, and free curcumin's impact on fasting blood glucose. The study showcased gradual, controlled curcumin release from nano micelles, suggesting their potential in type II diabetes treatment.

**Keywords:** Chitosan, Curcumin, nano micelles, polymer-prodrug, Type-II diabetic

## 1. Introduction

Diabetes mellitus (DM) is a chronic metabolic disorder marked by persistent high blood glucose levels, termed hyperglycemia. Prolonged hyperglycemia can cause significant harm to the body, impairing function and potentially leading to organ and tissue dysfunction.

According to the International Diabetes Federation (IDF) in 2021, approximately 10.5% of adults aged 20 to 79 have diabetes, with nearly half undiagnosed. IDF predicts that by 2045, diabetes prevalence among adults will rise to 1 in 8, affecting around 783 million people, marking a 46% increase from current levels.<sup>1,2</sup> Type 2 diabetes mellitus predominates among major diabetes categories, encompass-

ing around 90% of global diabetes cases.<sup>3,4</sup> Insufficiency of insulin production (Type 1 diabetes) or diminished cellular sensitivity to insulin (Type 2 and gestational diabetes) are the causes of prolonged hyperglycemia. Insulin-producing  $\beta$  cells are autoimmunely destroyed in type 1 diabetes; the destruction was previously linked to a T-cell-mediated attack. Nevertheless, the cause encompasses both environmental and genetic components, including viral infections, altered intestinal microbiota, and dietary patterns, as well as HLA alleles.<sup>5</sup> However, it is hypothesized to be associated with suboptimal dietary patterns characterized by high carbohydrate intake and a sedentary lifestyle. There is a gradual transition from a relative shortfall of insulin and lacking with its sensitivity leads to an absolute deficiency, which eventually requires the injection of exogenous insulin to regulate glucose levels.<sup>3,6,7</sup> Type 2 Diabetes Mellitus (T2DM) traditionally associated with the elderly, is now increasingly prevalent among children and young individuals. This rise is linked to inadequate dietary intake, sedentary lifestyles, and obesity rates. The phytochemical compounds produce a significant therapeutic response in the treatment of metabolic disorders such as diabetes mellitus due to their low toxicity. Curcumin, (CCMN) a polyphenolic phytochemical derived from the rhizome of the turmeric plant (*Curcuma longa*), has several medicinal properties (like anti-inflammatory, anti-cancer, antioxidant, wound healing, and anti-diabetic etc).<sup>8–10</sup> It has a wide range of potential applications and therapeutic activity. Still, its use is limited due to its very low aqueous solubility, chemical instability, photosensitivity, first-pass metabolism, insufficient tissue distribution, and inadequate absorption, resulting in inadequate bioavailability.<sup>11–13</sup> Studies have demonstrated that CCMN regulates lipid metabolism by suppressing key inflammatory transcription factors (MCP-1, IL-6, HbA1c, TNF- $\alpha$ ), reducing hepatic lipogenesis, and enhancing lipid mobilization enzyme activity. In animal models of diabetes, curcumin exhibits anti-hyperglycemic and anti-hyperlipidemic effects. Additionally, its antioxidant properties mitigate oxidative stress, a factor in Type 2 Diabetes Mellitus development. Curcumin has anti-inflammatory properties via its ability to reduce the levels of inflammatory factors, as well as through blocking signalling pathways such as NF- $\kappa$ B.<sup>14,15</sup> Moreover, it plays a crucial function in safeguarding heart health via its ability to mitigate apoptosis and inflammation in individuals with diabetic cardiomyopathy. The cumulative data indicate that curcumin may have therapeutic advantages in managing T2DM and its related problems.<sup>16,17</sup> A variety of approaches, including the encapsulation of CCMN in different lipid nanocarriers or the formation of polymer-prodrug complexes, are intended to address these challenges. Polymer-drug conjugates represent a prevalent and efficacious method for the delivery of hydrophobic drugs. This concept, initially introduced by Ringsdorf et al. in 1975, facilitates controlled drug release, enhances

therapeutic efficacy, reduces adverse effects, and improves patient compliance by increasing drug solubility in aqueous solvents.<sup>18,19</sup>

Chitosan (CHT), a biopolymer known for its biocompatibility, biodegradability, and ability to form gel-like structures in acidic conditions, is utilized in drug delivery applications. With its glucosamine unit containing hydroxyl and amine groups, chitosan enables the conjugation of many drugs and other substances.<sup>20</sup> This property can improve the drug's solubility, stability, and toxicity and facilitate the delivery of the drug to specific cells or tissues.<sup>21–23</sup> In this study, we proposed preparing the polymer prodrug conjugate by chemically binding curcumin and chitosan. The conjugation was done in the presence of succinic anhydride, which could act as a bridge between the chitosan and curcumin. This conjugate was converted to nano micelles in an aqueous environment, which may increase CCMN solubility and stability.<sup>24,25</sup> The *in vitro* hemocompatibility and physicochemical characteristics was investigated. The therapeutic potentiality, toxicity, and biochemical parameters of nano micelles was examined in *in-vivo* diabetic Balb/C mice induced by streptozotocin for 21 days.

## 2. Experimental

### 2. 1. Materials

Chitosan (low molecular weight ~ 50000 Da) purchased from Sigma-Aldrich, curcumin, succinic anhydride, dimethyl sulfoxide (DMSO), N, N' dicyclohexylcarbodiimide (DCC), 4-dimethylamino pyridine (DMAP), pyrene, pyridine, mono-tetrazolium salt (MTT) and other compounds were purchased from SRL Chem Pvt. Ltd (Mumbai, India). The blood was purchased from the certified blood bank in Kolkata, India. All the chemicals are used as analytical grades.

### 2. 2. Synthesis of Succinyl-Curcumin Conjugate (SUC-CCMN)

To synthesize SUC-CCMN, initially, CCMN (0.7368 g, 2 mmol) and succinic anhydride (0.2001 g, 2 mmol) were dissolved in 30 mL benzene and then added 2mL pyridine consequently refluxed for 36 h at 80 °C. After removal of the solvent under low pressure and lower temperature, the residue was purified by column chromatography, where hexane-ethyl acetate (95:5) was used as the mobile phase and silica gel as a stationary phase to get the final product SUC-CCMN (Yield = 0.32 g, 68.31%).<sup>26</sup>

### 2. 3. Synthesis of CHT-di(SUC-CCMN) Conjugates

To synthesize CHT-di(SUC-CCMN) conjugate, initially, in 20 mL DMSO carbohydrate polymer CHT

(1.52 gm, 1 mmol) and SUC-CCMN (0.93 mg, 2 mmol) were dissolved at room temperature. After both compounds were dissolved entirely, DCC (412 mg, 2 mmol) and DMAP (116 mg, 1 mmol) were added to the mixture while stirring continuously. This reaction was carried out in the dark at room temperature for 24 h. Following the completion of the reaction, the product was filtered to precipitate the CHT-di(SUC-CCMN) conjugate. The filtrate was added into a 50 mL solution containing a 1:1 (v/v) ratio of ethanol and ethyl ether to precipitate CHT-di(SUC-CCMN) conjugate. Figure 1 depicts the schematic processes for CHT-di(SUC-CCMN) synthesis.

## 2. 4. Preparation of CHT-di(SUC-CCMN) Conjugates Micelles

For the preparation of CHT-di(SUC-CCMN) conjugated micelles (CDSCM), 1 mg/mL CHT-di(SUC-CCMN) was prepared with DMSO by proper mixing. Then CHT-di(SUC-CCMN) mixture was taken into a dialysis bag (Mol.Wt 12 kDa), placed into double distilled water for 24 h, and replaced in 4 h intervals. The solvent remained in the reaction process, and other components were eliminated through dialysis. After completion of dialysis, it was passed through a filter of 0.45  $\mu\text{m}$  pore size to avoid the large particles, then lyophilized the product. The final micelles were stored in a cool and dry place for further use.<sup>27</sup> The yield of CDSCM was about 81 $\pm$ 6%.

## 2. 4. Physicochemical Characterizations of CDSCM

### 2. 4. 1. Characterizations of CDSCM

The structure of synthesized CHT-di(SUC-CCMN) was confirmed by different instrumental analyses, like an FTIR spectrophotometer (Shimadzu Corp No. 01988) with a spectral range of 4000  $\text{cm}^{-1}$  to 400  $\text{cm}^{-1}$ .  $^1\text{H}$ -NMR (Bruker-500 MHz spectrometer) spectral analysis was done with the solvent DMSO- $d_6$  and a UV-vis spectrophotometer (Shimadzu, Japan) over 200–700 nm. To know the morphology, hydrodynamic size, and zeta potential of the CDSCM, a zeta seizer (Nano-ZS 90, Malvern Instrument, UK), field emission scanning electron microscope; FEI, Quanta 200 (FE-SEM). To make the SEM sample, 1 mg/mL of lyophilized CDSCM powder was mixed with 1 mL of double distilled water. Then, the dispersion was placed on an aluminum sheet to make the thin film. The air-dried film was then coated with gold and evaluated under the SEM. A high-resolution transmission electron microscope (HR-TEM) (JEOL Japan, JEM-2100 Plus) was used, and TEM samples were prepared by placing a 0.001 mg/mL drop of CDSCM dispersion on the carbon-coated copper grid.

## 2. 4. 3. Critical Micelle Concentration (CMC) Determination

To determine the CMC of CHT-di(SUC-CCMN), different concentrations of CHT-di(SUC-CCMN) solutions ranging from 0.004 mg/mL to 2.5 mg/mL were vortexed with diluted fluorescent probe pyrene (used as fluorescent dye) solution. The CHT-di(SUC-CCMN) mixture was left overnight to record fluorescence using a fluorescence spectrophotometer at 390 nm emission (Infinite M200, TECAN).<sup>28</sup>

## 2. 5. Drug Loading Capacity

A specified high concentration of CCMN solution was prepared, and various concentrations of CCMN solution were prepared using the serial dilution procedure using DMSO as a solvent. The absorption was measured at 435 nm, and a standard curve was prepared. Absorption was measured after preparing a known concentration (1mg/mL) of CHT-di(SUC-CCMN) conjugate micelle (CDSCM) in DMSO solvent. The quantity of CCMN in the CHT-di(SUC-CCMN) conjugate micelle was determined using the standard line (equation). The following equation was used to compute the CCMN loading capacity of the CHT-di(SUC-CCMN) conjugate in micelles:

$$\text{CCMN loading capacity } \left( \frac{w}{w} \% \right) = \frac{\text{Amount of CCMN}}{\text{Amount of CCMN released from CDSCM}} \times 100 \quad (1)$$

## 2. 6. Stability of free CCMN and CDSCM in Physiological Conditions

The stability of the compound in different pH is different. The stability of free CCMN and CDSCM were analyzed in PBS buffer pH 7.4 for a specific incubation period at 37  $^{\circ}\text{C}$ , taken absorption by UV-vis spectrophotometer at 427 nm. The change of absorbance in the physiological condition of both compounds was noted and plotted graphically.<sup>29</sup>

## 2. 7. CCMN Release Study from CDSCM

In CDSCM, CCMN is conjugated with CHT through pH-sensitive succinyl ester bonds. The cumulative releases of CCMN from CDSCM were measured in PBS buffer pH 5.0 and 7.4. A fixed quantity of CDSCM (10 mg) was dispersed in each 10mL of PBS buffer pH 5.0 and 7.4 solutions. All those solutions were taken into two separate dialysis bags and transferred into 90 mL respective buffer solution containing beakers. Those were incubated at 37  $^{\circ}\text{C}$  for 7 days with moderate shaking. During the incubation period, with an increasing time interval, 2 mL of the sample was withdrawn from each beaker and replaced with the respective buffer.<sup>30</sup> A UV-vis spectrophotometer analyzed the concentration of CCMN at 427 nm.



## 2. 8. Blood Compatibility

A hemolysis study monitored the hemocompatibility of CDSCMs using a blood sample obtained from a local blood bank. RBCs were separated from the blood sample by centrifugation at 2000 rpm for 5 min. The collected RBCs were washed three times in PBS buffer. The stock RBC solution was made by combining 100  $\mu$ L of washed RBC with 10 mL of PBS (pH 7.4) buffer. To determine the hemoglobin release from RBC by CDSCM, 100  $\mu$ L of stock RBC solutions were subjected to 100  $\mu$ L different concentrations of CDSCM ranging from 0.5 to 2 mg/mL for 30 min at 37 °C. Then, all those solutions were centrifuged separately at 1500 rpm for 5 min, and the supernatant was taken for UV-visible absorbance at 541 nm.<sup>31,32</sup> PBS buffer pH 7.4 solution was utilized as a negative control, and distilled water as a positive control. The hemolysis percentage (Hp%) of CDSCM will be determined using the equation shown below:

$$Hp\% = \frac{A_s - A_n}{A_p - A_n} \times 100 \quad (2)$$

Where  $A_s$  = absorbance of the sample, the absorbance of the PBS buffer =  $A_n$ , and absorbance of distilled water =  $A_p$ . All the readings were taken in triplicate.

## 2. 9. In-vivo Experimental Protocol

### 2. 9. 1. Experimental Animals

For the *in vivo* antidiabetic activity study, male Balb/c mice weighing about 25–30 g were obtained from Chakraborty Enterprises (North 24 Parganas PIN-743312 West Bengal), registered breeders.<sup>33,34</sup> Before the start of experiments, they were kept for seven days to adjust standard laboratory conditions with a standard diet according to protocols. This experiment followed the guidelines of the “Institutional Animal Ethics Committee (Registration number: 1805/GO/Re/S/15/ CPCSEA)”, Jadavpur University, India (Approval of project proposal No: JU/IAEC-22/30), throughout the study, followed the National Institute of Health (NIH) recommendations.

### 2. 9. 2. Experiment Design of *In vivo* Study

A total of 30 Animals were taken and equally divided into five groups. Group I: Non-diabetic control animals (NDC) received a high fat-containing regular diet. Group II: Diabetic control (DC) received a high fat-containing regular diet with a single dose of diabetic inducer. Group III: Diabetic control free CCMN (DC-FCUR) received a high fat-containing regular diet with a single dose of diabetic inducer and treated orally with free CCMN at 100 mg/kg body weight for 21 days. Group IV: Diabetic control drug-containing nanoparticle (DC-DCN) received a high fat-containing regular diet with a single dose of diabetic inducer and treated orally with CDSCM equivalent to 100 mg/kg CCMN payload for 21 days. Group V: Diabetic control standard drug (DC-SD),

which received a high fat-containing regular diet with a single dose of diabetic inducer and treated orally with 2mg/kg b.w. glibenclamide for 21 days.

### 2. 9. 3. Induction of Type-II Diabetes Mellitus

To induce Type-II diabetes mellitus, a single intra-peritoneal injection of STZ (45 mg/kg to overnight fasting animals) followed by a 110 mg/kg intraperitoneal injection of nicotinamide after 15 min.<sup>35–37</sup> both solution was prepared separately by dissolving in citrate buffer pH 4.5 and saline solution, respectively. Non-diabetic control (Group I) animals were injected with saline instead of STZ. FBG levels of all animals were measured by an accu-check glucometer (Roche Diagnostics) on alternate days. Animals with FBG levels  $\geq$  200 mg/dl for three consecutive days after STZ injection were considered diabetic animals, and animals with blood glucose levels  $\leq$  145 mg/dl were considered non-diabetic animals and were excluded from the experiment.

### 2. 9. 4. Sampling of Blood to Estimate FBG Level

Blood samples were collected by pricking the tail and then gently milking it with warm water to evaluate the FBG level of each animal. The direction of milking was from the body side to the tail tip to enhance bleeding. One drop of blood was placed on a strip of the accu-check glucometer to take blood glucose levels, and it was done in duplicate to ensure the consistency of glucometer readings.<sup>38</sup>

### 2. 9. 5. Measurement of Body Weight

Every four days, the body weight of each animal in each group was measured. The variation in weight was documented. After 21 days, the liver weight of each animal was also recorded.

### 2. 9. 6. Estimation of Biochemical Parameters Level

For estimating the biochemical parameters, the blood of all animals was collected under mild anesthesia through cardiac puncture on the 21<sup>st</sup> day of the study. Blood samples were centrifuged for 15 min at 4000 rpm in a cooling centrifuge. Serums were correctly leveled and stored at –80 °C for further analysis. Auto-analyzer (USA) and ELISA kits for estimating the level of a lysosomal enzyme like alkaline phosphatase (ALP) (rAPid Alkaline Phosphatase; Roche), acid phosphatase (ACP) (CS0740, Sigma Aldrich), lipid profile components like HDL, LDL, serum triglycerides (TGL), total serum cholesterol, liver-specific enzymes like serum glutamate oxaloacetic transaminase (SGOT), serum glutamate pyruvic transaminase (SGPT), Hemoglobin A1c (HbA1c) (CS0740, Sigma Aldrich) and serum uric acid.<sup>38,39</sup>



### 2. 9. 7. Carbohydrate Metabolizing Enzymes Estimation

To estimate the level of hexokinase (HK), glucose-6-phosphate dehydrogenase (G6PD), and lactate dehydrogenase (LDH) parameters in the pancreas, liver, and kidney, all animals were euthanized with thiopental sodium after 21 days of treatment. Those tissues (0.3 g) were taken separately and homogenized in 3 mL of 0.01M Tris-HCL centrifuged at 10000 rpm for 20 min at 4 °C. Supernatants were treated with the corresponding colorimetric assay kits for HK, G6PD, and LDH.<sup>39,40</sup>

### 2. 10. Statistical Analysis

For the statistical analysis, all the readings were taken more than two times, standard deviation (SD) was calculated from obtained data, and the actual value of the readings was represented as mean  $\pm$  SD, were it possible. For the statistical processing of obtained results, one-way analysis of variance (ANOVA) with P-value < 0.05 was used to know the groups/category significant changes in another statistical tool, like a student t-test. Different software like Origin Pro 9.0 and GraphPad Prism 6.0 are used for the graphical representation of statistically processed data.

## 3. Results

The primary objective of our investigation was to synthesize the CHT-CCMN conjugate, which was subsequently synthesized and characterized using various in-

strumental methods. After confirming the synthesis of the conjugate, it was found that the conjugate was freely soluble in an aqueous and non-aqueous solvent. The tri-molecular conjugated polymer-prodrug, consisting of a hydrophilic polymer and hydrophobic drugs, can enhance aqueous solubility, improve drug targeting, prevent drug resistance, and minimize the toxic effect of the desired drug.<sup>41,42</sup> This study used CHT as a hydrophilic polymer, CCMN as a hydrophobic drug, and succinic anhydride as a bi-molecular pH-sensitive linker. CCMN, when conjugated with CHT via a succinyl ester link, creates an amphiphilic polymer-prodrug known as CHT-di (SUC-CCMN). This prodrug self-assembles into nano micelles when placed in an aqueous media. CHT has several hydroxyl groups that have the capability to form bonds with multiple SUC-CCMN molecules, enabling the transportation of CCMN for drug delivery purposes.

For the formation of CHT-di(SUC-CCMN) prodrug conjugate, CCMN refluxes with succinic anhydride in the presence of pyridine to form SUC-CCMN, which consists of a carboxylic acid group that can further react with a hydroxyl group of CHT to form an ester bond by a condensation reaction in the presence of pyridine, as shown in Figure 1. The FT-IR spectrum of CCMN clearly shows characteristic peaks of phenolic O-H stretching at 3507  $\text{cm}^{-1}$  for aromatic moiety C=C stretching peak at 1625  $\text{cm}^{-1}$ , benzene ring stretching vibrations peak at 1596  $\text{cm}^{-1}$ , for C=O and C=C vibrations peak at 1504  $\text{cm}^{-1}$ , for C-H bending vibrations of olefinic ( $>\text{C}=\text{C}<$ ) bond peak at 1424  $\text{cm}^{-1}$  and for stretching vibrations of the aromatic C-O bonding peak at 1276  $\text{cm}^{-1}$  could identify CCMN (Figure 2).<sup>43,44</sup> The FT-IR spectrum of SUC-CCMN shows a peak for phenolic O-H stretching at 3505  $\text{cm}^{-1}$ , a peak for aryl

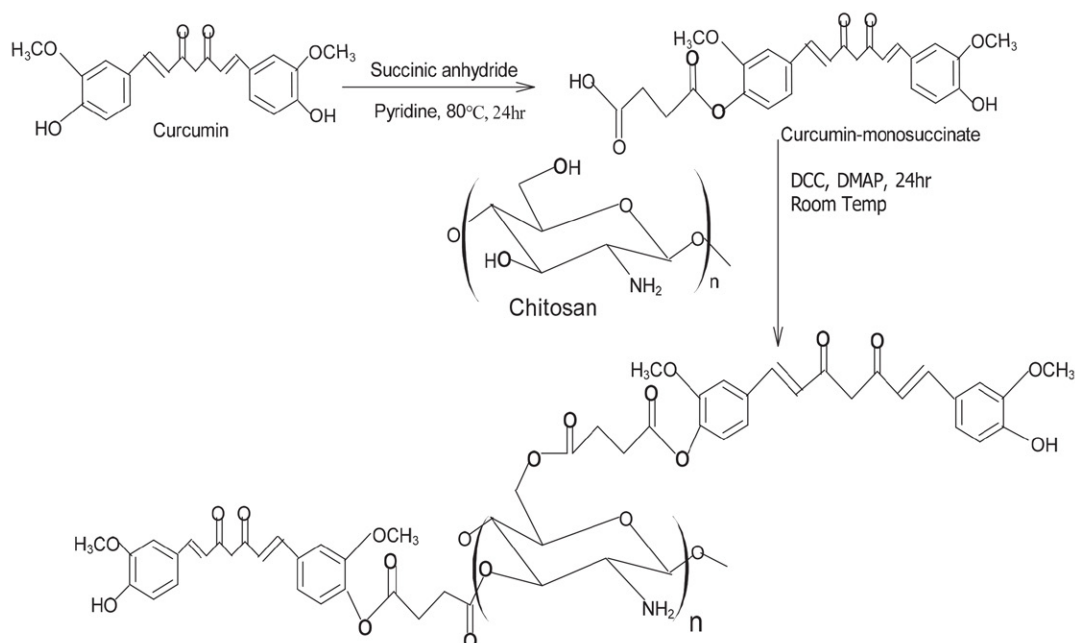
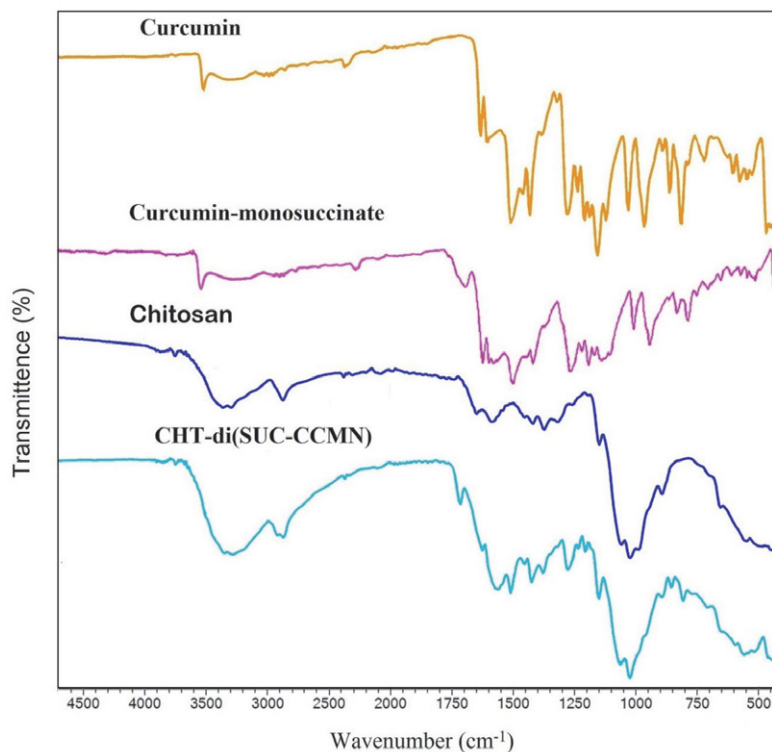


Figure 1. The schematic reactions for synthesizing SUC-CCMN and CHT-di(SUC-CCMN) conjugate.



**Figure 2:** FTIR spectra Curcumin, Curcumin-mono succinate, Chitosan, and CHT-di(SUC-CCMN)

(C-H) stretching at  $2942\text{ cm}^{-1}$ , peaks for C=O stretching frequencies of a conjugated succinic acid moiety at  $1697\text{ cm}^{-1}$ , peak for C=C of CCMN at  $1627\text{ cm}^{-1}$ , a peak for stretching frequencies of C=O and C-O (enol) groups of CCMN moiety at  $1510\text{ cm}^{-1}$  and  $1281\text{ cm}^{-1}$ . The peak at  $1028\text{ cm}^{-1}$  is attributed to the stretching frequencies of C-O-C. The presence of prominent peaks at  $3505\text{ cm}^{-1}$ ,  $1697\text{ cm}^{-1}$ , and  $1510\text{ cm}^{-1}$  corresponding to the -OH, C=O, and C-O bands, respectively, represent the successful conjugation of CCMN to SUC.<sup>25</sup> The FT-IR spectrum (Figure 2) of CHT-di(SUC-CCMN) conjugate exhibits a new peak at  $1735\text{ cm}^{-1}$  corresponding to the stretching frequency of the C=O group and a peak at  $1510\text{ cm}^{-1}$  corresponding to the C-O (enol) bands stretching frequencies in addition to peaks exhibited by CHT and SUC-CCMN, those peaks represent the existence of newly formed ester bond between CHT and SUC-CCMN.<sup>42</sup> The FTIR analysis demonstrates that the procedure begins with the reaction of CCMN and succinic anhydride, which results in the formation of SUC-CCMN with a reactive carboxylic acid group. The FTIR spectrum reveals that this acid group interacts with the hydroxyl group of CHT in the presence of pyridine to form an ester bond, leading to CHT-di(SUC-CCMN) prodrug-polymer synthesis. The enhanced solubility of curcumin in CHT-di(SUC-CCMN) could potentially be attributed to the formation of a tenuous hydrogen bond between the carbonyl group (C=O) in curcumin and the hydroxyl group in chitosan.<sup>45</sup>

To assure the formation of the conjugated structure of CHT-di(SUC-CCMN), CHT, CCMN, and SUC-CCMN

were initially analyzed through  $^1\text{H}$ -NMR spectroscopy. In Figure 3, it was observed that protons of CCMN show characteristic peaks between 5.4–9.4 ppm;<sup>45,46</sup> CHT shows its distinct peaks between 3.0–4.6 ppm for the protons of  $\beta(1\text{--}4)\text{-D-glucosamine}$  units,<sup>47</sup> including peak at 1.3 ppm for the presence of acetylated chitosan impurities; SUC-CCMN shows peak at 2.2 and 2.4 ppm for protons of  $-\text{CH}_2\text{-CH}_2-$  (Succinyl moiety) including the peaks at 9.4 and 12.5 ppm for the -OH proton of CCMN and succinyl moiety respectively in addition to peaks of CCMN. CHT-di(SUC-CCMN) conjugate exhibits its peaks consisting of characteristic peaks of CHT (3.0–4.6 ppm), CCMN (5.4–9.4 ppm), and succinyl (2.0 and 2.5 ppm) moiety excluding the peaks 12.5 ppm of succinyl moiety -OH proton were demonstrated the successful synthesis of desired conjugate.<sup>46,48</sup> Analysis of the CHT-di(SUC-CCMN) conjugate by  $^1\text{H}$ -NMR confirmed its successful synthesis. The characteristic peaks of CCMN, CHT, and SUC-CCMN were evident in their respective spectra. Notably, the conjugate's spectrum displayed peaks from all constituents except the -OH proton of the succinyl moiety. This absence and the presence of all other expected peaks strongly supported the construction of the designed conjugate.

To know the presence of CCMN in the CHT-di(SUC-CCMN) conjugate, CCMN and CHT-di(SUC-CCMN) were analyzed by UV-vis and fluorescence spectrometer. Both CCMN and CHT-di(SUC-CCMN) conjugate show peak UV-absorbance at 427 nm (Figure 4a, 4b), but conjugate shows a broader peak than the CCMN peak. The fluorescence emission spectral peak (the excita-

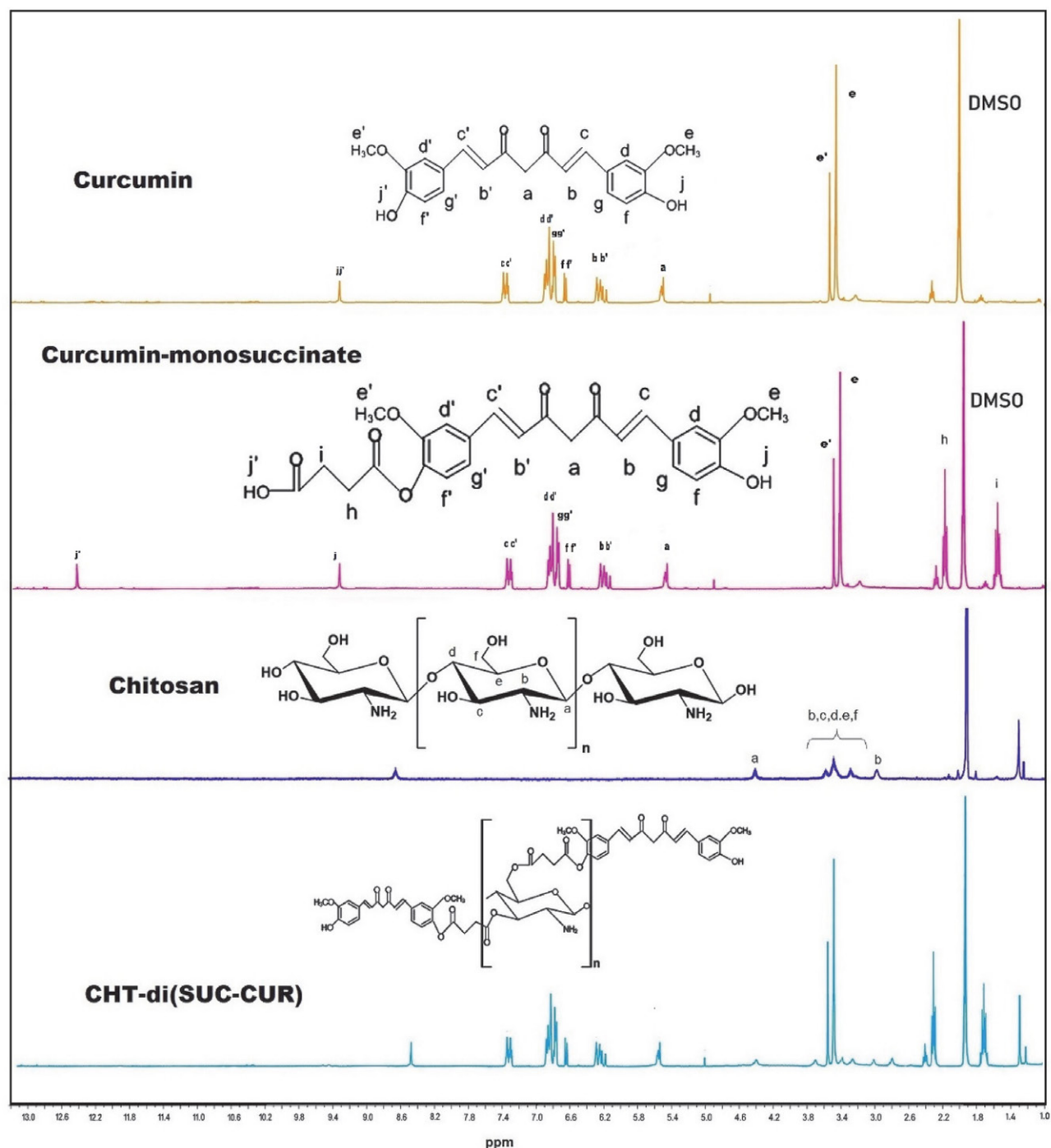


Figure 3:  $^1\text{H}$ -NMR of spectra of Curcumin, Curcumin-monosuccinate, Chitosan, and CHT-di(SUC-CCMN)

tion wavelength 427 nm) of CCMN and CHT-di(SUC-CCMN) shows at 550 nm and 522 nm, respectively, which help to conclude the formation of the conjugation within CHT and CCMN.<sup>49</sup>

The CHT-di(SUC-CCMN) conjugate consists of a free hydroxyl group containing the CHT moiety, which is the hydrophilic part. The CCMN moiety, the hydrophobic domain, jointly helps the amphiphilic to self-assemble into micelles (CDSCM) in an aqueous medium where the hydrophobic part forms the core and the hydrophilic part

remains outside of the micelle. Critical micelle concentration (CMC) signifies a concentration at which the amphiphilic polymeric compound can self-assemble into micelles in the solvent. The CMC of CDSCM was determined by employing the self-quenching agent pyrene as the fluorescence probe in an aqueous medium, and it helps to produce fluorescence for the presence of a lipophilic part of the micellar core. The intensity ratio of pyrene's (I335/I332) peaks depends on the medium's polarity.<sup>50,51</sup> The fluorescence intensity changed rapidly when pyrene transited

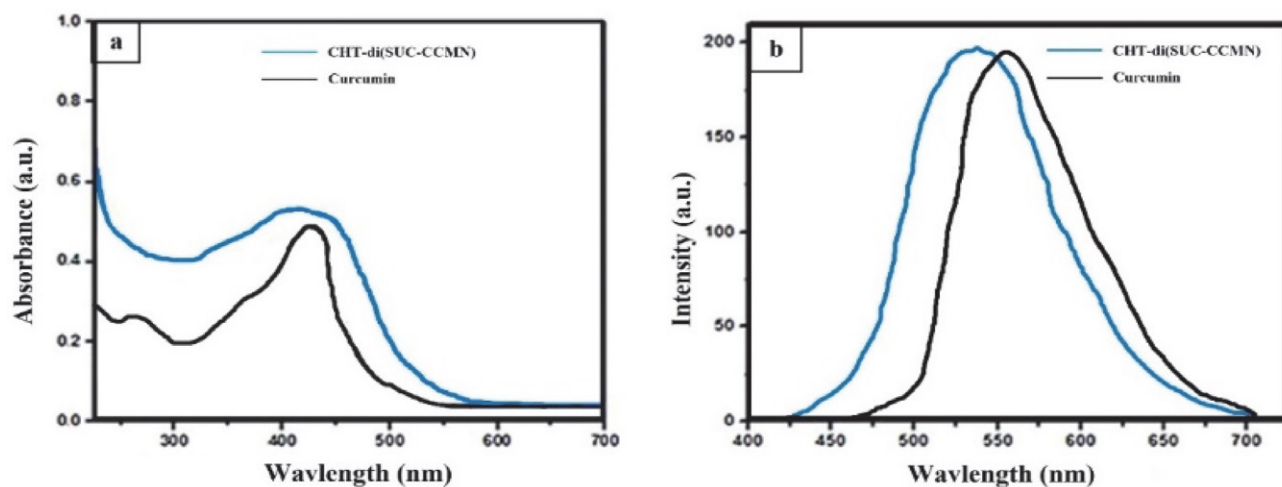


Figure 4: (a) UV-vis and (b) fluorescence spectra of CCMN and CHT-di(SUC-CCMN) conjugate

from hydrophilic media to the lipophilic core of CDSCM. Plotting the logarithm concentration of conjugate vs. intensity ratio constructs two straight lines intersecting at a point called CMC, which was 0.4644 mg/mL (Figure 5A). The lower CMC values signify its stability, prolonging blood circulation and accessibility to the drug's targeting.<sup>52</sup>

The hydrodynamic particle size and zeta potential of the CDSCM were determined by dynamic light scattering (DLS). The hydrodynamic particle size distribution of CDSCM is shown in Figure 5C, and zeta potential is shown in Figure 5B. It was observed that micelles were about  $57 \pm 6$  nm in size from and polydispersity index was found to be 0.19 Figure 5C. The zeta potential of CDSCM was meas-

ured to be  $-34.8$  mV, suggesting a significant negative charge. This negative charge is caused by the presence of unbound hydroxyl (-OH) groups in the glucosamine units of the CHT moiety on the surface of CDSCM. This accumulation of hydroxyl groups results in the formation of a highly negatively charged CDSCM surface. This negative change serves to maintain the CDSCM's stability. Higher negative surface charges repel each CDSCM from the other, thereby reducing nano-micelle accumulation.<sup>53</sup> The morphology of CDSCM was also determined through SEM and TEM (Figures 5D, 5E). Figure 5D indicates that CDSCM were roughly spherical and mostly uniform in size. The shape of the particle is distinguishable. For better

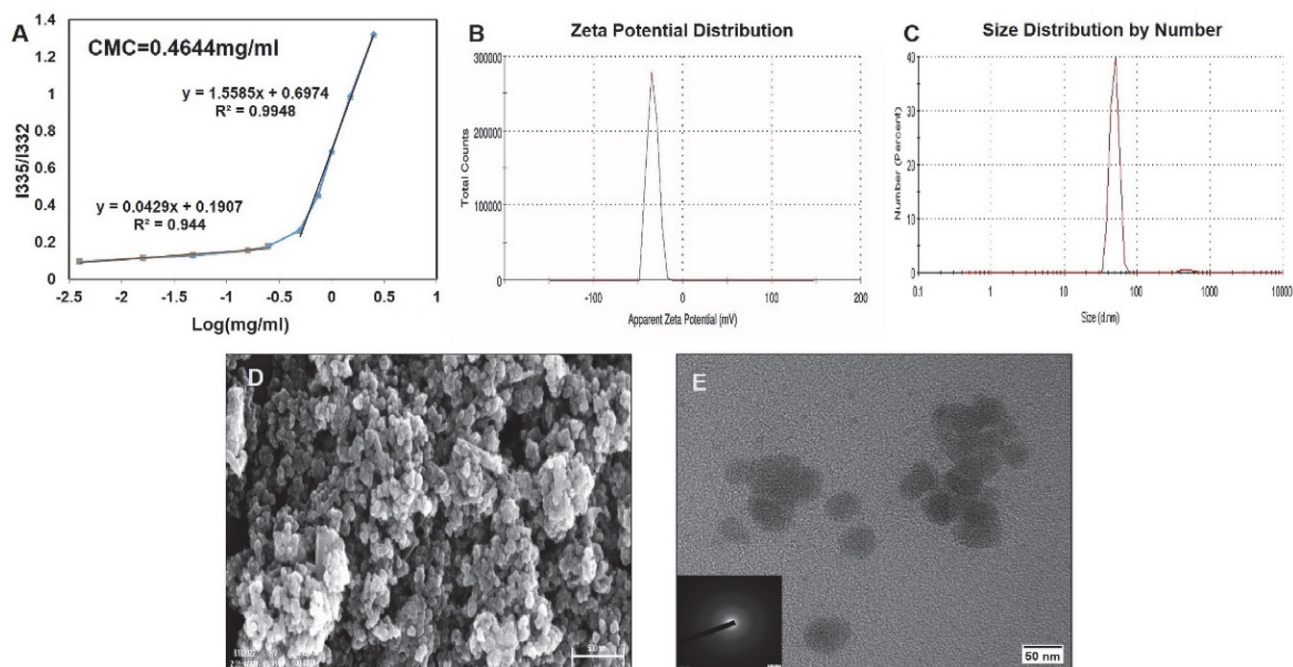


Figure 5: (A) CMC of CHT-di(SUC-CCMN) conjugate; (B) Zeta potential of CDSCM; (C) Particle size distribution of CDSCM; (D) FE-SEM Image of CDSCM; (E) TEM Image of CDSCM



morphological evaluation, another microscopic (TEM) study was done. Figure 5E shows that the CDSCM are spherical in shape and within the size range of  $50 \text{ nm} \pm 15 \text{ nm}$ . The selected area electron diffraction (SAED) pattern in the bottom left corner of the TEM image shows that the CDSCM samples don't have any crystalline particles. Based on the data shown in Figure 5, it is evident that the CDSCM was produced with precision, exhibiting higher zeta potential and smaller particle size. The size of the Nano micelles seen in the TEM analysis was primarily consistent with the hydrodynamic sizes of the Nano micelles determined by DLS analysis. Based on the aforementioned results, it is obvious that the CDSCM has the potential for use in the applications described above.

In physiological pH, the stability of free CCMN and CDSCM was compared. The stability of free CCMN and CCMN in CDSCM was evaluated at pH 7.4. The stability of free and formulated drugs at physiological pH is critical in drug delivery investigations. PBS was used to make a highly concentrated solution of free CCMN and CDSCM (pH 7.4). Absorbance was measured at 427 nm using a UV-vis spectrophotometer at set intervals from both solu-

tions up to a particular period. The percentage of degraded compounds for both compounds was calculated and presented in Figure 6a. It was observed that free CCMN was about to degrade entirely after 8 h, while more than 90% of CCMN in CDSCM was still present at the same time. As a result, conjugated CCMN exist in CDSCM and are much more stable than free CCMN. CCMN micelles developed by conjugation of CCMN with CHT significantly improve CCMN stability (Figure 6a).

The CCMN release pattern from CDSCMs was studied at physiological pH 7.4 and acidic pH 5, as shown in Figure 6b. It was observed that 97% of CCMN was released from CDSCM within 7 days in an acidic (pH 5) condition, whereas 49% of CCMN was released from CDSCM within the same time in a physiological pH 7.4 condition. The complete drug release was observed after 8 days of study in acidic pH 5, and it was observed that the CCMN presence in the CDSCM was about  $36.8 \pm 2\%$ , calculated using Equation 1. The higher release rate of CCMN in the acidic medium than in the basic medium is due to the acid-catalyzed hydrolysis of the ester linkage.<sup>54,55</sup> As a result, the rate of CCMN release in physiological pH is lower than in acidic

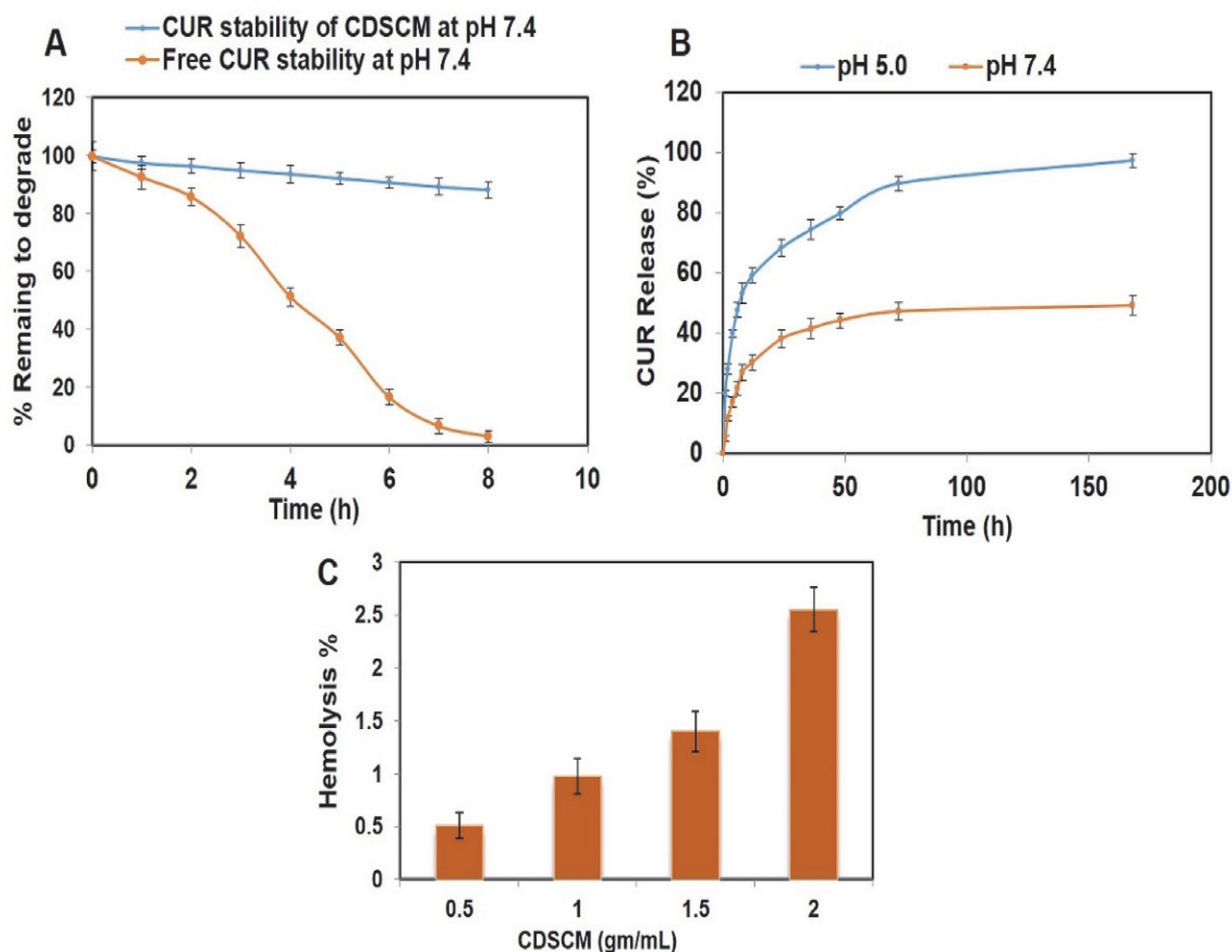


**Figure 6:** (a) Stability studies of CCMN and CDSCM, (b) Release profiles of CCMN from CDSCM under different conditions, and (c) Hemocompatibility assay of CDSCM

pH. Thus, CDSCM is applicable for sustained CCMN delivery and helps overcome first-pass metabolism.<sup>56,57</sup> The mechanism of drug release from CDSCM may depend on the release pattern in specific pH mediums. Release kinetic models were established for both acidic and basic medium, revealing that in the acidic medium, the release followed the first-order kinetic model, identified by its highest R<sup>2</sup> value of 0.943 (Table 1). This indicates that the rate of drug release decreases exponentially over time as the drug concentration in the delivery system decreases. This release mechanism likely involves diffusion through a matrix or dissolution of the drug from a reservoir. The acidic pH may facilitate this diffusion by swelling the nanomelles and breaking the ester bond, releasing CCMN into the medium. On the other hand, at pH 7.4, a basic medium, CCMN was released from the CDSCM following the Higuchi release kinetic model with the highest R<sup>2</sup> value of 0.802 suggests the release of CCMN diffusion through polymeric matrix.

Table 1: The release kinetics from the CDSCM

pH of the medium	pH 5 R <sup>2</sup> Value	pH 7.4 R <sup>2</sup> Value
Zero Ordar Model	0.5676	0.516
1st Order model	0.9432	0.581
korsmayar peppas model	0.5498	0.722
Higuchi model	0.8371	0.802
Hixson Crowell model	0.8313	0.559

Hemocompatibility is an essential criterion for evaluating compatibility regarding hemoglobin release from RBC by drug-loaded nanoparticles for the safety and biocompatibility of nano-drug formulation. Drugs associated with nanoparticles can damage the RBC partially or fully.

A hemolytic study determined the percentage of hemoglobin released from RBC. After CDSCM and RBCs interact, hemoglobin from the damaged RBCs could be released. A UV-visible spectrophotometer measured the absorbance of hemoglobin<sup>30</sup>, and was calculated in percentage. After sufficient time of incubation of CDSCMs with RBC, it was observed that around 2.5% of hemoglobin was released at the highest concentration of CDSCM (2mg/mL), as shown in Figure 6c. This signifies that our nano-formulation of CDSCM is compatible with RBC and blood, so these nano micelles are also applicable in intravenous administration.<sup>58–60</sup>

After three days of diabetic induction, it was observed that most of the animals had FBG levels of 284±9 mg/dL. Consider those animals as diabetic animals, and those with fasting blood glucose levels ≤145 mg/dL were not considered for the study. After the diabetic induction, a gradual body weight loss was observed (Figure 7C) in group II, but a slight increase in body weight in group III animals was observed. A significant increase in body weight of group-IV (CDSCM receiving group) was observed compared to group-V (diabetic control/standard drug) animals. The findings above highlight the significance of inducing diabetes about body weight and the possible contribution of CDSCM in addressing the alterations in body weight linked to diabetes.

The FBG level of overnight-fasted animals was measured every four days. A gradual increase in FBG level was observed (Figure 7A) in group II, but a gradual decrease in FBG level was observed in groups III, IV, and V. The non-diabetic control group I did not see any substantial alteration in fasting blood glucose (FBG) levels. The decrease in FBG level in users of CDSCM in group IV was substantially greater than in recipients of the conventional medicine in group V. The maximum decrease in blood glucose level was observed (Figure 7B) after 21 days of treatment in CDSCM recipients in group IV. The changes in

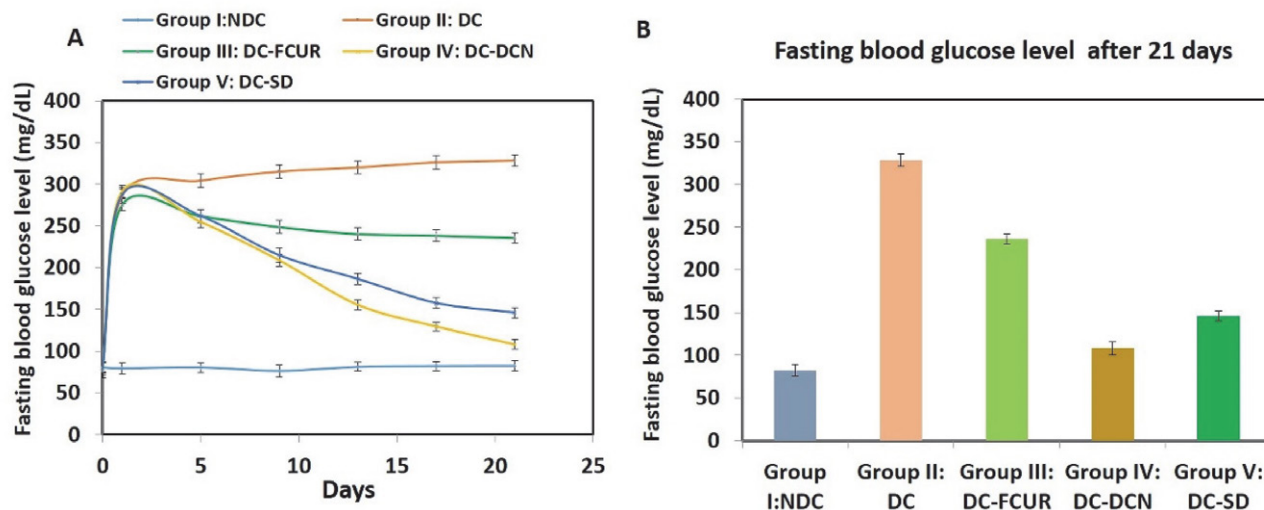


Figure 7: (A) Fasting blood glucose level after 21 days. (B) Change of body weight in 21 days.

Table 2. Biochemical parameters after 21 days of treatment

Parameter	Group I: NDC	Group II: DC	Group III: DC-FCUR	Group IV: DC-DCN	Group V: DC-SD
HbA1c (%)	5.70 ± 0.23	11.03 ± 0.31	8.55 ± 0.22	6.04 ± 0.20	6.89 ± 0.16
Serum creatinine (mg/dL)	0.81 ± 0.05	1.51 ± 0.04*	1.11 ± 0.03*	1.01 ± 0.04	1.17 ± 0.04
Serum uric acid (mg/dL)	3.10 ± 0.40**	5.30 ± 0.20*	4.12 ± 0.31**	3.62 ± 0.27*	4.51 ± 0.52
Serum cholesterol (mg/dL)	83.0 ± 1.1**	157.1 ± 1.7**	109.0 ± 1.2**	91.1 ± 0.9*	124.0 ± 2.1*
Serum triglycerides (mg/dL)	90.0 ± 1.2*	156.3 ± 1.9**	121.7 ± 2.2**	95.0 ± 1.4*	111.0 ± 3.1**
SGPT (IU/L)	70.0 ± 1.1	170.6 ± 3.8**	92.6 ± 3.1**	72.0 ± 1.0	80.1 ± 1.0
SGOT (IU/L)	121.2 ± 2.3**	255.3 ± 4.4**	200.3 ± 2.3**	136.2 ± 2.4**	140.3 ± 2.3**
HDL cholesterol (mg/dL)	51.1 ± 1.3**	32.1 ± 2.1**	38.5 ± 1.4**	44.5 ± 1.5*	43.1 ± 1.4*
LDL cholesterol (mg/dL)	21.0 ± 1.3*	88.8 ± 2.4**	44.2 ± 1.5*	33.5 ± 1.6*	61.8 ± 1.7**
ALP (IU/L)	170.0 ± 1.5**	233.0 ± 3.1**	203.1 ± 2.5**	185.1 ± 2.2**	211.1 ± 2.2**
Hexokinase (U/mL)	1.65 ± 0.11	0.25 ± 0.03	1.04 ± 0.12	1.47 ± 0.21	1.14 ± 0.32
G6PD (U/mL)	22.6 ± 1.4**	85.4 ± 2.1**	62.6 ± 2.5**	29.0 ± 2.8**	38.8 ± 1.8*
LDH (U/mL)	13.6 ± 0.7*	26.8 ± 1.4**	20.8 ± 0.8*	15.8 ± 0.8	17.7 ± 1.0

Data represent mean ± S.D (n = 3). \*\**p* < 0.05; \**p* < 0.01.

FBG concentrations reflect the effect of interventions on glucose metabolism. The observed reduction in fasting blood glucose (FBG) levels across groups III, IV, and V provides evidence of the potential efficacy of these therapies in managing diabetes. The observed difference in the rate of reduction in fasting blood glucose (FBG) level between group IV (the group receiving the CDSCM treatment) and group V may be attributed to the unique mechanism of action of CDSCM. The faster rate of decrease in FBG levels in the CDSCM group (IV) compared to the conventional drug group (V) demonstrates the potential of CDSCM as a promising strategy for controlling glucose in diabetes management.

Biochemical parameters of all the experimental animals were measured on the 21<sup>st</sup> days after induction of diabetes and before induction of diabetes (Table 2), which shows that, the levels of HbA1c, serum creatinine, serum uric acid, serum cholesterol, serum triglycerides, SGPT, SGOT, HDL, LDL, ALP, Hexokinase, G6PD, and LDH have no unexpected changes in the non-diabetic control group I but significant increases (except for HDL and Hexokinase) in the group II. Mild increases were observed in the group III animals, and significant inverse phenomena were observed in groups IV and V. Hexokinase and HDL remarkably increased in CDSCM-receiving group IV compared to diabetic control group II and standard drug-receiving group V. The consistency of high FBG levels in the animal group indicates high glycated hemoglobin (HbA1c).<sup>61</sup> After 21 days, the HbA1c levels of animals in group IV treated with CDSCM were lower. This decrease in HbA1c reflects the improved blood sugar management made possible by the administration of CDSCM. In addition, the investigation revealed a correlation between skeletal muscle mass and creatinine levels. As body weight decreased, creatinine levels increased, associated with an increased risk of type II diabetes.<sup>37</sup> Notably, animals treated with CDSCM had

significantly lower creatinine levels than those treated with free CCMN and the standard drug. This phenomenon suggests that CDSCM can potentially reduce the incidence of type II diabetes. The uric acid levels in the blood have emerged as valuable markers for various diseases, including stroke, hypertension, cardiac complications, and diabetes.<sup>38,62</sup> CDSCM also decreased serum uric acid levels, suggesting a potential improvement in the associated health risks. The investigation also explored diabetic dyslipidemia, a disorder characterized by abnormal lipid levels, including cholesterol, triglycerides, and distinct lipoprotein fractions. This condition is closely associated with type II diabetes.<sup>38,63</sup> Remarkably, animals treated with CDSCM exhibited fewer lipid abnormalities than the control group, indicating a potential function for CDSCM in diabetic dyslipidemia management.

The enzymatic focus of the investigation was on hexokinase, an enzyme with a negative correlation to diabetes. Notable was the increase in hexokinase levels in animals treated with CDSCM, which may have contributed to enhanced glucose metabolism. G6PD, an enzyme relevant to type II diabetes, is typically characterized by decreased tissue levels that contribute to increased blood levels due to metabolic alterations. Nonetheless, administration of CDSCM decreased blood levels of G6PD, indicating a return to metabolic equilibrium. Type II diabetes includes a variety of metabolic disorders involving enzymes such as hexokinase, G6PD, LDH, SGPT, SGOT, and ALP, among others.<sup>64,65</sup> These enzymes exhibit altered concentrations in associated tissues and blood. The CDSCM treatment significantly decreased the blood levels of these enzymes compared to other treatments, according to the study's findings. Our studies amalgamate chemical synthesis and nanotechnology to increase bioavailability and deliver poorly water-soluble, highly degradable phytochemical curcumin in treating type II diabetes.

## 4. Discussion

In this study, the CHT-CCMN conjugate was synthesized successfully. The polymer prodrug molecule was then converted to the nano micelles form, a transformation that not only demonstrates the versatility of our research but also its potential for practical applications. The FTIR and NMR evaluation confirms that the polymer and the drug curcumin were chemically conjugated, proving our success. It was discovered that the conjugate was readily soluble in both an aqueous and an organic solvent, a characteristic that enhances its potential applications. After conjugation, the lipophilic compound CCMN and the hydrophilic polymer CHT form an amphiphilic conjugate, a unique feature that further enhances its potential. In an aqueous environment, the amphiphilic conjugate self-assembled into a micelle at a concentration of 0.4644 mg/mL, a finding that underscores its stability and accessibility. Due to the low CMC value, the nano micelles signify its stability, prolonging blood circulation and making it accessible for the drug's targeting. This feature in stills confidence in its potential for drug delivery systems.<sup>66</sup> The nano micelles exhibited an average hydrodynamic size range of  $57 \pm 6$  nm, as measured by a zeta seizer. The majority of the particles were concentrated within a very limited range. The micelle's polydispersity index was found to be 0.19, which signifies the homogeneity of micelle size. From these, it is understood that micelles are not aggregated and create a proper dispersion in aqueous medium. The zeta potential of the micelle was  $-34.8$  mV, which suggests that the micelles' surface are highly negatively charged, which could help them repel each other, accumulate into the aqueous medium, and provide better stability. These negative surface charges and smaller sizes may help micelles escape reticuloendothelial system internalization.<sup>67,68</sup> The SEM and TEM examination were conducted to morphologically characterize the CDSC micelles by microscopic inspection. The scanning electron microscope (SEM) picture revealed that the lyophilized powder of the CDSCM formed a nearly spherical and aggregated thin film. However, in order to get a precise comprehension, these micelles are examined using transmission electron microscopy (TEM), revealing their spherical shape and particle sizes ranging from around  $50 \pm 10$  nm. This provides the similarity with the hydrodynamic size of the prepared nano micelles. The morphological evaluation of the nano micelles provides a clear understanding of the size and shape of the nano micelles, which is acceptable for the *in vivo* characterization, and better homogeneous biodistribution will occur.<sup>69</sup>

The degradation study found that at physiological pH 7.4, more than 90% of CDSCM remained to degrade within eight hours. In comparison, free CCMN degraded almost entirely under the same conditions. This contrast emphasizes the stability of CDSCM to maintain its structural strength in the physiological environment. Moreover, CDSCM showed a longer drug release duration at the

physiological pH compared to the medium's acidic pH level. This extended drug release profile presents the potential for achieving controlled drug delivery by assuring a constant drug release from micelles. In addition, CDSCM's ability to release drugs under acidic pH conditions enables its use in various medical conditions where drug release is required in acidic environments, thereby expanding its versatility in drug delivery systems.<sup>70,71</sup> The effect of fasting blood glucose (FBG) levels on animals treated with CDSCM was significantly greater than that of unbound CCMN and the standard drug glibenclamide.

Interestingly, the effects of CDSCM on body weight in diabetic-induced animals were found to be less severe than those of free CCMN and the conventional drug. The difference suggests that CDSCM may have a more targeted and potent effect on glucose regulation, potentially allowing for a more targeted method of treating elevated FBG levels. In addition, the consistent elevation of FBG levels in these animals suggests the presence of an elevated amount of glycated hemoglobin (HbA1c), highlighting the chronic nature of the diabetic condition under study.<sup>72</sup> After 21 days, HbA1c levels were significantly reduced in animals treated with CDSCM, according to this research. This correlation can be explained by the direct relationship between skeletal muscle mass and creatinine levels, where creatinine levels progressively increase as body weight decreases, increasing the risk of type II diabetes.<sup>73</sup> Notably, the creatinine levels of CDSCM-treated animals were substantially lower than those of CCMN-free and standard-drug-treated animals. Notably, treatment with CDSCM increased hexokinase enzyme levels, which may have improved glucose metabolism. Glucose-6-phosphate dehydrogenase (G6PD) is an additional enzyme associated with type II diabetes.

Nevertheless, administration of CDSCM reduced blood glucose-6-phosphate dehydrogenase (G6PD) levels, suggesting a restoration of metabolic equilibrium. Several metabolic disorders involving enzymes such as hexokinase, G6PD, LDH, SGPT, SGOT, and ALP, which exhibit altered concentrations in tissues and blood, are associated with Type II diabetes. Compared to other interventions, the CDSCM treatment substantially decreased blood enzyme levels. The above results could indicate that CDSCM restores the normal metabolic process in group IV more efficiently than in other diabetic groups. The effect of FBG on CDSCM capacity was significantly more than that of accessible CCMN and standard drug glibenclamide, and the impact on body weight of CDSCM-treated animals was less than that of free CCMN and standard drug-treated diabetic induced animals.

## 5. Conclusion

In this study, we have successfully synthesized a prodrug of chitosan-curcumin conjugate that self-assem-



bled in an aqueous environment as nano-micelles, where chitosan provided the hydrophilic outer backbone and curcumin the lipophilic core of the micelles. The chitosan di-succinyl curcumin micelles have curcumin in their backbone and entrap curcumin in their inner core, enhancing the solubility and stability of curcumin in many folds. Curcumin is sustainably released from micelles at physiological and acidic pH because there are ester bonds between chitosan and curcumin. The micelles play a pivotal role in declining the fasting blood glucose level and normalizing the related biochemical parameters of type II diabetic animals. The findings suggest that nano micelles have a notable effect in restoring the metabolic pathway that is disrupted in Type-II diabetes mellitus, as compared to both glibenclamide (the conventional treatment) and free curcumin. In future studies, these developments explore multidrug delivery in the form of conjugated prodrugs and entrapment in the micelle core. The amount of drug to be delivered can be increased as needed, prolonging the delivery time, and can be used for multiple other chronic biomedical conditions.

**Author Contributions:** Conceptualization: Sk Mosiur Rahaman and Ranu Biswas, Abimanyu Sugumaran.; Study execution, Data collection, Analysis, and interpretation of results: Sk Mosiur Rahaman, Ranu Biswas and Gouranga Dutta; Writing—original draft: Sk Mosiur Rahaman and Gouranga Dutta; Writing—review and editing: Sk Mosiur Rahaman, Ranu Biswas, Abimanyu Sugumaran, Mohamed M. Salem, Mounir M. Salem-Bekhit, Mohamed Abd El Rahman and Mohammed Gamal. Figures and Tables: Sk Mosiur Rahaman, Gouranga Dutta. All the authors have confirmed the manuscript for the submission proceedings.

**Funding:** The authors would like to extend their sincere appreciation to the Researchers Supporting Project Number (RSPD2024R986), King Saud University, Riyadh, Saudi Arabia.

**Institutional Review Board Statement:** The Institutional Animal Ethics Committee of Jadavpur University, Kolkata, India (JU/IAEC-22/30) approved the animal study protocol.

**Data Availability Statement:** Current study data are available from the corresponding author upon reasonable request

**Acknowledgments:** The authors are thankful to Head, Department of Pharmaceutical Technology, Jadavpur University, Kolkata, West Bengal, India.

**Conflicts of Interest:** The author declares that there is no financial or personal conflict of interest associated with the work reported in this paper.

## 6. Reference

1. QX. Zhang, E. Kupczyk, P. Schmitt-Kopplin, C. Mueller, *Drug Discov. Today*. **2022**, *27*, 103331. DOI:10.1016/j.drudis.2022.07.016
2. S. Park, H. Lee, W. Cho, H. G. Woo, H. Lim, S. Kim, S. Y. Rhee, D. K. Yon, *Obes. Rev.* **2024**, *25*, e13714. DOI:10.1111/obr.13714
3. N. Esser, S. Legrand-Poels, J. Piette, A. J. Scheen, N. Paquot, *Diabetes Res. Clin. Pract.* **2014**, *105*, 141–150. DOI:10.1016/j.diabres.2014.04.006
4. D. A. Domingo-Lopez, G. Lattanzi, L. H. J. Schreiber, E. J. Wallace, R. Wylie, J. O'Sullivan, E. B. Dolan, G. P. Duffy, *Adv. Drug Deliv. Rev.* **2022**, *185*, 114280. DOI:10.1016/j.addr.2022.114280
5. L. A. DiMeglio, C. Evans-Molina, R. A. Oram, *Lancet*. **2018**, *391*, 2449–2462. DOI:10.1016/S0140-6736(18)31320-5
6. S. E. Kahn, *Diabetologia*. **2003**, *46*, 3–19. DOI:10.1007/s00125-002-1009-0
7. Y. Li, W. Zhang, R. Zhao, X. Zhang, *Bioact. Mater.* **2022**, *15*, 392–408. DOI:10.1016/j.bioactmat.2022.02.025
8. W. Lu, F. Khatibi Shahidi, K. Khorsandi, R. Hosseinzadeh, A. Gul, V. Balick, *J. Food Biochem.* **2022**, *46*, e14358. DOI:10.1111/jfbc.14358
9. B. Salehi, Z. Stojanović-Radić, J. Matejić, M. Sharifi-Rad, N. V. Anil Kumar, N. Martins, J. Sharifi-Rad, *Eur. J. Med. Chem.* **2019**, *163*, 527–545. DOI:10.1016/j.ejmech.2018.12.016
10. A. Sugumaran, J. Sadhasivam, P. Gawas, V. Nitalapati, R. Pandian, S. Kumar Perumal, *Mater. Sci. Eng. B.* **2022**, *286*, 116047. DOI:10.1016/j.mseb.2022.116047
11. S. Fuloria, J. Mehta, A. Chandel, M. Sekar, N. N. I. M. Rani, M. Y. Begum, V. Subramaniyan, K. Chidambaram, L. Thangavelu, R. Nordin, et al., *Front. Pharmacol.* **2022**, *13*, 820806. DOI:10.3389/fphar.2022.820806
12. N. Agrawal, M. Jaiswal, *Eur. J. Med. Chem. Reports*. **2022**, *6*, 100081. DOI:10.1016/j.ejmcr.2022.100081
13. V. Ruiz de Porras, L. Layos, E. Martínez-Balibrea, *Semin. Cancer Biol.* **2021**, *73*, 321–330. DOI:10.1016/j.semcancer.2020.09.004
14. Y. Zhong, C. Liu, J. Feng, J. Li, Z. Fan, *Exp. Ther. Med.* **2020**, *20*, 1856–1870. DOI:10.3892/etm.2020.8915
15. S. K. Jain, J. Rains, J. Croad, B. Larson, K. Jones, *Antioxid. Redox Signal.* **2009**, *11*, 241–249. DOI:10.1089/ars.2008.2140
16. O. Bozkurt, B. Kocaadam-Bozkurt, H. Yildiran, *Food Funct.* **2022**, *13*, 11999–12010. DOI:10.1039/D2FO02625B
17. F. Pivari, A. Mingione, C. Brasacchio, L. Soldati, *Nutrients*, **2019**, *11*, 1837. DOI:10.3390/nu11081837
18. S. Ibrahim, T. Tagami, T. Kishi, T. Ozeki, *Int. J. Pharm.* **2018**, *540*, 40–49. DOI:10.1016/j.ijpharm.2018.01.051
19. H. Ringsdorf, *J. Polym. Sci. Polym. Symp.* **1975**, *51*, 135–153. DOI:10.1002/polc.5070510111
20. A. Anand, B. R. Iyer, C. Ponnusamy, R. Pandiyan, A. Sugumaran, *Cardiovasc. Hematol. Agents Med. Chem.* **2020**, *18*, 45–54. DOI:10.2174/1871525718666200203112502
21. I. Aranaz, A. R. Alcántara, M. C. Civera, C. Arias, B. Elorza, A. Heras Caballero, N. Acosta, *Polymers (Basel)*. **2021**, *13*,

3256. DOI:10.3390/polym13193256
22. J. Sharifi-Rad, C. Quispe, M. Butnariu, L. S. Rotariu, O. Sytar, S. Sestito, S. Rapposelli, M. Akram, M. Iqbal, A. Krishna, et al., *Cancer Cell Int.* **2021**, *21*, 318. DOI:10.1186/s12935-021-02025-4
  23. D. Ghosh Dastidar, S. Saha, G. Dutta, S. Abat, N. Guha, D. Ghosh, *Mater. Res. Express.* **2020**, *7*, 015031. DOI:10.1088/2053-1591/ab637f
  24. A. Sugumaran, V. Mathialagan, *Curr. Pharm. Des.* **2020**, *26*, 5174–5187. DOI:10.2174/1381612826666200625110950
  25. V. Krishnaswami, A. Sugumaran, V. Perumal, M. Manavalan, D. P. Kondeti, S. K. Basha, M. A. Ahmed, M. Kumar, S. Vijayaraghavalu, *Curr. Drug Targets.* **2022**, *23*, 1330–1344. DOI:10.2174/1389450123666220822094248
  26. S. Jain, R. Jain, M. Das, A. K. Agrawal, K. Thanki, V. Kishwah, *RSC Adv.* **2014**, *4*, 29193–29201. DOI:10.1039/C4RA04237A
  27. M. Li, M. Gao, Y. Fu, C. Chen, X. Meng, A. Fan, D. Kong, Z. Wang, Y. Zhao, *Colloids Surf. B Biointerfaces.* **2016**, *140*, 11–18. DOI:10.1016/j.colsurfb.2015.12.025
  28. R. Raveendran, C. K. S. Pillai, G. S. Bhuvaneshwar, C. P. Sharma, *J. Nanopharmaceutics Drug Deliv.* **2014**, *2*, 36–51. DOI:10.1166/jnd.2014.1046
  29. S. Dey, K. Sreenivasan, *Carbohydr. Polym.* **2014**, *99*, 499–507. DOI:10.1016/j.carbpol.2013.08.067
  30. Sauraj, S. U. Kumar, P. Gopinath, Y. S. Negi, *Carbohydr. Polym.* **2017**, *157*, 1442–1450. DOI:10.1016/j.carbpol.2016.09.096
  31. S. V. Lale, A. Kumar, S. Prasad, A. C. Bharti, V. Koul, *Biomacromolecules.* **2015**, *16*, 1736–1752. DOI:10.1021/acs.biomac.5b00244
  32. C. Ponnusamy, A. Sugumaran, V. Krishnaswami, R. Kandasamy, S. Natesan, *IET Nanobiotechnol.* **2019**, *13*, 868–874. DOI:10.1049/iet-nbt.2019.0130
  33. F. Shafiee, E. Khoshvishkaie, A. Davoodi, A. Dashti Kalantar, H. Bakhshi Jouybari, R. Ataee, *Medicines.* **2018**, *5*. DOI:10.3390/medicines5010001
  34. M. Wahab, A. Bhatti, P. John, *Polymers (Basel).* **2022**, *14*, 3138. DOI:10.3390/polym14153138
  35. P. L. Cruz, I. C. Moraes-Silva, A. A. Ribeiro, J. F. Machi, M. D. T. de Melo, F. dos Santos, M. B. da Silva, C. M. C. Strunz, E. G. Caldini, M.-C. Irigoyen, *BMC Endocr. Disord.* **2021**, *21*, 133. DOI:10.1186/s12902-021-00795-6
  36. P. Rathore, A. Mahor, S. Jain, A. Haque, P. Kesharwani, *RSC Adv.* **2020**, *10*, 43629–43639. DOI:10.1039/D0RA07640F
  37. G. Chandrasegaran, C. Elanchezhian, K. Ghosh, *Biomed. Pharmacother.* **2018**, *99*, 227–236. DOI:10.1016/j.biopha.2018.01.007
  38. M. U. Akbar, K. M. Zia, M. S. H. Akash, A. Nazir, M. Zuber, M. Ibrahim, *Int. J. Biol. Macromol.* **2018**, *120*, 2418–2430. DOI:10.1016/j.ijbiomac.2018.09.010
  39. Y. M. El-Far, M. M. Zakaria, M. M. Gabr, A. M. El Gayar, L. A. Eissa, I. M. El-Sherbiny, *Nanomed.* **2017**, *12*, 1689–1711. DOI:10.2217/nnm-2017-0106
  40. M. F. Elsayed, B. M. Ahmed, *Saudi J. Biol. Sci.* **2022**, *29*, 1402–1406. DOI:10.1016/j.sjbs.2021.11.035
  41. S. Manandhar, E. Sjöholm, J. Bobacka, J. M. Rosenholm, K. K. Bansal, *J. Nanotheranostics.* **2021**, *2*, 63–81. DOI:10.3390/jnt2010005
  42. J. Pan, K. Rostamizadeh, N. Filipczak, V. Torchilin, *Molecules.* **2019**, *24*, 1035. DOI:10.3390/molecules24061035
  43. Sauraj, S. U. Kumar, V. Kumar, R. Priyadarshi, P. Gopinath, Y. S. Negi, *Carbohydr. Polym.* **2018**, *188*, 252–259. DOI:10.1016/j.carbpol.2018.02.006
  44. J. Wang, J.-Z. Jiang, W. Chen, Z.-W. Bai, *Carbohydr. Polym.* **2016**, *145*, 78–85. DOI:10.1016/j.carbpol.2016.03.022
  45. A. Praveen, D. Prasad, S. Mishra, S. Nagarajan, S. R. Chaudhari, *Food Chem.* **2021**, *341*, 128646. DOI:10.1016/j.foodchem.2020.128646
  46. B. N. Waghela, A. Sharma, S. Dhumale, S. M. Pandey, C. Pathak, *PLoS One.* **2015**, *10*, e0117526. DOI:10.1371/journal.pone.0117526
  47. N. M. L. Hansen, D. Plackett, *Polym. Chem.* **2011**, *2*, 2010–2020. DOI:10.1039/c1py00086a
  48. M. Huo, Y. Zhang, J. Zhou, A. Zou, D. Yu, Y. Wu, J. Li, H. Li, *Int. J. Pharm.* **2010**, *394*, 162–173. DOI:10.1016/j.ijpharm.2010.05.001
  49. P. R. Sarika, N. R. James, P. R. A. Kumar, D. K. Raj, T. V. Kumary, *Carbohydr. Polym.* **2015**, *134*, 167–174. DOI:10.1016/j.carbpol.2015.07.068
  50. A. Sahu, U. Bora, N. Kasoju, P. Goswami, *Acta Biomater.* **2008**, *4*, 1752–1761. DOI:10.1016/j.actbio.2008.04.021
  51. H. Li, D. Hu, F. Liang, X. Huang, Q. Zhu, *R. Soc. Open Sci.* **2020**, *7*, 192092. DOI:10.1098/rsos.192092
  52. X. Zhang, Y. Huang, S. Li, *Ther. Deliv.* **2014**, *5*, 53–68. DOI:10.4155/tde.13.135
  53. Y. Liu, K. Liu, C. Li, L. Wang, J. Liu, J. He, J. Lei, X. Liu, *RSC Adv.* **2017**, *7*, 36256–36268. DOI:10.1039/C7RA05913B
  54. L. Hu, P. Zhang, X. Wang, X. Cheng, J. Qin, R. Tang, *Carbohydr. Polym.* **2017**, *178*, 166–179. DOI:10.1016/j.carbpol.2017.09.004
  55. L. Nicolle, C. M. A. Journot, S. Gerber-Lemaire, *Polymers (Basel).* **2021**, *13*, 4118. DOI:10.3390/polym13234118
  56. J. J. Milligan, S. Saha, *Cancers (Basel).* **2022**, *14*, 1741. DOI:10.3390/cancers14071741
  57. M. Ghezzi, S. Pescina, C. Padula, P. Santi, E. Del Favero, L. Cantù, S. Nicoli, *J. Control. Release.* **2021**, *332*, 312–336. DOI:10.1016/j.jconrel.2021.02.031
  58. M. Rai, R. Pandit, S. Gaikwad, A. Yadav, A. Gade, *Nanotechnol. Rev.* **2015**, *4*, 161–172. DOI:10.1515/hsz-2015-0001
  59. N. Ghalandarlaki, A. M. Alizadeh, S. Ashkani-Esfahani, *Biomed Res. Int.* **2014**, *2014*, 1–23. DOI:10.1155/2014/394264
  60. Z. Li, M. Shi, N. Li, R. Xu, *Front. Chem.* **2020**, *8*, 589957. DOI:10.3389/fchem.2020.589957
  61. G. Chao, Y. Zhu, L. Chen, *J. Diabetes Res.* **2021**, *2021*. DOI:10.1155/2021/6626587
  62. Q. Xiong, J. Liu, Y. Xu, *Int. J. Endocrinol.* **2019**, *2019*, 1–8. DOI:10.1155/2019/9691345
  63. T. Hirano, *J. Atheroscler. Thromb.* **2018**, *25*, 771–782. DOI:10.5551/jat.RV17023
  64. M. Taher, T. M. F. S. Tg Zakaria, D. Susanti, Z. A. Zakaria, *BMC Complement. Altern. Med.* **2016**, *16*, 135. DOI:10.1186/s12906-016-1118-9

65. S. K. Choudhary, G. Chhabra, D. Sharma, A. Vashishta, S. Ohri, A. Dixit, *Evidence-Based Complement. Altern. Med.* **2012**, *2012*, 1–10. DOI:10.1155/2012/293650
66. G. Ottaviani, S. Wendelspiess, R. Alvarez-Sánchez, *Mol. Pharm.* **2015**, *12*, 1171–1179. DOI:10.1021/mp5006992
67. K. Xiao, Y. Li, J. Luo, J. S. Lee, W. Xiao, A. M. Gonik, R. G. Agarwal, K. S. Lam, *Biomater.* **2011**, *32*, 3435–3446. DOI:10.1016/j.biomaterials.2011.01.021
68. M. Zhang, S. Gao, D. Yang, Y. Fang, X. Lin, X. Jin, Y. Liu, X. Liu, K. Su, K. Shi, *Acta Pharm. Sin. B.* **2021**, *11*, 2265–2285. DOI:10.1016/j.apsb.2021.03.033
69. J. M. Caster, S. K. Yu, A. N. Patel, N. J. Newman, Z. J. Lee, S. B. Warner, K. T. Wagner, K. C. Roche, X. Tian, Y. Min, et al., *Nanomed. :Nanotechnol. Biol. Med.* **2017**, *13*, 1673–1683. DOI:10.1016/j.nano.2017.03.002
70. Z. Yu, L. Ma, S. Ye, G. Li, M. Zhang, *Carbohydr. Polym.* **2020**, *236*, 115972. DOI:10.1016/j.carbpol.2020.115972
71. N. A. Nasab, H. H. Kumleh, M. Beygzadeh, S. Teimourian, M. Kazemzad, *Artif. Cells Nanomed. Biotechnol.* **2018**, *46*, 75–81. DOI:10.1080/21691401.2017.1290648
72. S. I. Sherwani, H. A. Khan, A. Ekhzaimy, A. Masood, M. K. Sakharkar, *Biomark. Insights* **2016**, *11*, 95–104. DOI:10.4137/BMI.S38440
73. N. Harita, T. Hayashi, K. K. Sata, Y. Nakamura, T. Yoneda, G. Endo, H. Kambe, *Diabetes Care.* **2009**, *32*, 424–426. DOI:10.2337/dc08-1265

## Povzetek

Sladkorna bolezen je kronična presnovna motnja, za katero je značilna povišana raven sladkorja v krvi, ki povzroča motnje v delovanju organov. Kurkumin, pridobljen iz kurkume, kaže obetavne lastnosti pri zdravljenju sladkorne bolezni tipa II. Amfipatska polimerna predzdravila so sintetizirali s konjugiranjem kurkumina s hitosanom prek sukcinil anhidrida. Nanomiceli, ki so nastali z dializo amfipatskega polimernega predzdravila, so bili sferični s povprečno hidrodinamsko velikostjo 57 nm. Študije sproščanja *in vitro* so pokazale 97-odstotno sproščanje kurkumina pri pH 5 v 7 dneh. V 21-dnevnem poskusu na diabetičnih miših so primerjali vpliv nanomicel, standardnih zdravil in prostega kurkumina na glukozo v krvi na tešče. Študija je pokazala postopno in nadzorovano sproščanje kurkumina iz nanomicel, kar kaže na njihov potencial pri zdravljenju sladkorne bolezni tipa II.



Except when otherwise noted, articles in this journal are published under the terms and conditions of the Creative Commons Attribution 4.0 International License





# National Seminar

On  
"Recent Advances in Drug Discovery and Development"

July 29<sup>th</sup> & 30<sup>th</sup>, 2022

Venue: Calcutta Institute of Pharmaceutical Technology & AHS Seminar Hall




Organized by: Calcutta Institute of Pharmaceutical Technology & AHS  
Banitabla, Uluberia, Howrah-711316, West Bengal, India

## Certificate of Presentation

This is to certify that Prof./Dr./Mr./Ms. Sk Mosiur Rahamon  
has presented paper in ~~Oral/Poster Session~~ in the National Seminar on "Recent Advances in  
Drug Discovery and Development", organized by Calcutta Institute of Pharmaceutical  
Technology & AHS on 29<sup>th</sup> and 30<sup>th</sup> July 2022.

  
Dr. S. M. Firdous  
Coordinator

  
Prof. (Dr). M. E. Bhanaji Rao  
Organizing Chairman





**RB SCIENCE**  
ENTERPRISING BIOSCIENCE RESEARCH

Registered with  
**MSME**



## NATIONAL CONFERENCE ON

# DRUG REPOSITIONING: A NOVEL APPROACH TO DRUG DISCOVERY

## *Certificate*

**Sk Mosiur Rahaman**

This certificate is being awarded to Dr./Mr./Mrs. ....

of **Jadavpur University** .....

for his/her ..... on the topic: Type-II Antidiabetic Potential of Solid Dispersion of Curcumin & resveratrol containing

D-α-tocopheryl polyethylene glycol succinate and mannitol formulation ..... in the National Conference organized on 18-09-2022.

*Dr. Devendra Nath Neekhara*

**Er. Devendra Nath Neekhara**  
Patron

*Dr. Richa Mishra*

**Dr. Richa Mishra**  
Founder & Director

*Prof. Brijeshkunvar Mishra*

**Prof. Brijeshkunvar Mishra**  
Co-Founder